LIITE 1

LUT, Syöttövesipumppaus-projekti
- yhteenveto 18.8.2013

Open your mind. LUT.
Lappeenranta University of Technology

Open your mind. LUT.
Lappeenranta University of Technology

Syöttövesipumpppujen optimaalinen valinta

Lappeenranta University of Technology
Prof. Esa Vakkilainen

Tarkasteltavat tapaukset

Open your mind. LUT.
Lappeenranta University of Technology

- Saatu dataa Suomesta neljästä kattilasta
  - Kaukopää SK6
  - Kaukopää SK5
  - Joutseno
  - Kymi
- Jokaisesta kattilasta kerätty vähintään vuoden ajalta tuntidata syöttövesivirtauksesta ja paineesta
- Kattiloiden toiminnan perusteella valittu tyypilliset toimintapisteet
- Saatujen SV-pumppujen datojen perusteella saatiin tyypillinen pumpun hyötysuhdekäyrä
- Investointikustannus perustuu saatuihin kustannuksiin (Wisa, Kymi-projektit)
- Pumppauskustannus perustuu kussakin toimintapisteessä pumppaustehon minimointiin valitsemalla sopiva määrä pumppuja

Tarkasteltavissa tapauksissa pysyvyyskäyrät samanlaisia

Open your mind. LUT.
Lappeenranta University of Technology

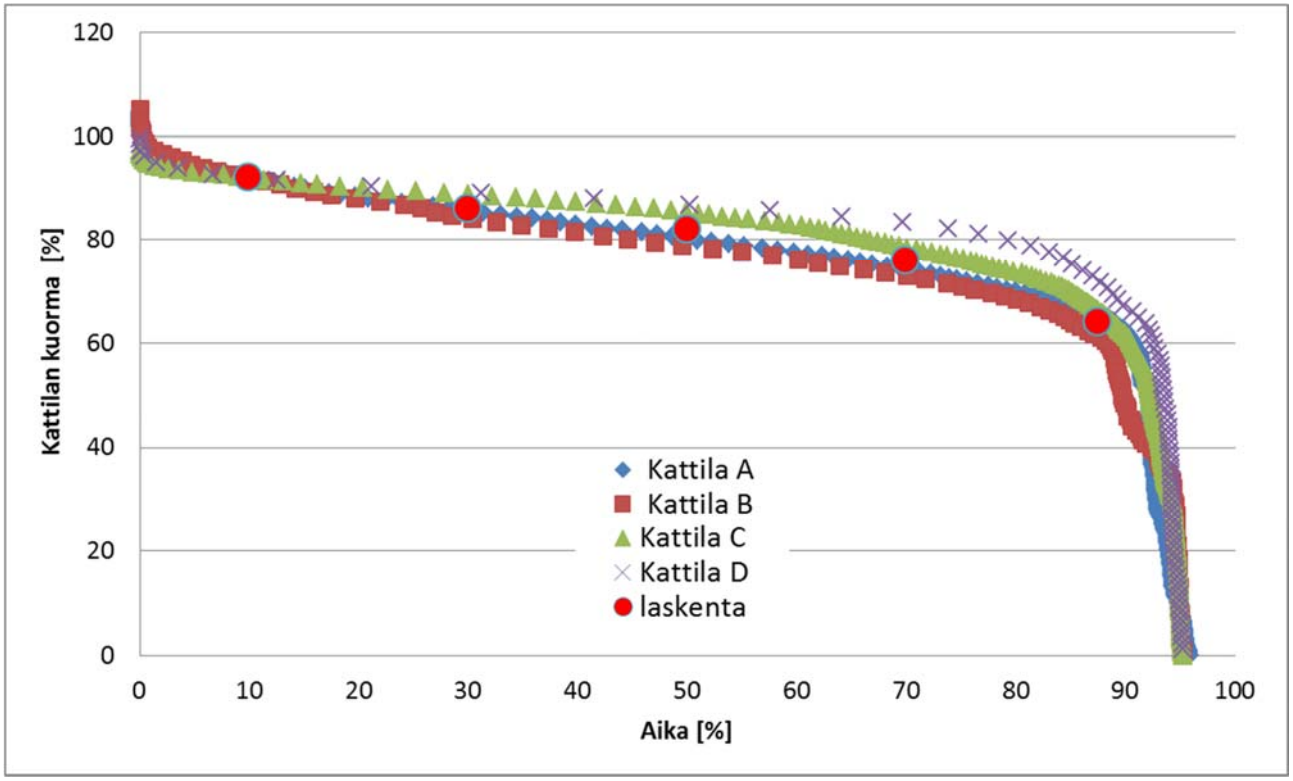

Tyypillinen pumpun hyötysuhdekäyrä

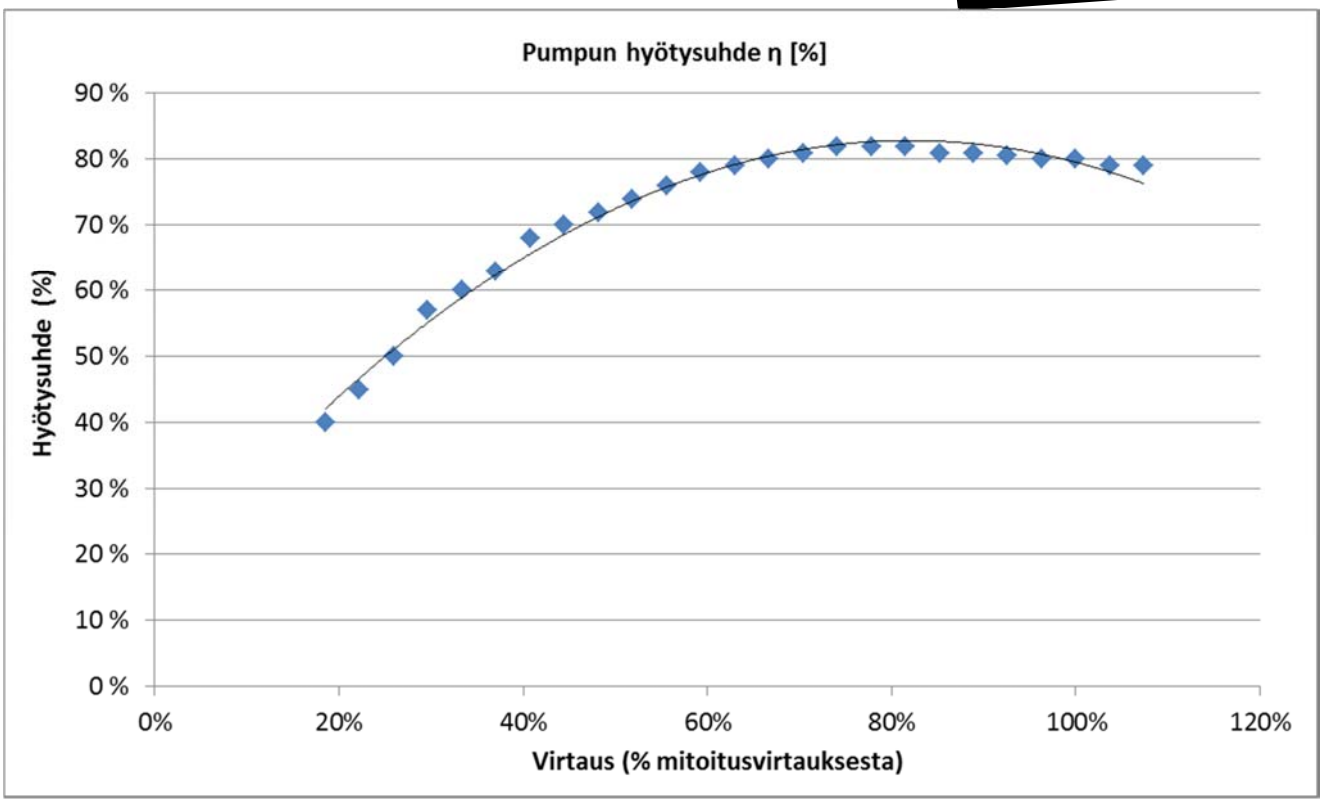

Tyypillinen pumpun nostokorkeus (kuristussäätö)

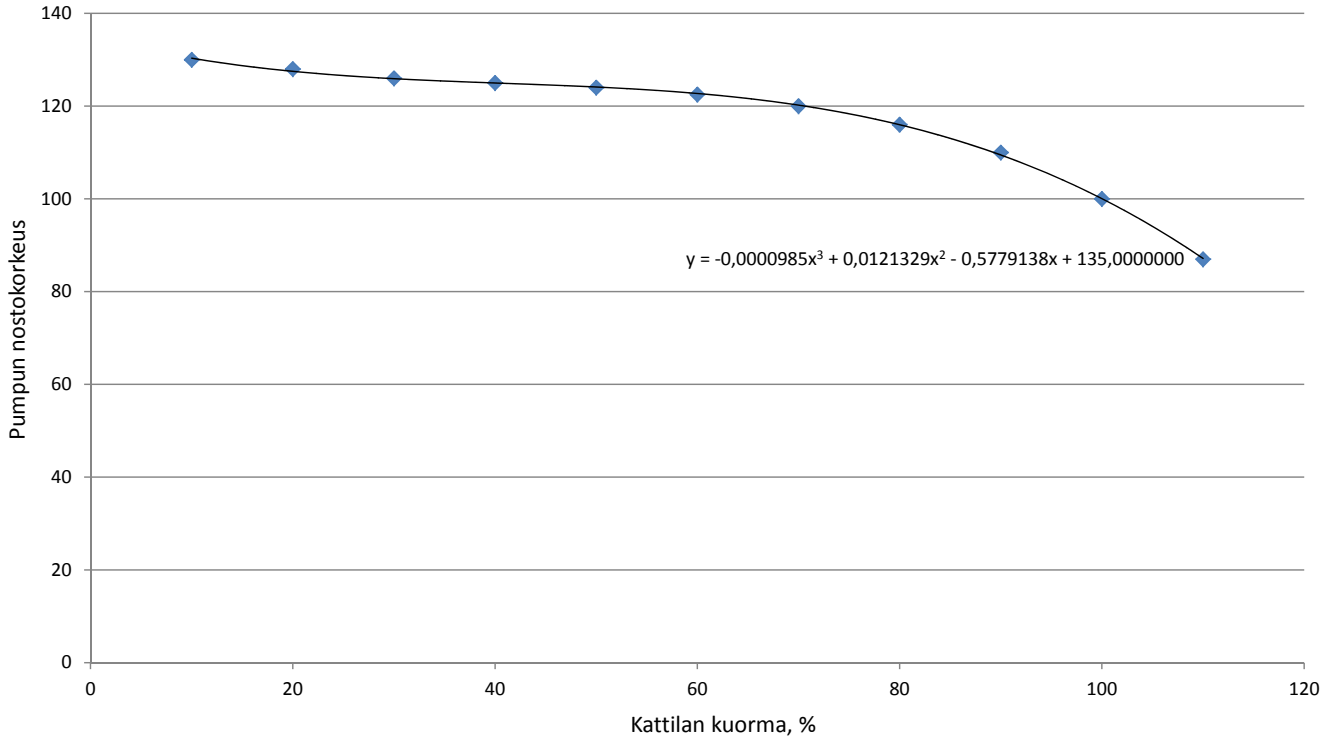

Laskennassa käytetyt arvot (valittiin tyypillinen tapaus)

virtaus[MCR]	100	kg/s
paine sisään	0.5	MPa
paine ulos	10.3	MPa
SV-paineennousu	9.8	MPa
josta virtaushäviöt	1.2	MPa
tiheys	922	kg/m^3
sähkön hinta	40	€/MWh
ajoaika	8313	h/a
Moottorin η	92 %	

Laskentatapaukset (varalla turbopumppu)

	1					
Käytössä olevat pumput	1*140					
Pumpun mitoitusvirtaus [kg/s]	168					
	2	1				
Käytössä olevat pumput	2*70	1*70				
Pumpun mitoitusvirtaus [kg/s]	84	84				
	3	2	1			
Käytössä olevat pumput	3*45	2*45	1*45			
Pumpun mitoitusvirtaus [kg/s]	54	54	54			
	4	3	2	1		
Käytössä olevat pumput	4*33	3*33	2*33	1*33		
Pumpun mitoitusvirtaus [kg/s]	40	40	40	40		
	5	4	3	2	1	
Käytössä olevat pumput	5*25	4*25	3*25	2*25	1*25	
Pumpun mitoitusvirtaus [kg/s]	30	30	30	30	30	
	6	5	4	3	2	1
Käytössä olevat pumput	6*20	5*20	4*20	3*20	2*20	1*20
Pumpun mitoitusvirtaus [kg/s]	24	24	24	24	24	24

Laskentaesimerkki

Open your mind. LUT.
Lappeenranta University of Technology

	1	2	1	3	2	1	4	3	2	1	5	4	3	2	1	6	5	4	3	2	1
käytössä olevat pumput	**1*140**	**2*70**	1*70	**3*45**	2*45	1*45	**4*33**	3*33	2*33	1*33	**5*25**	4*25	3*25	2*25	1*25	6*20	5*20	4*20	3*20	2*20	1*20
Pumpun suunnittelu %MCR	168	84	84	54	54	54	40	40	40	40	30	30	30	30	30	24	24	24	24	24	24
0-1750 0-20 %	168			162			158.4				150					144					
Ajopiste mcr/pumppu	**92.0**	**46.0**	92.0	30.7	**46.0**	92.0	23.0	**30.7**	46.0	92.0	18.4	**23.0**	30.7	46.0	92.0	15.3	**18.4**	23.0	30.7	46.0	92.0
mcr/mcr_design	**0.55**	**0.55**	1.10	0.57	**0.85**	1.70	0.58	**0.77**	1.16	2.32	0.61	**0.77**	1.02	1.53	3.07	0.64	**0.77**	0.96	1.28	1.92	3.83
η [%]	**75 %**	**75 %**	75 %	76 %	**83 %**	31 %	77 %	**83 %**	71 %	31 %	79 %	**83 %**	79 %	31 %	31 %	80 %	**83 %**	81 %	62 %	31 %	31 %
Paine MCR	**98 %**	**90 %**	98 %	89 %	**90 %**	98 %	88 %	**89 %**	90 %	98 %	88 %	**88 %**	89 %	90 %	98 %	88 %	**88 %**	88 %	89 %	90 %	98 %
η,paine	**95 %**	**95 %**	92 %	95 %	**99 %**	78 %	97 %	**99 %**	96 %	66 %	97 %	**99 %**	90 %	67 %	45 %	98 %	**99 %**	90 %	85 %	48 %	32 %
kust. [k€]	**102**	**94**	106	91	**82**	302	88	**81**	99	357	86	**80**	93	320	523	84	**80**	90	126	452	736
1750-3500 20-40%																					
Ajopiste mcr/pumppu	**86.0**	43.0	**86.0**	28.7	**43.0**	86.0	21.5	**28.7**	43.0	86.0	17.2	**21.5**	28.7	43.0	86.0	14.3	**17.2**	21.5	28.7	43.0	86.0
mcr/mcr_design	**0.51**	0.51	**1.02**	0.53	**0.80**	1.59	0.54	**0.72**	1.09	2.17	0.57	**0.72**	0.96	1.43	2.87	0.60	**0.72**	0.90	1.19	1.79	3.58
η [%]	**73 %**	73 %	**79 %**	74 %	**83 %**	31 %	75 %	**82 %**	76 %	31 %	77 %	**82 %**	81 %	45 %	31 %	78 %	**82 %**	82 %	69 %	31 %	31 %
Paine max [%]	**97 %**	90 %	**97 %**	89 %	**90 %**	97 %	88 %	**89 %**	90 %	97 %	88 %	**88 %**	89 %	90 %	97 %	88 %	**88 %**	88 %	89 %	90 %	97 %
η,paine [%]	**92 %**	90 %	**85 %**	92 %	**99 %**	82 %	94 %	**98 %**	92 %	68 %	95 %	**98 %**	90 %	76 %	48 %	92 %	**97 %**	95 %	92 %	77 %	34 %
kust. [k€]	**100**	95	**101**	90	**76**	265	87	**77**	90	319	84	**77**	85	184	453	85	**77**	79	98	262	639
3500-5250 40-60 %																					
Ajopiste mcr/pumppu	**82.0**	41.0	**82.0**	27.3	**41.0**	82.0	20.5	**27.3**	41.0	82.0	16.4	**20.5**	27.3	41.0	82.0	13.7	16.4	**20.5**	27.3	41.0	82.0
mcr/mcr_design	**0.49**	0.49	**0.98**	0.51	**0.76**	1.52	0.52	**0.69**	1.04	2.07	0.55	**0.68**	0.91	1.37	2.73	0.57	0.68	**0.85**	1.14	1.71	3.42
η [%]	**72 %**	72 %	**80 %**	73 %	**82 %**	33 %	74 %	**81 %**	78 %	31 %	75 %	**81 %**	82 %	53 %	31 %	77 %	81 %	**83 %**	73 %	31 %	31 %
Paine max [%]	**96 %**	90 %	**96 %**	89 %	**90 %**	96 %	88 %	**89 %**	90 %	96 %	88 %	**88 %**	89 %	90 %	96 %	88 %	88 %	**88 %**	89 %	90 %	96 %
η,paine [%]	**90 %**	90 %	**90 %**	90 %	**98 %**	84 %	95 %	**98 %**	92 %	70 %	95 %	**98 %**	97 %	82 %	51 %	97 %	98 %	**98 %**	96 %	89 %	38 %
kust. [k€]	**99**	92	**88**	90	**74**	227	84	**74**	83	293	82	**74**	74	138	403	79	74	**72**	84	216	540
5250-7000 60-80 %																					
Ajopiste mcr/pumppu	**76.0**	38.0	**76.0**	25.3	**38.0**	76.0	19.0	**25.3**	38.0	76.0	15.2	**19.0**	25.3	38.0	76.0	12.7	15.2	**19.0**	25.3	38.0	76.0
mcr/mcr_design	**0.45**	0.45	**0.90**	0.47	**0.70**	1.41	0.48	**0.64**	0.96	1.92	0.51	**0.63**	0.84	1.27	2.53	0.53	0.63	**0.79**	1.06	1.58	3.17
η [%]	**69 %**	69 %	**82 %**	70 %	**81 %**	48 %	71 %	**80 %**	81 %	31 %	73 %	**79 %**	83 %	63 %	31 %	74 %	79 %	**83 %**	77 %	31 %	31 %
Paine max [%]	**95 %**	90 %	**95 %**	89 %	**90 %**	95 %	88 %	**89 %**	90 %	95 %	88 %	**88 %**	89 %	90 %	95 %	88 %	88 %	**88 %**	89 %	90 %	95 %
η,paine [%]	**90 %**	90 %	**98 %**	90 %	**95 %**	88 %	90 %	**95 %**	94 %	72 %	90 %	**94 %**	98 %	34 %	56 %	91 %	93 %	**98 %**	88 %	74 %	40 %
kust. [k€]	**94**	88	**72**	86	**71**	138	85	**72**	72	261	82	**73**	67	258	336	80	73	**67**	80	240	470
7000-8313 80-95 %																					
Ajopiste mcr/pumppu	**64.0**	32.0	**64.0**	21.3	**32.0**	64.0	16.0	21.3	**32.0**	64.0	12.8	16.0	**21.3**	32.0	64.0	10.7	12.8	16.0	**21.3**	32.0	64.0
mcr/mcr_design	**0.38**	0.38	**0.76**	0.40	**0.59**	1.19	0.40	0.54	**0.81**	1.62	0.43	0.53	**0.71**	1.07	2.13	0.44	0.53	0.67	**0.89**	1.33	2.67
η [%]	**63 %**	63 %	**83 %**	65 %	**78 %**	69 %	65 %	75 %	**83 %**	31 %	67 %	75 %	**82 %**	77 %	31 %	69 %	75 %	80 %	**82 %**	56 %	31 %
Paine max [%]	**93 %**	89 %	**93 %**	88 %	**89 %**	93 %	88 %	88 %	**89 %**	93 %	88 %	88 %	**88 %**	89 %	93 %	88 %	88 %	88 %	**88 %**	89 %	93 %
η,paine [%]	**87 %**	87 %	**96 %**	88 %	**93 %**	90 %	88 %	93 %	**98 %**	82 %	88 %	90 %	**95 %**	93 %	78 %	89 %	90 %	93 %	**97 %**	85 %	54 %
kust. [k€]	**87**	84	**61**	80	**64**	77	79	66	**57**	189	77	68	**59**	65	199	75	68	61	**57**	97	287
KUST. YHT [k€]/a	481	410		367			360				357					354					

Laskentatulokset kuristussäätö (edullisimman pumppumäärän ajon mukaan)

Open your mind. LUT.
Lappeenranta University of Technology

Käyttöaika 7 vuotta						
Pumppu [kpl]	1	2	3	4	5	6
Mit. virtaus/pumppu [kg/s]	168	84	54	40	30	24
Nostokorkeus [MPa]	11.27	11.27	11.27	11.27	11.27	11.27
Sähkömoottorit [kW]	3100	1500	1000	700	600	400
Turbopumppu	2567	1283	825	605	458	367
Kustannukset [k€]						
- Pumput	202	249	274	294	303	311
- Sähkömoottorit	272	245	246	240	258	227
- Turbopumppu	506	312	229	184	152	130
- Asennus ym.	142	197	244	286	325	362
YHTEENSÄ [k€]	1122	1003	993	1005	1038	1030
INV. KUST. YHT [k€]/a	184	143	142	144	148	147
PUMPPAUS [k€]/a	684	609	593	593	588	586
KOKONAISKUST. [k€]/a	**844**	**752**	**735**	**736**	**737**	**733**

Laskentatulokset nestekytkinsäätö (edullisimman pumppumäärän ajon mukaan)

Käyttöaika 7 vuotta						
Pumppu [kpl]	1	2	3	4	5	6
Mit. virtaus/pumppu [kg/s]	168	84	54	40	30	24
Nostokorkeus [MPa]	11.27	11.27	11.27	11.27	11.27	11.27
Sähkömoottorit [kW]	3100	1500	1000	700	600	400
Nestekytkin [kW]	3400	1700	1100	800	700	400
Turbopumppu	2567	1283	825	605	458	367
Kustannukset [k€]						
- Pumput	202	249	274	294	303	311
- Sähkömoottorit	272	245	246	240	258	227
- Nestekytkin	290	357	395	421	480	389
- Turbopumppu	506	312	229	184	152	130
- Asennus ym.	112	148	179	207	233	257
YHTEENSÄ [k€]	1382	1311	1323	1347	1425	1314
INV. KUST. YHT [k€]/a	197	187	189	192	204	188
PUMPPAUS [k€]/a	543	420	404	404	381	377
KOKONAISKUST. [k€]/a	**740**	**607**	**593**	**597**	**585**	**564**

Laskentatulokset invertterisäätö (edullisimman pumppumäärän ajon mukaan)

Käyttöaika 7 vuotta						
Pumppu [kpl]	1	2	3	4	5	6
Mit. virtaus/pumppu [kg/s]	168	84	54	40	30	24
Nostokorkeus [MPa]	11.27	11.27	11.27	11.27	11.27	11.27
Sähkömoottorit [kW]	3100	1500	1000	700	600	400
Invertteri [kW]	3400	1700	1100	800	700	400
Turbopumppu	2567	1283	825	605	458	367
Kustannukset [k€]						
- Pumput	202	249	274	294	303	311
- Sähkömoottorit	272	245	246	240	258	227
- Invertterit	304	367	415	433	483	444
- Turbopumppu	506	312	229	184	152	130
- Asennus ym.	142	197	244	286	325	362
YHTEENSÄ [k€]	1427	1370	1408	1437	1522	1474
INV. KUST. YHT [k€]/a	204	197	201	207	220	205
PUMPPAUS [k€]/a	481	410	367	360	357	354
KOKONAISKUST. [k€]/a	**685**	**607**	**568**	**567**	**574**	**559**

Vertailu (turbopumppu varalla)

Open your mind. LUT.
Lappeenranta University of Technology

Käyttöaika 7 vuotta						
Pumppu [kpl]	1	2	3	4	5	6
Kuristussäätö						
YHTEENSÄ [k€]	1122	1003	993	1005	1038	1030
INV. KUST. YHT [k€]/a	160	143	142	144	148	147
PUMPPAUS [k€]/a	684	609	593	593	588	586
KOKONAISKUST. [k€]/a	**844**	**752**	**735**	**736**	**737**	**733**
Nestekytkinsäätö						
YHTEENSÄ [k€]	1382	1311	1323	1347	1425	1314
INV. KUST. YHT [k€]/a	197	187	189	192	204	188
PUMPPAUS [k€]/a	543	420	404	404	381	377
KOKONAISKUST. [k€]/a	**740**	**607**	**593**	**597**	**585**	**564**
Invertterisäätö						
YHTEENSÄ [k€]	1427	1370	1408	1437	1522	1474
INV. KUST. YHT [k€]/a	204	197	201	207	220	205
PUMPPAUS [k€]/a	481	410	367	360	357	354
KOKONAISKUST. [k€]/a	**685**	**607**	**568**	**567**	**577**	**559**

Tulokset

Open your mind. LUT.
Lappeenranta University of Technology

- Näyttää siltä että **kolme pumppua ja turbopumppu** on kaikissa tapauksissa edullisin tai ainakaan eroa neljä pumppua ja turbopumppu on pieni.
- Kaksi pumppua ja turbopumppu on aina kallis vaihtoehto
- Yksi pumppu ja turbopumppu on aina kallein vaihtoehto
- Syöttövesipumppujen teho on ylimitoitettu osittain standardin vaatimuksesta
  - Syöttövesipumppuilla pitää pystyä pumppaamaan 115 %kattilan höyrystys kaikilla kattilan painehäviöillä ja toisaalta 100 %:n kapasiteetti niin, että paine vastaa lieriön varojen aukeamispainetta (= 10 % yli vastuksista lasketun painetarpeen).
- Turbopumpun tarve on kyseenalainen koska soodakattila on suunniteltu siten että se voidaan tarvittaessa tyhjentää vaurioittamatta kattilaa. Tällöin veden pinta lasketaan pari metriä pohjan alinta tasoa korkeammalle. Varapumpun tarvetta taas perustellaan sillä että veden pintaa pitää lieriössä näkyvillä, koska muutoin kattila vaurioituu. Tässä on ristiriita.

LIITE 2

Aalto/Labtium, Mustalipeän Ei-Newtonilaisuus ja pisaroituminen – raportti 30.11.2015

Mustalipeän ei-Newtonilaisuus

Ari Kankkunen, Jorma Torniainen, Mika Järvinen

Aalto-yliopisto, Insinööritieteiden korkeakoulu, Energiatekniikan laitos
Labtium Oy

23.10.2015

TIIVISTELMÄ

Polttoon menevän mustalipeän kuiva-ainepitoisuutta on nostettu viime vuosikymmeninä. Samalla on lisääntynyt todennäköisyys mustalipeän ei-Newtonilaiseen käyttäytymiseen. Ei-Newtonilaisen nesteen viskositeetti riippuu lämpötilan ja kuiva-aineen lisäksi myös leikkausnopeudesta, kun taas Newtonilaisen nesteen viskositeetti pysyy vakiona vaikka leikkausnopeus muuttuu.

Projektin tuloksena saatiin tietoa erilaisten mustalipeiden ei-Newtonilaisesta käyttäytymisestä sekä vaikutuksesta soodakattilan toimintaan, erityisesti mustalipeän ruiskutukseen. Tutkimuksessa mitattiin lehtipuulipeän, havupuulipeän, sekalipeän ja eukalyptuslipeän viskositeetti. Lämpötiloiksi valittiin neljä ruiskutuksen ja konsentroinnin kannalta sopivaa lämpötilaa (120 – 150 °C). Leikkausnopeutta muutettiin alueella 5 – 800 1/s. Kaikki lipeät olivat ei-Newtonilaisia pienillä leikkausnopeuksilla. Tämä vaikuttaa pisaroitumiseen, palamiseen ja mahdollisesti haihduttamon viimeisen yksikön toimintaan. Pisaroitumiseen liittyvää ei-Newtonilaisuuden vaikutusta simuloitiin ASYS Fluentilla. Ei-Newtonilaisuus vaikuttaa merkittävästi etenkin suurten pisaroiden muodon muutokseen. Tällöin myös pisaroiden lentorata ja palaminen muuttuvat. Ei-Newtonilaisinta oli lehtipuulipeä, jolla viskositeetti pienillä leikkausnopeuksilla oli moninkertainen verrattuna mustalipeän viskositeetin mittauksessa normaalisti käytettävään leikkausnopeuteen 288 1/s. Putkistoissa ja suuttimella leikkausnopeus on suuri eikä lipeän ei-Newtonilaisuus vaikuta merkittävästi painehäviöön.

Ei-Newtonilaisuuden vaikutusta pisaroiden muodon muutokseen simuloitiin Fluent virtauslaskentaohjelmistolla. Laskennassa huomioitiin vain viskositeetin ja pintajännityksen vaikutus. Pisarakoon ollessa 8 mm, vaatii ei-Newtonilaisen rihman muuttuminen palloksi noin 20 % pitemmän ajan kuin olettaessa Newtonilainen viskositeetti.

Tutkimuksen yhteydessä kehitettiin kapillaariviskometri, joka mahdollistaisi viskositeetin online-mittaukset tehtaalla. Laboratoriossa viskometri kalibroitiin standardiöljyllä, jolloin tarkkuudeksi saatiin 15 %. Tehdasmittauksessa tarkkuuden todettiin olevan huonompi johtuen mm. lämpötilaeroista. Kehitetty laite on tällä hetkellä vaikeakäyttöinen ja vaatii kehitystyötä ennen soveltamista tehtaan jokapäiväiseen käyttöön.

Tutkimusta varten kehitettiin paineistettava mustelipeän näytteenotin. Näin varmistettiin kuumassa mustalipeässä olevan höyryn pysyminen näytteessä ja siten todellisen kuiva-ainepitoisuuden mittaaminen. Mustalipeän kuiva-ainepitoisuus on tärkeä suure, koska monet muut mustalipeän ominaisuudet, kuten kiehumapisteennousu ja viskositeetti esitetään kuiva-aineen funktiona. Yhden prosenttiyksikön virhe vaikuttaa kuiva-aineeltaan 80 % olevan mustalipeän kiehumapisteeseen 1 ºC ja viskositeettiin enimmillään jopa yli 30 %. Ruiskutuksen ja pisaroitumisen kannalta erot ovat merkityksellisiä.

Uudella menetelmällä otettuja näytteitä verrattiin vanhalla menetelmällä otettuihin näytteisiin. Kahdessa tapauksessa kolmesta kuiva-ainepitoisuus aleni, kuten oletetaan höyryn päätyessä lipeään. Kolmannessa tapauksessa kuiva-aine kohosi käytettäessä paineistettua näytteenotinta. Näytteen ottaminen ja käsittely tai sulfidin hapettuminen voivat aiheuttaa ko. virheen. Tulosten varmistaminen vaatisi useamman näytteenoton ja analysoinnin. Koska kaikki aiemmat kuiva-aineen määritykset on tehty normaalilla menettelyllä, jossa osa höyrystä karkaa, on jatkossakin perusteltua käyttää vanhaa näytteenottomenetelmää.

KÄYTETYT MERKINNÄT

Symbolit

A	Pinta-ala, m^2
a	Cassonin viskositeettimallin vakio
K	Vakio
n	Ei-Newtonilaisuuteen liittyvä vakio
T	Absoluuttinen lämpötila, K
u	Nopeus, m/s
v	Nopeus, m/s
$\dot{\gamma}$	Leikkausnopeus, 1/s
μ	Dynaaminen viskositeetti, Pa·s
μ_a	Näennäinen (apparent) viskositeetti, Pa·s
μ_0	Nollaleikkausnopeuden viskositeetti, Pa·s
τ	Leikkausjännitys, N/m^2

1 JOHDANTO

1.1 Tausta

Aikaisemmissa tutkimuksissa mustalipeällä on todettu olevan ei-Newtonilaisia ominaisuuksia kun kuiva-aine on korkea [1,2] tai jopa alle 70 % kuiva-aineilla [3]. Erityisesti suomalaiset koivulipeät olivat ei-Newtonilaisia Söderhjelmin [4] käyttämissä olosuhteissa ko. lipeille. Sellunkeittoprosessit sekä käytetyt puulajit ovat erilaisia eri tehtailla ja prosessit ovat muuttuneet Söderhjelmin 1988 julkaisemien tutkimusten jälkeen.

Mustalipeiden ei-Newtonilaisuudesta ei kuitenkaan ole ollut saatavilla paljoakaan tietoa. Sopivia laitteita ei ole myöskään yleisesti käytössä. Labtiumissa on käytettävissä erityisesti mustalipeän mittaamiseen tarkoitettu viskometri. Erityispiirteinä siinä on helppo lämpötilan säätö, helppo kuiva-aineen muuttaminen ja kiehumisen estävä paineistettu mittaustila kiehumispisteen yläpuolisissa lämpötiloissa tapahtuvalle viskositeetin määritykselle.

Ei-Newtonilaisuuden vaikutuksesta pisaroitumiseen on vähän tutkimustietoa. Nesteet, joiden viskositeetti kasvaa leikkausnopeuden pienentyessä, ovat periaatteessa huonosti pisaroituvia. Pisaroitumisen välivaiheissa, rihmojen ja pisaroiden muodostumisessa ovat leikkausvoimat ja muutosnopeudet pieniä. Tällöin pisaran muodostus voi jäädä kesken suuren viskositeetin takia ja syntyy isoja ei-pyöreitä pisaroita.

1.2 Viskositeetti

Viskositeetti on yksi olennaisimmista mustalipeän ruiskutukseen liittyvistä ominaisuuksista jotka vaikuttavat soodakattilan toimintaan. Viskositeetti kuvaa nesteen kykyä vastustaa liikettä. Kuvassa 1 on esitetty viskositeetin vaikutus yksinkertaisessa tilanteessa. Vedetään A kokoista levyä nopeudella v, etäisyydellä z pinnasta, voimalla F. Leikkausjännitys on tällöin (1)

$$\tau = \frac{F}{A} = \mu \frac{dv}{dz} = \mu \frac{v}{z} \tag{1}$$

jossa μ on viskositeetti.

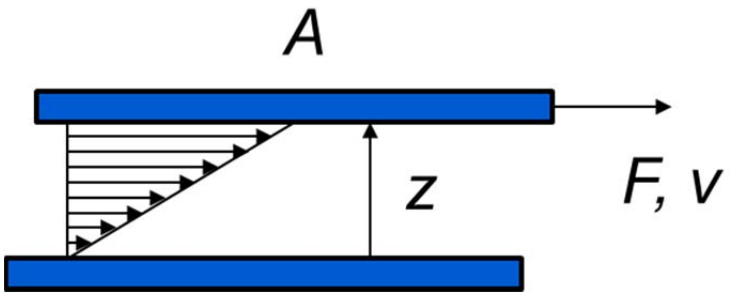

Kuva 1. Nopeusjakauma nesteessä levyjen välissä.

Nesteiden käyttäytyminen voidaan jakaa Newtonilaisiin sekä ei-Newtonilaisiin. Esitetään leikkausjännityksen ja leikkausnopeuden riippuvuus seuraavasti.

$$\tau = \mu \left(\frac{du}{dz}\right)^n = \mu \dot{\gamma}^n = \mu_a(\dot{\gamma})\dot{\gamma} \tag{2}$$

jossa μ_a on näennäinen (apparent) viskositeetti, joka on leikkausnopeuden $\dot{\gamma}$ funktio. Potenssi n on 1 Newtonilaisille nesteille ja erisuuri kuin 1 ei-Newtonilaisille nesteille.

Newtonilaisen nesteen viskositeetti pysyy vakiona, vaikka leikkausnopeus muuttuu. Ei-Newtonilaisen nesteen viskositeetti riippuu leikkausnopeudesta. Leikkausohenevien, pseudoplastisten, nesteiden näennäinen viskositeetti alenee, kun leikkausnopeus kohoaa. Leikkausohenevuus on yleisin ei-Newtonilaisen viskositeetin muoto. Dilatanttisten nesteiden viskositeetti kohoaa, kun leikkausnopeus kohoaa. Jos näennäinen viskositeetti riippuu sekä leikkausnopeudesta että leikkaavan tilanteen kestosta, on kyseessä thiksotrooppinen neste. Viskoplastisten nesteet käyttäytyvät kuten kiinteät elastiset aineet myötörajaan asti. Kuvassa 2. on esimerkki näistä tilanteista.

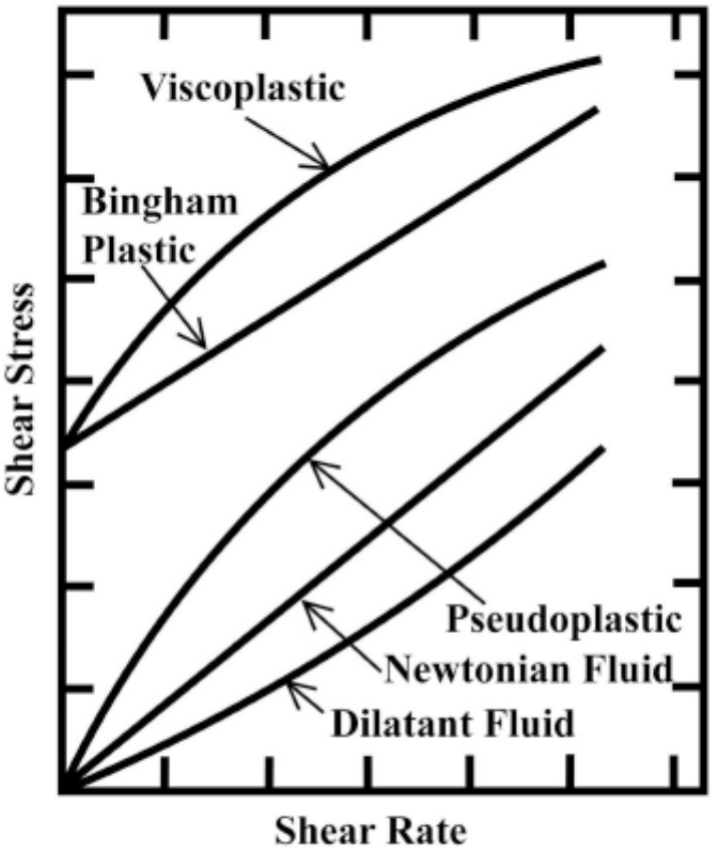

Kuva 2. Newtonilaisen ja ei-Newtonilaisten nesteiden leikkausjännityksen riippuvuus leikkausnopeudesta [1].

Mustalipeän käyttäytyminen on leikkausohenevaa, silloin kun mustalipeä on ei-Newtonilaista. Leikkausoheneminen voi johtua ei-pyöreiden partikkelien asettumisesta virtauksen suuntaisiksi, rihmasykeröiden oikenemisesta tai klustereiden hajoamisesta, kuten kuvassa 3 on esitetty.

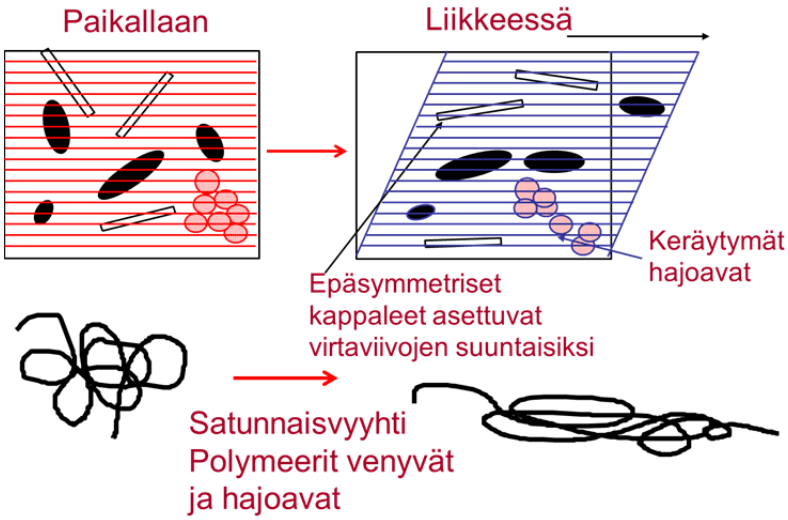

Kuva 3. Leikkausohenemisen syyt

Mustalipeää pidetään Newtonilaisena alhaisilla kuiva-ainepitoisuuksilla ja korkeilla lämpötiloilla. Korkeilla kuiva-ainepitoisuuksilla mustalipeä saattaa olla ei-Newtonilaista, joskin korkea lämpötila vähentää ei-Newtonilaisuuden merkitystä Zamanin ja Fricken [5] mukaan. Bagassimustalipeä on Yangin ym. [6] mukaan ei-Newtonilaista jo 43 ja 56 %:n kuiva-aineilla, kun lämpötila on alle 65°C. Söderhjelmin [7] mukaan korkea kuiva-aineinen ei-Newtonilainen mustalipeä on joskus pseudoplastista ja havupuun viskositeetti on hiukan alhaisempi kuin lehtipuun.

Ei-Newtonilaista virtausta on tutkittu laajimmin liittyen erilaisten polymeerien ominaisuuksiin. Polymeereille soveltuvia yhtälöitä on hyödynnetty mustalipeän ei-Newtonialaisten ominaisuuksien määrittämisessä, mm. Wight [8] ja Fricke ja Zaman [2]. Kuvasta 4 nähdään erään polymeerin seoksen näennäinen viskositeetti eri leikkausnopeuksilla sekä nollaleikkausnopeutta (käyrän vasen pää) ja ääretöntä leikkausnopeutta (käyrän oikea pää) vastaavat tasaantuneet näennäisen viskositeetin alueet. Lisäksi kuvassa on esitetty eri leikkausnopeusalueille soveltuvat viskometrityypit. Kapillaariviskometri sopii alueelle 900–200000 1/s.

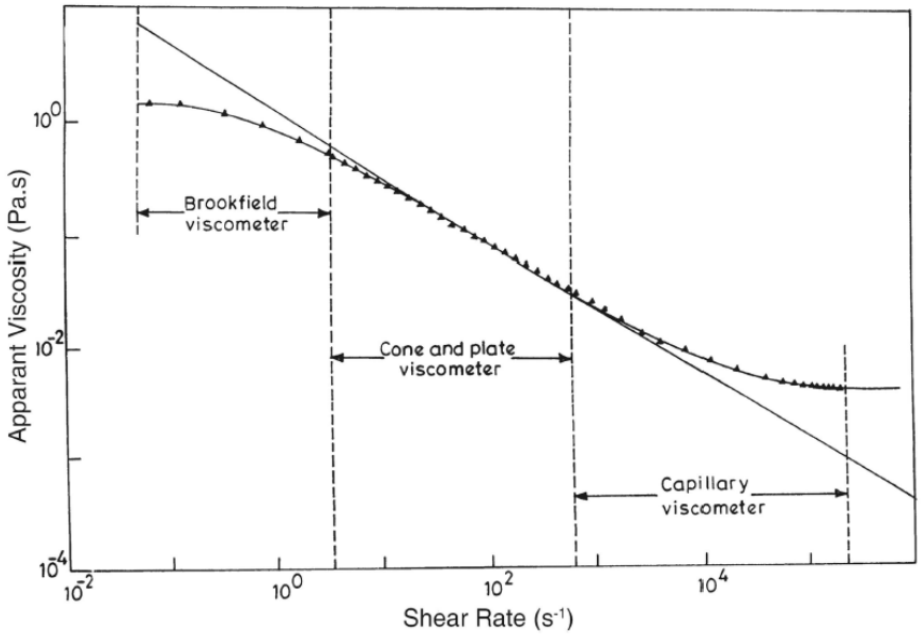

Kuva 4. Nollaleikkausnopeus ja äärellisiä leikkausnopeuksia eräälle polymeerille [1].

Kattavimman tutkimuksen mustalipeän viskositeetista ovat julkaisseet Fricke ja Zaman [2] 1998. He totesivat, että kaikista mustalipeän ominaisuuksista juuri viskositeetti vaihtelee eniten. Vaihteluväli voi olla jopa satakertainen. Erilaisiin mittaustilanteisiin Frickellä ja Zamanilla oli kahdeksan erilaista viskometria, monet modifioitu juuri mustalipeälle soveliaiksi. Tämä mahdollisti laajat viskositeettialueet ja myös viskoelastisuuden tutkimisen. Mittareita voitiin myös vertailla keskenään paremman luotettavuuden saavuttamiseksi.

Fricken ja Zamanin [2] tutkimuksessa korkeimmat kuiva-aineet jäivät hiukan pienemmälle huomiolle. Kuiva-ainepitoisuudet ovat kohonneet viimeisen viidentoista vuoden aikana, joten nykyisten mustalipeiden viskositeetin tutkiminen on nähty tarpeelliseksi.

Mielenkiintoinen uusi menetelmä on kehitetty VTT:llä, Haavisto et al. [9]. Siinä mitataan ultraäänen avulla mustalipeän virtausnopeusprofiili putkessa ja lasketaan sen perusteella näennäinen viskositeetti. Menetelmällä voinee selvittää tulevaisuudessa mustalipeän ei-Newtonilaisia ominaisuuksia.

1.3 Mustalipeän ei-Newtonilaiseen viskositeettiin vaikuttavat tekijät

Zaman and Fricke [10] esittävät, että alle 50 % kuiva-aineella oleellisia viskositeettiin vaikuttavia muuttujia ovat lämpötila ja kuiva-ainepitoisuus. Muita muuttujia ovat keittotapa, joka vaikuttaa mm. kiintoaineiden koostumukseen ja ligniinin molekyylipainoon. Kuvassa 5 on esitetty erään mustalipeän viskositeetin riippuvuus lämpötilasta ja kuiva-ainepitoisuudesta Miikkulaisen [11] mukaan.

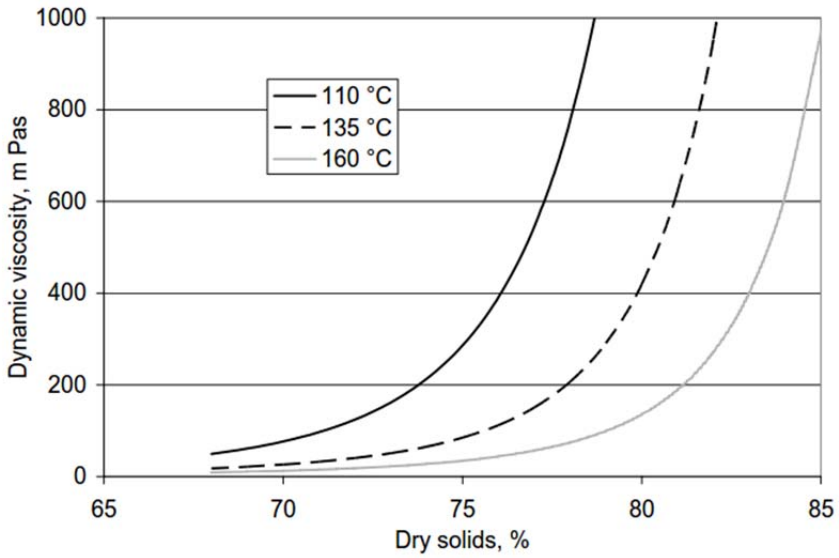

Kuva 5. Mustalipeän viskositeetin riippuvuus kuiva-ainepitoisuudesta ja lämpötilasta (leikkausnopeus 288 1/s).

Suuri molekyylisen ligniinin osuus vaikuttaa viskositeettiin merkittävästi Söderhjelmin [12] mukaan. Polysakkaridit lisäävät koivumustalipeän viskositeettia. Jäännösalkalin kohoaminen korottaa mustalipeän viskositeettia.

Ruiskutuksen kannalta relevantein tutkimus mustalipeän kuiva-aineesta on Zamanin ja Fricke [5] tutkimus vuodelta 1991. Kuvissa 6 ja 7 on esitetty mustalipeän viskositeetti kahdella eri kuiva-ainepitoisuudella. Korkeissa lämpötiloissa ei-Newtonilaisuus on vähäistä, mutta korkealla kuiva-aineella kuitenkin havaittavissa. Kyseisessä tutkimuksessa ei kuitenkaan mitattu pieniä

leikkausnopeuksia, alle 20 1/s.

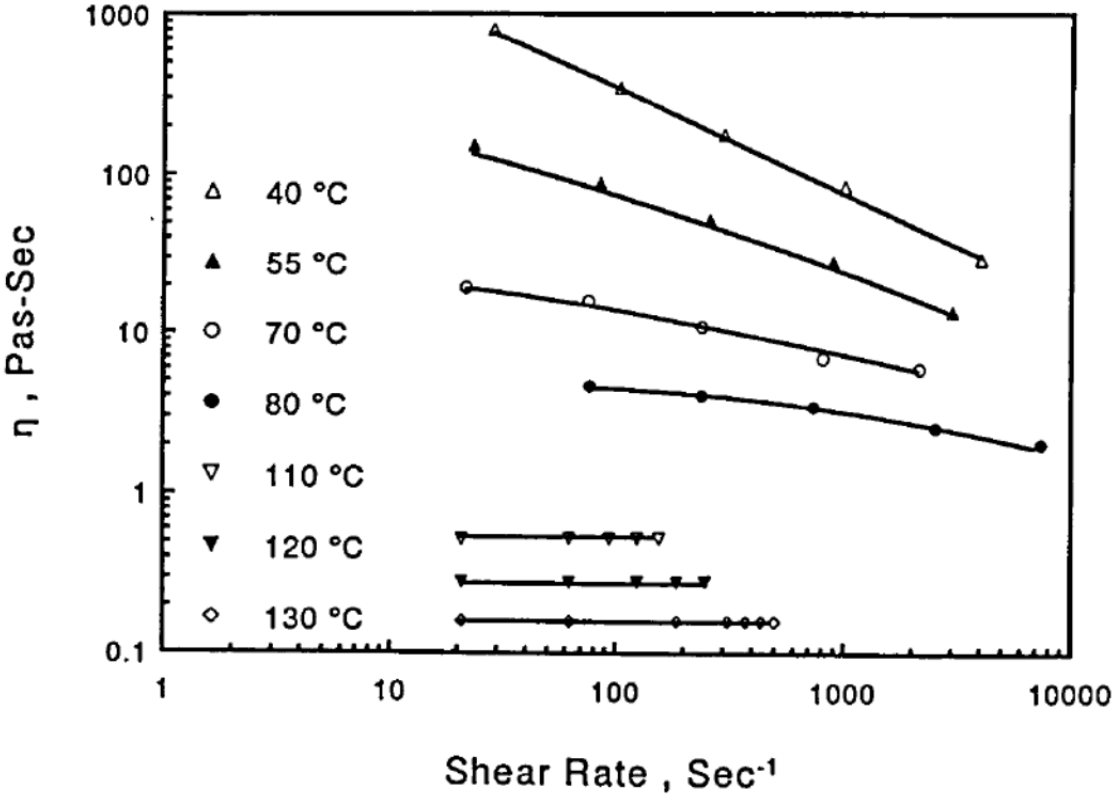

Kuva 6. Viskositeetti kuiva-ainepitoisuudella 75.4 % [5].

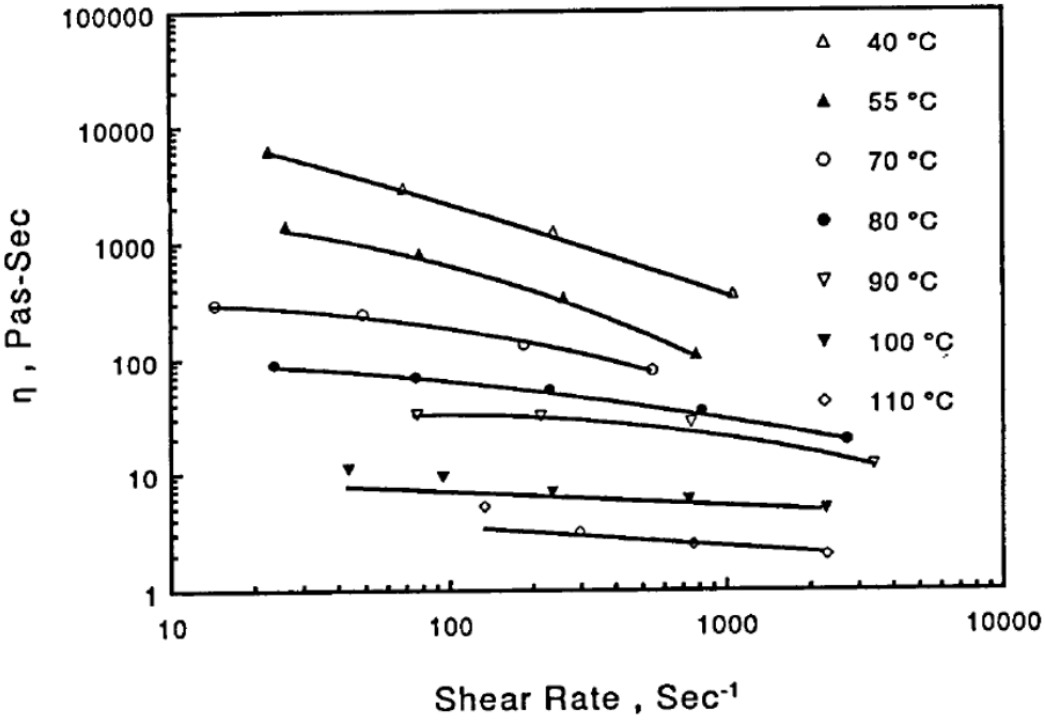

Kuva 7. Viskositeetti kuiva-ainepitoisuudella 84.1 % [5].

1.4 Mustalipeiden ei-Newtonilaisuutta kuvaavia yhtälöitä

Pseudoplastisten nesteiden leikkausjännitystä kuvataan yksinkertaisimmillaan yhtälöllä

$$\tau = K\dot{\gamma}^n \tag{3}$$

jossa K on vakio, $\dot{\gamma}$ on leikkausnopeus ja n on vakio, jonka arvo on alle yhden.

Zaman ja Fricke [5] ehdottivat nollaleikkausnopeuden viskositeetin yhtälömuodoksi korkeilla kuiva-aineilla

$$\mu_0 = A\exp\left(\frac{BT_0}{T - T_0}\right) \tag{4}$$

jossa μ_0 on nollaleikkausnopeuden viskositeetti, T absoluuttinen lämpötila, T_0 on lämpötila, jossa vapaatilavuus on nolla, A on vakio ja B on vakio suhteessa molekyyliketjujen pyörimiseen.

Zaman ja Fricke [5] määrittivät lasittumislämpötilan (T_g) muutamille lipeätyypeille DSC:llä (Differential Scanning Calorimetry). Lasittumislämpötilaa he käyttivät lipeän viskositeetin laskemiseen. Menetelmä on monimutkainen ja tulokset eivät ole yleistettävissä kaikille lipeille ilman kokeellisia mittauksia. Suomalaisille mustalipeille lasittumislämpötilanmittausta ei ole tehty.

Huomionarvoista on, että Zaman ja Fricke [5,13] eivät mitanneet viskositeetteja pienillä alle 100 1/s leikkausnopeuksilla korkeissa lämpötiloissa. Söderhjelm [12] mittasi korkeilla kuiva-aineilla 70 1/s asti, mutta ei tätä alemmilla leikkausnopeuksilla. Pisaranmuodostuksen kannalta juuri pienet leikkausnopeudet ovat oleellisia. Mahdollisesti siis kannattaa etsiä oma paremmin soveltuva yhtälömuoto, joka perustuu tässä projektissa mitattuihin viskositeetteihin.

Järvinen [14] ehdotti yhtälömuodoksi Cassonin viskositeettimallia

$$\mu = \mu_\infty \left(1 + a\dot{\gamma}^{-0.5}\right)^2 \tag{5}$$

jossa μ_∞ on viskositeetti suurilla leikkausnopeuksilla lämpötilan ja kuiva-aineen funktiona ja a on vakio. Malli ei huomioi lämpötilaa tai kuiva-ainetta muuttujaksi, joten sitä voidaan käyttää vain tilanteille, joista on ainakin yksi viskositeettimittaus ko. lämpötilalle. Kuvassa 8 on esitetty leikkausnopeuden ja näennäisen viskositeetin riippuvuus eräälle mustalipeälle.

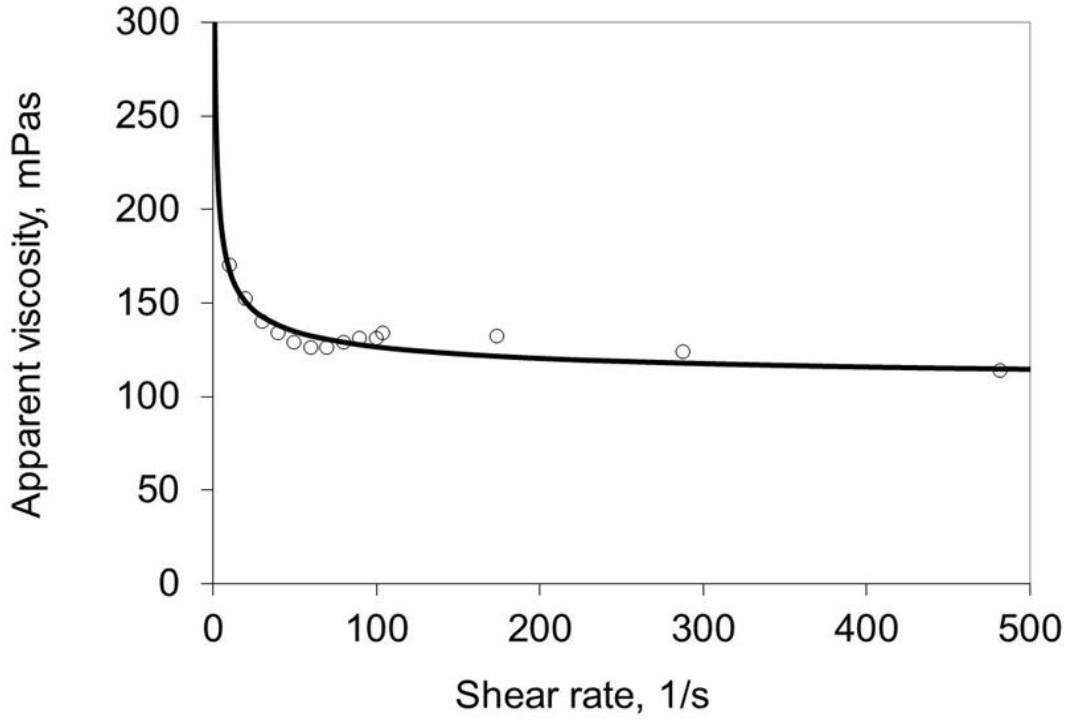

Kuva 8. Cassonin mallin mukainen mustalipeän viskositeetti ja vastaava mitattu data (mustalipeän ka = 71 % ja T= 140 °C)

Adamsin [15] ehdottama yhtälömuoto on

$$\log_{10}(\mu_\infty / \mu_w) = \frac{y_s / T}{b - c y_s / T} \tag{6}$$

jossa μ_w on veden viskositeetti ja T on absoluuttinen lämpötila. b ja c ovat kokeellisia vakioita.

Mustalipeiden viskoelastisuutta ovat tutkineet Zaman ja Fricke [13]. Viskoelastisuus kuvaa materiaalin kykyä palautua aiempaan muotoonsa. Mustalipeät olivat viskoelastisia alhaisissa, alle 85°C, lämpötiloissa. Korkeammissa lämpötiloissa viskoelastisuutta ei esiintynyt, vaikka kuiva-ainepitoisuus oli korkea. Pisaranmuodostuksen viimeisissä vaiheissa viskoelastisuuden merkitys olisi joka tapauksessa vähäinen, koska nopeasti palautuvia tapahtumia ei esiinny. Lusikalla ja suuttimen ulostuloaukossa nopeiden pakotettujen suunnanmuutosten yhteydessä viskoelastisuudella voisi olla merkitystä, jos ruiskutettavan mustalipeän lämpötila olisi epänormaalin alhainen.

2 KOKEET

2.1 Näytteenotto

Normaalisti mustalipeänäyte otetaan tehtailla siten, että kiehuvasta lipeästä karkaa höyryä näytteenoton yhteydessä. Riippuen mm. tehtaan näytteenottojärjestelmästä, lipeästä, ruiskutuslämpötilasta, kuiva-ainepitoisuudesta voi karanneen höyryn määrä vaikuttaa mitattuun kuiva-ainepitoisuuteen. Tämän tutkimuksen yhteydessä näyte otettiin paineistettavalla näytteenottimella, jossa höyryä ei päässyt karkaamaan ja vertailunäyte normaalilla menettelyllä. Eukalyptuslipeälle näyte on otettu pelkästään normaalilla menetelmällä. Kuvassa 9 on esitetty paineistettava näytteenotin.

Kuva 9. Paineistettava näytteenotin.

2.2 Viskositeetinmittausmenetelmä

Tutkittiin 4 erilaisen lipeän viskositeettia Labtiumin Haake RheoStress 6000 with Haake Pressure Cell D100/200 viskometrillä. Kuvassa 10 on esitetty koejärjestely. Lämmitys/kuivatusastiassa (evaporation unit) mustalipeän lämpötila ja kuiva-aine säädetään sopiviksi, jonka jälkeen mustalipeä siirretään paineilman avulla viskometrin mittatilaan. Mittatilan kuorenlämpötila säädetään automaattisesti haluttuun lämpötilaan tietokoneohjelman avulla. Tasaantumisajan jälkeen tietokone ajaa viskositeettimittauksen eri leikkausnopeuksilla ja muodostaa viskositeettikäyrän. Viskositeetti perustuu aina viskositeettikäyrään, jolloin yksittäisten mittapisteiden aiheuttama virhe voidaan karsia manuaalisesti hylkäämällä ko. piste.

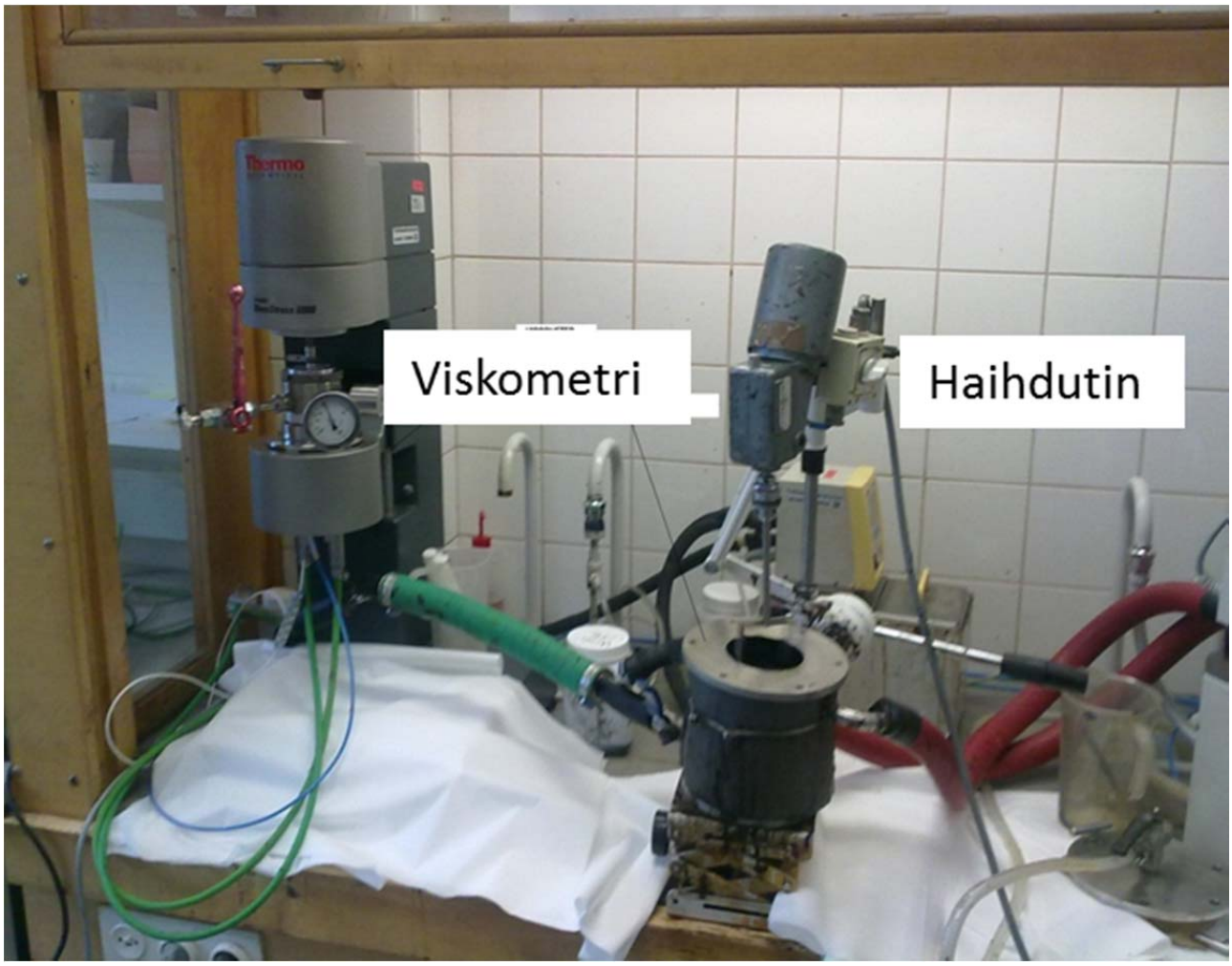

Kuva 10. Viskometri ja lämmitys/haihdutusastia.

2.3 Koelipeät

Taulukko 1. Koelipeät

Lipeälaatu	Ruiskutus		Kuiva-aine pitoisuus			Kiehumispisteen	
	lämpötila	Tehdas	Lab. normaali	Lab. paineistettu	Teoreettinen	nousu	
	°C	%	%	%	%		°C
Havupuu	134.6	75.7	73.7	73.1	74.5		18.3
Lehtipuu	126	70	73.1	71.2	72.1		15
Seka	144	81.8	81.8	82.7	82.7		28
Eukalyptus	-	-	77.8	-			16

Taulukossa 1 on esitetty neljä kuiva-ainepitoisuutta. Ensimmäinen on tehdasinstrumentoinnin antama, toinen perinteisellä näytteenottomenetelmällä otettu mustalipeänäyte ja kolmas on paineistetulla menetelmällä otettu näyte. Neljäs on teoreettinen tapaus, jossa kaikki höyry on karannut näytteestä. Paineistettu näytteenotin alensi kuiva-ainepitoisuutta 0.6 % ja 1.9 % havu- ja lehtipuulipeillä. Sekalipeällä kuiva-ainepitoisuus näytti kohonneen 0.9 %, joka on yllättävä tulos. Eukalyptuslipeälle ei saatu paineistettua näytettä.

Kuiva-aine on määritetty laboratoriossa menetelmän SCAN-N 22:77 mukaisesti (ns. hiekkamenetelmä). Menetelmän mittausepävarmuus vahvoille mustalipeille on ± 1 %. On kuitenkin

huomattava, että yleisesti käytössä olevalla mustalipeän kuiva-ainemenetelmällä (SCAN-N 22) saadaan liian suuria tuloksia, koska sulfidi hapettuu pääasiassa tiosulfaatiksi näytettä kuivattaessa. Ero on riippuvainen sekä näytteen sulfidipitoisuudesta että kuiva-aineesta, kuten kuvassa 11 on esitetty.

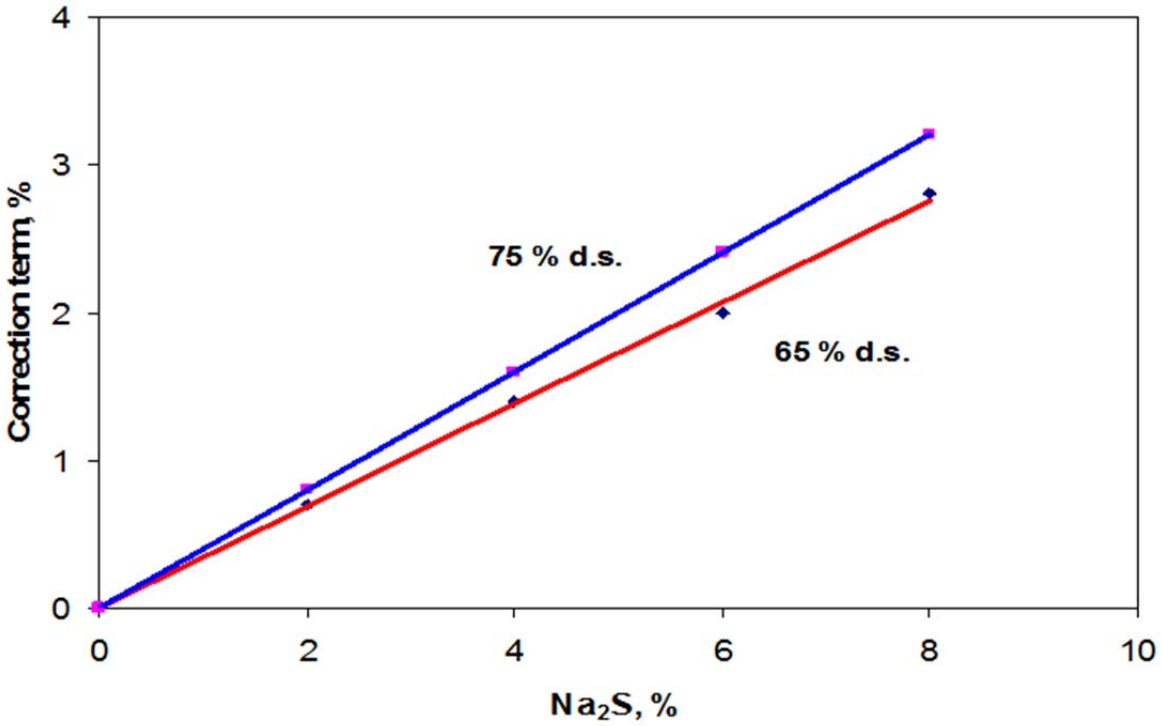

Kuva 11. Teoreettisesti lasketut, sulfidin hapettumisesta johtuvat virheet kuiva-aineen sulfidipitoisuuden funktiona kuiva-ainepitoisuuksilla 65 % ja 75 %.

Taulukossa 2. on laskettu kaikille SCAN-N 22:27 mukaan määritetyille kuiva-aineille myös sulfidikorjatut kuiva-ainepitoisuudet. Eli korjauksissa on oletettu, että kaikki näytteen sisältämä sulfidi on hapettunut kuiva-ainemäärityksessä tiosulfaatiksi. Tämä hapettunut osuus on vähennetty mitatusta arvosta ja saatu sulfidikorjattu kuiva-aine.

Taulukko 2. Sulfidikorjatut kuiva-aineet

Lipeälaatu	Lab. normaali %	Lab. normaali sulfidikorjattu, %	Lab. paineistettu %	Lab. paineistettu sulfidikorjattu, %
Havupuu	73,7	71,0	73,1	70,4
Lehtipuu	73,1	71,4	71,2	69,5
Seka	81,8	79,8	82,7	80,7
Eukalyptus	77,8	75,9	-	

2.4 Viskositeetit leikkausnopeuden muuttuessa

Viskositeetin leikkausnopeuden riippuvuus kolmella kuiva-ainepitoisuudella on esitetty kuvissa 12–14. Kuiva-ainepitoisuudet on redusoitu samaan kuiva-aineeseen mittausdatasta (Liitteet 1-4) vertailun mahdollistamiseksi. Eri tehtaiden tai puulajien viskositeettien vertailu keskenään on vaikeaa koska haihduttamolla käytössä oleva lipeän lämpökäsittely (lämpötila/kesto) vaikuttaa lipeän ominaisuuksiin kuten viskositeettiin. Havaitaan, että kaikissa tapauksissa pienillä leikkausnopeuksilla mustalipeä on ei-Newtonilaista. Lehtipuun ja eukalyptuksen viskositeetit

muuttuvat eniten pienillä leikkausnopeuksilla, kun kuiva-ainepitoisuus on 75 %. Korkeimmalla kuiva-ainepitoisuudella 85 % muuttuu lehtipuun viskositeetti moninkertaiseksi pienillä leikkausnopeuksilla, kun taas eukalyptuksen viskositeetti kohoaa vain vähän. Havupuulla muutos on pienin, alle 100 %, mutta kuitenkin merkittävä. Yhtenä selittävänä tekijänä voi olla näytteen polysakkaridipitoisuus, joka havu- ja sekalipeillä on alle 2 %, eukalyptuslipeällä 2.6 % ja koivulla 4 %. Näytteiden alkuperäinen mittausdata on esitetty liitteissä 1-5.

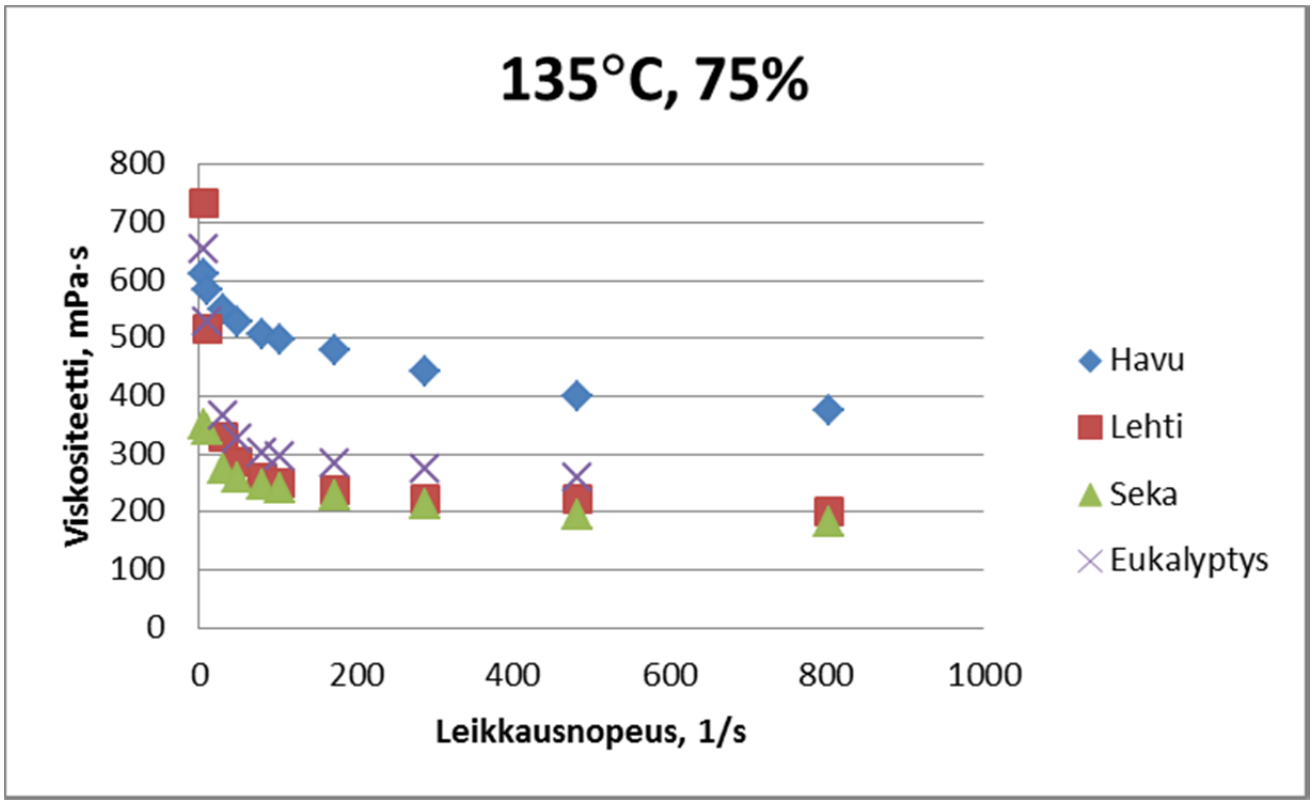

Kuva 12. Viskositeetin leikkausnopeusriippuvuus 75 % kuiva-ainepitoisuudella.

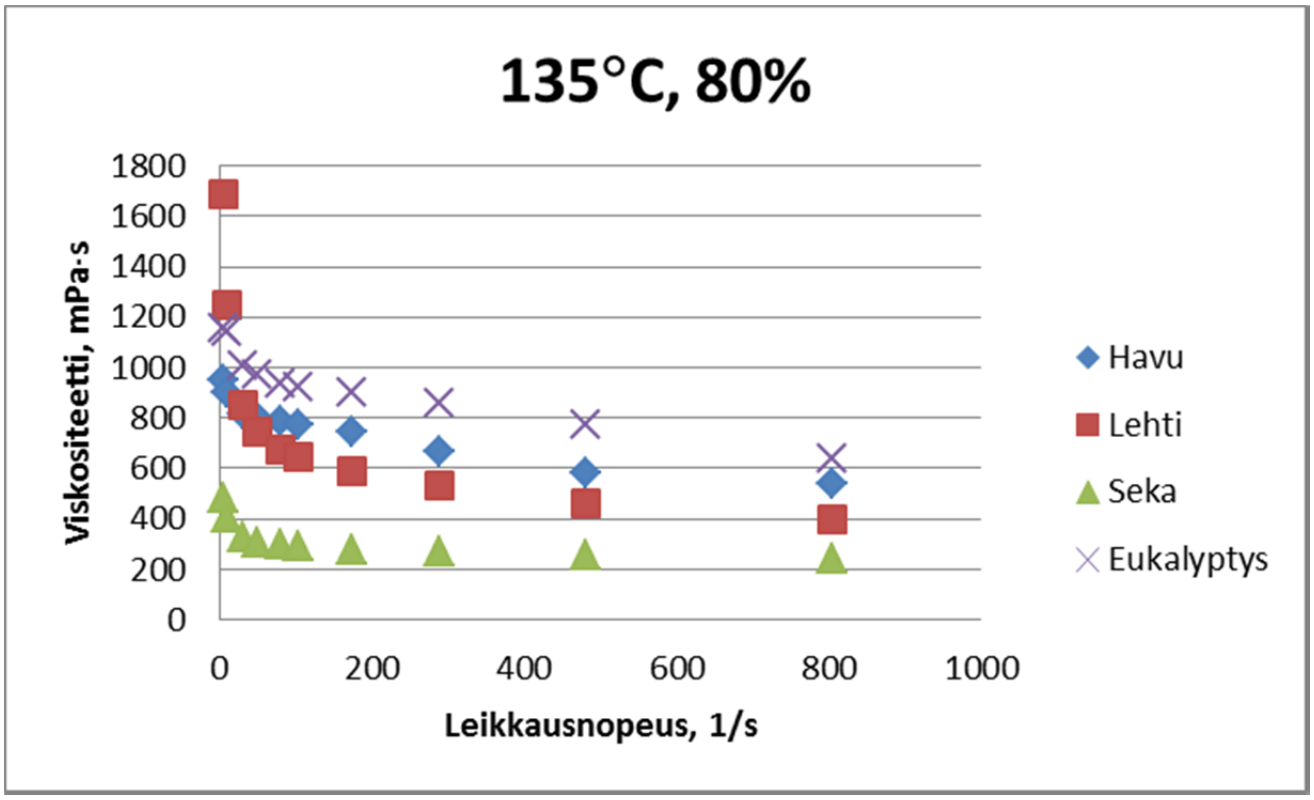

Kuva 13. Viskositeetin leikkausnopeusriippuvuus 80 % kuiva-ainepitoisuudella.

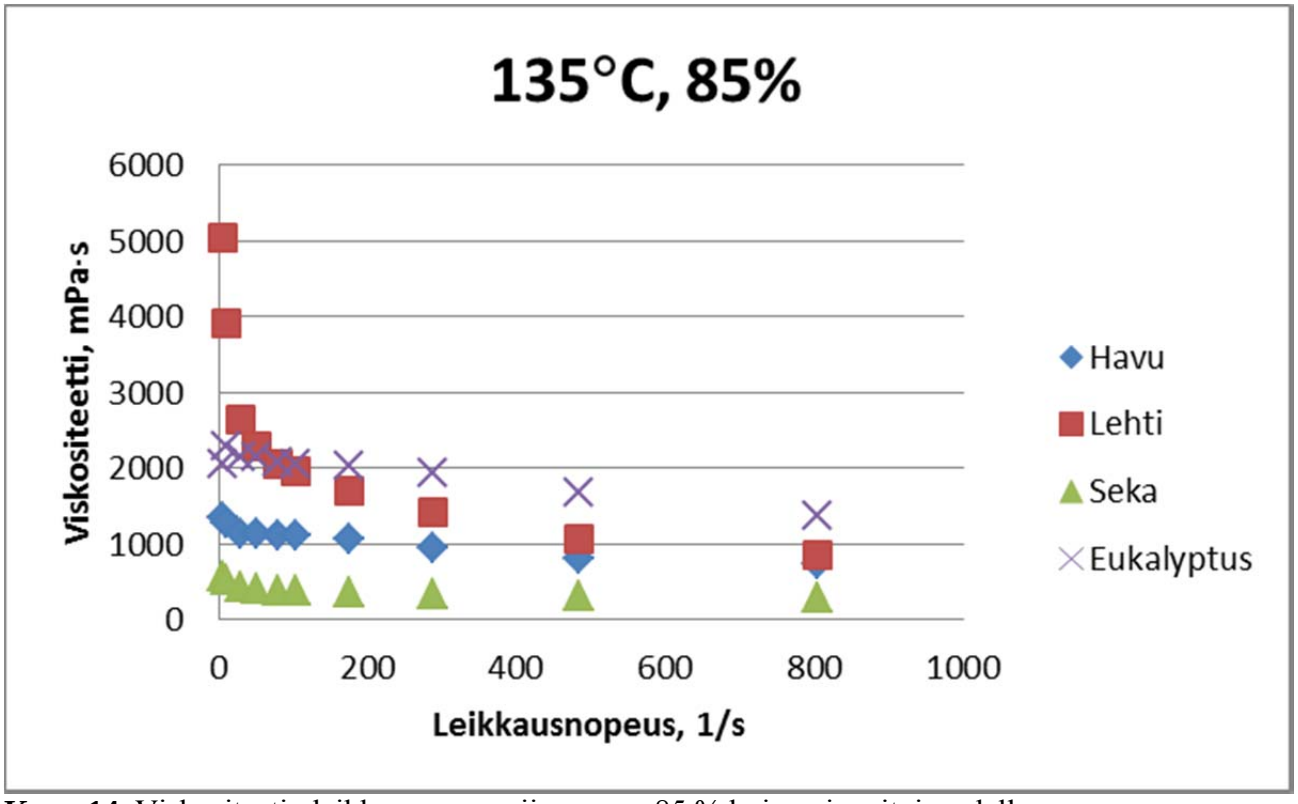

Kuva 14. Viskositeetin leikkausnopeusriippuvuus 85 % kuiva-ainepitoisuudella.

Viskositeetin leikkausnopeusriippuvuutta eri lämpötiloissa on tutkittu kuvasarjassa 15–17. Lehtipuun viskositeetti muuttuu eniten, 4-6 kertaiseksi, alhaisilla leikkausnopeuksilla ja myös eukalytuksen viskositeetti kasvaa paljon leikkausnopeuden pienentyessä. Havupuun viskositeetti kohoaa vähiten, mutta kuitenkin yli 50 %, leikkausnopeuden pienentyessä arvoon 5 1/s.

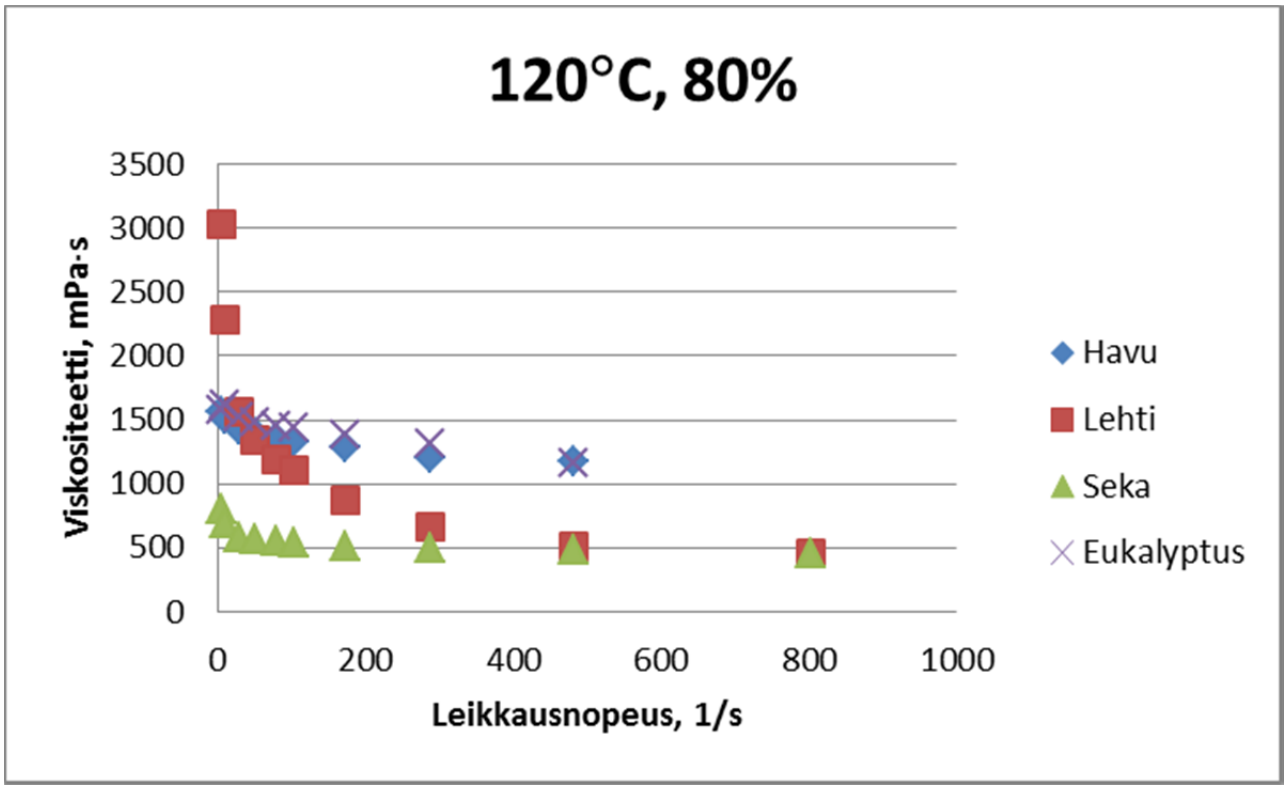

Kuva 15. Viskositeetin leikkausnopeusriippuvuus 120 °C:een lämpötilassa.

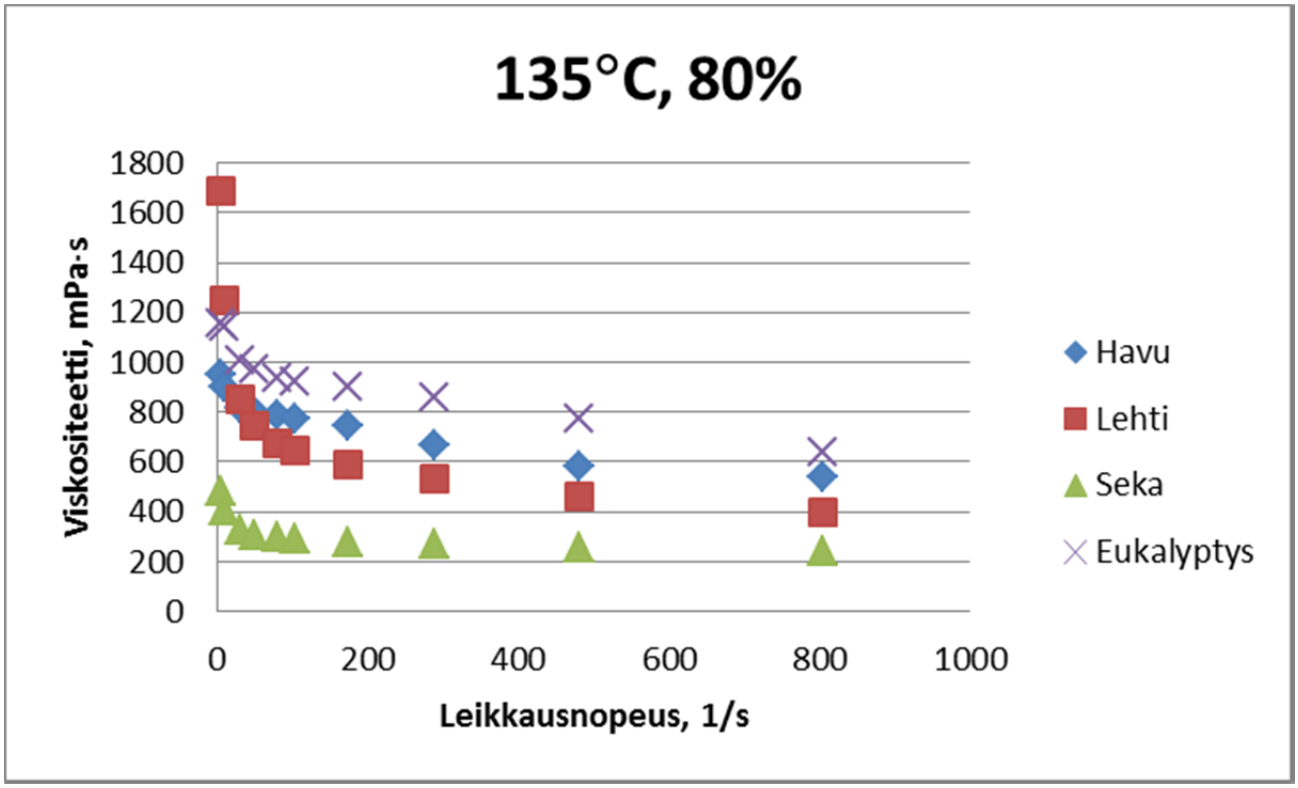

Kuva 16. Viskositeetin leikkausnopeusriippuvuus 135 °C:een lämpötilassa.

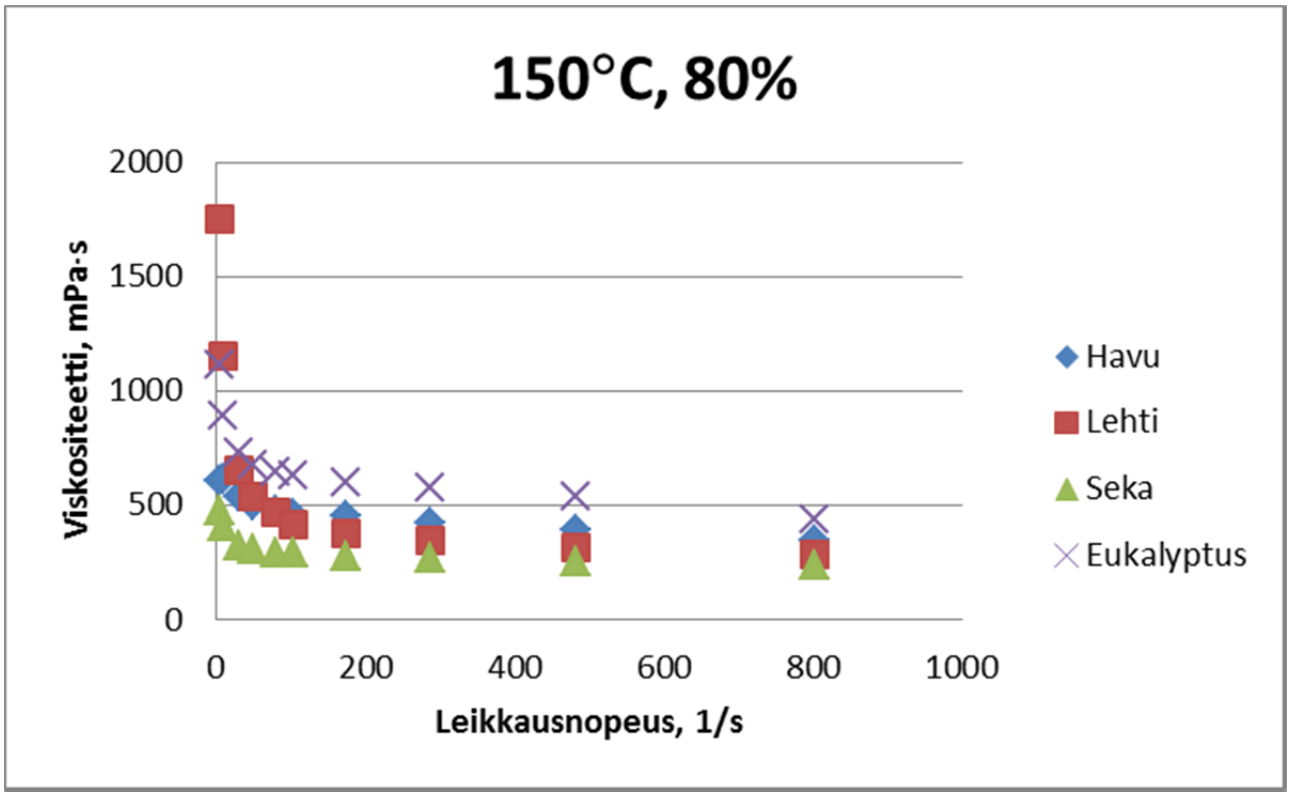

Kuva 17. Viskositeetin leikkausnopeusriippuvuus 150 °C:een lämpötilassa.

Merkillepantavaa on, että kaikilla lipeillä viskositeetti kohosi leikkausnopeuden pienentyessä, joskin alin mitattu leikkausnopeus oli vain 5 1/s. Yhtälössä (5) ei oleteta nollaleikkausnopeudelle äärellistä viskositeettia, päinvastoin kuin Zaman ja Fricke [5] olettivat polymeereihin perustuvien yhtälöidensä perusteella. Oikeaa yhtälömuotoa ei voi tietää ennen mittauksia nyt toteutettua pienemmillä leikkausnopeuksilla.

Viskositeettiin merkittävästi vaikuttavat polysakkaridipitoisuudet on esitetty liitteessä 5. Korkein polysakkaridipitoisuus on lehtipuulipeällä. Lehtipuu on myös ei-Newtonilaisin yhdessä eukalyptuksen kanssa. Havu- ja sekalipeän polysakkaridipitoisuudet olivat alhaiset.

Jäännösalkalipitoisuus lehtipuulipeällä oli 3.2 %. Havu- ja sekalipeän jäännösalkalipitoisuudet olivat 4.6 % ja 4.3 %.

2.5 Viskositeettimittauksen kalibrointi

Haake RheoStress 6000 with Haake Pressure Cell D100/200 kalibroitiin käyttäen kalibrointiöljyä ISO 170251 / ISO Guide 34 VISCOSITY AND DENSITY REFERENCE STANDARD N4000. Liitteessä 6 on esitetty kalibrointiöljyn kuvaus tarkemmin. Taulukossa 2 on esitetty kalibroinnin tulos. Kuvassa 18 on esitetty referenssinesteen viskositeetti ja mitatut viskositeetit leikkausnopeuksilla 100 1/s ja 288 1/s. Silmämääräisesti arvioiden mittaustulos seuraa kohtuullisen hyvin referenssinesteen viskositeettia eri lämpötiloissa. Kuvissa 19 ja 20 on esitetty virheen prosentuaalinen suuruus. Virheen suuruus on jokseenkin lineaarisesti riippuvainen lämpötilasta. Koska virhe on merkittävä korkealla ja matalalla viskositeettiarvolla, ei yritetä etsiä vakioita lipeiden ei-Newtonilaisuuden yhtälöissä 3-6. Labtium on ryhtynyt selvittämään viskometrin valmistajan kanssa syytä lämpötilariippuvaan virheeseen.

Taulukko 2. Viskositeetti lämpötilan muuttuessa. Punaisella merkitty mustalipeille tyypillinen mittausalue

Lämpötila, °C	Sertifioitu arvo mPas	Mitattu arvo, 100 1/s mPas	Mitattu arvo, 288 1/s mPas	Ero 100 1/s mPas	Ero 288 1/s mPas	Ero 100 1/s %	Ero 288 1/s %
40	2921	2195	2080	-726	-841	-24.9	-28.8
50	1423	1245	1218	-178	-205	-12.5	-14.4
60	744.7	810	802	65.3	57.3	8.8	7.7
80	247.6	290	288	42.4	40.4	17.1	16.3
100	102.1	165	158	62.9	55.9	61.6	54.8

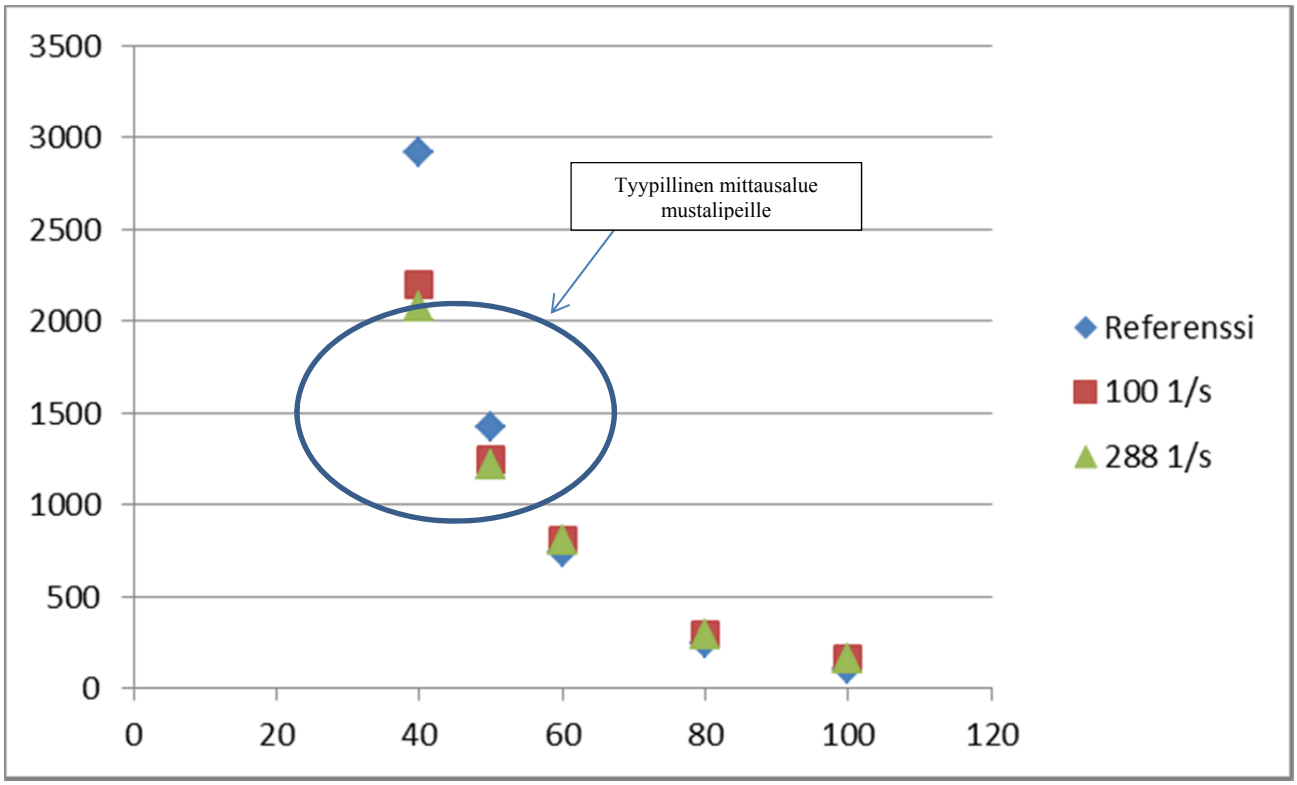

Kuva 18. Referenssinesteen ilmoitettu viskositeetti ja kahdella leikkausnopeudella mitattu viskositeetti lämpötilan funktiona.

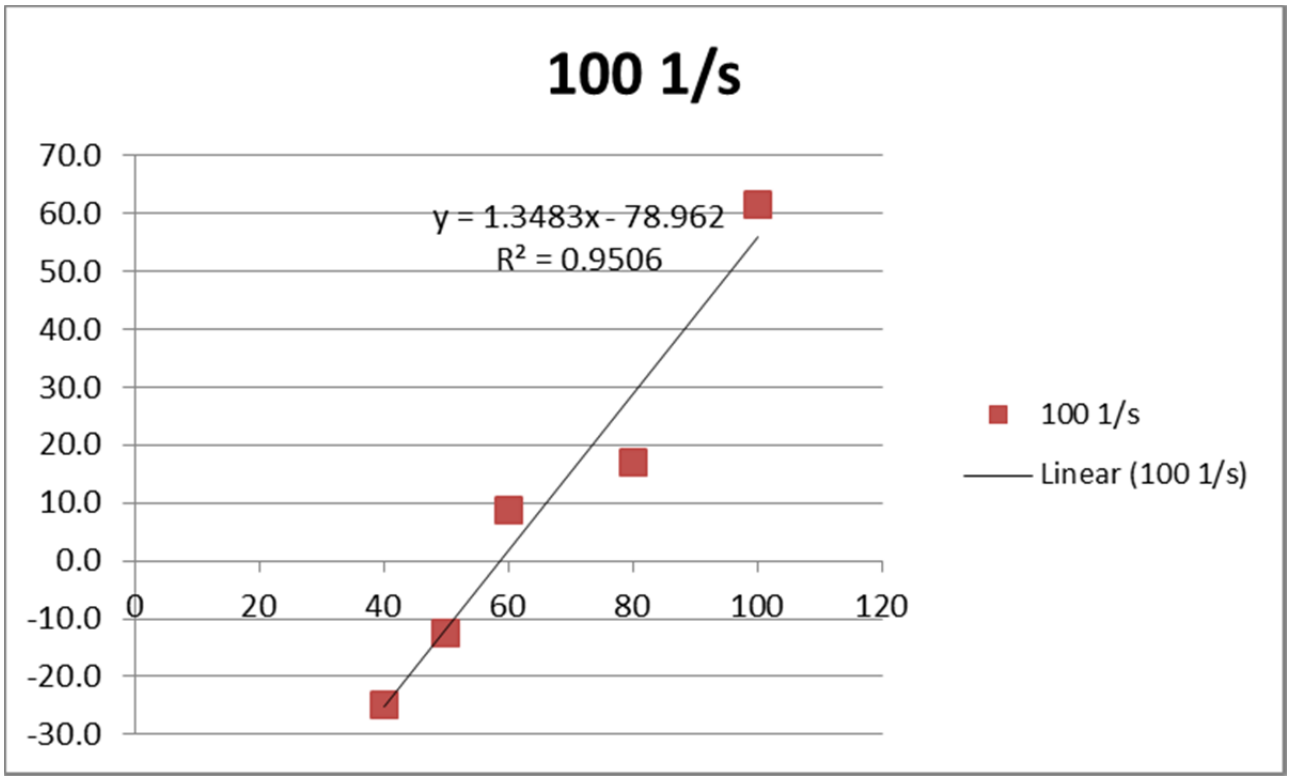

Kuva 19. Virhe % leikkausnopeudella 100 1/s.

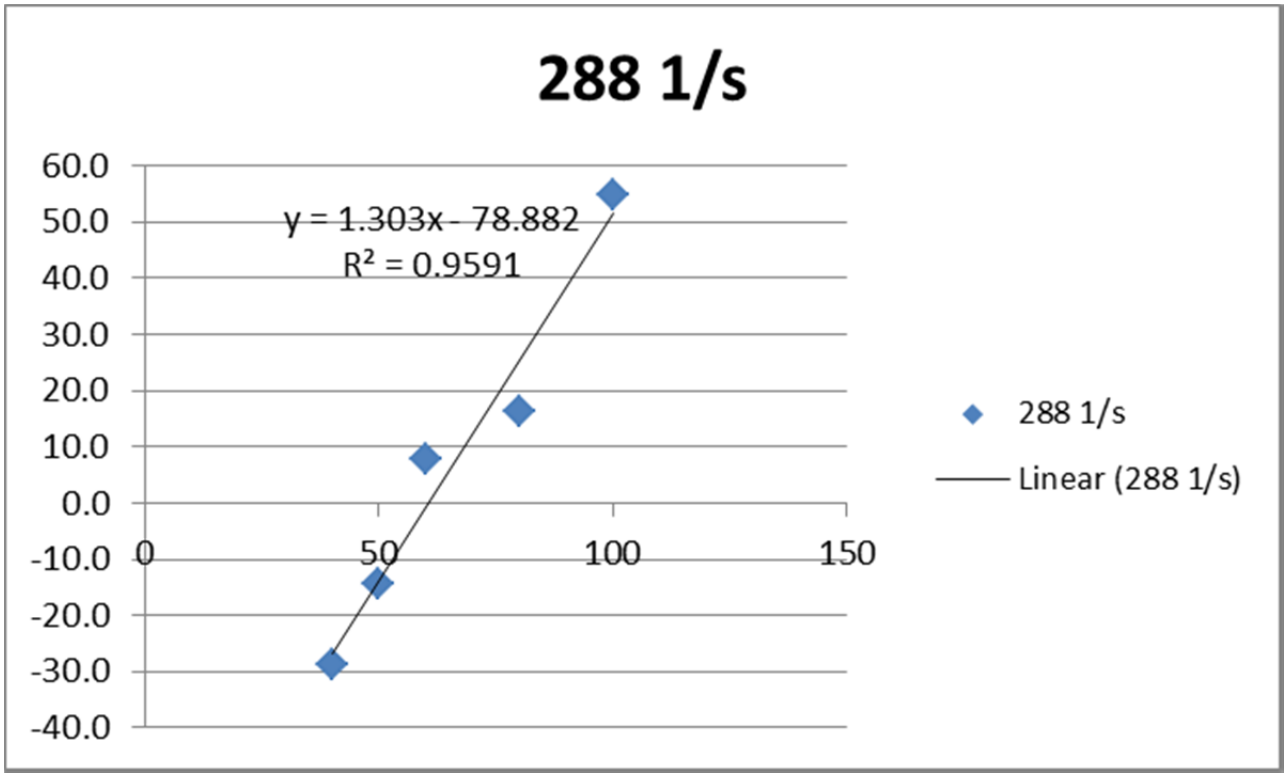

Kuva 20. Virhe % leikkausnopeudella 288 1/s.

2.6 Kapillaariviskometri

Viskositeetti mitattiin yksinkertaisella kapillaariviskometrillä soodakattilalla. Laitteisto on esitetty kuvassa 21. Mustalipeä otetaan lipeärenkaalta ja johdetaan pienen massavirtamittarin läpi kapillaariviskometriin ja siitä edelleen taustalla näkyvään ruiskutuskammioon.

Kuvassa 22 on kuvattu laitteiston periaate. Venttiilien 1 ja 2 avulla säädetään virtausta siten, ettei lipeä pääse kiehumaan. Kaksoisvaippaputkella ja ulommassa putkessa virtaavalla lämmitetyllä termoöljyllä pidetään lipeän lämpötila vakiona. Lämpötila laski 2-3 °C matkalla lipeärenkaalta koelaitteistolle. Paine-eroanturilla mitattiin mustalipeän paineen muutos koelaitteistossa, jolloin näennäinen viskositeetti voidaan laskea. Kuvassa 23 on esitetty kapillaariviskometrilla mitattu näennäinen viskositeetti leikkausnopeuden muuttuessa ja vastaava tilanne redusoituna HaakeRheometer viskometrin mittaustuloksista. HaakeRheometrin antama viskositeetti on yli kolminkertainen verrattuna kapillaarimittarin tulokseen. Kapillaariviskometrilla ei päästä pieniin leikkausnopeuksiin, alle 200 1/s.

Kuva 21. Koelaitteisto soodakattilalla.

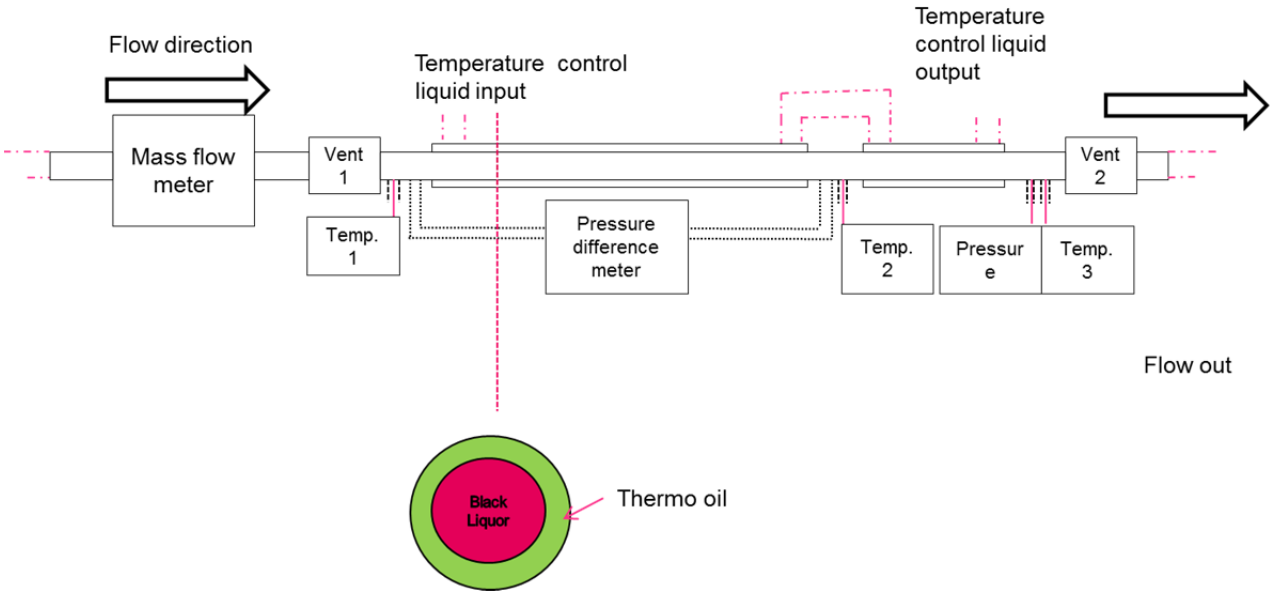

Kuva 22. Kapillaariviskometrin periaatekaavio.

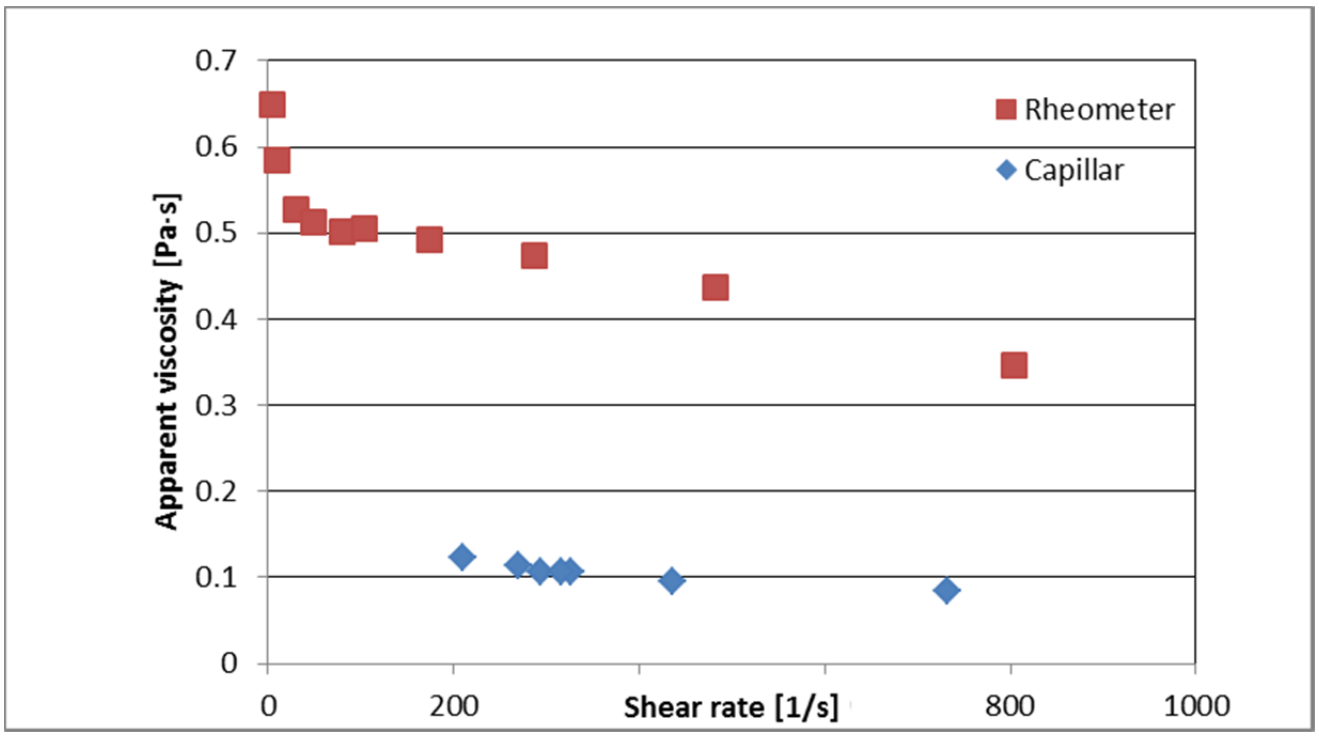

Kuva 23. Näennäinen viskositeetti eri leikkausnopeuksilla mitattuna HaakeRheometrilla ja kapillaariputkella. Havulipeä 73.1 % ja 129 ºC.

2.7 Kapillaariviskometrin kalibrointi

Kapillaariviskometri kalibroitiin standardiöljyn ISO 17025 avulla. Liitteessä 7 on esitetty kalibrointiöljyn tiedot tarkemmin. Tarkkuudeksi laboratoriossa saatiin 15 %. Tehtaalla laitetta ei kalibroitu ja mittaukset olivat merkittävästi epätarkempia. Sopivilla massavirroilla laite soveltuu tehdasmittauksiin, mutta laitteen käyttäminen on työlästä ja huolellisuutta vaativaa. Kuvassa 24 on esitetty laboratoriossa suoritetun kalibrointimittauksen tulos eri leikkausnopeuksilla. Kalibrointimittaus on esitetty tarkemmin Jukka Koskenrannan erikoistyössä [16].

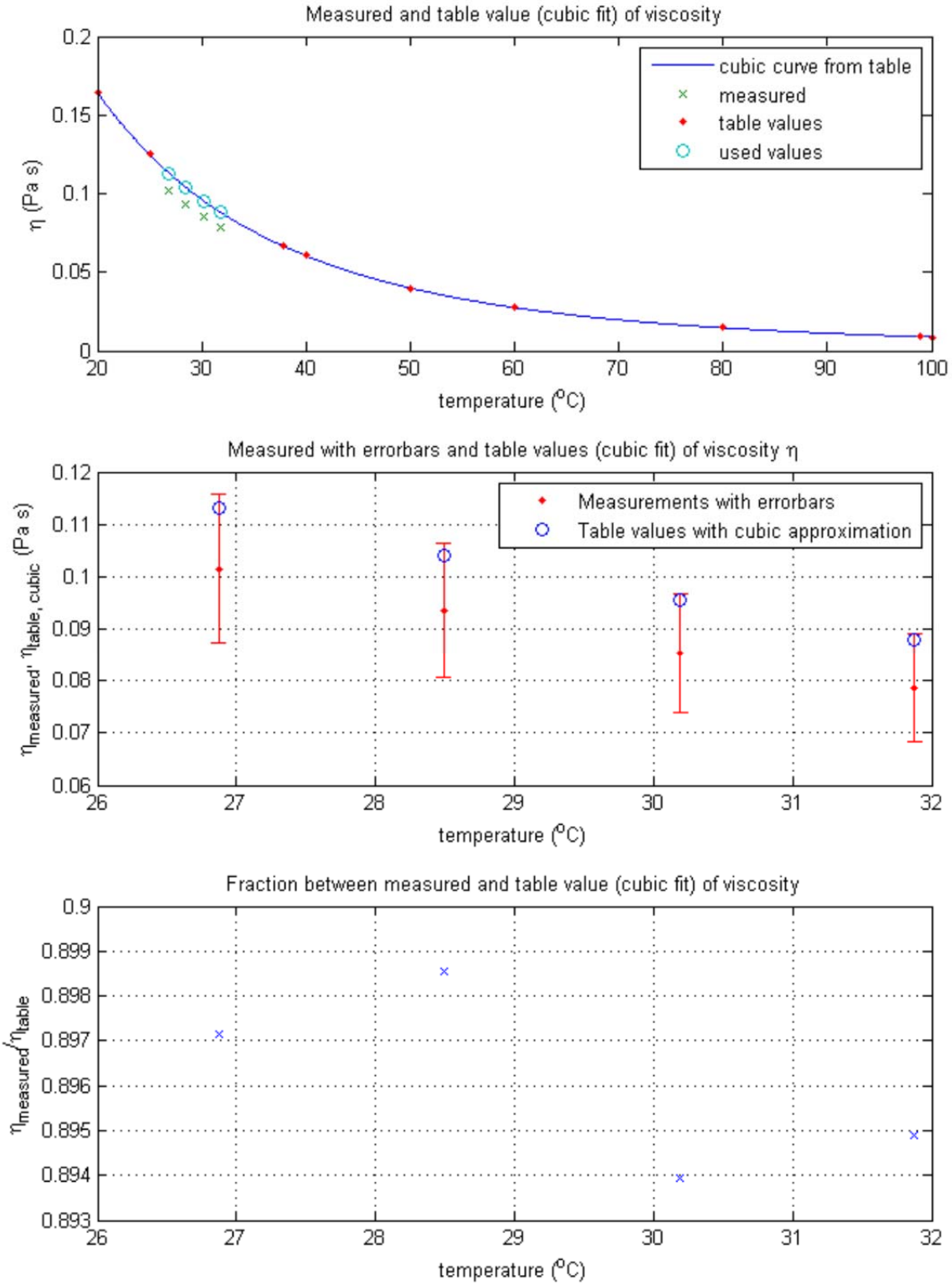

Kuva 24. Kapillaariviskometrin kalibrointimittaus laboratoriossa.

3 MUSTALIPEÄN KÄSITTELYN VAIHEET

3.1 Haihduttamo

Jos tarkastellaan mustalipeän elinkaarta tehtaalla haihduttamolta lähtien, viskositeetin vaikutus on suurin haihduttamon väkevässä päässä ja vaikuttaa olennaisesti valuvan nestekalvon käyttäytymiseen sekä lämmön- ja aineensiirron osalta että likaantumisen kannalta. Leikkausnopeudet ovat pieniä, joten mustalipeän ei-Newtonilaisuus voi haihduttamon viimeisissä yksiköissä olla merkitsevää.

3.2 Pumput

Viskositeetti vaikuttaa myös pumppujen ja sekoittimien vaatimaan tehoon sekä virtaukseen putkistoissa. Pumpuissa leikkausnopeudet ovat suuria eikä ei-Newtonilaisuus siten ole oleellista pumpun toiminalle.

3.3 Putkistot

Putkistot on mitoitettu suuriksi, jota painehäviö olisi alhainen. Esimerkiksi mustalipeää pumpataan soodakattilalle putkissa, joiden sisähalkaisija on 110 mm. Massavirta on esimerkiksi 60 l/s sisältäen takaisinkierrätykseen menevän osuuden. Leikkausnopeudeksi saadaan noin 500 1/s. Näennäinen viskositeetti ei muutu merkittävästi ei-Newtonilaisuuden takia.

3.4 Suutinputki

Putkistoissa ja juuri ennen ruiskua mustalipeän paine on korkeampi kuin sen kiehumispaine, eikä kiehumista siis voi tapahtua. Juuri ennen suuttimen ulostuloa aukkoa (0-20 cm) alkaa kiehuminen paineen laskiessa riittävän alas. Tällöin mustalipeän kuiva-ainepitoisuus kohoaa kiehumista vastaavan kuiva-aine muutoksen verran ja samalla mustalipeän viskositeetti kohoaa hiukan.

Suutinputkessa virtausnopeudet ovat muutamia metrejä sekunnissa ja vastaavat leikkausnopeudet paljon yli 100 1/s. Suutinputkessa ei-Newtonilaisuus ei siis vaikuta merkittävästi.

3.5 Lusikka

Lusikalla ja juuri ennen lusikkaa virtausnopeudet ja leikkausnopeudet ovat suuria verrattuna virtauksen poikkipinta-alaan. Ei-Newtonilaisuus ei ole oleellista näennäisen viskositeetin arvolle.

3.6 Mustalipeäkalvo, rihmat ja pisarat

Kuvassa 25 on esitetty kalvon muodostuminen heti lusikan jälkeen. Kun mustalipeä kalvo on jättänyt lusikan, pienevät leikkausta aiheuttavat voimat. Samalla viskositeetti kohoaa, jos mustalipeä käyttäytyy ei-Newtonilaisesti, kuten mittaukset osoittivat pienille leikkausnopeuksille.

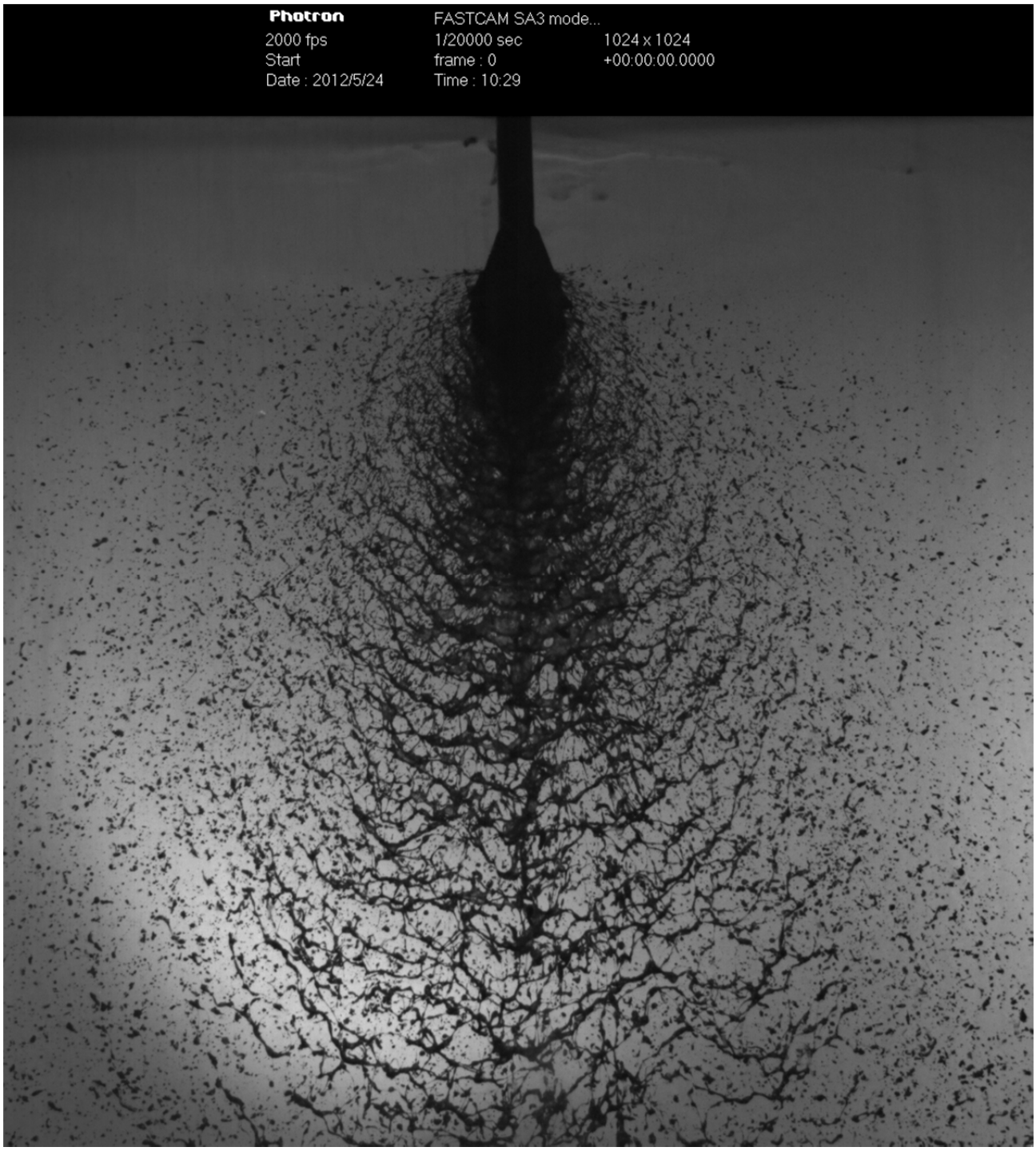

Kuva 25. Mustalipeäkalvo, rihmat ja pisarat heti suuttimen jälkeen koeruiskutuskammiossa kuvattuna.

Viskositeetin kohoaminen jatkuu suuttimen ulkopuolella tulipesässä. Mustalipeän sisältämä paineistettu höyry pullistaa ja rikkoo syntyvää mustalipeäkalvoa ja siitä muodostuvia rihmoja ja pisaroita. Kuiva-aine pitoisuus etenkin kalvon, rihmojen ja pisaroiden pinnalla laskee. Samanaikaisesti leikkausnopeus pienenee, kun leikkausta aiheuttavat voimat pienenevät ja viskositeetti kasvaa. Tässä tilanteessa mustalipeän ei-Newtonilaiset ominaisuudet ovat voimakkaimmillaan ja vaikuttavat pisaroiden kehittymiseen, kuivumiseen ja palamiseen oleellisesti.

4 PISARAN MUODONMUUTOS

4.1 Simulointi OpenFoam-ohjelmalla

Käytettiin ANSYS FLUENT ohjelmaa pisaroitumisen laskentaan, vapaan pinnan laskenta, 3D kuvaus. Kärnän ja Järvisen [17] laskennassa 1 mm, 3 mm ja 8 mm pisarat venytettiin 8:1 sylintereiksi ja päästettiin vapaaksi ja annettiin pintajännityksen vetää ne kokoon. Ei-Newtonilaisen lipeän viskositeetin oletettiin olevan suurella leikkausnopeudella 300 mPa·s ja Newtonilaisen lipeän 300 mPa·s. Kuvasarjassa 26-28 on esitetty tuloksia muodonmuutosnopeudesta.

Ei-Newtonilaisuus hidastaa esimerkkitapauksessa oleellisesti muodonmuutosta. Tämän seurauksena palaminen olisi nopeampaa ja pisaroiden hidastuvuus suurempi kuin Newtonilaisen nesteen samassa tilanteessa. Ei-Newtonilaisen lipeän pisarat päätyisivät siis eri kohtaan keossa ja niiden hiilipitoisuus poikkeaisi Newtonilaisen lipeän hiilipitoisuudesta keon pinnalla.

Laskennassa on huomioitu pelkästään viskositeetin ja pintajännityksen vaikutus muodon muutokseen. Kuvassa 29 on esitetty lisäksi muodonmuutos eri ajanhetkinä 8 mm:n pisaralle. Ei-Newtonilaisen pisaran muodon muutos on noin 20 % hitaampi kuin Newtonilaisen pisaran. Todellisuudessa pisaran lämpötila, kuiva-ainepitoisuus ja muoto muuttuisivat tulipesässä. Etenkin höyryn vapautuminen rihmoista ja pisaroista sekä pintajännityksen väärä arvo voivat vaikuttaa merkittävästi pisaroiden muotoon, lentorataan ja palamiseen. Ilman huolellista simulointia tai kokeellista mittausta, on vaikea sanoa kuinka suuri vaikutus ei-Newtonilaisuudella on soodakattilan toimintaan.

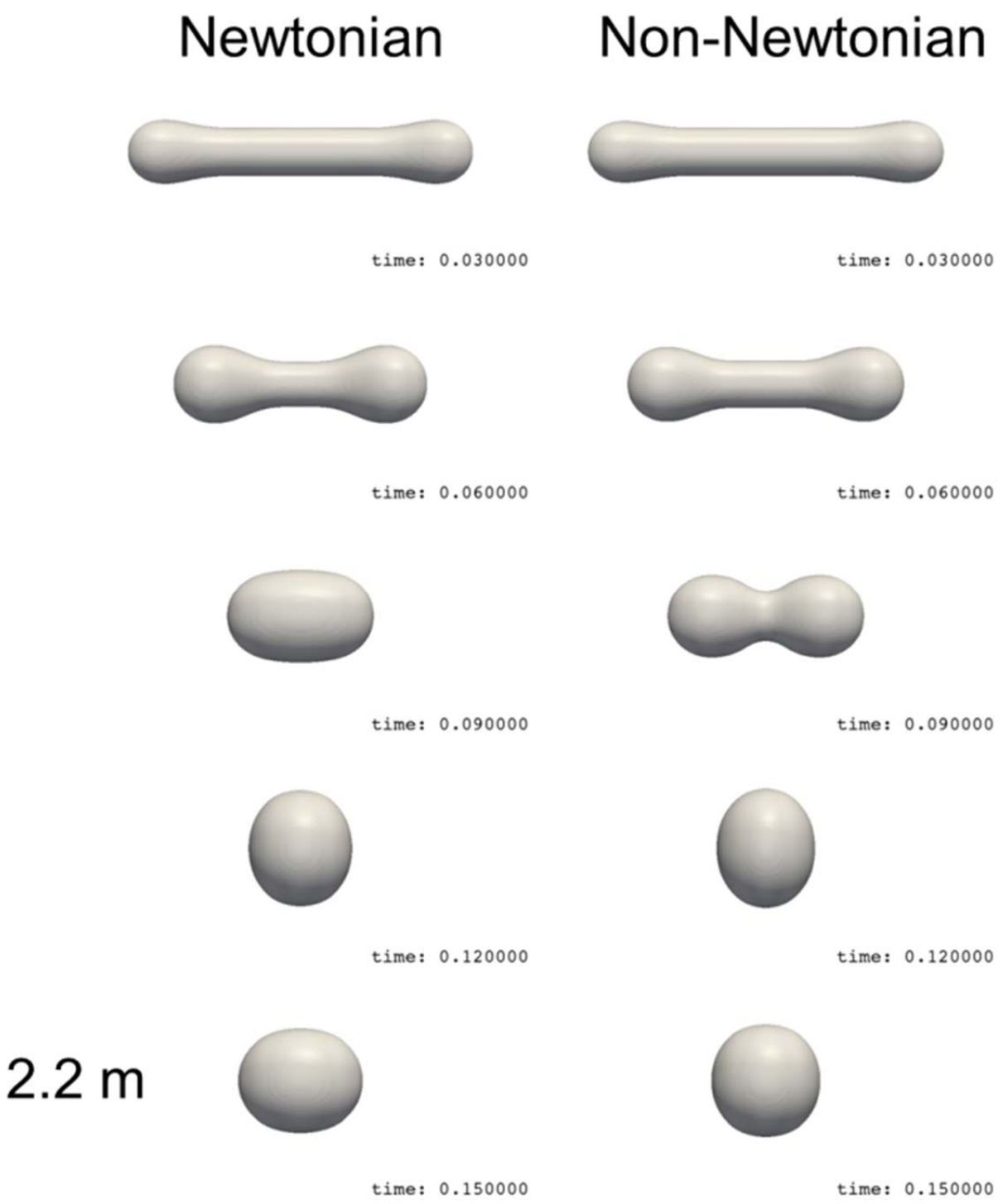

Kuva 26. 1 mm pisarat, 300 mPa·s, 0-0.15 s.

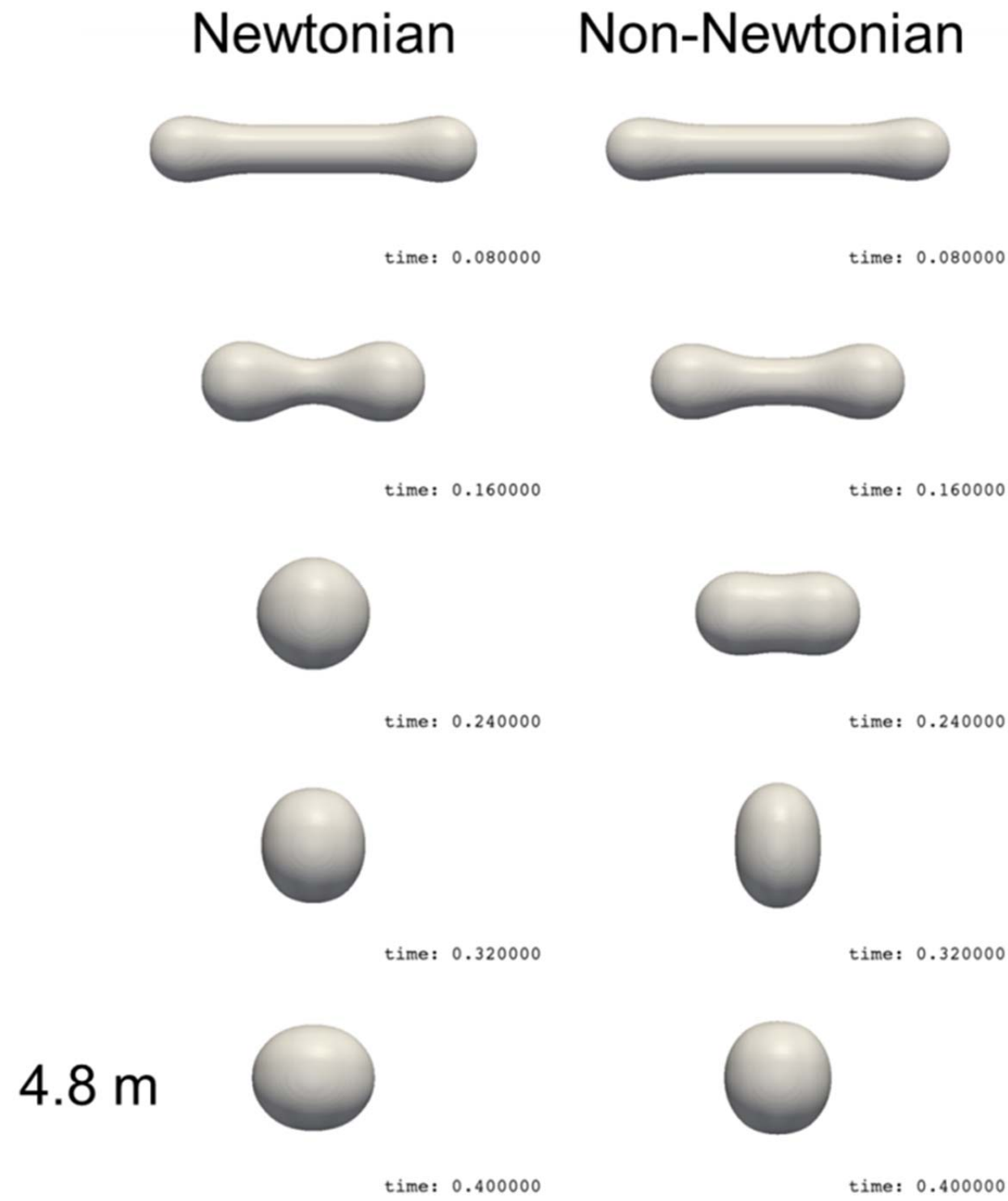

Kuva 27. 3 mm pisarat, 300 mPa·s, 0-0.4 s.

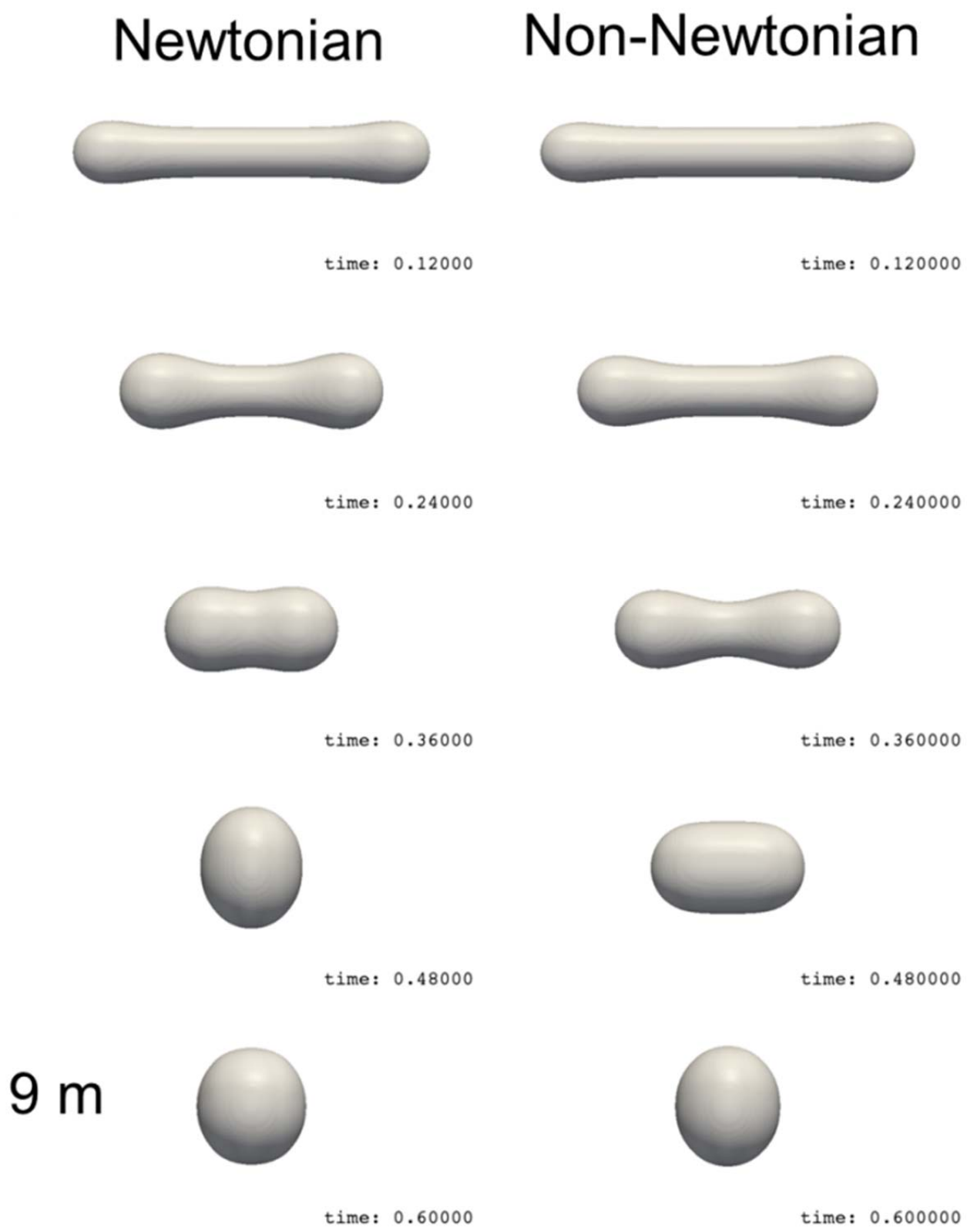

Kuva 28. 8 mm pisarat, 300 mPa·s, 0-0.6 s.

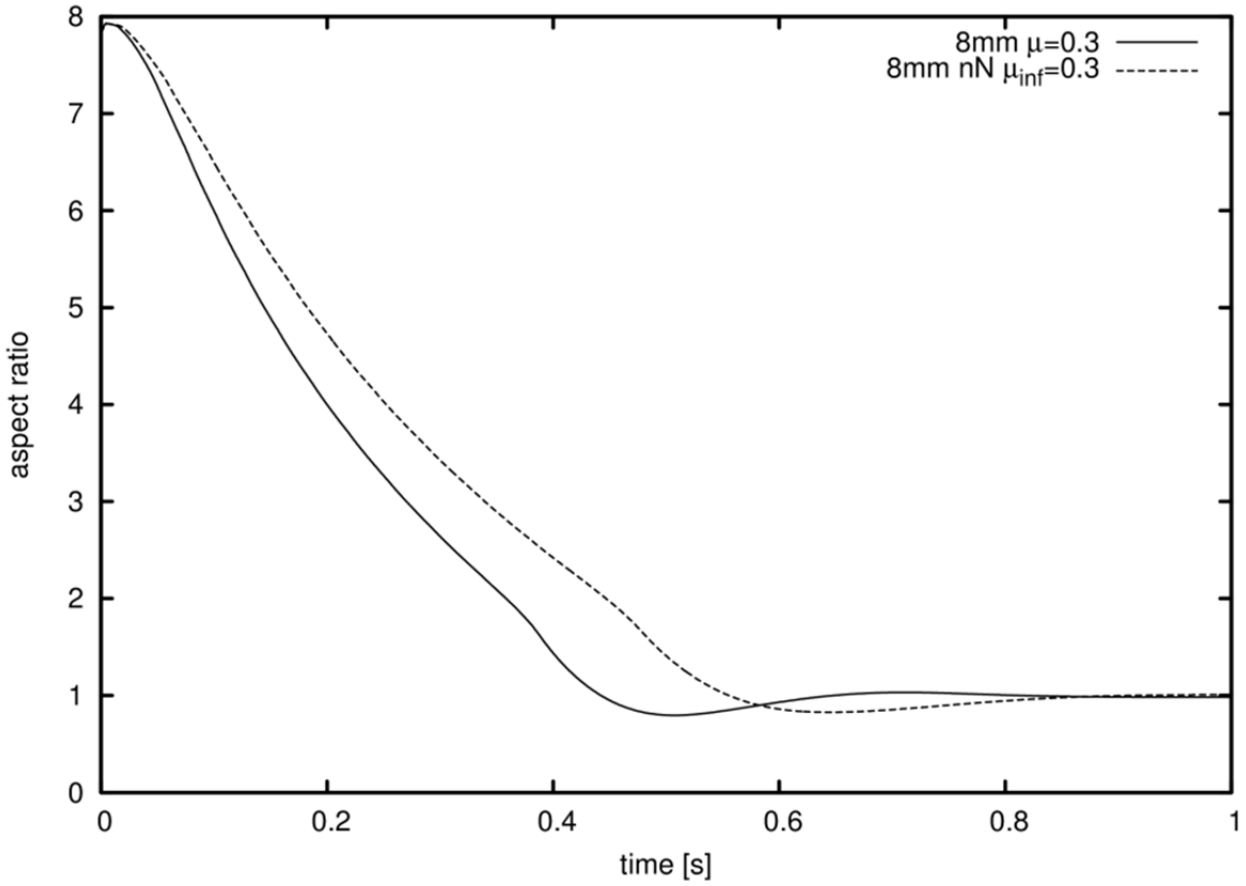

Kuva 29. Newtonilaisen ja ei-Newtonilaisen 8 mm:n pisaran muodonmuutos.

5 JOHTOPÄÄTÖKSET

5.1 Ei-Newtonilainen viskositeetti

Pienillä leikkausnopeuksilla, alle 50 1/s, ovat kaikki tutkitut lipeät ei-Newtonilaisia, pseudoplastisia. Viskositeetti kohoaa ja ei-Newtonilaisuus lisääntyy, kun mustalipeän lämpötilaa alennetaan tai kuiva-ainepitoisuutta kohotetaan. Kirjallisuuden perusteella viskoelastisuus ei ole merkittävää mustalipeälle käytetyissä lämpötiloissa ja kuiva-ainepitoisuuksilla.

5.2 Merkitys soodakattilan toimintaan

Alhaisilla kuiva-ainepitoisuuksilla ei-Newtonilaisuus ei vaikuta haihduttamon toimintaan. Haihdutinsarjan loppupäässä korkeilla kuiva-ainepitoisuuksilla ei-Newtonilaisuus voi vaikuttaa haihdutinyksiköiden toimintaan. Pumpuissa leikkausnopeudet ovat korkeita, joten ei-Newtonilaisuuden merkitys on vähäistä. Putkistoissa ei-Newtonilaisuus voi alentaa hiukan näennäistä viskositeettia. Mustalipeän siirtoputket on takaisinkierrätyksineen mitoitettu niin, että leikkausnopeus on tasaisen viskositeetin alueella eikä viskositeetti siis alene. Myös suutinputkessa ja lusikalla leikkausnopeudet ovat suuria, eikä ei-Newtonilaisuutta tarvitse huomioida.

Lusikan jälkeen tilanne on erilainen. Mustalipeäkalvon ja pisaroiden ympärillä leikkausvoimat ja leikkausnopeudet ovat pieniä ja ei-Newtonilaisuus korottaa viskositeettia. Viskositeettia lisää myös kalvon, rihmojen ja pintojen kuivuminen tulipesäolosuhteiden takia. Rihmojen ja pisaroiden muodonmuutokset hidastuvat, jolloin pisaroiden lentoradat lyhenevät ja samalla kuivuminen ja palaminen tehostuvat rihmojen pisaroita suuremman pinta-alan takia. Tämä vaikuttaa keon muotoon ja koostumukseen sekä intensiivisimmän palamisen sijaintiin tulipesässä.

Tutkijoille ja tuotekehittelijöille, jotka kehittävät soodakattilan ruiskutusta tai haihdutinyksiköitä, havainnot mustalipeän ei-Newtonilaisista ominaisuuksista ovat tärkeitä. Näiden tulosten pohjalta voidaan kehittää tarkempia pisaroitumis- ja ruiskunmalleja sekä tehokkaampia haihduttamoja.

5.3 Pohdintaa tulosten hyödyntämisideoista

Tulokset ovat uusia ja mielenkiintoisia. Pienillä leikkausnopeuksilla korkeakuiva-aineinen mustalipeä on ei-Newtonilaista jopa käytetyillä korkeilla lämpötiloilla. Suurilla leikkausnopeuksilla mustalipeä käyttäytyy Newtonilaisen nesteen tavoin normaalisti käytetyillä kuiva-ainepitoisuuksilla ja lämpötiloilla.

Pumpuissa, putkistoissa ja suuttimissa mustalipeä käyttäytyy Newtonilaisen nesteen tavoin. Ruiskutuksen jälkeen tulipesässä leikkausnopeudet ovat pieniä ja mustalipeä tämän takia ei-Newtonilaista. Pelkän ei-Newtonilaisuuden huomioiminen pisaran muodonmuutokseen on tehtävissä luvussa neljä esitetyllä tavalla käyttäen Fluent virtauslaskentaohjelmistoa. 8:n millimerin pisaroilla muodon muutos hidastui tässä laskelmassa 20 %. Todellisessa tulipesässä muodostuneiden rihmojen ja pisaroiden muodon muutoksen laskeminen on vaikeaa, koska samanaikaisesti mustalipeä kokee höyrynkuplien laajenemisen ja höyryn vapautumisen, tulipesäsäteilyn kuivattavan vaikutuksen ja tulipesän kuumat kaasuvirtaukset. Mittaus- ja laskentamenetelmiä pisaroiden todelliselle käyttäytymiselle tulipesässä pitäisi kehittää, jotta tulipesän käyttäytymistä voitaisiin luotettavasti ennustaa. Aiempiin laskelmiin nähden pisaroiden muodonmuutos on todellisille ei-Newtonilaisille pisaroille hitaampaa, kuin Newtonilainen viskositeetti antaa olettaa. Oletettavasti viskositeetin kasvaessa lämpötilaa tulisi hiukan kohottaa, jotta ruiskutus- ja polttamisolosuhteet pysyisivät ennallaan. Samanaikaisesti pitäisi huomioida ruiskutuslämpötilan ja kiehumispisteen välinen lämpötilaero, joka vaikuttaa suihkun nopeuteen ja

pisarakokoon. Täydellisessä optimoinnissa huomioitaisiin mm. tarvittava uusi ruikutuskulma ja uudelle tilanteelle optimoitu ilmanjako.

Tutkimuksessa käytetyn on-line viskometrin tarkkuudeksi arvioitiin laboratoriossa huoneenlämpöisellä kalibrointinesteellä 15 %. Tehtaalla tarkkuus on huonompi, koska lämpötilan ja virtauksen säätö ovat vaikeampia. Laitteen asettelu ja virittely vaati paljon etukäteisvalmisteluja. Kapillaariviskometrista olisi kuitenkin kehitettävissä jatkuvatoiminen mittalaite. Laitetta voitaisiin käyttää esimerkiksi ruiskutuksen ohjaukseen, jolloin voitaisiin reagoida viskositeettimuutoksiin jo ennen keossa tai palamisessa havaittuja muutoksia. Samansuuntaista tietoa syntyy kuiva-ainemittauksella, mutta aina kuiva-ainepitoisuus ei ennusta viskositeettia tarkasti, esimerkiksi suolan lisäyksen, puulaadun, jäännösalkalin muutoksen tai muun prosessimuutoksen yhteydessä. On myös mahdollista, että viskositeetin mittaaminen jälkikäteen laboratoriossa johtaa erilaiseen lopputulokseen, kuin viskositeetin mittaaminen jatkuvatoimisesti tehtaalla. Mustalipeän jäähdyttäminen ja laboratoriossa tapahtuva uudelleen lämmittäminen ja näytteenkäsittely voivat vaikuttaa mustalipeän mitattaviin ominaisuuksiin.

Useammasta erikokoisesta putkesta koostuvalla kapillaarityyppisellä viskometrilla voitaisiin tutkia ruiskutettavan mustalipeän ei-Newtonilaisuutta jatkuvatoimisesti. Tällöin vältyttäisiin näytteenkäsittelystä aiheutuvalta viiveeltä ja mahdollisilta muutoksilta mustalipeässä. Toisaalta kapillaariviskometrin tarkkuus huononee pienillä leikkausnopeuksilla, joten pisaroitumisen kannalta mittaamisen tarkkuus on ongelmallista. Ei-Newtonilaisuus liittyy ligniinin ja polysakkaridien pitoisuuksiin, joten mahdollisesti liuosten ei-Newtonilaisuutta voitaisiin käyttää näiden pitoisuuksien määrittämiseen.

Normaalisti näytteenotto tapahtuu paineistamattomaan astiaan, jolloin osa mustalipeän höyrystä pääse karkaamaan. Nyt testattu paineistettu näytteenotin vangitsi kaiken höyryn näytteen sisään myöhempää kuiva-ainepitoisuuden määrittämistä varten. Havu- ja lehtipuulipeän tapauksessa paineistetun näytteenottotavan kuiva-ainepitoisuus aleni 0.6 ja 1.9 prosenttiyksikköä, kun se olisi voinut alentua teoreettisesti maksimissaan 1.4 ja 0.9 prosenttiyksikköä. Sekalipeällä paineistetun näytteenottotavan kuiva-ainepitoisuus oli kohonnut 0,9 prosenttiyksikköä, kun se olisi voinut alentua maksimissaan 1.5 prosenttiyksikköä. Osa tuloksista viittaa virheeseen näytteenoton tai käsittelyn jossain vaiheessa. Kuten aiemmin on jo mainittu, käytetyn kuiva-ainemenetelmän (SCAN-N 22:77, ns. hiekkamenetelmä) mittausepävarmuus (95 % luottamustasolla) on ± 1 %.

Mustalipeän kuiva-ainepitoisuus on tärkeä suure, koska monet muut mustalipeän ominaisuudet, kuten kiehumapisteennousu ja viskositeetti esitetään kuiva-aineen funktiona. Yhden prosenttiyksikön virhe vaikuttaa kuiva-aineeltaan 80 % olevan mustalipeän kiehumapisteeseen 1 ºC ja viskositeettiin enimmillään jopa yli 30 %. Ruiskutuksen ja pisaroitumisen kannalta erot ovat merkityksellisiä. Kuiva-aineen ollessa tätä korkeampi, yhden prosenttiyksiön epätarkkuus vaikuttaa vielä enemmän. Koska kaikki aiemmat kuiva-aineen määritykset on tehty normaalilla menettelyllä, jossa osa höyrystä karkaa, on jatkossakin perusteltua käyttää vanhaa näytteenottomenetelmää. Samalla vältetään uuden paineistetun menetelmän aiheuttamat lisäkustannukset.

5.4 Jatkotutkimus

Varmistetaan Haake RheoStress 6000 viskometrin toiminta mustalipeälle soveltuvissa lämpötiloissa. Kalibroinnin yhteydessä mitattu viskositeetti etenkin korkeissa lämpötiloissa vaikutti seuraavan huonosti kalibrointiöljyn viskositeettia. Toisaalta korkeassa lämpötilassa kalibrointiöljyn viskositeetti oli melko alhainen (n. 100 mPas), sillä nykyisin tyypillisten mustalipeiden merkittävä mittausalue on 200-1000 mPas.

Pisaroitumiseen ja haihduttamon viimeisissä yksiköissä leikkausnopeudet ovat pieniä ja ei-Newtonilaisuus vaikuttaa merkittävästi. Viskositeettia ei mitattu alle 5 1/s leikkausnopeuksille. Ei tiedetä, kasvaisiko viskositeetti äärettömiin pienillä leikkausnopeuksilla vai olisiko viskositeetille olemassa vakioarvo pienillä leikkausnopeuksilla. Tällainen vakioarvo (eli nollaviskositeetti) esiintyy polymeereillä pienillä leikkausnopeuksilla. Mustalipeän käyttäytyminen erittäin pienillä leikkausnopeuksilla pitäisi selvittää.

Ligniinin molekyylipaino olisi hyvä mitata liittyen tutkittaviin mustalipeisiin. Molekyylipaino, varsinkin ligniinin suurimolekyylinen osuus (HMML), liittyy olennaisesti viskositeettiin ja etenkin ei-Newtonilaiseen viskositeettiin.

Viskoelastisuutta ei tämän tutkimuksen yhteydessä tutkittu. Kirjallisuuden perusteella viskoelastisuutta esiintyy Zaman ja Fricke [13] mukaan alle 85 ºC lämpötiloissa, mutta ei yli 120 ºC lämpötiloissa. Mustalipeälle aihetta ei ole tutkittu merkittävästi, vaikka esimerkiksi polymeereilla viskoelastisuus on tärkeä suure.

Pisaran muodonmuutoksen mallinnusta on jatkettava OpenFoam-ohjelmalla. Mallia voidaan validoida kokeellisesti esimerkiksi ei-Newtonilaisen ksanttaaniseoksen avulla. Viritetään ksanttaanirihma pysty-tai vaakasuuntaisesti, jolloin voidaan kuvata rihman kasaan vetäytyminen hallitusti katkaistulle rihmalle. Vaikka tilanne ei kuvaa mustalipeäpisaraa tulipesässä, on mallin validointi yksi askel mustalipeäpisaran tulipesäkäyttäytymisen ymmärtämisessä. Pisaroitumisen, kuivumisen ja palamisen todellinen eteneminen tulipesäolosuhteissa on selvitettävä. Yhdistämällä pisaran käyttäytymisen mallintaminen ja kuvaukset tulipesässä hallituissa olosuhteissa mahdollistavat tulevaisuudessa entistä paremman pisaroiden palamisen, keon muodostumisen ja likaantumisen hallinnan tulipesässä.

LÄHDELUETTELO

1. Chhabra, R.P. Richardson, J.F. (2008). Non-Newtonian Flow and Applied Rheology - Engineering Applications (2nd Edition). Elsevier.

2. Fricke, A., L., Zaman, A., A., A Comprehensive Program to Develop Correlations for Physical Properties of Kraft Black Liquor, Final Report, The University of Florida, May 1998.

3. Söderhjelm, Liva, Factors Affecting the Viscosity of Strong Black Liquor, Appita Journal 41(1988):5, 389-392.

4. Söderhjelm, L., Viscosity of Strong Black Liquor from Birch, Paper and Timber, vol 70, 1988, 348-355.

5. Zaman A. A., Fricke A. L., Viscosity of Black Liquor up to 130°C and 84% Solids, AIChE Proceedings, 1991Forest Products Symp., pp. 59-77 (1991).

6. Yang R., Chen K., Liu Y. Chen Q., Shear-Thinning Properties of Non-Wood Kraft Pulping Waste Liquor, J. Cent. South Univ. Technol. (2007) s1−0522−04.

7. Söderhjelm, L., Characterization of Kraft Black Liquor with Respect to Evaporation and Combustion, Dissertation, Helsinki University of Technology, Laboratory of Pulping Technology, Helsinki, 1998.

8. Wight, M., Co, A., Fricke, A.L., Viscosity of Black Liquor by Cone and Plate and Parallel Disk Viscometry, AIChE Symposium Series: 77(207), 9-12 (1981).

9. Haavisto, S., Salmela, J., Järvinen, M., Kankkunen, A., Koponen, A., Application Of Ultrasound Velocity Profiling For Measuring Flow Behavior Inside Black Liquor Nozzles, International Chemical Recovery Conference, Tampere, Tampere-Talo, Finland, 8-13 June, 2014. Helsinki 2014, Finnish Recovery Boiler Committee, 2014, pp. 271-278.

10. Zaman A. A., Fricke A. L., Correlations for Viscosity of Kraft Black Liquors at Low Solids Concentrations. AIChE Journal, Vol. 40, No. 1, 1994, 187-192.

11. Miikkulainen, P., Spray Formation of High Dry Solids Black Liquor in Recovery Boiler Furnaces, Dissertation, Department of Mechanical Engineering, Helsinki University of Technology, 2006.

12. Söderhjelm, L., Viscosity of Strong Black Liquor, Paperi ja Puu, 68 (1986):9, 642-652.

13. Zaman, A. A., Fricke, A. L., Viscoelastic Properties of High Solids Softwood Kraft Black Liquors, Ind. Eng. Chem. Res., 1995, 34 (1), pp 382–391.

14. Järvinen, M., Kankkunen, A., Virtanen, R., Miikkulainen, P., Heikkilä, V.P, A One-Dimensional 2-Phase Flow Model and Experimental Validation for a Flashing Viscous Liquid in a Splash Plate Nozzle, Atomization and Sprays, to be published 2015.

15. Adams, T.N, Frederick, J.M., Grace, T.M., Hupa, M., Iisa, K., Jones, A.K, Tran, H., Kraft Recovery Boilers, Tappi Press, Atlanta, 1997.

16. Koskenranta J., Calibration of Black Liquor Viscometer, 15 June, 2014, Aalto University, School of Engineering, Department of Energy.

17. Kärnä, A., Järvinen, M., Kankkunen, A., CFD Modeling and Experiments of Droplet Formation of Non-Newtonian Liquids, to be submitted 2015

LIITE 1

Havulipeän viskositeettikäyrät

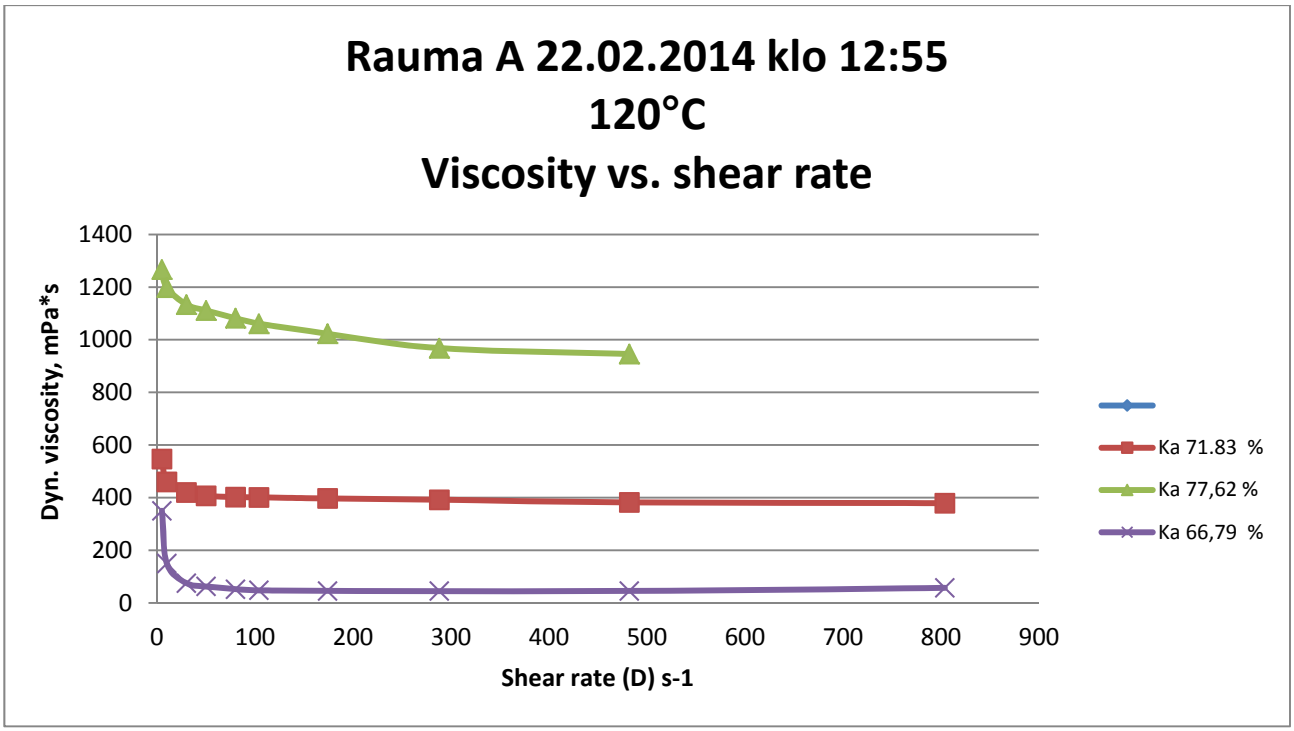
Rauma A 22.02.2014 klo 12:55
120°C
Viscosity vs. shear rate
Dyn. viscosity, mPa*s
1400
1200
1000
800
600
400
200
0
0
100
200
300
400
500
600
700
800
900
Shear rate (D) s-1
Ka 71.83 %
Ka 77,62 %
Ka 66,79 %

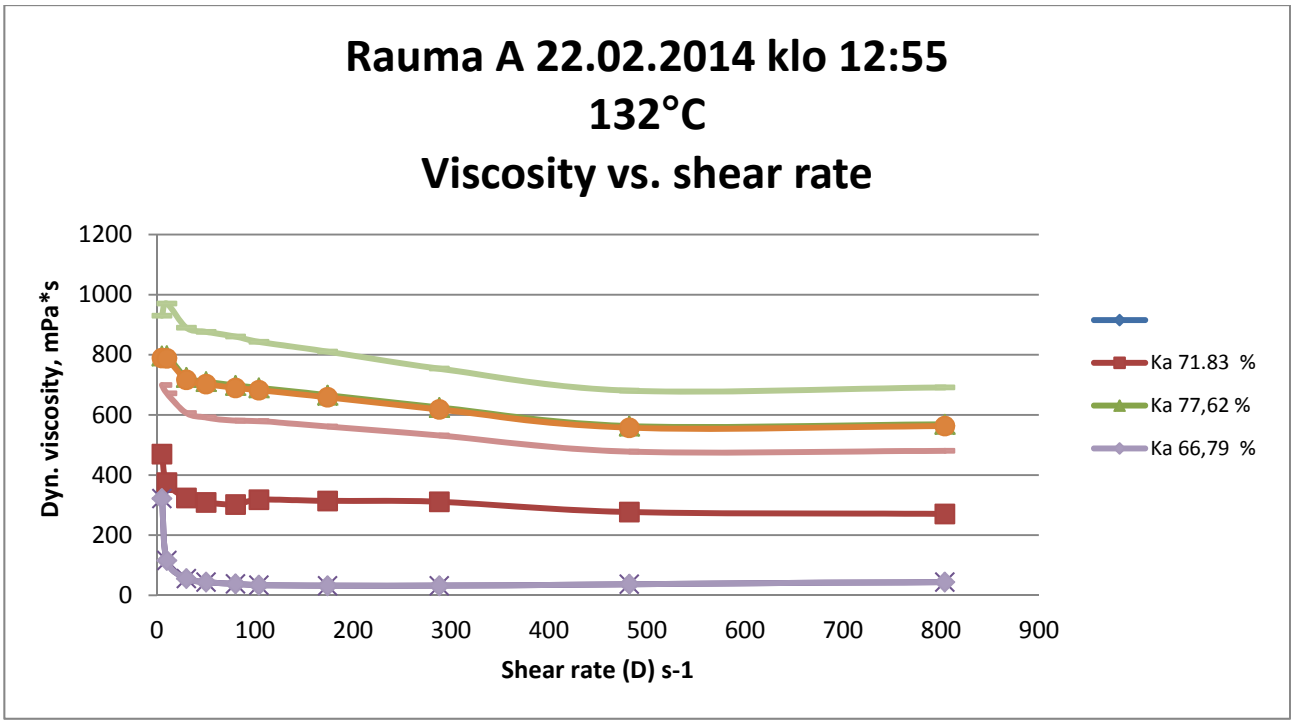
Rauma A 22.02.2014 klo 12:55
132°C
Viscosity vs. shear rate
Dyn. viscosity, mPa*s
1200
1000
800
600
400
200
0
0
100
200
300
400
500
600
700
800
900
Shear rate (D) s-1
Ka 71.83 %
Ka 77,62 %
Ka 66,79 %

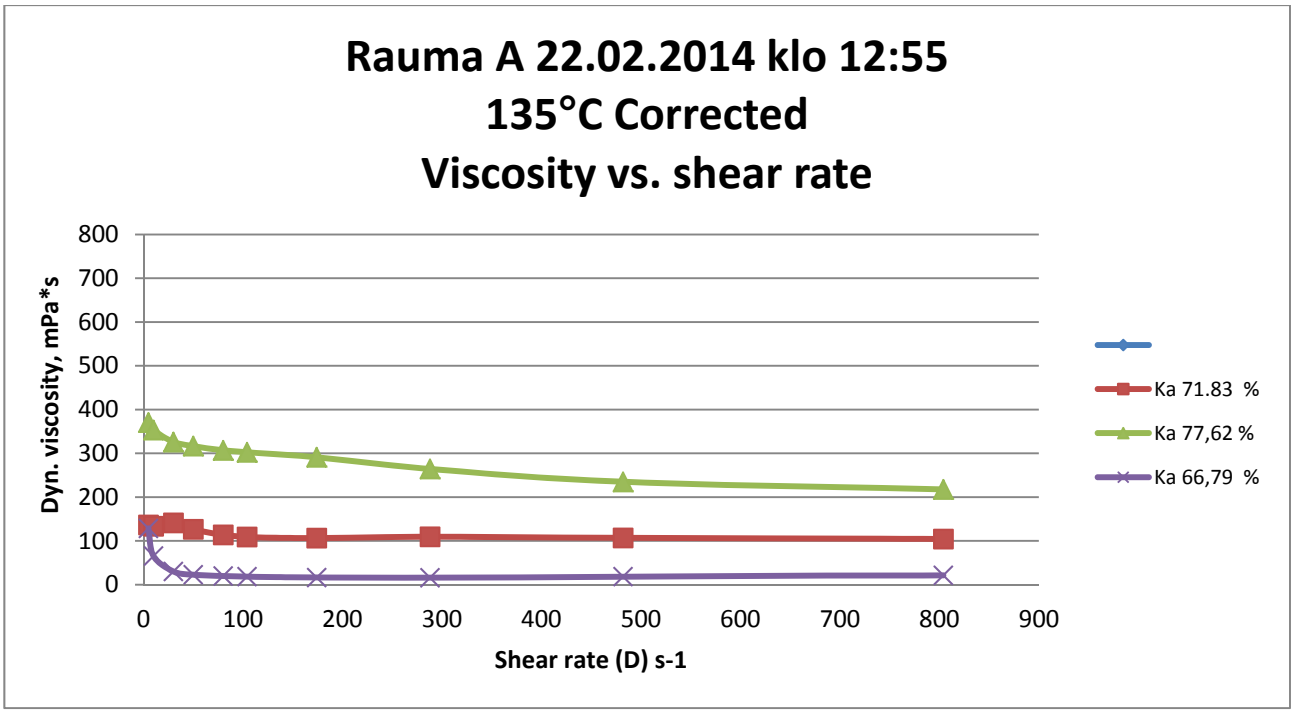
Rauma A 22.02.2014 klo 12:55
135°C Corrected
Viscosity vs. shear rate
Dyn. viscosity, mPa*s
800
700
600
500
400
300
200
100
0
0
100
200
300
400
500
600
700
800
900
Shear rate (D) s-1
Ka 71.83 %
Ka 77,62 %
Ka 66,79 %

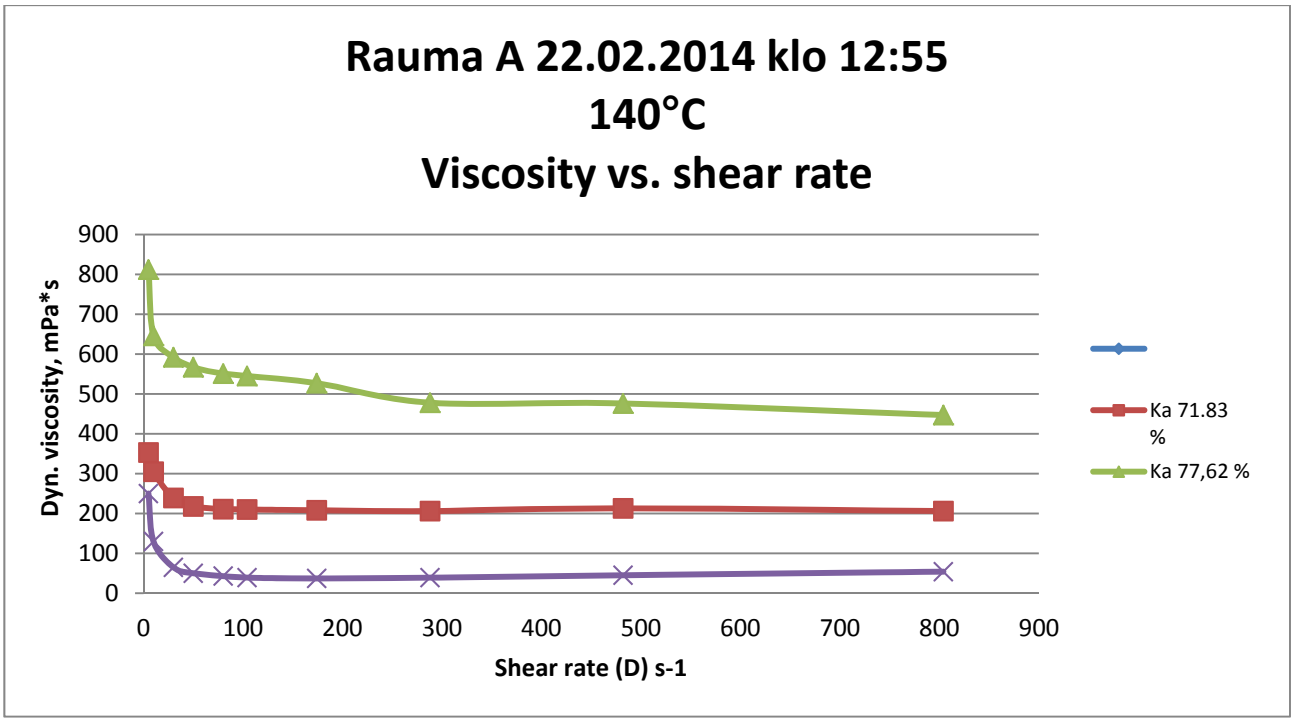
Rauma A 22.02.2014 klo 12:55
140°C
Viscosity vs. shear rate
Dyn. viscosity, mPa*s
900
800
700
600
500
400
300
200
100
0
0
100
200
300
400
500
600
700
800
900
Shear rate (D) s-1
Ka 71.83 %
Ka 77,62 %

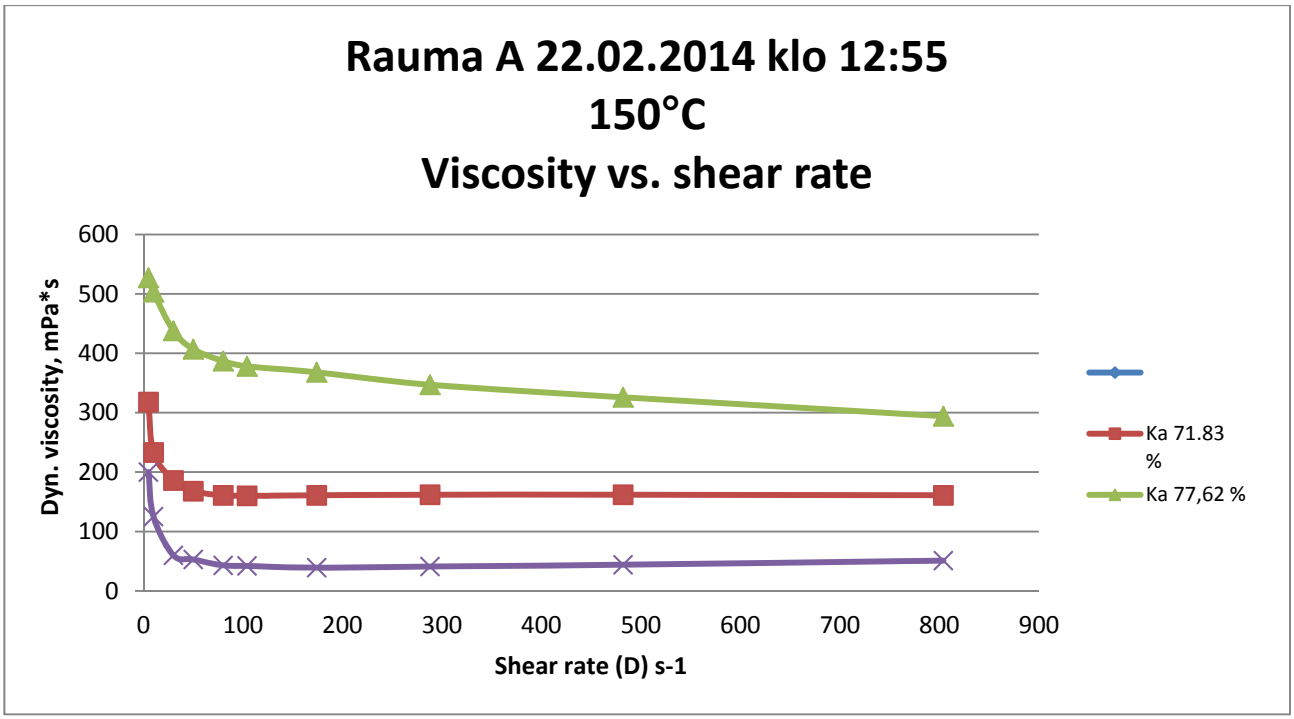
Rauma A 22.02.2014 klo 12:55
150°C
Viscosity vs. shear rate
Dyn. viscosity, mPa*s
600
500
400
300
200
100
0
0
100
200
300
400
500
600
700
800
900
Shear rate (D) s-1
Ka 71.83 %
Ka 77,62 %

LIITE 2

Lehtipuulipeän viskositeettikäyrät

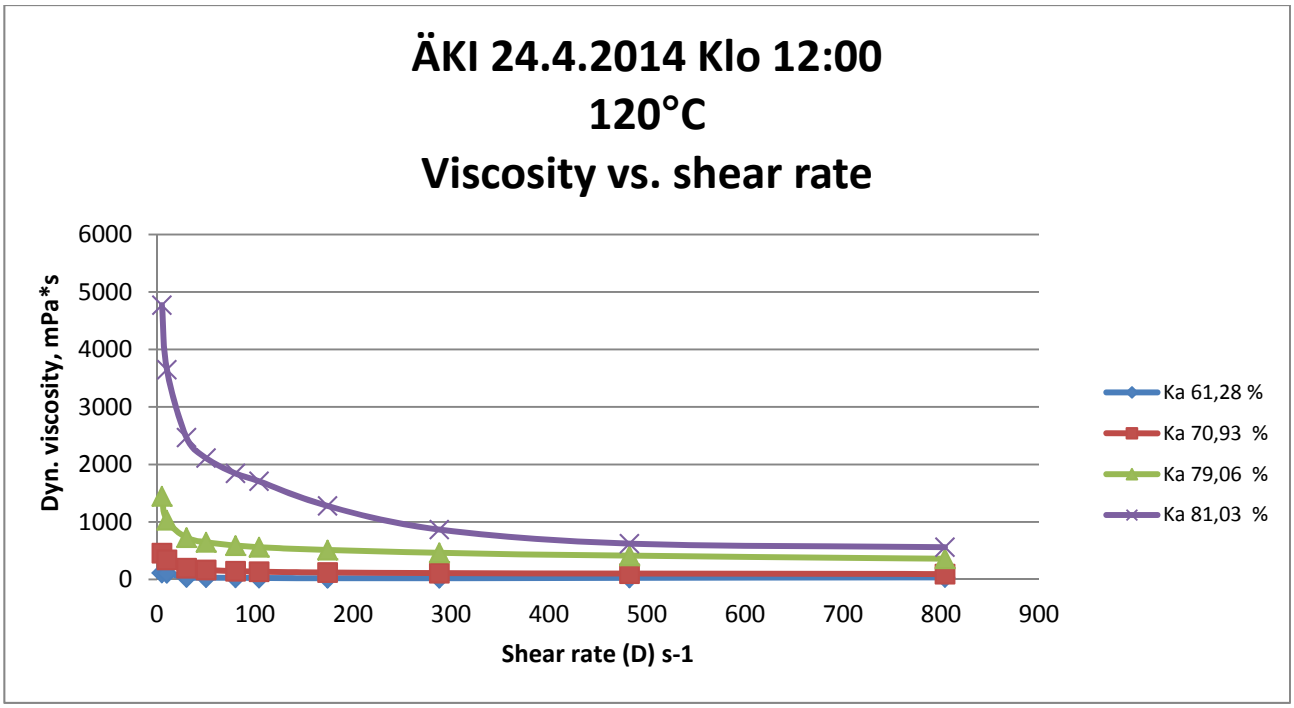
ÄKI 24.4.2014 Klo 12:00
120°C
Viscosity vs. shear rate
Dyn. viscosity, mPa*s
6000
5000
4000
3000
2000
1000
0
0
100
200
300
400
500
600
700
800
900
Shear rate (D) s-1
Ka 61,28 %
Ka 70,93 %
Ka 79,06 %
Ka 81,03 %

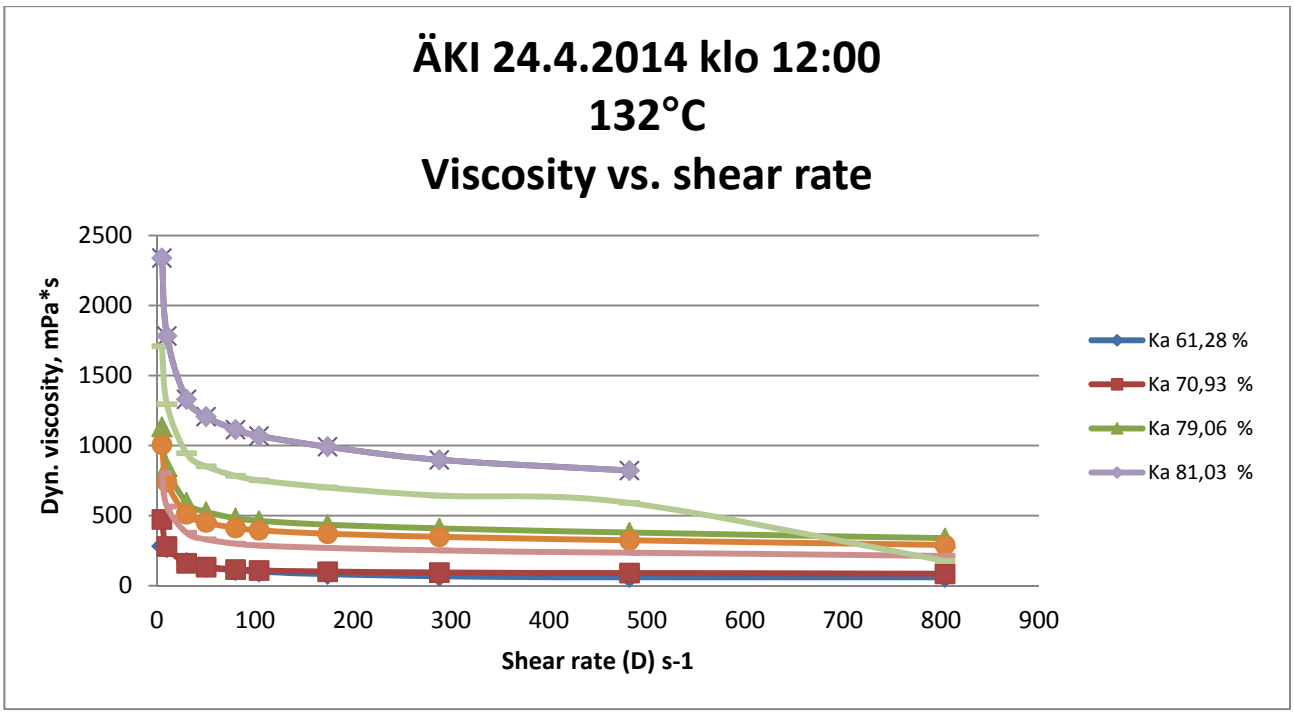
ÄKI 24.4.2014 klo 12:00
132°C
Viscosity vs. shear rate
Dyn. viscosity, mPa*s
2500
2000
1500
1000
500
0
0
100
200
300
400
500
600
700
800
900
Shear rate (D) s-1
Ka 61,28 %
Ka 70,93 %
Ka 79,06 %
Ka 81,03 %

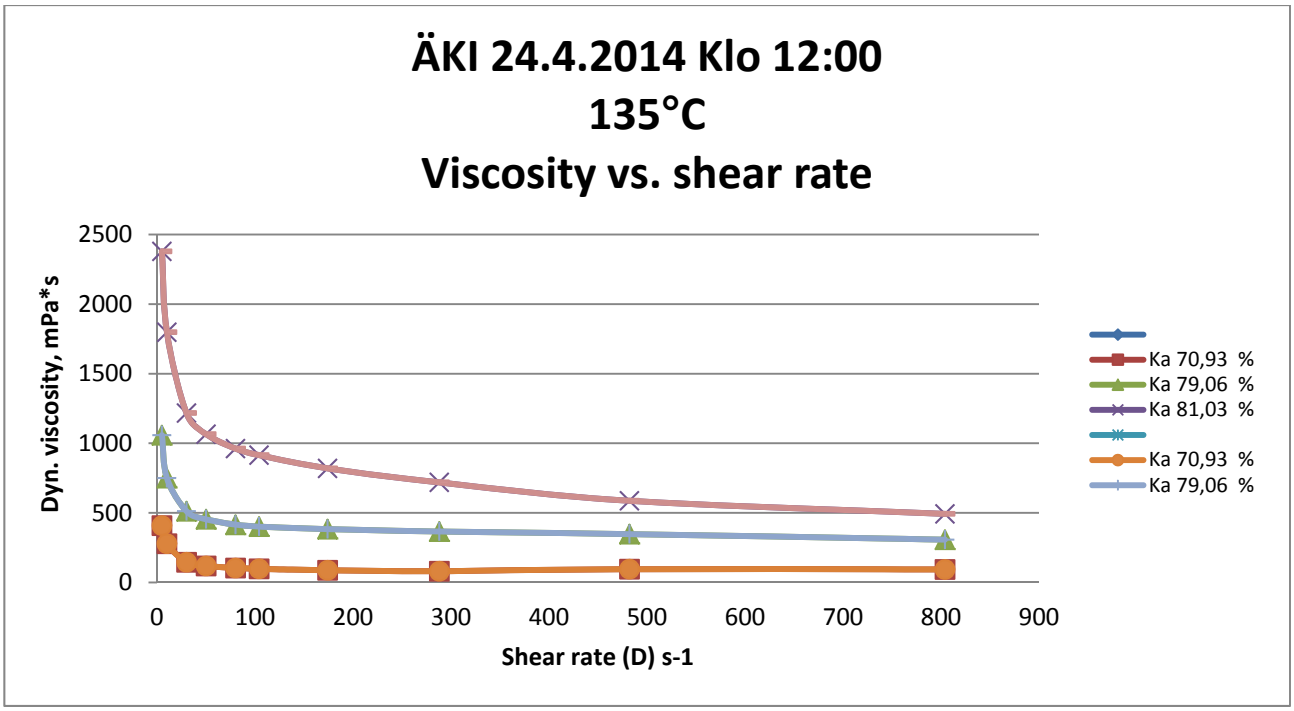
ÄKI 24.4.2014 Klo 12:00
135°C
Viscosity vs. shear rate
Dyn. viscosity, mPa*s
2500
2000
1500
1000
500
0
0
100
200
300
400
500
600
700
800
900
Shear rate (D) s-1
Ka 70,93 %
Ka 79,06 %
Ka 81,03 %
Ka 70,93 %
Ka 79,06 %

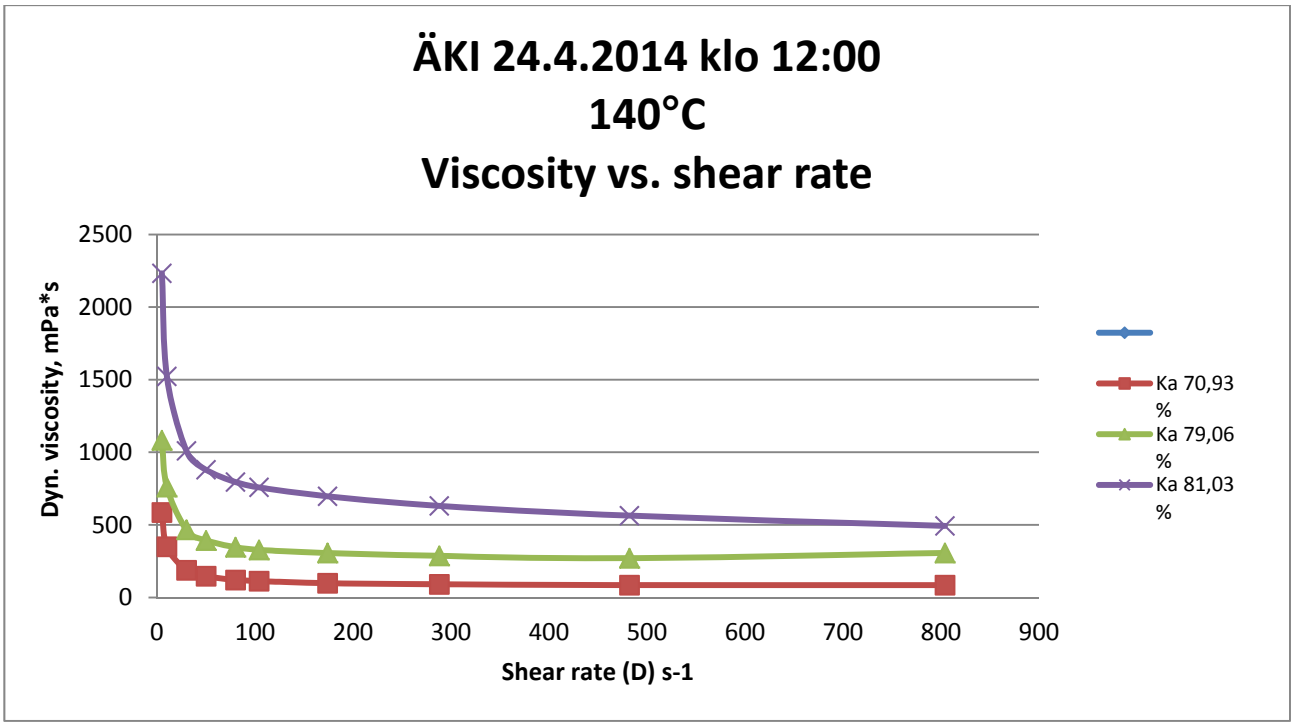
ÄKI 24.4.2014 klo 12:00
140°C
Viscosity vs. shear rate
Dyn. viscosity, mPa*s
2500
2000
1500
1000
500
0
0
100
200
300
400
500
600
700
800
900
Shear rate (D) s-1
Ka 70,93 %
Ka 79,06 %
Ka 81,03 %

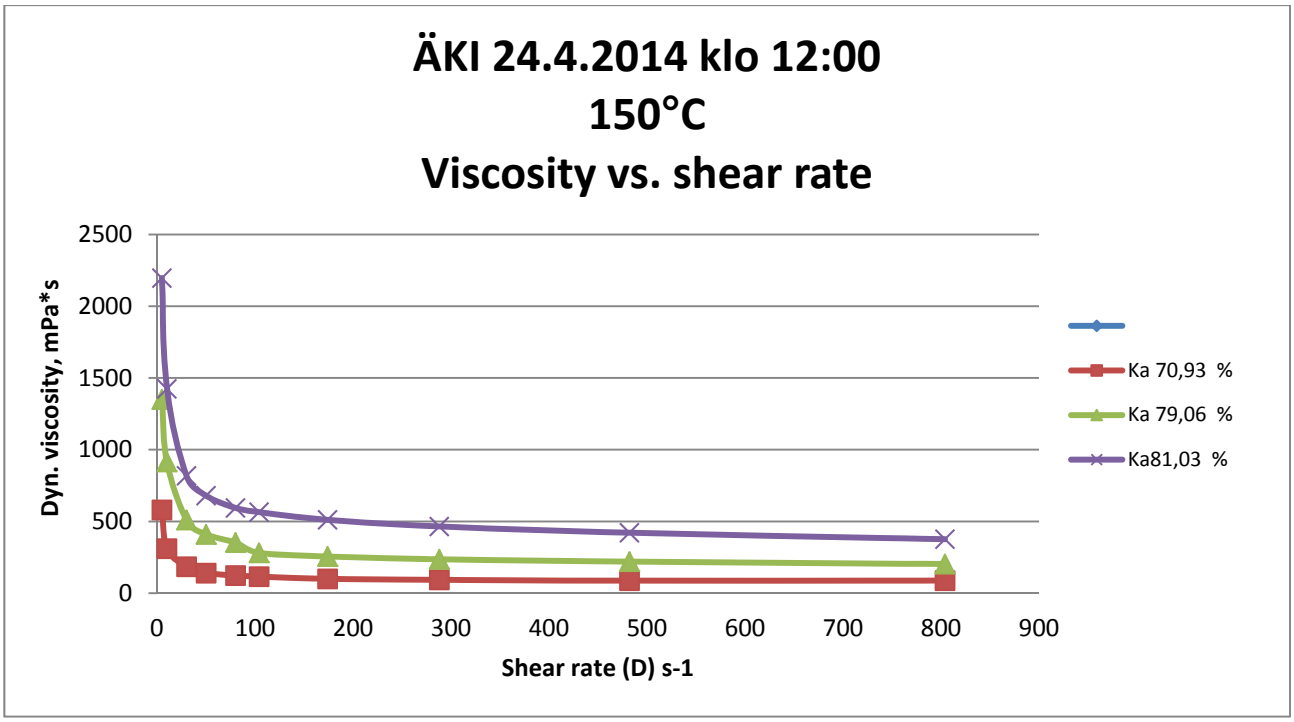
ÄKI 24.4.2014 klo 12:00
150°C
Viscosity vs. shear rate
Dyn. viscosity, mPa*s
2500
2000
1500
1000
500
0
0
100
200
300
400
500
600
700
800
900
Shear rate (D) s-1
Ka 70,93 %
Ka 79,06 %
Ka81,03 %

LIITE 3

Sekalipeän viskositeettikäyrät

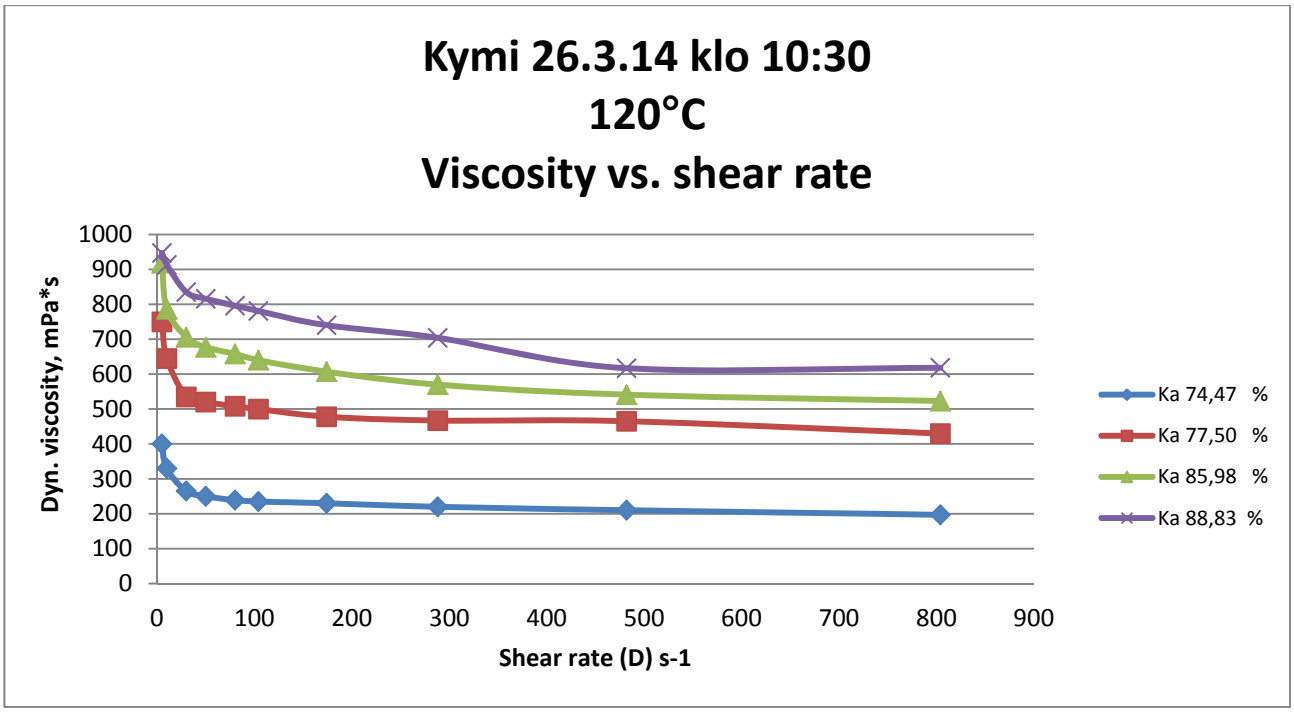
Kymi 26.3.14 klo 10:30
120°C
Viscosity vs. shear rate
Dyn. viscosity, mPa*s
1000
900
800
700
600
500
400
300
200
100
0
0
100
200
300
400
500
600
700
800
900
Shear rate (D) s-1
Ka 74,47 %
Ka 77,50 %
Ka 85,98 %
Ka 88,83 %

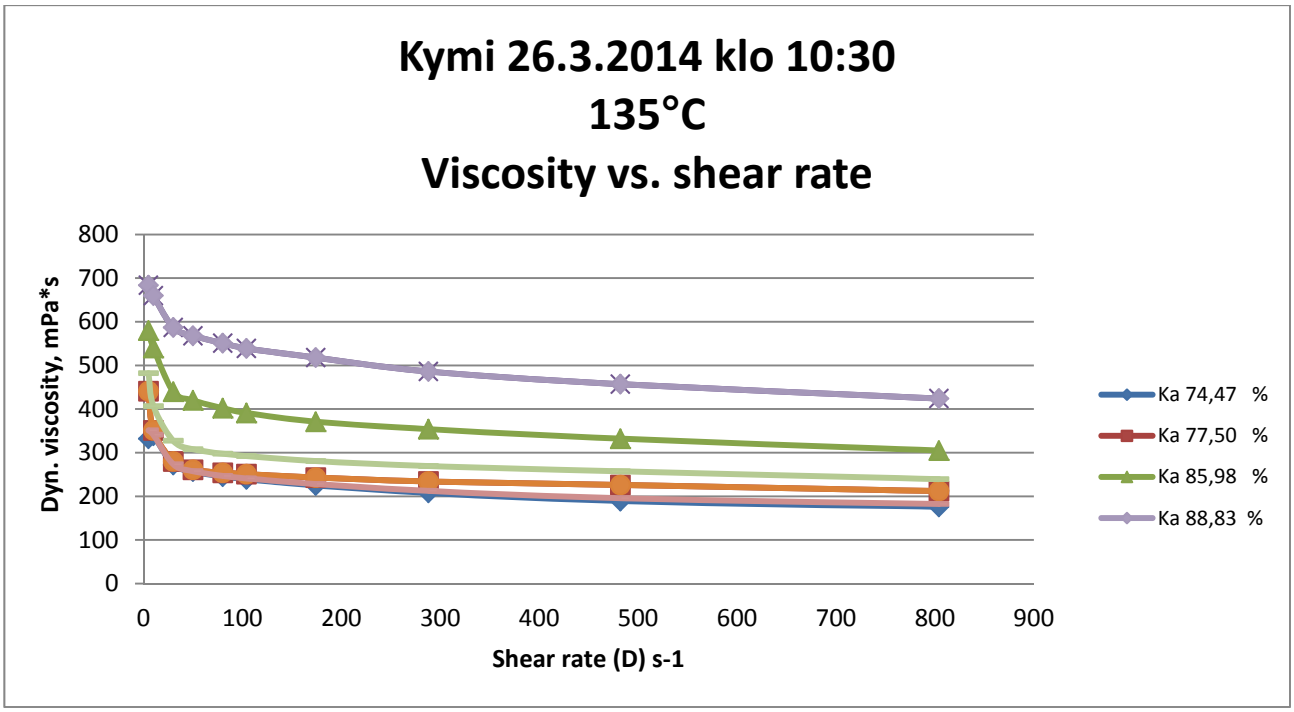
Kymi 26.3.2014 klo 10:30
135°C
Viscosity vs. shear rate
Dyn. viscosity, mPa*s
800
700
600
500
400
300
200
100
0
0
100
200
300
400
500
600
700
800
900
Shear rate (D) s-1
Ka 74,47 %
Ka 77,50 %
Ka 85,98 %
Ka 88,83 %

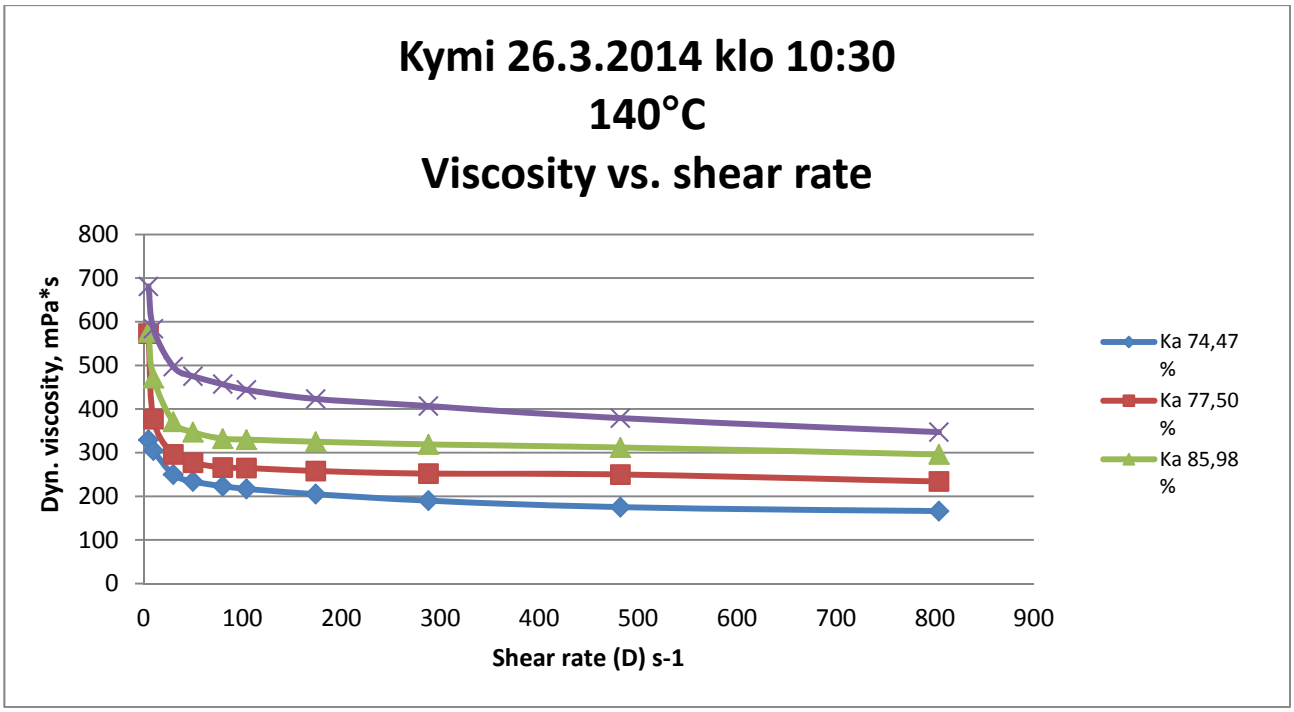
Kymi 26.3.2014 klo 10:30
140°C
Viscosity vs. shear rate
Dyn. viscosity, mPa*s
800
700
600
500
400
300
200
100
0
0
100
200
300
400
500
600
700
800
900
Shear rate (D) s-1
Ka 74,47 %
Ka 77,50 %
Ka 85,98 %

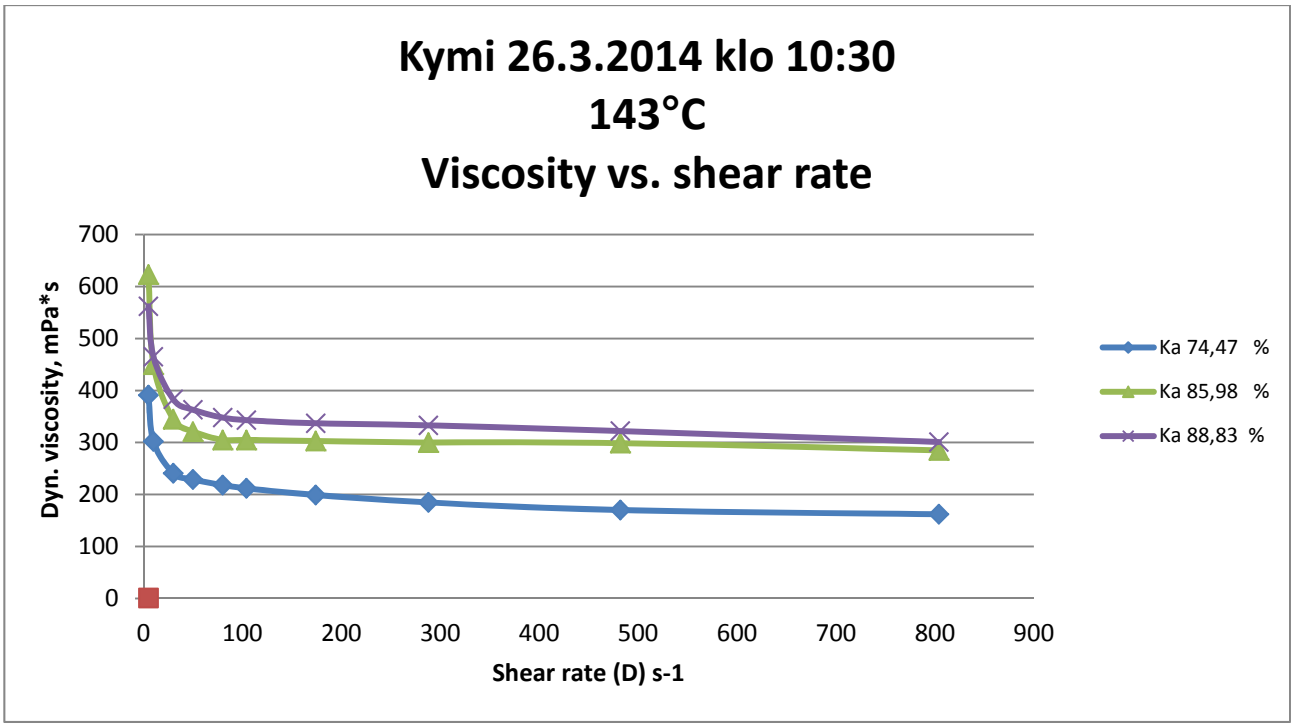
Kymi 26.3.2014 klo 10:30
143°C
Viscosity vs. shear rate
Dyn. viscosity, mPa*s
700
600
500
400
300
200
100
0
0
100
200
300
400
500
600
700
800
900
Shear rate (D) s-1
Ka 74,47 %
Ka 85,98 %
Ka 88,83 %

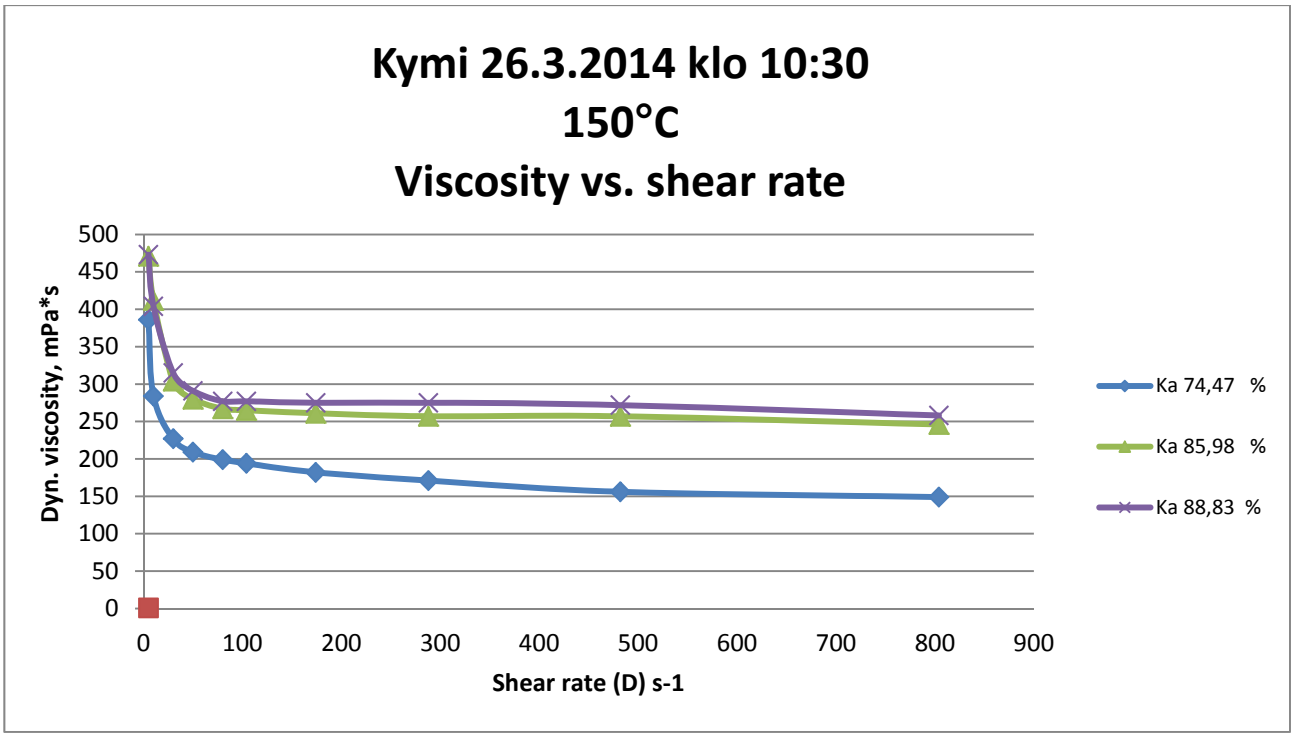
Kymi 26.3.2014 klo 10:30
150°C
Viscosity vs. shear rate
Dyn. viscosity, mPa*s
500
450
400
350
300
250
200
150
100
50
0
0
100
200
300
400
500
600
700
800
900
Shear rate (D) s-1
Ka 74,47 %
Ka 85,98 %
Ka 88,83 %

LIITE 4

Eukalyptuslipeän viskositeettikäyrät

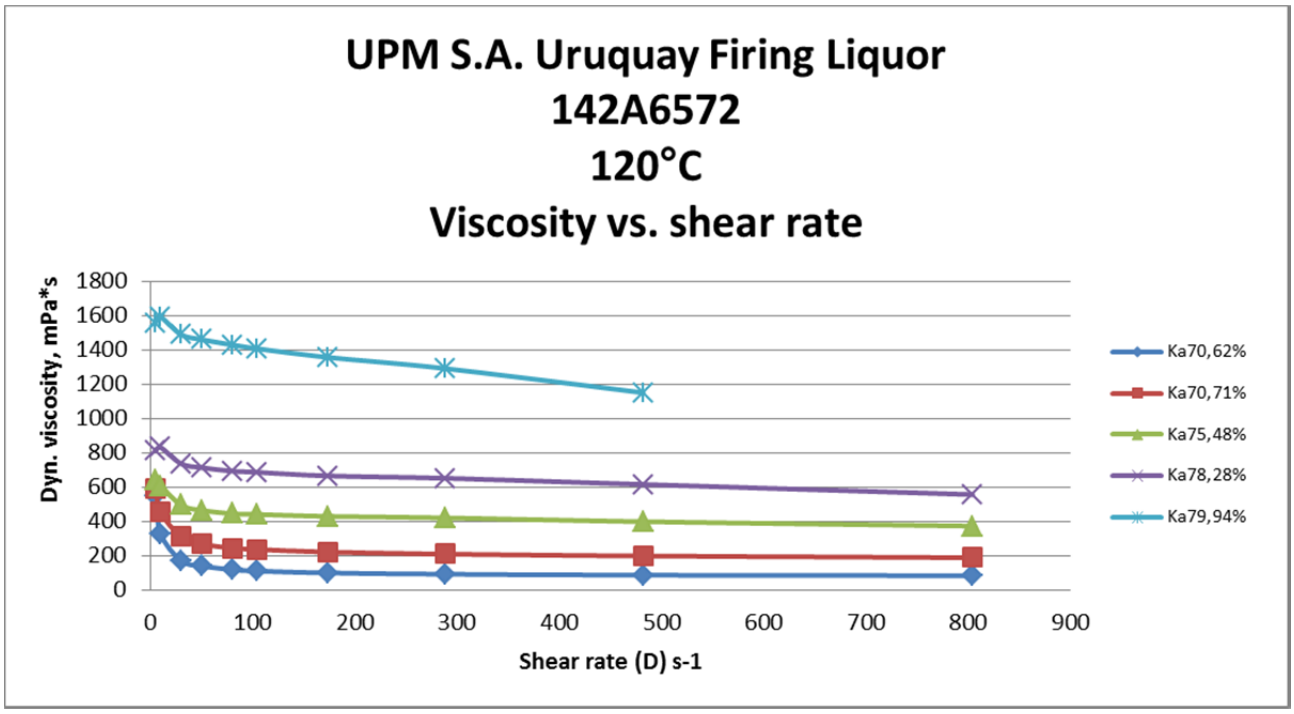
UPM S.A. Uruquay Firing Liquor
142A6572
120°C
Viscosity vs. shear rate
Dyn. viscosity, mPa*s
1800
1600
1400
1200
1000
800
600
400
200
0
0
100
200
300
400
500
600
700
800
900
Shear rate (D) s-1
Ka70,62%
Ka70,71%
Ka75,48%
Ka78,28%
Ka79,94%

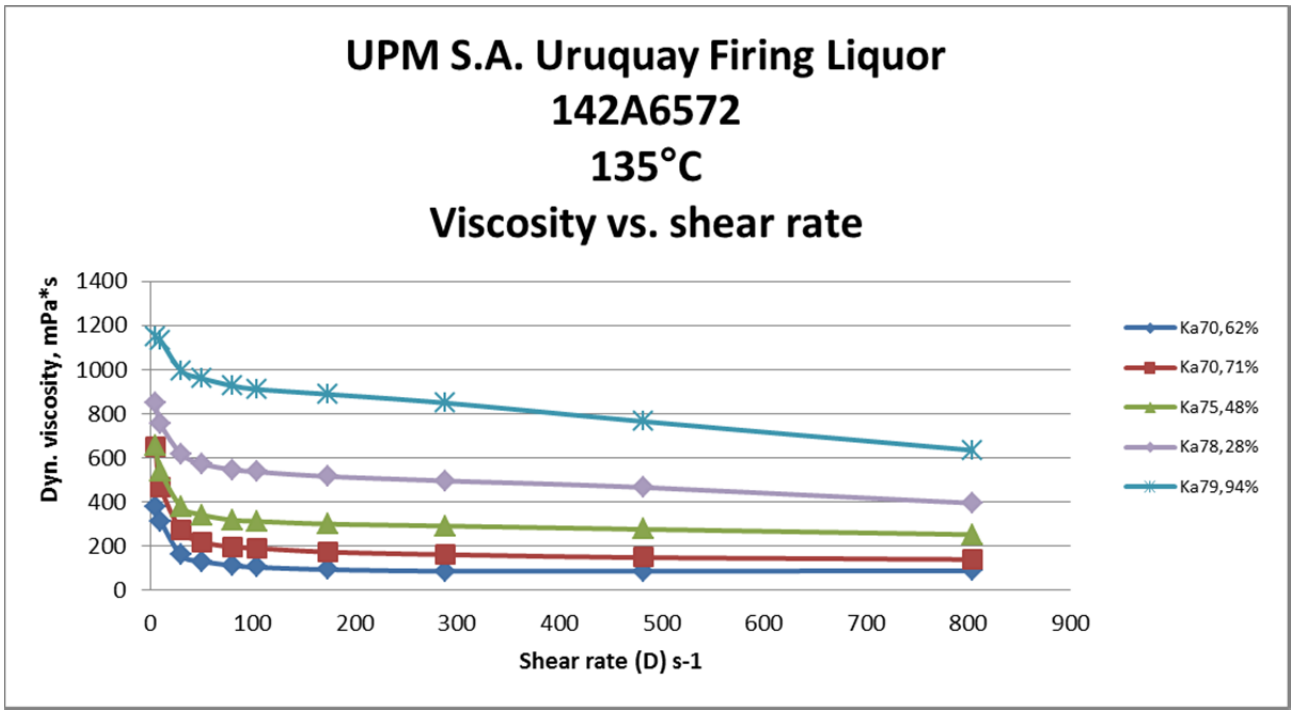
UPM S.A. Uruquay Firing Liquor
142A6572
135°C
Viscosity vs. shear rate
Dyn. viscosity, mPa*s
1400
1200
1000
800
600
400
200
0
0
100
200
300
400
500
600
700
800
900
Shear rate (D) s-1
Ka70,62%
Ka70,71%
Ka75,48%
Ka78,28%
Ka79,94%

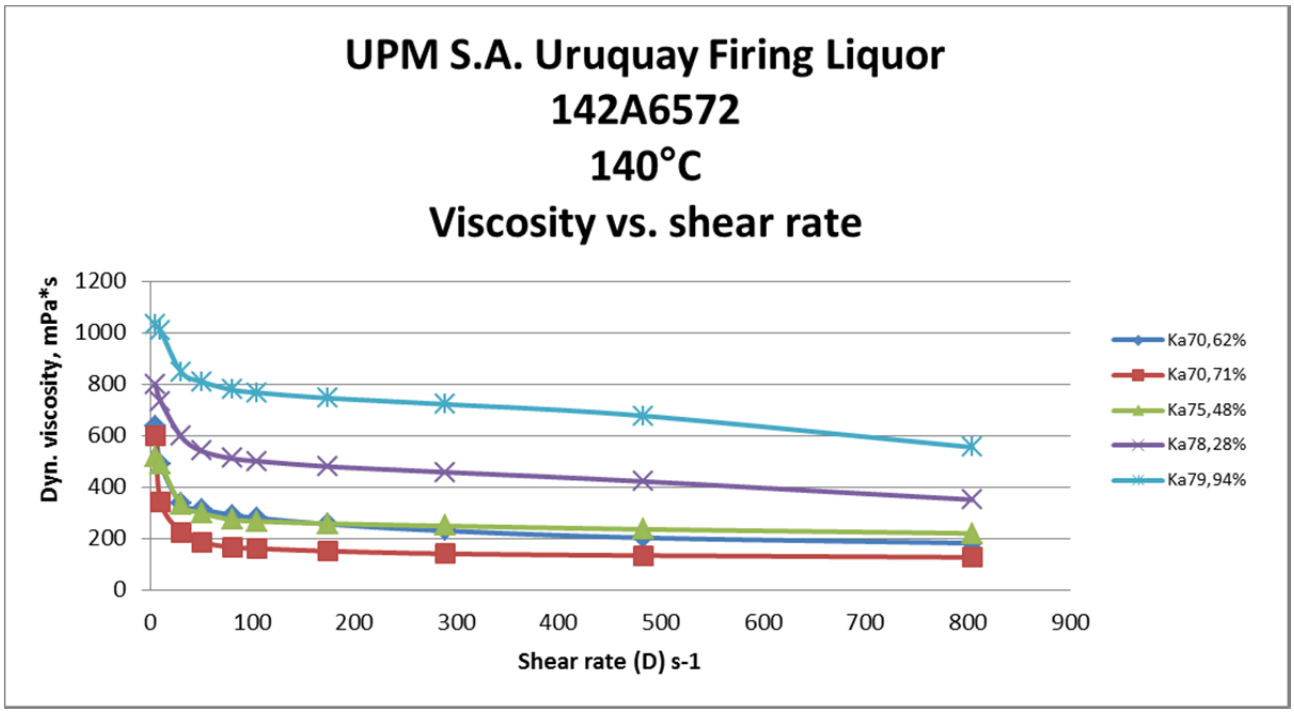
UPM S.A. Uruquay Firing Liquor
142A6572
140°C
Viscosity vs. shear rate
Dyn. viscosity, mPa*s
1200
1000
800
600
400
200
0
0
100
200
300
400
500
600
700
800
900
Shear rate (D) s-1
Ka70,62%
Ka70,71%
Ka75,48%
Ka78,28%
Ka79,94%

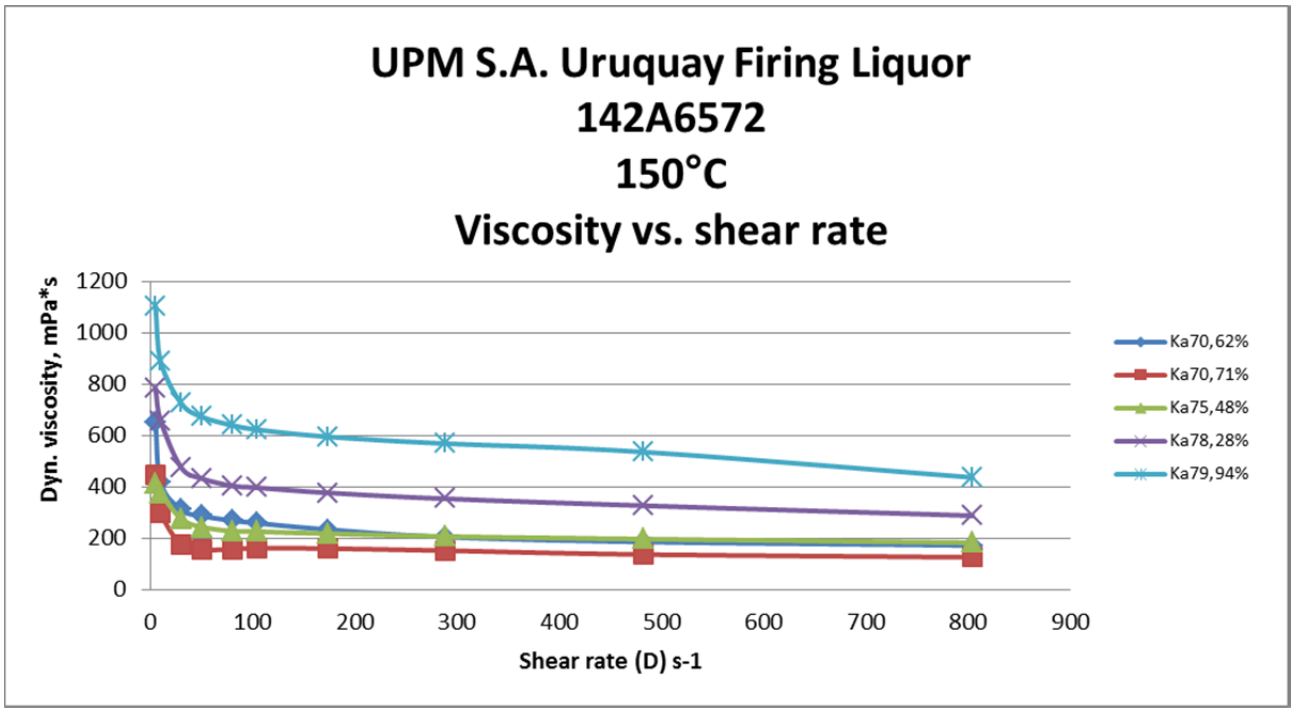
UPM S.A. Uruquay Firing Liquor
142A6572
150°C
Viscosity vs. shear rate
Dyn. viscosity, mPa*s
1200
1000
800
600
400
200
0
0
100
200
300
400
500
600
700
800
900
Shear rate (D) s-1
Ka70,62%
Ka70,71%
Ka75,48%
Ka78,28%
Ka79,94%

LIITE 5

Kemialliset analyysit

				Havulipeä	*Koivulipeä*	*Sekalipeä*	*Eukalyptus*
Kuiva-aine		%	SCAN-N 22:77	73,1	82,7	71,2	77,8
Kuiva-aineen							
tuhka		%	KCL 59:83	56,3	58,2	56,3	52,4
hiili	C	%	ASTM D 5373	31,1	28,9	30,5	33,1
vety	H	%	ASTM D 5373	4,4	3,4	3,7	3,3
typpi (Kjeldahl)	N	%	SFS 5505 modif.	0,062	0,073	0,116	0,093
natrium	Na	%	SCAN-N 37:98	21,7	22,1	21,6	21,2
kalium	K	%	SCAN-N 37:98	2,7	3,4	2,8	1,7
alumiini	Al	mg/kg	SCAN-N 38:10	32	23	22	64
barium	Ba	mg/kg	SCAN-N 38:10	4,4	8,0	5,6	15
kalsium	Ca	mg/kg	SCAN-N 38:10	360	230	120	690
kupari	Cu	mg/kg	SCAN-N 38:10	2,5	< 1	< 1	1,6
rauta	Fe	mg/kg	SCAN-N 38:10	17	12	8,7	33
magnesium	Mg	mg/kg	SCAN-N 38:10	390	160	190	300
mangaani	Mn	mg/kg	SCAN-N 38:10	63	60	66	48
fosfori	P	mg/kg	SCAN-N 38:10	89	120	130	170
pii	Si	mg/kg	SCAN-N 38:10	290	260	180	500
vanadiini	V	mg/kg	SCAN-N 38:10	15	< 5	15	20
sinkki	Zn	mg/kg	SCAN-N 38:10	15	29	24	2,7
rikki	S	%	SCAN-N 38:10	8,2	7,2	5,9	7,8
kloori	Cl	%	AOX-laite	0,2	0,2	0,2	0,4
karbonaatti	$CO_3^=$	%	SCAN-N 32:98	5,2	6,2	6,1	5,3
sulfaatti	$SO_4^=$	%	KCL 71:81	7,2	7,0	6,3	5,4
sulfidi	$S^=$	%	SCAN-N 31:94	3,6	2,7	2,3	2,6
jäännösalkali	NaOH	%	SCAN-N 33:94	4,6	4,3	3,2	2,3
polysakkaridit		%	HPAEC-PAD	1,2	1,6	4,0	2,6
oksalaatti	$C_2O_4^=$	g/kg	SCAN-N 39:05	2,5	2,6	2,4	5,9
epäorg./org.-suhde			KCL 61:83	0,67	0,71	0,64	0,56
kalorimetrinen lämpöarvo		MJ/kg	Autom. kalorimetri	13,2	12,2	12,7	13,2
tehollinen lämpöarvo		MJ/kg		9,6	9,2	10,1	10,0
Näytteen tehollinen lämpöarvo		MJ/kg		6,4	7,1	6,5	7,2

LIITE 6

Kalibrointiöljyjen N4000ja N75 ominaisuudet

CERTIFICATE OF CALIBRATION

ISSUED BY PARAGON SCIENTIFIC LIMITED

Date of Issue: **23-Jul-13** Certificate No. **UHD1322**

0649 4589

Paragon Scientific Ltd

UKAS-accredited calibration laboratory No. 0649 accredited to ISO/IEC 17025
UKAS accredited reference material producer No. 4589 accredited to ISO Guide 34
2 Kelvin Park, Dock Road, Birkenhead, Wirral, CH41 1LT, England
Telephone: +44 (0) 151 649 9955 Fax: +44 (0) 151 649 9977
e-mail: sales@paragon-sci.com Web Site: www.paragon-sci.com

Page 1 of 1 pages
Approved Signatory

Name Mr. J. Morris

Signature

ISO 17025 / ISO Guide 34 VISCOSITY AND DENSITY REFERENCE STANDARD

Standard type: **N4000** Lot No: **110401** Expiry Date: **23-Jul-15**

Temperature (°C)	Temperature (°F)	Viscosity mm²/s (cSt) Kinematic	Viscosity mPa·s (cP) Dynamic	SUS	SFS	Density (g/mL)
20.00	68.00	17952	15852			0.8830
25.00	77.00	11395	10030			0.8802
37.78	100.00	3965	3461			0.8729
40.00	104.00	3351	2921			0.8718
50.00	122.00	1643	1423			0.8661
60.00	140.00	865.2	744.7			0.8607
80.00	176.00	291.5	247.6			0.8494
98.89	210.00	127.2	106.7			0.8389
100.00	212.00	121.8	102.1			0.8384

Paragon Scientific Ltd. certifies that the kinematic viscosity measurements have been made in accordance with ASTM D 2162 using long capillary Master Viscometers at all temperatures. See also ASTM D 445, D 446, D 2171, ISO 3104, ISO 3105, IP 71 Sections 1 and 2 and IP 222. The viscosity data reported is based on the primary standard of pure water at 20°C (ITS-90) having a value of 1.0034 mm2/s (cSt) ± 0.17%, as adopted by NIST, ASTM, IP and ISO (ISO 3666). Density measurements were made in accordance with ASTM D 1480. Temperature measurements were made using thermometers specified in ASTM D 2162 which have a current calibration traceable to the National Physical Laboratory (NPL), National Institute Standards and Technology (NIST) and other recognised national standards laboratories. SUS and SFS values have been calculated in accordance with ASTM D 2161 where stated. The calibrations of this product are traceable to NIST.

Uncertainties:

Viscosity Range	Expanded Uncertainty Kinematic Viscosity mm²/s (cSt)	Expanded Uncertainty Dynamic Viscosity mPa·s (cP)
0.3 to 7.4	± 0.07 %	± 0.07 %
7.4 to 10	± 0.09 %	± 0.09 %
10 to 30	± 0.12 %	± 0.12 %
30 to 72	± 0.14 %	± 0.14 %
72 to 180	± 0.15 %	± 0.15 %
180 to 520	± 0.17 %	± 0.17 %
520 to 1000	± 0.19 %	± 0.19 %
1000 to 2700	± 0.20 %	± 0.20 %
2700 to 8000	± 0.22 %	± 0.22 %
8000 to 82 500	± 0.23 %	± 0.23 %

Uncertainties stated on this certificate do not include the uncertainty for the value of the viscosity of water at 20°C (ITS-90) having a value of 1.0034 mm²/s (cSt) ± 0.17%.

Density Uncertainties: Expanded Uncertainty ± 0.01 %

The reported expanded uncertainty is based on a combined standard uncertainty multiplied by a coverage factor of $k=2$, providing a level of confidence of approximately 95%.

The evaluation has been carried out in accordance with UKAS requirements.

Notes: The shelf life of this product is guaranteed until the expiry date, provided the bottle is unopened and stored at ambient temperature (15 to 30°C). The guarantee is void if the bottle seal is broken but the product should remain stable for 3 months after opening if stored correctly. Filtration of product before use is not necessary. No minimum volume is required to guarantee homogeneity.

Units: Kinematic Viscosity: 1 cSt = 10^{-2} St = 10^{-6} m²/s = 1 mm²/s
Dynamic Viscosity: 1 mPa·s = 10^{-3} Pa·s = 1 cP = 10^{-2} P
Dynamic Viscosity = Kinematic Viscosity x Density (at the same temperature)

CERTIFICATE OF CALIBRATION

ISSUED BY PARAGON SCIENTIFIC LIMITED

Date of Issue: **25-Apr-14** Certificate No. **U1713**

0649 4589

Paragon Scientific Ltd

Page 1 of 1 pages
Approved Signatory

Name Mr. J. Morris

Signature

UKAS accredited calibration laboratory No. 0649 accredited to ISO/IEC 17025
UKAS accredited reference material producer No. 4589 accredited to ISO Guide 34
6 Prenton Way, North Cheshire Trading Estate, Prenton, Wirral, UK. CH43 3DU.
Telephone: +44 (0) 151 649 9955 Fax: +44 (0) 151 649 9977
e-mail: sales@paragon-sci.com Web Site: www.paragon-sci.com

ISO 17025 / ISO Guide 34 VISCOSITY AND DENSITY REFERENCE STANDARD

Standard type: **N75** Lot No: **1123110** Expiry Date: **24-Apr-16**

Temperature		Viscosity				Density
(°C)	(°F)	mm^2/s (cSt) Kinematic	mPa·s (cP) Dynamic	SUS	SFS	(g/mL)
20.00	68.00	196.9	164.0			0.8327
25.00	77.00	150.5	124.9			0.8297
37.78	100.00	81.33	66.84			0.8218
40.00	104.00	73.78	60.53			0.8204
50.00	122.00	49.03	39.93			0.8144
60.00	140.00	34.09	27.55			0.8083
80.00	176.00	18.41	14.66			0.7961
98.89	210.00	11.46	8.992			0.7846
100.00	212.00	11.18	8.764			0.7839

Paragon Scientific Ltd. certifies that the kinematic viscosity measurements have been made in accordance with ASTM D2162 using long capillary Master Viscometers at all temperatures. See also ASTM D445, D446, D2171, ISO 3104, ISO 3105, IP 71 Sections 1 and 2 and IP 222. The viscosity data reported is based on the primary standard of pure water at 20°C (ITS-90) having a value of 1.0034 mm^2/s (cSt) ± 0.17%, as adopted by NIST, ASTM, IP and ISO (ISO 3666). Density measurements were made in accordance with ASTM D1480. Temperature measurements were made using thermometers specified in ASTM D2162 which have a current calibration traceable to the National Physical Laboratory (NPL), National Institute Standards and Technology (NIST) and other recognised national standards laboratories. SUS and SFS values have been calculated in accordance with ASTM D2161 where stated. The calibrations of this product are traceable to NIST.

Uncertainties:

	Expanded Uncertainty	
Viscosity Range	**Kinematic Viscosity mm^2/s (cSt)**	**Dynamic Viscosity mPa·s (cP)**
0.3 to 7.4	± 0.07 %	± 0.07 %
7.4 to 10	± 0.09 %	± 0.09 %
10 to 30	± 0.12 %	± 0.12 %
30 to 72	± 0.14 %	± 0.14 %
72 to 180	± 0.15 %	± 0.15 %
180 to 520	± 0.17 %	± 0.17 %
520 to 1000	± 0.19 %	± 0.19 %
1000 to 2700	± 0.20 %	± 0.20 %
2700 to 8000	± 0.22 %	± 0.22 %
8000 to 82 500	± 0.23 %	± 0.23 %

Uncertainties stated on this certificate do not include the uncertainty for the value of the viscosity of water at 20°C (ITS-90) having a value of 1.0034 mm^2/s (cSt) ± 0.17%.

Density Uncertainties: Expanded Uncertainty ± 0.01 %

The reported expanded uncertainty is based on a combined standard uncertainty multiplied by a coverage factor of $k=2$, providing a level of confidence of approximately 95%.

The evaluation has been carried out in accordance with UKAS requirements.

Notes: The shelf life of this product is guaranteed until the expiry date, provided the bottle is unopened and stored at ambient temperature (15 to 30°C). The guarantee is void if the bottle seal is broken but the product should remain stable for 3 months after opening if stored correctly. Filtration of product before use is not necessary. No minimum volume is required to guarantee homogeneity.

Units: Kinematic Viscosity: 1 cSt = 10^{-2} St = $10^{-6} m^2/s$ = 1 mm^2/s

Dynamic Viscosity: 1 mPa·s = 10^{-3} Pa·s = 1 cP = 10^{-2} P

Dynamic Viscosity = Kinematic Viscosity x Density (at the same temperature)

LIITE 3

ÅA, Understanding Low Temperature Corrosion in BL Combustion
Phase 2 – diplomityö 29.10.2015

ÅBO AKADEMI

Master's Thesis

Low temperature corrosion in black liquor recovery boilers due to hygroscopic salts

Henri Holmblad

[Pick the date]

[Type the abstract of the document here. The abstract is typically a short summary of the contents of the document. Type the abstract of the document here. The abstract is typically a short summary of the contents of the document.]

List of content

1. Introduction

The main target with this project was to investigate hygroscopic and corrosive properties of different salts present in recovery boiler ash, to clarify at which temperatures and water vapor concentrations they absorb water and cause corrosion in low temperature areas of a recovery boiler. For this purpose a laboratory set-up was built to test these hygroscopic and corrosive properties at different temperatures ranging from 70°C to 150°C at different water vapor concentrations: 25, 40, 60 or 80 vol%. The highest levels are representative of the locally high concentration of water in the flue gas near the soot blowers. Sufficiently stable temperatures and water vapor concentrations were maintained and the corrosion of carbon steel coupons was identified by: visual inspections, measured as weight change, and by SEM/EDX for more comprehensive analysis. The different salts and ashes investigated were: Na_2SO_4, $NaHSO_4$, Na_2CO_3, NaCl, KCl, and two samples of modern recovery boiler (ESP) ash from a location in Scandinavia, with the difference that one ash sample is from the processing of softwood and the other from hardwood. At a given temperature, the humidity at which a salt absorbs water is called the humidity of deliquescence. The observed corrosion is consistent with sorption of water by the salts. The main conclusion is that hygroscopic salts will absorb water above the water dew point and in such cases enhance the probability of corrosion on carbon steel surfaces.

2. Background

The underlying cause of low temperature corrosion in recovery boilers has not been clearly documented, and the main reason for maintaining an elevated flue gas temperature has been based on the hypothesis of an assumed sulfuric acid dew point. New corrosion probe studies and SO_3/H_2SO_4 measurements have shown that there is no H_2SO_4 and thus no acid dew point in modern recovery boilers [1]. Furthermore, in one study at a sulfite mill where there was high SO_2, an elevated dew point that was above the water dew point was recognized, but well below the acid dew point [1]. This gives a good reason to further investigate low temperature corrosion in recovery boilers. It is important to understand the cause of low temperature corrosion and to map the conditions in which it can occur, especially in such cases where companies are considering lowering their flue gas temperatures.

The fly ash in recovery boilers contains hygroscopic salts, such as Na_2CO_3, Na_2SO_4, and $NaHSO_4$ etc. Hygroscopic salts will absorb moisture from the flue gas at a temperature higher than the pure water dew point. When the humidity in the flue gas reaches a critical level, the solid salt particle transforms into an aqueous solution, which can lead to corrosion of the steel surfaces. This sort of behavior is very apparent with $NaHSO_4$. Different salts have their own specific relative humidity at which the particle starts to absorb moisture. This is referred to as the relative humidity of deliquescence. Thus, one leading hypothesis is that if hygroscopic salts are present, water can be absorbed during periods of high humidity and form an aqueous solution at the steel surface, resulting in corrosion.

3. Modern Recovery Boilers

Recovery boilers are used in pulp mills throughout the world with the twin objective of recovering both chemicals and thermal energy. This makes recovery boiler design more complex than virtually any other boiler application, why it is not just the largest unit by size in a paper mill, but also the most expensive one to build [2].

The sodium sulfate or Kraft pulping process was patented in 1884. The design of the black liquor recovery boiler is attributed to G.H. Tomlinson and the first unit having water walls was constructed in 1934 by Babcock and Wilcox. The Kraft process would not be economically viable without the black liquor recovery boiler (BLRB). The purpose of the BLRB is to reclaim the spent pulping chemicals in the black liquor by the process of combustion and to capture the heating value as steam to generate electricity and supply process steam demands [3]. A contemporary BLRB may be either two drum design, which is popular for operating pressures less than 6.2 MPa, or single drum design, which is popular for pressures above 6.2 MPa. The single drum design has the advantages of removing the drum from the corrosive flue gases and eliminating potential leakage from rolled tube joints. The combustion gases are highly corrosive, particularly at temperatures necessary for operation above 6.2 MPa. Above 6.2 MPa, special corrosion protection, such as composite tubes, chromizing, metal spray coating and stainless weld overlay, is provided for furnace tubes [2]. The furnace of a BLRB is generally taller than a utility or industrial water tube boiler of similar steam generating capacity, due to the poor heat transfer in the furnace area [3].

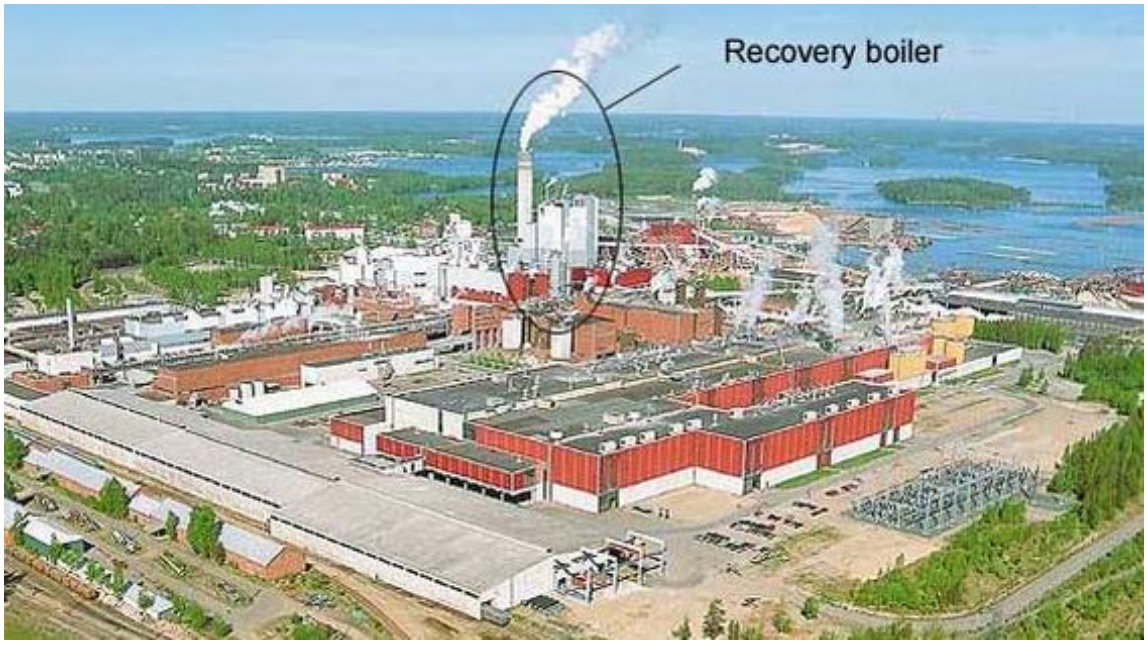

Figure 3.1. Black liquor recovery boiler and its location in a pulp mill (Courtesy of UPM-Kymmene).

The pulp production capacity of a mill determines the size of a BLRB. For each ton of pulp, about 1400 kg of dry solids are generated. A typical large BLRB will process up to 3000 tons/day dry solids and be rated for 10.4 MPa maximum allowable working pressure (MAWP) and up to 400 tons/h steam [2]. The biggest boilers to date have the capacity of 6000 tons/day of dry solids [4] and a boiler with the capacity of 11,600 tons/day is scheduled for start-up in the second quarter of 2016 [5].

BLRBs have auxiliary fuel (gas or oil) burners located near the floor to raise the temperature for initiating combustion of the black liquor and to stabilize combustion if an upset occurs. Auxiliary burners may also be provided higher in the furnace to supplement the heat input during times of limited liquor availability or other upsets. Generally, auxiliary fuel is shut off once firing of black liquor has become self-sustaining and stabilized [2].

3.1 Operational overview of a black liquor recovery boiler

Recovery boilers (figure 3.2) are constructed to burn black liquor and recover inorganic chemicals used in pulp mills. The heat from black liquor combustion is recovered and used for generating superheated steam that is released through turbines in order to generate electricity. The generated steam is also used in the mill [3].

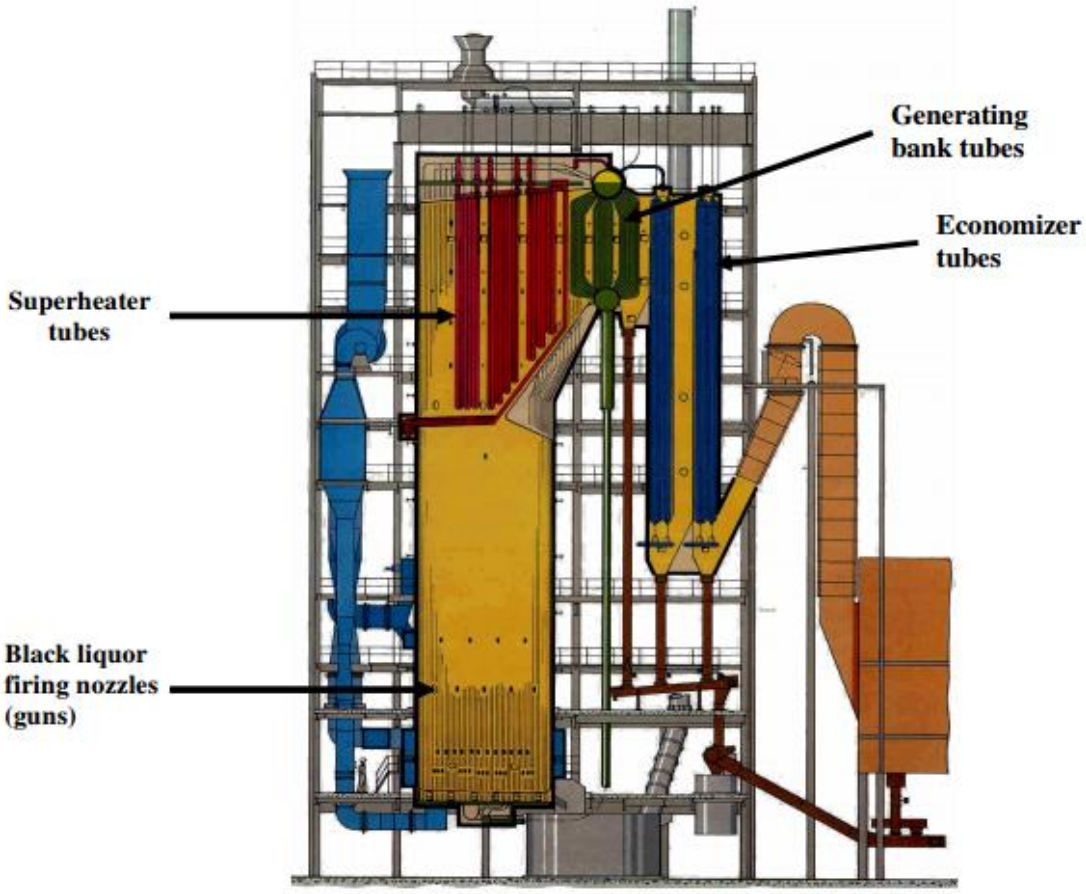

Figure 3.2. Modern recovery boiler. The furnace section is in the lower part of the recovery boiler, where the black liquor guns are mounted. The Superheater generates superheated steam for power production, while the generating bank and the economizer increase the efficiency of the heat convection. The electrostatic precipitator (ESP) can be seen to the far right in the figure as an orange colored box. The flue gas stack would follow the ESP [6].

The recovery of thermal energy released from the combustion of black liquor in the furnace, is managed by a system of water pipes, which enables the heat convection needed in the steam and power production. The feedwater is first preheated in the economizer by the flue gases, in the back end of the boiler, after which the preheated water enters the waterwall, which is a system of water pipes inside the walls, surrounding the furnace in the lower section of the recovery boiler. Here the water is heated to saturated steam. From the waterwall, the water is led to the boiler bank, or generating bank, where saturated steam is being separated in the drum. The saturated steam is afterwards even further heated and transformed into superheated steam in the superheater and used for power production when released through turbines, to generate electricity [7].

In the lower parts of a recovery boiler is the furnace section, which is schematically depicted in figure 3.3. The furnace is basically a rectangular box with openings for nozzles (liquor guns) that spray black liquor into the furnace, where the liquor droplets are mixed with the combustion air. In the bottom section of the furnace lays the char bed, which consists mainly of a smelt of the inorganic salts, mainly Na_2S and Na_2CO_3. In the floor section, beneath the char bed, are the smelt outlets or spouts, through which the inorganic smelt can leave the furnace to be recovered and processed for reuse in the mill [7].

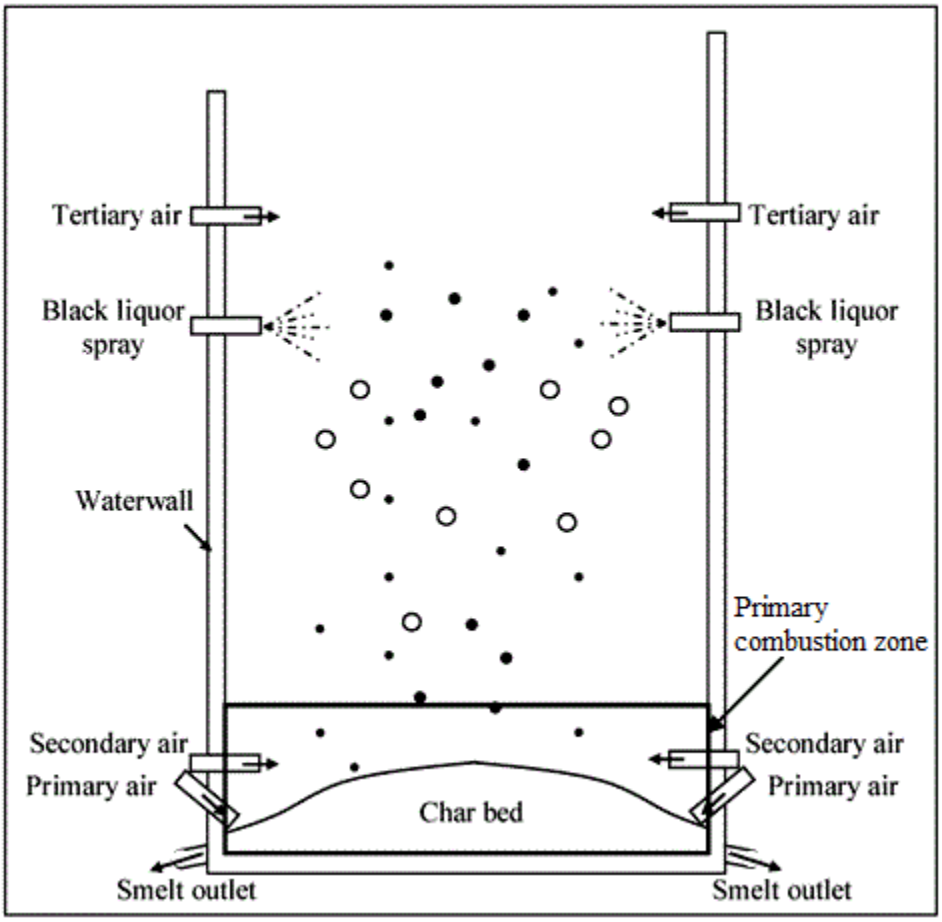

Figure 3.3. A schematic depiction of the combustion of black liquor in a typical recovery boiler furnace [7].

The recovery of inorganic compounds, mainly sodium and sulfur, from the black liquor makes up its own complex challenges. Ideally all the diverse sulfur and sodium compounds would be transformed in a recovery boiler to sodium sulfide (Na_2S) and sodium carbonate (Na_2CO_3) and be contained in the smelt at the bottom in the furnace. This would mean that none of the sodium or sulfur would be released into the furnace gas. In reality this process is complex and the reduction or molar ratio (Na_2S)/total S) in the smelt of an actual process is typically 90 – 95% [8].

3.2 Black liquor

Kraft black liquor is the spent liquor from the process of pulping wood with an aqueous solution of NaOH and Na_2S. The chemicals, NaOH and Na_2S, are used in a strong solution referred to as cooking liquor, which after digestion turns black from the organics, mainly lignin, contained in the wood [9]. It consists of a complex mixture of water, inorganic salts, and digested organics. The elemental composition for a typical open cycle Kraft process can be seen in table 3.1. The contents of particularly sodium and sulfur may vary considerably between two processes. For example the sulfidity and the S/Na_2 ratio of the process tend to be notably higher in Scandinavian pulp mills than in North American pulp mill [10]. To recover these chemicals from the used liquor, it is first concentrated by evaporation to 65% - 80% dry solids, before it is used as fuel in the recovery boiler [9].

In addition to the main compounds of sodium and sulfur there are also present other elements, such as chlorine and potassium, which come from the wood and chemicals used in the pulp mill. The chlorine content in mills is usually 0.1 – 0.5 % of the liquor dry solids, but does vary greatly. Chlorine originates from the wood itself or from an outer source, for example sea water, depending on the wood handling and storage. Potassium is a natural mineral found in wood and constitutes approximately 1 to 3 % of the liquor dry solids content [8]. Potassium and chlorine are controlled by ash dumping, crystallization or ash leaching systems in the precipitator ash.

Table 3.1. An example of the elemental composition of Kraft black liquor before the mixing tank [8]

	Wt% dry solids
C	38.2
H	3.4
O	31.1
N	0.1
S	5.2
Na	19.8
K	1.9
Cl	0.10
Others (Ca,Si,Fe,Mg,Al,Mn)	0.2
S/Na_2 = 0.38 mol/mol	

Sulfur is one of the major elements in black liquor and has a great impact on the process in general and on the flue gas chemistry in particular. The various formations of sulfur are given in table 3.2. Different combinations of sulfuric compounds will, when the temperature drops, start to condense and form ash particles in the flue gas [3]. Sulfur is thereby of much interest when investigating low temperature corrosion, because of its tendency to react with alkali compounds and form hygroscopic salts which can cause corrosion to carbon steel, due to water absorption from the flue gas in black liquor recovery boilers.

Table 3.2. An example of the distribution of sulfur compounds in black liquor [8]

	% sulphur of total sulphur
Sulphide, S^{2-}	11
Thiosulphate, $S_2O_3^{2-}$	36
Sulphite, SO_3^{2-}	13
Sulphate, SO_4^{2-}	5
Organic sulphur (balance)	35
Total	100

The combustion of black liquor droplets can be divided into different stages: drying, pyrolysis, and finally the combustion of carbon in the char conversion, figure 3.4. All of the emitted substances are to take part as constituents in the flue gas and will form

various compounds, such as salts, by condensation to fume particles. Approximately 90% of the fumes come from the burning of black liquor droplets during the flight. About 10% of the fumes are vaporized from the smelt bed, through oxidation and reduction reactions of the remaining inorganic constituents in the smelt [7].

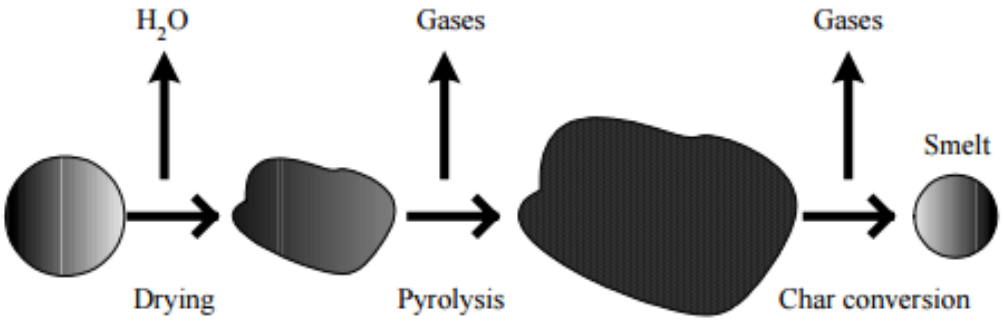

Figure 3.4. Conversion stages of a black liquor droplet [11].

3.3 Flue gas composition in recovery boilers

The flue gas composition in a recovery boiler consists of a complex gas mixture of various gaseous- and solid components. The main flue gas components are nitrogen (N_2), water (H_2O), carbon dioxide (CO_2), and oxygen (O_2). The sulfur is usually present in the furnace gas as hydrogen sulfite (H_2S), carbonyl sulfide (COS), and sulfur dioxide (SO_2). Sodium appears as sodium hydroxide (NaOH) and metallic sodium (Na) [12]. In figure 3.5, the conceptual chemical reactions are displayed in accordance to the physical presence of different combustion products in the lower parts of a recovery boiler. Typical pyrolysis gases that are formed are for example H_2S, NH_3, H_2, CO, and different hydrocarbons. The coke remaining after pyrolysis takes the longest time to combust and is recognized as the main source of CO and some CO_2 in the lower parts, close to the smelt bed, while higher up in the boiler the CO will react with O_2 and form CO_2 [13].

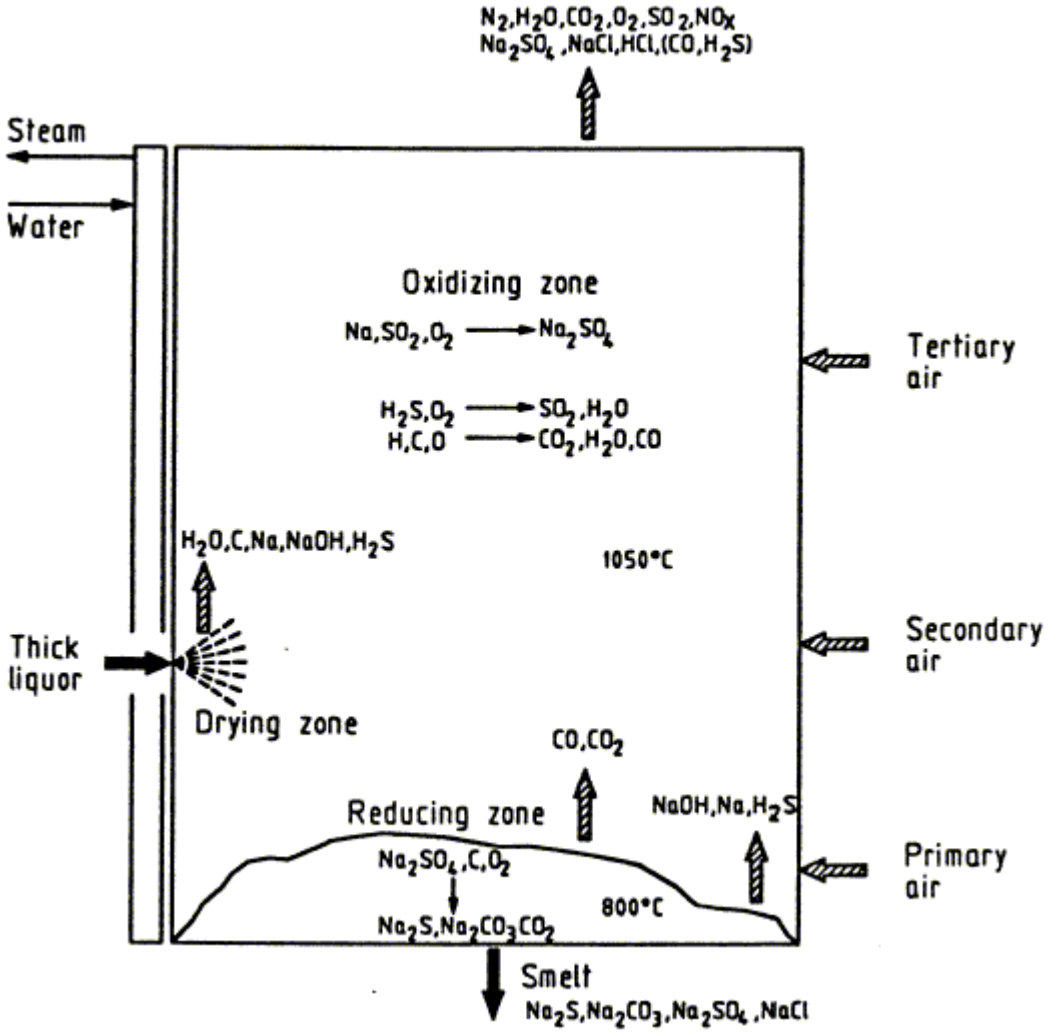

Figure 3.5. Conceptual chemical reactions and combustion products in a recovery boiler [14].

3.3.1 Vapors of sodium and sulfur

Black liquor contains approximately 20 wt% sodium, of which most of it is released into the furnace gas during char burning due to the reactions of sodium carbonate (Na_2CO_3) and char carbon at temperatures where the salts are in a molten state [3][16][17]. These reactions become significant when the temperature exceeds 900°C [3]. Gasified sodium reacts quickly with water vapor and chlorides in the furnace gas to form sodium

hydroxide and sodium chloride [16]. In figure 3.6 is a general depiction of the sodium balance in a recovery boiler. The values represent the amount of sodium in grams per kilogram of black liquor burned.

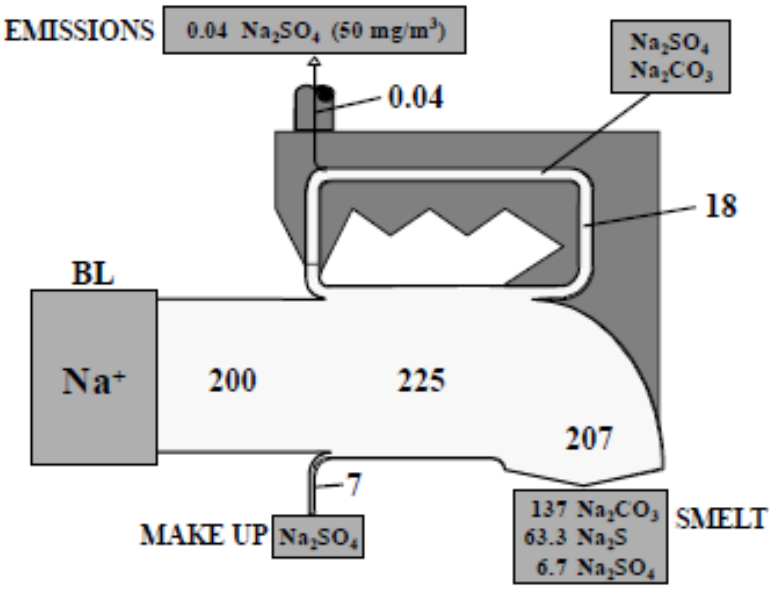

Figure 3.6. Sodium balance in a recovery boiler. The values in the figure represent the amount of sodium in gram / kg solids of black liquor [8].

The flue gas contains also sulfur, often as hydrogen sulfite (H_2S), methanethiol or methyl mercaptan (CH_3SH), dimethyl sulfide ($(CH_3)_2S$), and dimethyl disulfide ($(CH_3)_2S_2$) [15]. The sulfur in the furnace gas originates from the pyrolysis of black liquor and is released by a completely different mechanism than sodium [3]. A significant fraction of sulfur is in black liquor in the form of sulfide and is released in a relatively narrow window of 300 - 400°C during black liquor droplet heating [3]. Sulfur is typically to be found at concentrations around 200 – 1000 ppm in the lower section of a boiler [13]. Higher up in the boiler the different sodium compounds are oxidized by the secondary and tertiary air inlets to form sulfur dioxide (SO_2) [15]. A schematic presentation of the sulfur flows released in a recovery boiler is given in figure 3.7.

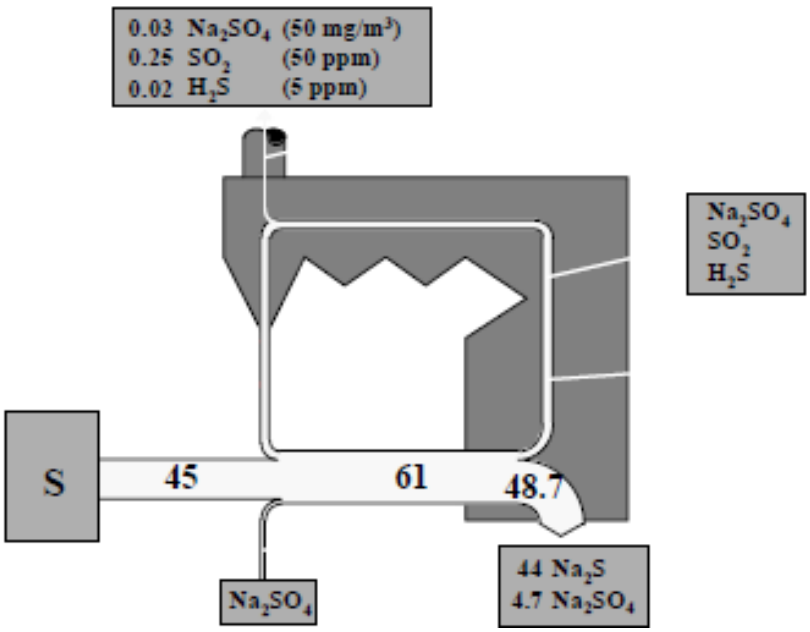

Figure 3.7. Sulfur balance in a recovery boiler. The values in the figure represent the amount of sulfur in gram / kg solids of black liquor [8].

The lower furnace and char bed are crucial for the entire recovery boiler chemistry. The conditions in the lower furnace almost exclusively determine how sulfur and alkalines are distributed. Black liquor spraying, dry solids content and air delivery into the lower furnace have a major impact on the lower furnace temperatures. High lower furnace temperatures promote sodium fuming and decrease sulfur release [3]. The concentration of gasified sodium increases rapidly at temperatures over 1000°C, while the concentration of sulfur decreases accordingly, figure 3.8 [10].

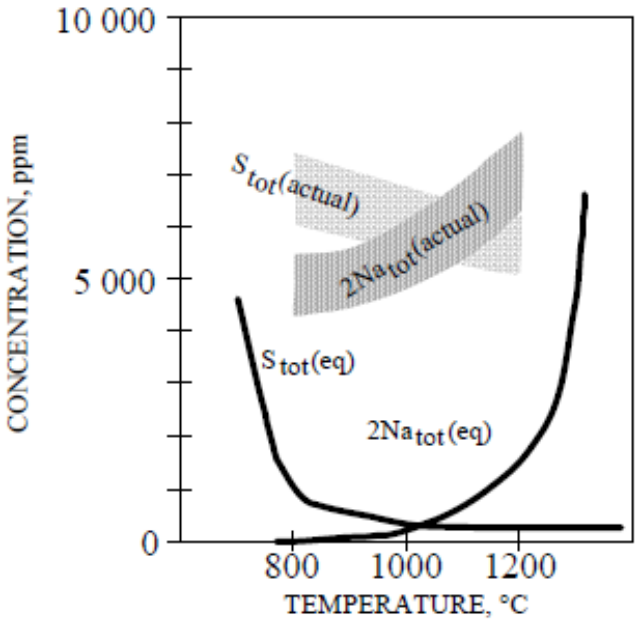

Figure 3.8. The concentrations of gasified sulfur and sodium in a recovery boiler as function of temperature, based on equilibrium and empirical values [8].

Alkali hydroxides and alkali chlorides react with sulfur dioxide to form sulfates (reaction 1 and 2). If there is not a sufficient amount of sulfur dioxide available, carbonates are formed instead through surface reactions [17]. The surface reaction mechanism (reaction 3) is thought to function by CO_2 molecules adsorbing to the surface of a sodium hydroxide particle. These reactions take place higher up in the boiler, where the temperature is lower. Alkali carbonates and alkali sulfates will condense to small particulate when the temperature drops. Hereafter they are to be removed from the flue gas by the electrostatic precipitator (ESP) [17].

$$2NaOH\,(g) + SO_2\,(g) + 1/2O_2 \rightarrow Na_2SO_4\,(g, c) + H_2O\,(g) \quad (1)$$

$$2NaCl\,(g) + SO_2\,(g) + 1/2O_2 \rightarrow Na_2SO_4\,(g, c) + 2HCl\,(g) \quad (2)$$

$$2NaOH\,(g) + CO_2\,(g) \rightarrow 2NaOH\,(c) + CO_2\,(g) \rightarrow Na_2CO_3\,(c) + H_2O\,(g) \quad (3)$$

The chemical reactions taking place in the flue gas are strongly affected by the molar ratio of sodium and sulfur, and temperature. This can be seen in figures 3.9 and 3.10 at different levels in a recovery boiler. Figure 3.9 illustrates the case of a low furnace

temperature and a high sulfidity in the black liquor. This relation is reversed in figure 3.10, so that the furnace temperature is high and the black liquor has a low sulfidity. Actual boilers generally operates somewhere between these two extremes. The widths of the lines, describing material flow, are proportional to the magnitude of each flow in these two figures [10].

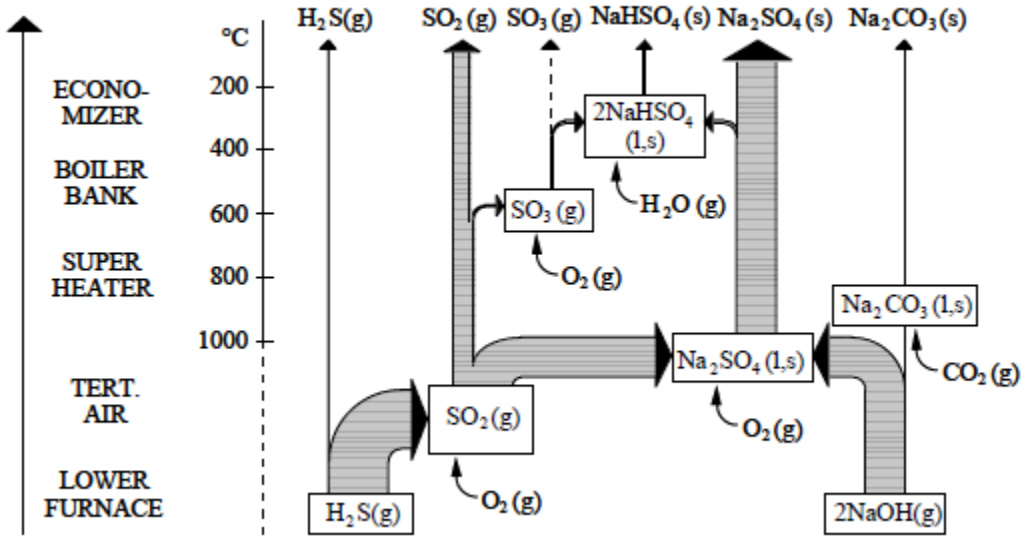

Figure 3.9. Reactions and products of different gasified compounds in the flue gas throughout a recovery boiler system with low furnace temperature and high sulfidity. The molar ratio in the flue gas is $S/Na_2 = 1.5$, in this particular case. Low temperature (mainly 200°C or less) corrosion due to hygroscopic salts is foremost to be found in this figure in the economizer region [10].

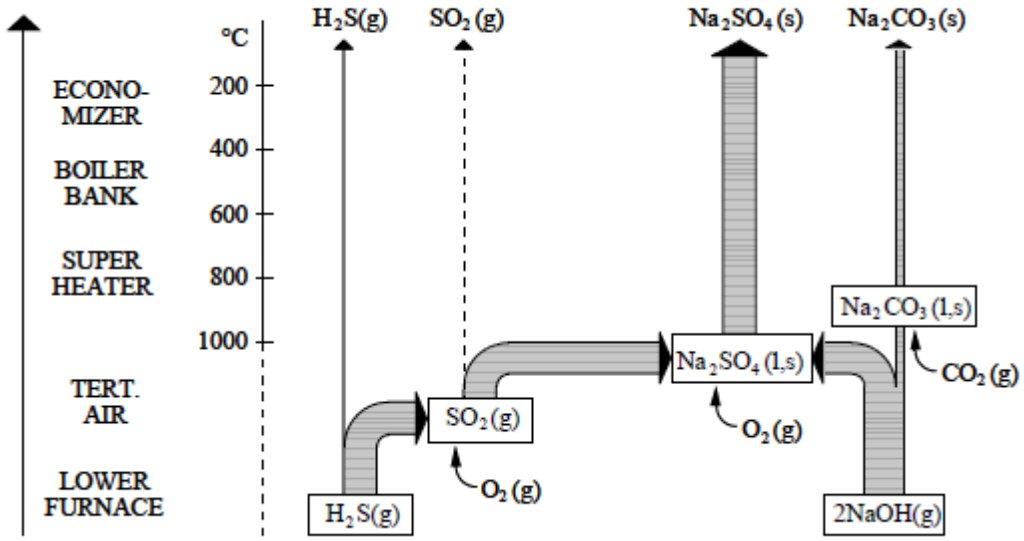

Figure 3.10. Reactions and products of different gasified compounds in the flue gas throughout a recovery boiler system with high furnace temperature and low sulfidity. The molar ratio in the flue gas is $S/Na_2 = 0.8$, in this particular case. Low temperature (mainly 200°C or less) corrosion due to hygroscopic salts is foremost to be found in this figure in the economizer region [10].

In both figure 3.9 and 3.10, the first reaction that tend to take place is the oxidation of sulfur to sulfur dioxide. The completeness of this oxidation is governed by the air ratio and efficiency of mixing the air with the combustion gases [8][10]. In figure 3.11 is a more detailed schematic of the oxidation of sulfur and sodium containing compounds in a modern Kraft recovery boiler, burning high dry solids black liquor. Sulfur is mainly released during the devolatilization stage, mostly as H_2S and methyl mercaptan (MM) [18][19].

The air ratio, expressed as $\lambda<1$ and $\lambda>1$, tilts the reaction products towards H_2S and SO_2 or Na_2SO_4, depending on the amount of oxygen in the furnace, as seen in figure 3.11. If the conditions are sub-stoichiometric ($\lambda<1$), H_2S and SO_2 may coexist, as high as above the tertiary air level, with Na_2SO_4, which is formed by SO_2 reacting with Na, NaOH and $NaCO_3$ in the presence of oxygen [20][21]. Virtually all the gaseous sulfur species will

eventually be captured and become a part of the fly ash, why SO_2 emissions in modern Kraft recovery boilers are rare [21].

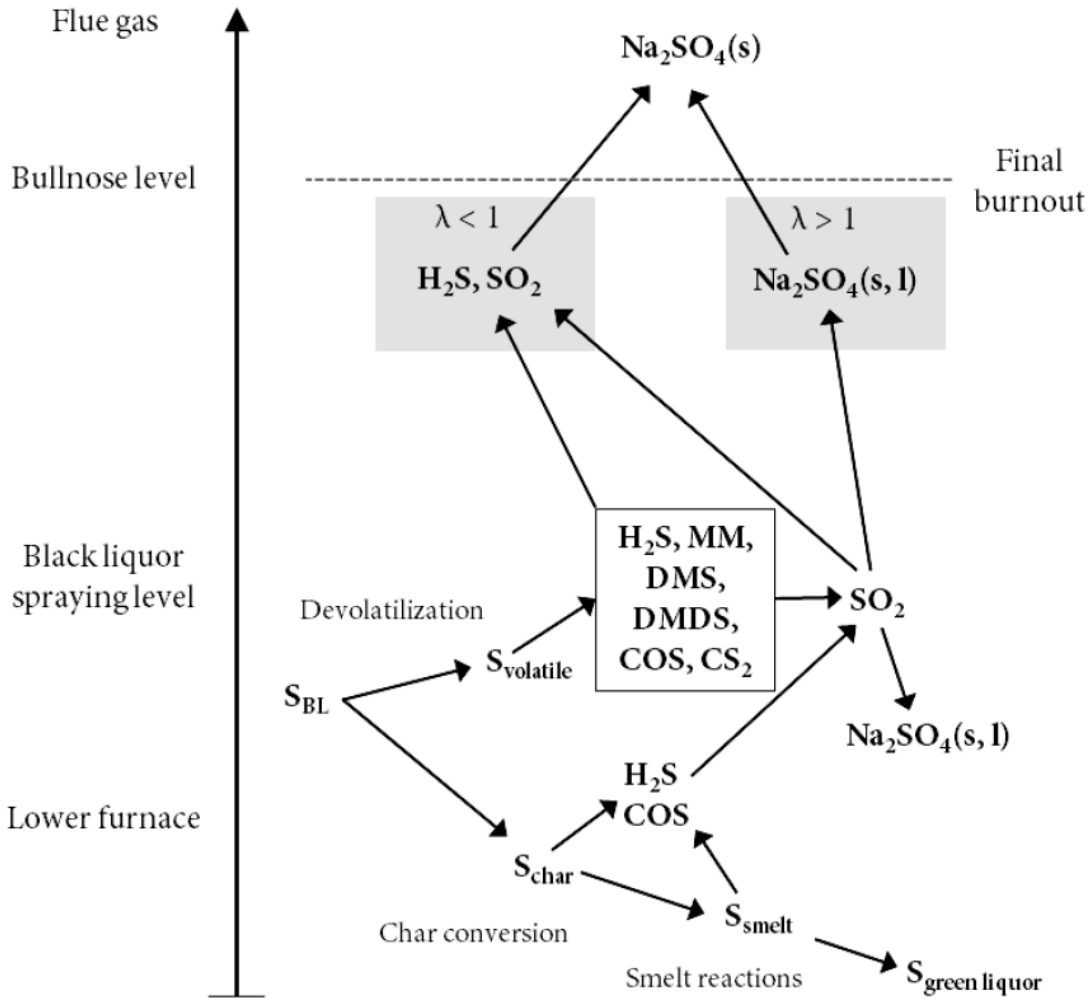

Figure 3.11. Main sulfur pathways in the Kraft recovery boiler. MM = methyl mercaptan, DMS = dimethyl sulfide, DMDS = dimethyl disulfide [21]

3.3.2 Vapors of chlorine and potassium

Chlorine occurs almost exclusively as alkali chlorides NaCl and KCl in the lower part of the furnace in a black liquor recovery boiler. Main compounds of potassium in the lower furnace are KOH and KCl. The vaporization of chlorine and potassium compounds into the flue gas is strongly dependent on temperature, with potassium compounds being more volatile than sodium compounds. Potassium is therefore enriched in the fume. The vaporized chlorine and potassium compounds will condense and form ash, as the flue gases cool on the way to the chimney. The ash captured by electrostatic precipitators consists of this type of fine particulate ash, in the size range of 0.2 – 1 µm. In addition to this type of ash, coarser particles in a size range of 10 – 100 µm occur in large quantities in the super heater area and in the first dust hoppers [8].

3.4 Formation of deposits

Deposits are formed in different parts of the boiler by three types of particulate matter; *carryover*, *fume* and *intermediate sized particles* [22]. The presence and quantity of different types of deposit varies throughout the locations in a recovery boiler [22][23]. In figure 3.12 is a schematic depiction of the types of deposits forming in a recovery boiler.

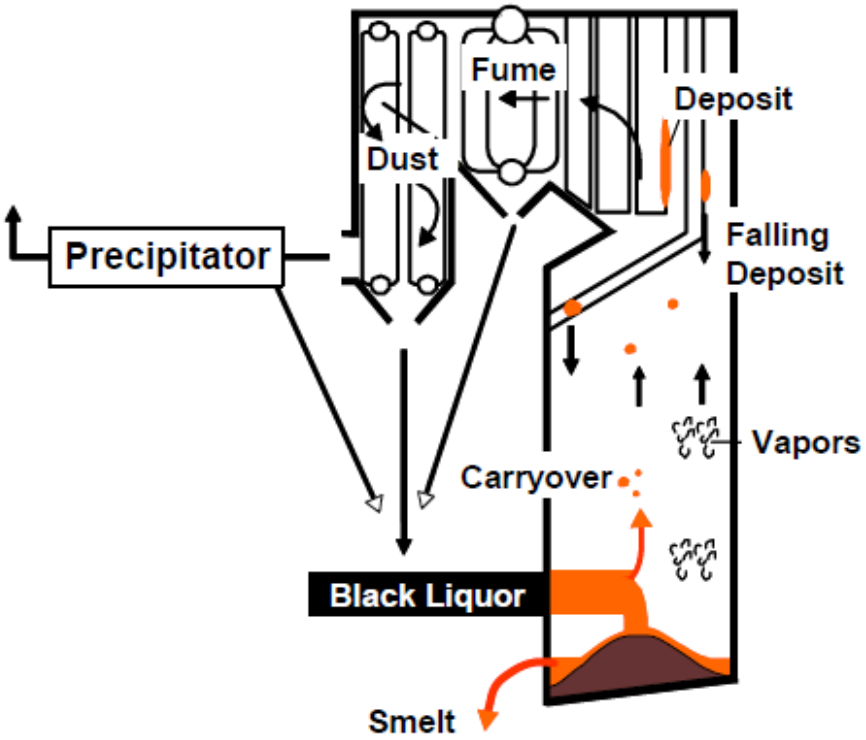

Figure 3.12. Deposit formation in a black liquor recovery boiler [22].

Carryover deposits are usually pink in color, fused and very hard smelt-like formations on tube surfaces. They are a result of collisions on the tube surface of relatively large (0.01 – 3mm) molten or partially molten smelt particles, and/or of partially burned black liquor solids droplets entrained in, and carried up with the gases [22].

Fume deposits consists of condensed vapors of sodium and potassium compounds in the flue gas and form a white and usually soft deposit layer. Fume deposits are a result of either direct condensation on cooler surfaces, or indirectly by the formation of condensed fume particles in the flue gas stream and transferred to the steel surface by turbulent deposition. The size of these fume particles varies from 0.1 to 1 µm [22].

Intermediate sized particles (ISP) are believed to form as a result of fragmentation of black liquor droplets during combustion and/or ejection of material from molten smelt pool during char burning. ISP deposits tend to have a similar appearance to carryover

deposits, with an average particle size distribution of 1 to 100 µm. These sorts of deposits are to be recognized as a white layer, containing no char [22].

3.4.1 Precipitator ash composition

It has been estimated that precipitator ash (or dust) contains about 95 wt. % fume and 5 wt. % carryover and ISP. This mixture is quite similar to that of the fume found in the upper boiler region. The chemical composition is for the most part sodium sulfate (Na_2SO_4) and some sodium carbonate (Na_2CO_3), combined with some enrichment of chloride and potassium. The fume composition, and thereby precipitator ash composition, is greatly influenced by the bed temperature in the lower furnace and the black liquor sulfidity. A high bed temperature in the furnace produce more fume and also fume with higher carbonate content and less sulfate [3].

3.4.2 Precipitator ash pH

Measurements of the pH in ash taken from the flue gas duct or the electrostatic precipitator (ESP), gives information about whether the ash contains carbonate or bisulfate. The presence of carbonate results in an alkaline water solution, while only a few percent of bisulfate reduces the pH in the water solution by several units. Pure sodium sulfate does not affect the pH and it will stay at pH 7. The relationship, and impact on pH in a water solution, between concentrations of sodium carbonate (Na_2CO_3) or sodium bisulfate, and water is shown in figure 3.13 [8].

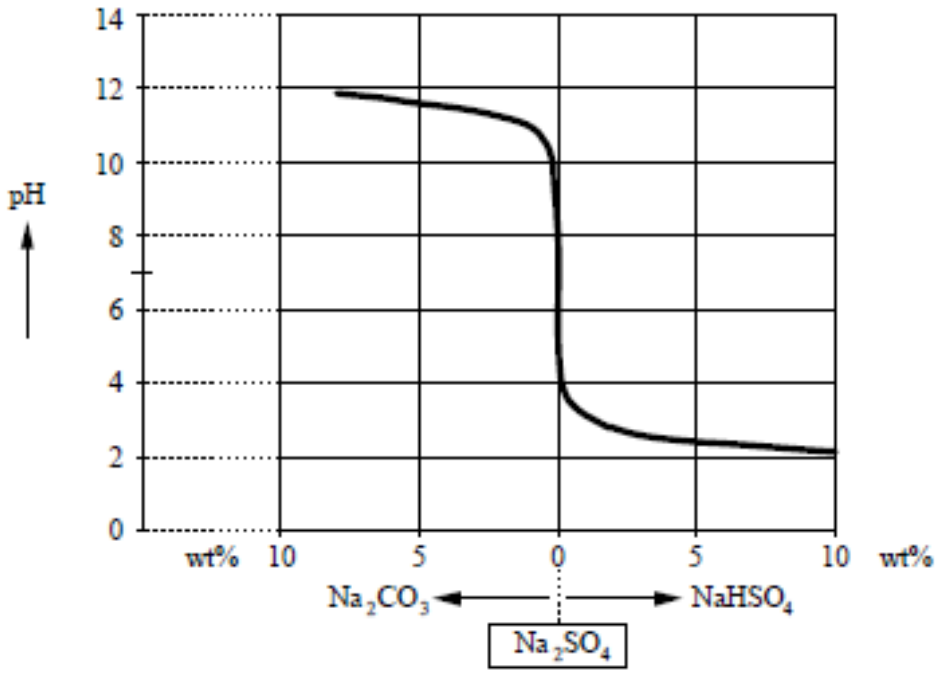

Figure 3.13. Precipitator ash pH as a function of the concentration of sodium carbonate (Na_2CO_3) and sodium bisulfate ($NaHSO_4$) in a water solution with 1% ash [8].

4. Corrosion in recovery boilers

The large quantity on inorganics and the low temperature of the ash make black liquor one of the most troublesome industrial fuels used for steam and power generation [24]. Corrosion can be found in all parts of the boiler and it occurs in various forms, for example: sulfidation, thermal oxidation, stress corrosion cracking, molten salt corrosion, pitting corrosion, and aqueous corrosion. In order for corrosion to occur, a steel surface must be exposed to corrosive gases and/or deposits. Massive deposit accumulation will decrease the heat transfer efficiency of the boiler and can locally form a corrosive environment and damage the construction [24].

4.1 Low temperature corrosion in recovery boilers

Corrosion at elevated and high temperatures in recovery boilers has gone through quite extensive inspection and the knowledge and understanding of such behavior is fairly well understood, compared to low temperature corrosion caused by salts. Often the steel properties have been the main targets in such studies. The experiments and results presented in this work are entirely focused on the properties of different salts, often occurring in the fly ash and to be more specific, it is the corrosion enabling interaction between salt, water vapor and temperature that is studied. The aim is to see whether there is corrosion or not, and under which conditions it happens.

4.2 Corrosion due to acid dew point

Several authors have throughout the years pointed out the dangers of sulfuric acid corrosion in black liquor recovery boilers. Sulfuric acid in the flue gas would lead to severe corrosion of components, such as economizers, air preheaters, and the flue gas duct, if their material temperature is below the sulfuric acid dew point temperature [25]. The concept of an acid dewpoint has been the driving force in maintaining an elevated temperature in e.g. the feed water in the economizer. According to Honghi Tran, a feedwater temperature at about 130°C - 150°C is necessary for avoiding the formation of condensed H_2SO_4 at cooled tube surfaces at the feedwater entrance, especially in boilers which burn low solids and high sulfidity liquor. Furthermore the conclusion is that acid dew point corrosion does occur in electrostatic precipitators [24].

In a study submitted for consideration for publication in the Tappi Journal (1987), on behalf of the Institute of paper chemistry (IPC), about corrosion in electrostatic precipitators by David C. Crow [26], it was concluded that the principal cause of corrosion in precipitators is dewpoint corrosion; and that this form of corrosion involves the condensation of acid vapors, primarily sulfuric acid, onto structural surfaces and consequent attack of the material [26]. Sharp [27] highlights the risk of corrosion in

economizers, precipitators and stacks by acid furnace gases (e.g. CO_2, NO_x, SO_x) dissolving in, on steel surfaces, condensed moisture; and forming an acidic condensate that will dissolve carbon steel.

New in-situ probe measurements by Vainio et al. [1], shows however that the fear of an acid dewpoint might be based on false premises, at least in modern Kraft recovery boilers. An in-situ implementation of a salt method was used in field measurements, in which the presence of sulfuric acid in the flue gas in both a Kraft and a sulfite recovery boiler was studied. These in-situ measurements by Vainio et al., showed that corrosion due to sulfuric acid condensation during normal operation did not occur. The SO_2 level before the scrubber in the sulfite recovery boiler was above 1000 ppmv; however, no H_2SO_4 was detected in the flue gas. This implies, according to Vainio et al., that all the H_2SO_4 formed in the combustion had reacted with the ash particles to form sulfates.

Table 3.3. Sulfur dioxide and H2SO4 measured in a Kraft and sulfite recovery boiler [1]

	SO_2 (ppmv, dry)	H_2SO_4 (ppmv, dry)
Kraft recovery boiler	<2	0
Sulfite recovery boiler	1000-1400	<1

The H2SO4 concentration was also measured during the start-up of a Kraft recovery boiler. Heavy fuel oil was combusted during the start-up and conditions were challenging, due to a heavily-sooting flame and a highly-diluted flue gas. The excess O_2 in the flue gas measured 19.5 vol%. Some H_2SO_4 was measured while the concentrations were low due to the highly diluted flue gas. No significant amount of sulfur was found in the particle filter. The 1.4 ppmv H_2SO_4 measured below the superheater tubes corresponds to a 4% conversion of SO_2 to H_2SO_4 [1].

The gases could nonetheless contribute to the formation of acidic sulfates such as sodium bisulfate ($NaHSO_4$) and potassium bisulfate ($KHSO_4$), which can be responsible

for the pitting corrosion associated with sulfuric acid in economizers and electrostatic precipitators [24]. These acidic sulfates would however show their presence in pH measurements, considering that already a few percent of bisulfates in precipitator ash would give a pH readily below 7 [8]. According to own measurements (chapter 5.3) of electrostatic precipitator ash from a pulp mill in Scandinavia, the pH values were about 10 - 11, why acidic sulfates would not be responsible for any observed corrosion with such a high pH.

4.3 Effect on corrosion of alkaline solutions

Investigations have shown that corrosion of steel decreases with increasing concentrations of an alkali in water, compared with pure water, although there is an intermediate region where the rate of corrosion is actually increased through a certain range of increasing alkalinity. If the alkaline concentration of pure water is increased, the rate of corrosion gradually increases to a maximum and then rapidly falls off to zero [28]. The concentration of the alkaline solution whose strength is just below that in which local corrosion, or pitting, first appears has been called the *lower-limit concentration*. The one in which the rate of corrosion is a maximum has been termed the *critical concentration*, and the one just above, in which the lasts signs of corrosion appear, the *upper-limit concentration*. Sodium carbonate (Na_2CO_3) has an upper limit of 1.3 g (salt) / liter (water), a critical limit of 0.4 g/l, and a lower limit of 0.08 g/l [28]. However, in the case of salt absorbing water, it will always be above the upper limit.

As a general rule, acid solutions (pH < 7) are more corrosive than neutral solutions (pH = 7) or alkaline solutions (pH > 7). Ordinary carbon steel corrodes rapidly in solutions with a pH at 4.5 or less [29]. For pH values above about pH 7, the corrosion rate is observed to fall as pH is increased [30]. This is believed to be due to an increase in the rate of reaction of oxygen with $Fe(OH)_2$ (hydrated FeO) in the oxide layer to form the more protective Fe_2O_3 [30]. According to Ameer et al. [31], is the passivation of carbon

steel in alkaline environments due to the formation of a protective oxide/hydroxide layer, which corresponds to a double layer consisting of an inner magnetite and an outer ferric oxide, according to a Fe_3O_4/Fe^{3+} structure. The passivity of this layer occurs by addition of Cl^- to the alkaline solution, which would enable corrosion of the carbon steel as a result [31].

4.4 Hygroscopic salts and corrosion

Hygroscopy is the ability of a substance to attract and hold water molecules from the surrounding environment. This is achieved through either absorption or adsorption. Many different salts are so hygroscopic that they readily dissolve in the water they absorb. This property is called deliquescence. A saturated solution formed by deliquescent salts with corrosion enabling properties, can attack as an electrolyte in points on a small area, leaving pits and troughs in the steel surface. Depending on the salt, the corresponding iron-sulfate and/or iron-chloride compounds can be formed, in addition to iron oxides [32]. Increasingly thick layers of deposit however, can impede the flue gas humidity from entering the steel surface and thus reduce the risk of corrosion. An increasingly thick layer raises the surface temperature of the deposit, which increasingly reduces the adsorption of flue gas humidity by the hygroscopic salts [32].

4.4.1 The humidity of deliquescence

Deliquescent relative humidity (DRH) is a term generally used in atmospheric chemistry to describe how salt infused aerosols interact with moisture in the atmosphere [33]. To further explain the phenomena, the term DRH can be divided into two categories, where *deliquescence* is a process by which a particle takes up liquid water, lowering its saturation vapor pressure, and where *deliquescence relative humidity* (DRH) is the

relative humidity at which an initially-dry solid first takes on liquid water during an increase in relative humidity. Above the DRH, the solid may not exist [34]. In figure 4.1, DRH is drawn as a function of temperature for salts of KCl, NaCl and (K, Na) Cl. In figure 4.2 the function of DRH and temperature is with respect to 15 vol% water in the gas.

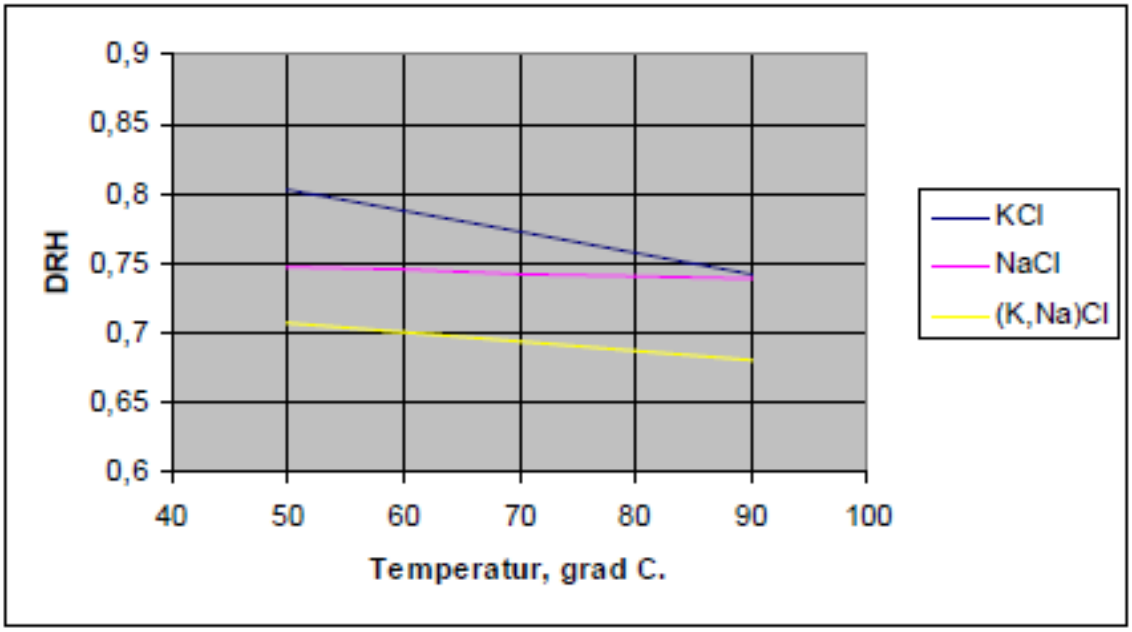

Figure 4.1. DRH as function of temperature for KCl, NaCl and (K, Na)Cl [33].

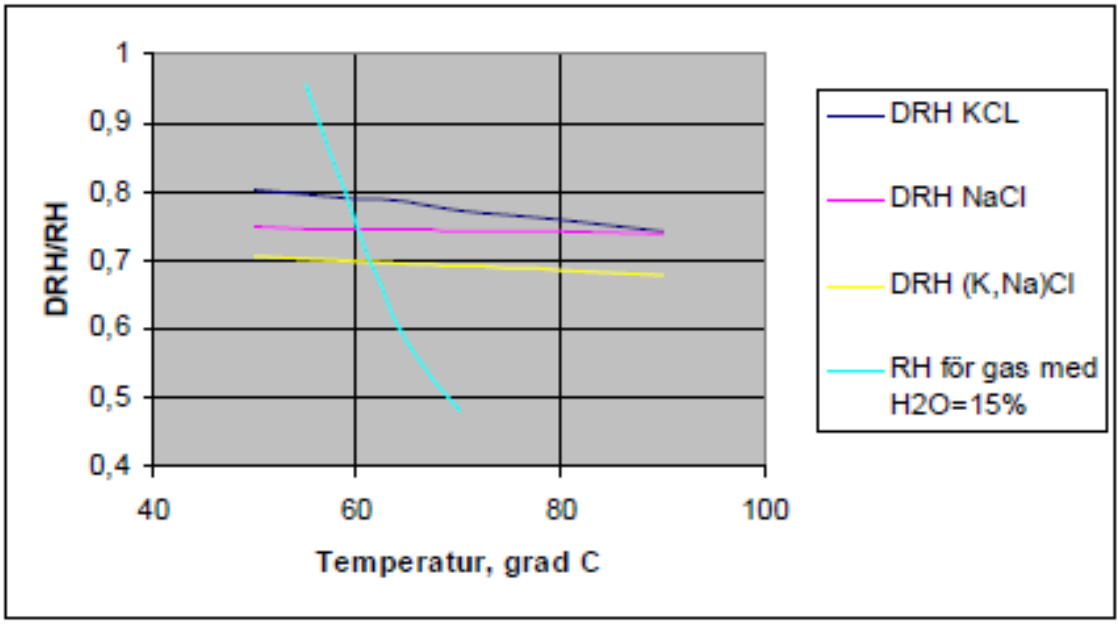

Figure 4.2. The function of DRH and temperature is with respect to 15 vol% water in the flue gas. DRH temperature by salt at 15 vol% H_2O: KCl at 58°C, NaCl at 60°C, and (K, Na) Cl at 63°C [33].

The relative humidity (RH) of air is a function of both water content and temperature. Thus the relative humidity (RH) for a water vapor-gas mixture at the temperature T, is given by

$$RH = p_w / p_0\,(T) \qquad (1)$$

with p_w being the partial pressure of water in the gas phase and $p_0(T)$ being the saturation vapor pressure of pure water at temperature T. Relative humidity is normally expressed as a percentage and thereby should calculations made by equation 1 above, be multiplied by 100. At a temperature, $T_{w,}$ that equals the water dew point, the partial pressure p_w of water is equal to p_0

$$p_w = p_0(T_w) \qquad (2)$$

If there instead of pure water is a salt solution, with the concentration c of a salt with the solubility c_0, the equilibria between the water phase and the gas phase is altered, so that the salt solution has lower partial pressure p_s at temperature T than pure water p_w. This is also the reason behind a higher boiling point at a given pressure for water containing salt, compared to the boiling point of pure water. The water-steam pressure p_s for a salt solution is a function of the salt concentration c in the water-salt solution and temperature:

$$p_s = p_s(T, c) \tag{3}$$

$$p_s(T, c) < p_0(T_w) \tag{4}$$

And:

$$p_s(T, c) < p_s(T, c_0) \tag{5}$$

The lowering of the partial pressure of water, increases with increasing salt concentration c in the solution and is at its lowest when the solution is fully saturated ($c = c_0$). The more soluble a salt, the greater the decrease in partial pressure for a solution.

The deliquescence of relative humidity, or DRH, relates to both relative humidity (RH) and the concentration of a salt by

$$DRH = p_s(T, c_0) / p_0(T) \tag{6}$$

There is a DRH value for every salt and possible double salt as a function of temperature. For condensation of water to occur, the partial pressure of water p_w in the gas phase must exceed the equilibrium partial pressure above the salt solution [35], meaning

$$P_w > p_s(T) \tag{7}$$

which results in

$$RH > DRH \quad (8)$$

This allows the water to be absorbed by the salt and condense to the metal surface at a higher temperature than the pure water dew point, so that an electrolytic interaction between the salt and the steel material can arise, subsequently leading to corrosion of the metal [35]. A situation where the RH is greater than the DRH, as in equation (8), would result in a salt that is liquefied and thus dissolved in its own absorbed water. This is usually not a must for corrosion to occur, which can in fact be initiated at lower RH than the DRH.

Each salt and combination of salts, and double salts, have specific dew points depending on the temperature and volume-% of water vapor [35]. Usually salts with a high solubility (often is >1 mol/liter regarded as highly soluble), are the ones of most importance concerning hygroscopic properties and eventual corrosion enabling behavior [33]. In table 4.1 and 4.2, are the solubilities of some salts in water at different temperatures and at 100°C respectively. If the solubility of a salt increases with temperature, does the DRH decrease accordingly. The DRH of any salt mixture is lower than the DRH of any single salt present in the salt mixture [36]. When two salts with roughly the same DRH are mixed, the DRH of the salt mixture is usually significantly lower than the DRH of any of the single salts in the mixture. If the DRH between two mixed salts is significant, the DRH of the mixture of dose two salts is usually lower, but close to the DRH for the more deliquescent of the two single salts [36]. Graphs of the DRH of different salts as a function of temperature are presented in figures 4.3 and 4.4.

Table 4.1. The solubility of different salts (wt%) in water at different temperatures. The solubility values are expressed as mass percent of solute, $100 \cdot w_2$, where $w_2 = m_2 / (m_1 + m_2)$ and m_2 is the mass of solute and m_1 the mass of water [37]

Salt	25°C	50°C	60°C	70°C	80°C	90°C	100°C
Na_2SO_4	21.95	31.55	30.90	30.39	30.02	29.97	29.67

$NaHSO_4$	22.20						33.30
Na_2CO_3	23.50	32.20	31.70	31.10	31.10	30.90	30.90
NaCl	26.45	26.84	27.03	27.25	27.50	27.78	28.05
KCl	26.22	30.04	31.40	32.66	33.86	34.99	36.05

Table 4.2. The solubility of different salts according to n mol salt per liter H_2O, and n gram salt / 100 cm^3 H_2O at 100°C [36]

Solubility	Na2SO4	NaHSO4	Na2CO3	NaCl	KCl
*mol / l	3.0	4.0	4.3	6.7	7.6
g / 100 cm^3	42.7	47.9	45.5	39.1	56.7

*The solubility values (in mol/l) are calculated from the given values of solubility according to g/ 100 cm^3.

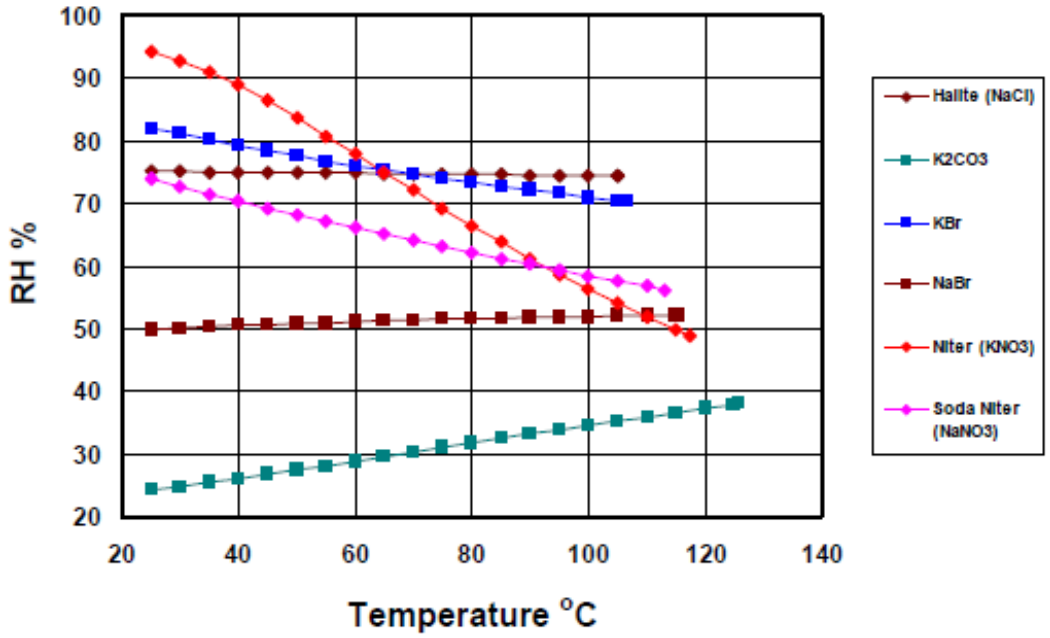

Figure 4.3. The deliquescence RH (DRH) as a function of temperature for some salts [36].

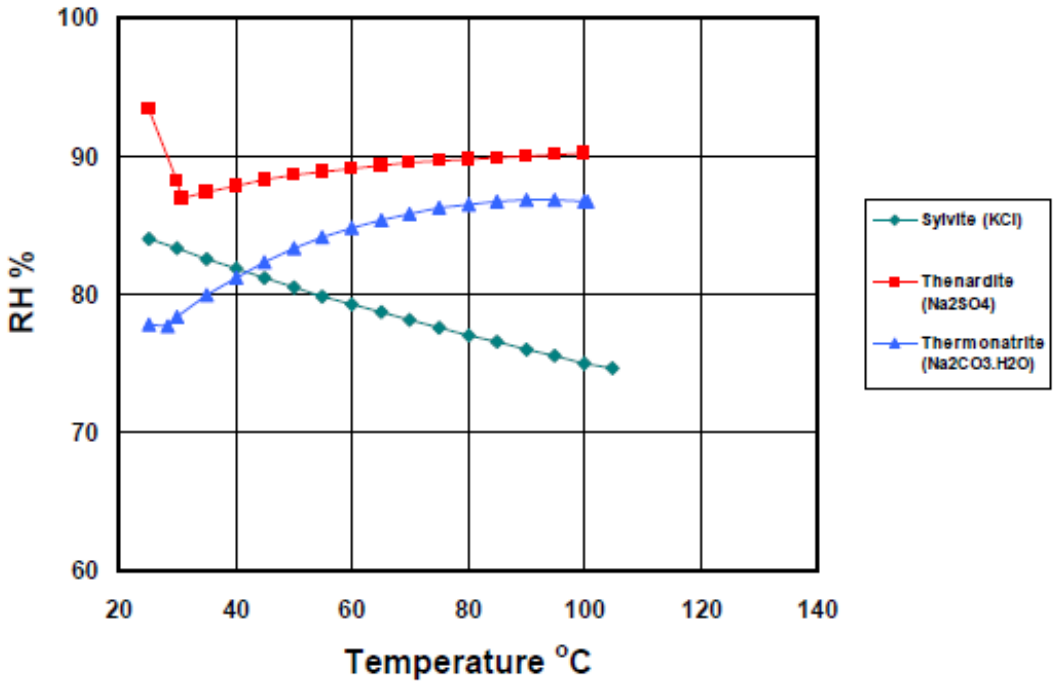

Figure 4.4. The deliquescence RH (DRH) as a function of temperature for some salts. The curve for Na_2SO_4 takes a sharp turn near 30.7°C due to reactions with water at low temperatures. A similar temperature driven reaction can be recognized for Na_2CO_3 [36].

Worth to also consider when discussing water adsorption by salts is the thermodynamic aspect of adsorption. Tang and Munkelwitz [38] give equations based on enthalpy in a study on deliquescence where they calculate deliquescence properties for both single- and mixed-salt particles. Equations are derived expressing % RHD (relative humidity of deliquescence) as a function of composition and temperature. For example: a solid NaCl particle at a temperature *T* K at its DRH, corresponding to a water vapor partial pressure of *p* atm, the particle transforms into a droplet by condensing 1 mol $H_2O(g)$ onto n mol NaCl(c) to form a saturated aqueous solution of m_s molar. The vapor-liquid equilibrium can be expressed by the following reactions:

$$H_2O(g) = H_2O(l) \quad (9)$$

$$H_2O(l) + nNaCl(c) = nNaCl(aq, m_s) \quad (10)$$

Here the symbols g, l, c and aq in the parentheses means: g = vapor, l = liquid, c= crystalline, and aq = aqueous solution. The saturation molarity is expressed by m_s. The heat that is released in reaction (9) is the heat of condensation of water vapor, which is equal to its heat of vaporization, $-\Delta H_v$. The heat that is absorbed in reaction (10) is the integral heat of solution, ΔH_s, which may be calculated from the heats of formation in standard thermodynamics tables. The overall heat involved in the process is the sum of two heats:

$$\Delta H = n\Delta H_s - \Delta H_v \tag{11}$$

The difference in enthalpy is of importance considering a spontaneous reaction such as absorption of water and dissolution of particles in a solvent. The first step in reaction (9) consumes energy and would discourage solubility, but the second reaction releases energy and has the opposite effect [38].

It is unclear whether there are deliquescence relative humidities at higher temperatures, than what was presented for some salts previously in figures 4.3 and 4.4. If for example NaCl has no DRH after 105°C (as in figure 4.3), would this indicate that the observed corrosion of carbon steel under NaCl (chapter 6), at 110°C with 80 vol% H_2O, happens at a higher temperature than what is physically possible (in a non-pressurized system) for NaCl to have a deliquescence RH. This would mean that the DRH for a salt must not be achieved for the corrosion mechanism to thrive. This phenomenon, when corrosion is initiated at a RH below the DRH for a salt, is called "the critical relative humidity" (CRH). Worth also to consider is the fact that the atmospheric boiling temperature for a saturated water solution with NaCl is 108.76°C [36].

The initiation of aqueous corrosion of a metal is believed to occur at a critical relative humidity (CRH), which is lower than the DRH of the salt causing the corrosion. To determine the CRH, of some salts compared to their DRH at 50°C, the electric currents imposed by the corrosion mechanism were measured by Yang et al [39] in an experiment with a multi electrode array sensor under different salts. They found out that

the initiation of non-uniform corrosion on carbon steel and type 316 stainless steel occurs at a relative humidity that is 14 percentage points (RH = 67.2% versus DRH = 81.3%) lower than the deliquescence relative humidity (DRH) of potassium chloride (KCl). It was also found out that once significant corrosion had occurred, the non-uniform corrosion process for the carbon steel material under the salt deposit continues at relative humidities as low as 27% [39]. Additionally they also concluded that the conductivity of a salt, or mixture of a salt, generally starts to increase at relative humidities that are 15 – 20 percentage points lower than their DRH at 50°C [40]. The experiments were conducted to study the non-uniform corrosion behavior to determine the CRH for sodium chloride (NaCl) and potassium chloride (KCl).

Figure 4.5 shows the response of the non-uniform corrosion currents from the carbon steel and stainless steel sensors under the KCl powder to changes in RH during a 64-day test, conducted by Yang et al [39]. The non-uniform corrosion current from each sensor is represented by three times the standard deviation of the currents from a total of 16 electrodes, in order to simulate one piece of metal, with some electrodes acting as anodic sites and others acting as cathodic sites. Each anodic coupling current represents the degree of charge transferred from a corroding (or more corroding) site to a non-corroding (or less corroding) site, which is part of the non-uniform corrosion process. For the carbon steel sensor, the non-uniform corrosion current increased with an increase in RH and reached a constant value at the DRH of KCl. Further raising the RH above the DRH for KCl seemed interestingly to have no significant effect on the corrosion current. Because of technical limitations, the RH could not be lowered past 27% [39].

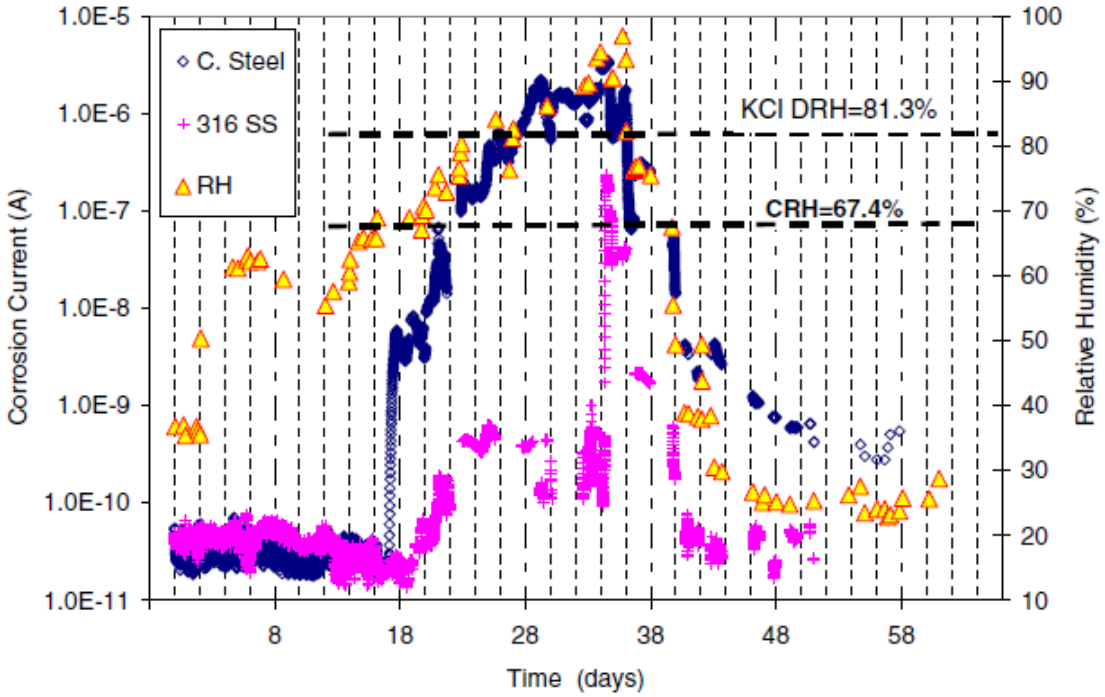

Figure 4.5. Responses of the non-uniform corrosion currents from the multielectrode sensors under KCl salt to changes in relative humidity in the chamber. The dark blue and pink symbols represent the measured currents for carbon steel (blue) and type 316 stainless steels (pink) respectively. The yellow triangles represent the actual relative humidity at a specific point in time. The stronger the current, the more pervasive is the corrosion [39].

4.4.2 Corrosion mechanism

The corrosion reaction can be considered as taking place by two simultaneous reactions: the oxidation of a metal at an anode (a corroded end releasing electrons) and the reduction of a substance at a cathode (a protected end receiving electrons). In order for the reaction to occur, a chemical potential difference must exist between adjacent sites on a metal surface and an electrolyte to provide solution conductivity and as a source of material to be reduced at the cathode [29].

When the metallic surface is exposed to an aqueous solution containing ionic substances (salts), galvanic corrosion can occur in the metallic surface. The galvanic corrosion reaction is caused by an anodic portion and a cathodic portion occurring simultaneously at discrete points on the metallic surface. Flow of electricity from the anodic to the cathodic areas may be generated by local sites either on a single metallic surface because of local point-to-point chemical potential differences or at the interface of different metals. The driving force to cause galvanic corrosion results from a difference in the electromotive force. The anodic and cathodic areas on a metal surface are formed by such variables as inhomogeneities in the metal composition, differential surface conditions, metal stresses, or variation in the solution concentration [29].

Concentration-cell corrosion is a type of localized corrosion caused by variations in the concentration of oxygen, change in acidity, buildup of ions, or depletion of an inhibitor. Common forms of these reactions are called “oxygen concentration-cell corrosion”, or “crevice corrosion”. The oxygen concentration-cell is an electrolytic cell in which the driving force causing corrosion results from a difference in the amount of oxygen in the solution at one point as compared with other locations. Crevice corrosion occurs within or adjacent to a crevice formed by contact with another piece of the same metal, another metal, or with nonmetallic material. Metal at the area of low oxygen availability becomes anodic to other areas. Because the cathodic area is large compared to the anodic area, the intensity of attack is usually more severe than on surrounding areas of the same surface. In water with high concentrations of sodium chloride, crevice corrosion is attributed to the combination of depletion of oxygen and the accumulation of chloride and hydrogen ions in the crevice. As the oxygen in the crevice is depleted, ferrous ions from the corrosion reaction are accumulated, and negatively charged chloride ions must enter the crevice to maintain electrical neutrality [29].

Pitting occurs as small areas of localized corrosion which vary in size, frequency of occurrence, and depth. Rapid penetration of the metal may occur, leading to petal perforation. Pits are often initiated because of inhomogeneity of the metal surface, deposits or scale on the surface or breaks in a protective film. Once a pit is initiated, a

concentration-cell is developed since the base of the pit is less accessible to oxygen than the metal surface is. Halide ions such as chlorides often stimulate pitting corrosion. The mechanism is similar to that described for crevice corrosion. The depletion of oxygen in the pit slows down the generation of hydroxyl ions. The accumulation of positive charges in the form of Fe^{++} then attracts negatively charged chloride ions. The resulting ferrous chloride hydrolyzes to produce insoluble ferrous hydroxide plus excess hydrogen and chloride ions; both of these ions then accelerate the corrosion at the bottom of the pit [29].

5. Experimental

In order to investigate the hygroscopic and corrosion enabling properties of different salts, a reactor system (figure 5.1) with a stable temperature and water vapor concentration was built and tested. Maintaining stable conditions throughout the experiment is crucial when studying low temperature corrosion due to water absorption by salts. Fluctuations in the water vapor concentration or temperature could lead to false interpretation of the results.

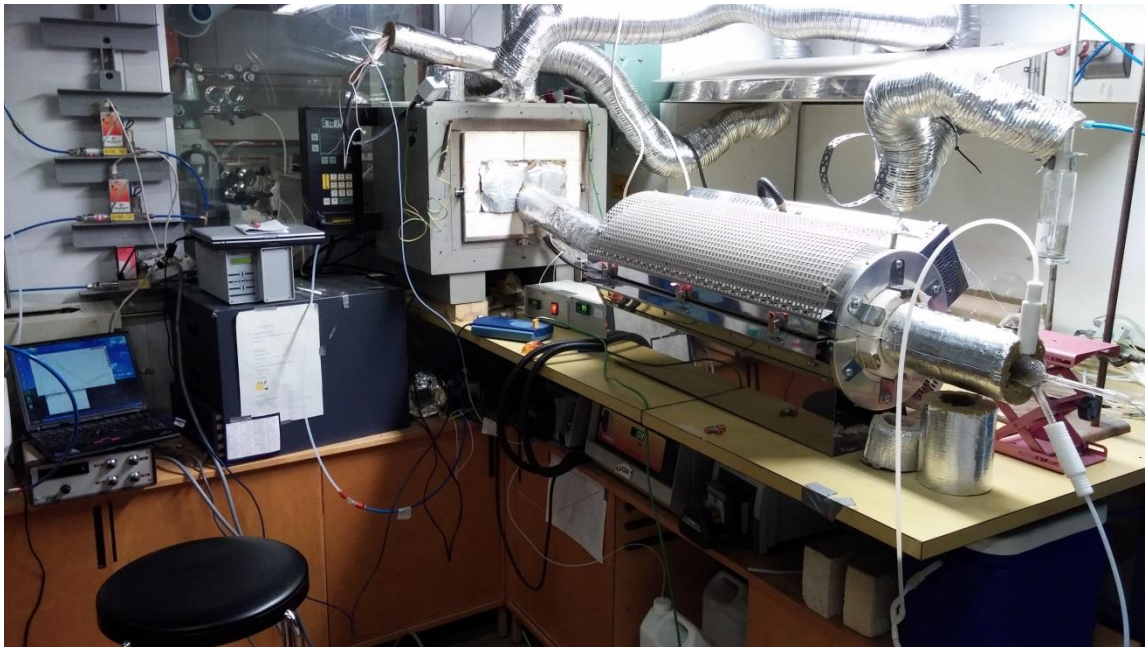

Figure 5.1. The setup.

In table 5.1 is the experimental plan, according to which the experiments were conducted. The different salts that are listed in the plan were chosen because of their occurrence in actual ash and deposits in a black liquor recovery boiler. All of them have hygroscopic properties.

Table 5.1. The experimental plan

Salt	H2O (vol%)	Temp (°C)	Time (h)	Coupons	Additional	Order
Na_2SO_4	**25**	80	4	3		Run26
		90	4	3		Run25
	60	100	4	5		Run1
		100	24	4		Run2
		110	24	5		*RunX
$NaHSO_4$	**25**	80	4	3		Run8
		90	4	3		Run7
	60	120	4	3		Run3
		130	4	3		Run4
		140	4	3		Run5
		150	4	3		Run6
	0	**150**	**4**	**3**		**Run9**
Na_2CO_3	**80**	90	4	3		Run28
		100	4	3		Run27
		110	24	3		Run11
		120	24	3		Run10
NaCl	**80**	110	24	3		Run12
		120	24	3		Run13
KCl	**80**	110	24	3		Run14
		110	4	4	SEM/EDX	Run24
		120	24	3		Run15
PA1	**25**	70	24	3		Run16
		80	24	3		Run17
		90	24	3		Run18
		100	24	3		Run19
		110	24	3		Run20
	60	100	4	4	SEM/EDX	Run23
		110	4	4		Run22
		120	4	4		Run21
PA2	**25**	100	4	4	SEM/EDX	Run29
		110	4	3		Run30
	60	100	4	3		Run32
		110	4	3		Run31

*RunX was carried out with the very same equipment in a previous study.

5.1 Corrosion tests with hygroscopic salts

To create a constant feed of water vapor, the water was pumped with a Masterflex L/S pump at a constant flow to the steam generator. The calculated average water vapor concentrations are given in table 5.2, along with the maximum and minimum values. The minimum water feed rate with this set-up translates to 27 vol% H_2O, although 20 vol% was the initially planned minimum. The steam generator consists of a thin pipe with heating tape. The temperature in the steam generator was set to 200°C in order to insure that water was vaporized at a constant rate. The hot steam was carried by a gas containing N_2, O_2 and CO_2, and flowed through a thin tube in an oven, called the "temperature regulator" in figure 5.2, in which the temperature of the wet gas was cooled to the desired temperature. After the "temperature regulator" unit the wet gases flowed through a preheater before entering the tube furnace, where the corrosion samples were placed. The back end of the tube furnace was well insulated to minimize water condensation to prevent water from flowing back into the reactor. The wet gases exited the tube furnace to a water condenser unit where water was condensed and finally dry gases were vented out. With this setup, which is schematically depicted in figure 5.2, the gas composition, gas flow, water vapor content and temperature can easily be adjusted.

Table 5.2. Minimum and maximum water concentrations (vol%) in the gas stream for a given target vol%. Average water concentrations are calculation based on all the runs at a given target vol% H_2O. The minimum and maximum values and their respective test runs are shown in brackets

Target:	27 vol%	60 vol%	80 vol%
Min:	(Run18) 26.81	(Run1) 59.06	(Run28) 76.31
Max:	(Run29) 27.88	(Run4) 61.13	(Run24) 79.44
Average:	27.17	60.56	78.71

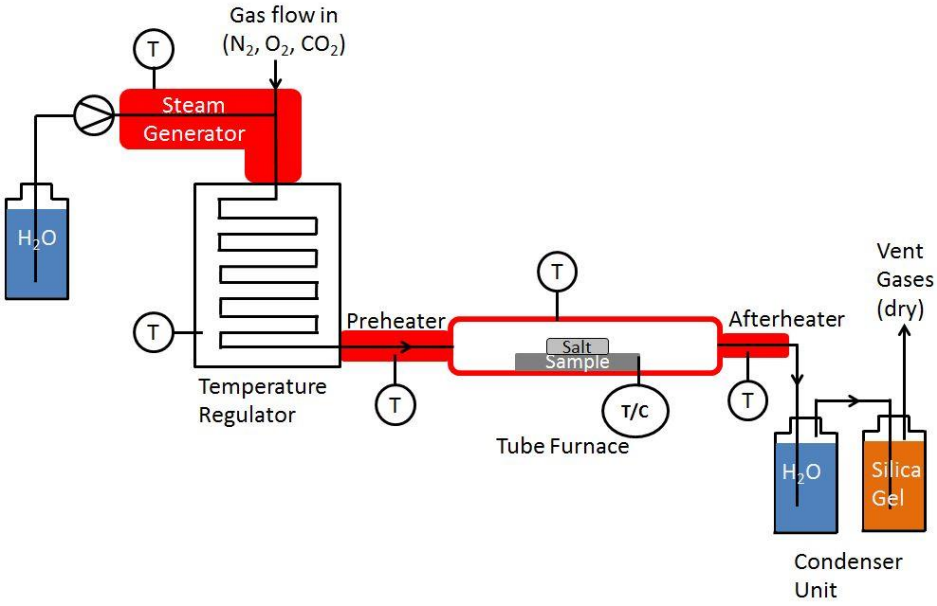

Figure 5.2 Schematic picture of the experimental setup.

5.2 Test procedure

The procedure is visualized, step by step, in figure 5.3 and begins with preparations, which include the cutting, polishing, and weighing of st45 carbon steel coupons. The salt is dried at 105°C in an oven over night and then kept in a desiccator for the rest of the test period. Roughly 0.1 g of dry salt is placed on top of each coupon of three or four, whereafter the samples are placed on the sample tray (figure 5.4) and inserted in the tube furnace, to heat up to the designated temperature in an inert N_2 atmosphere. When the target temperature is in close reach, the gas flow of N_2 is accompanied by flows of O_2 and CO_2. The composition of the simulated flue gas becomes at this stage: N_2 = 0.62 l_n/min; CO_2 = 0.14 l_n/min; O_2 = 0.04 l_n/min. The sum of gas flows equals 2 l_n/min. The feed of water into the gas flow starts when the gas temperature in the tube furnace has reached the target temperature and the test run can begin. Exposure times for the samples in each run were either 4 or 24 hours at the conditions given in table 5.1.

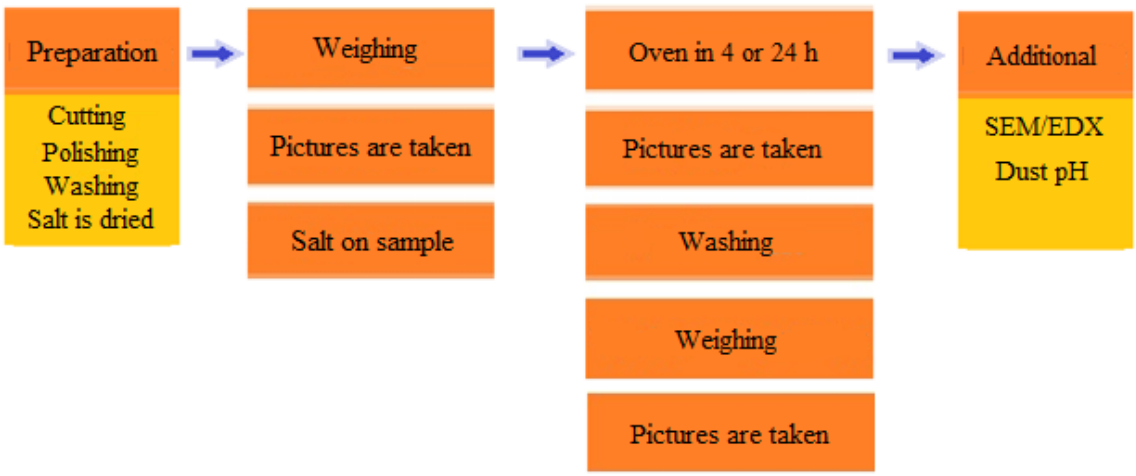

Figure 5.3. Workflow scheme: for the study of hygroscopic and corrosion enabling properties, for salts and electrostatic precipitator ash.

Figure 5.4. Carbon steel coupons with salt placed on the sample tray. The thermocouple was at the end of the sample holder.

After the exposure, pictures of the samples were taken, whereafter the steel coupons were washed with water and ethanol to wash off salts and excessive corrosion products. The weight change was determined by weighing the coupons before and after exposure. The weight loss, when all corrosion products are removed, is then used as measure of the corrosion. The weight loss numbers where extrapolated to annual tube wall thickness loss (mm/year), assuming a constant corrosion rate over the whole year. This extrapolation is an oversimplification - corrosion rate in the first two hours is typically higher than the average rate over a full year under same conditions. Consequently the mm/year numbers are higher than the real full year exposures would be.

In figure 5.5 and 5.6, are the temperature profiles for the sodium chloride (NaCl) and potassium chloride (KCl) runs respectively, at different temperatures with 80 vol% water in the synthetic flue gas and with 24h exposure time. These figures are examples of the stable temperatures maintained throughout all of the experiments that were conducted. As previously stated, it is important that the temperature is kept as stable and close to target temperature as possible. The deviation in the mentioned temperature profiles can be deemed to be within the 1°C, and thus accurate enough to be valid. All temperature profiles can be found in appendix B.

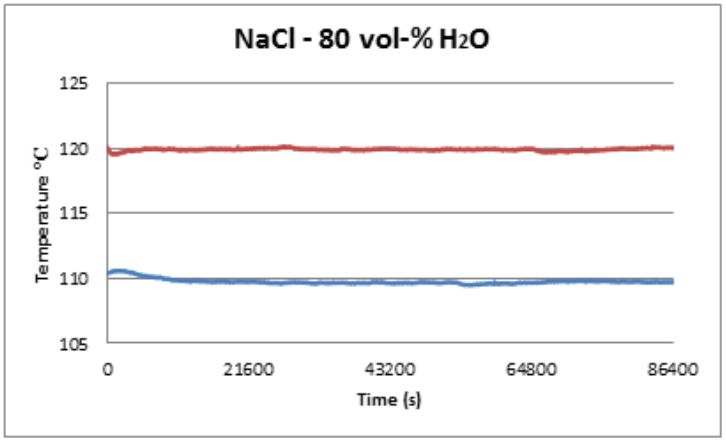

Figure 5.5. Temperature profiles for the experiments with NaCl at 110°C and 120°C, 24h run with 80 Vol-% H_2O.

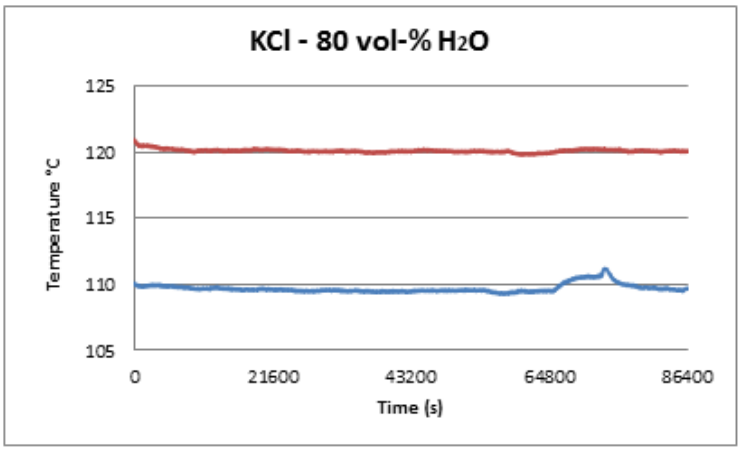

Figure 5.6. Temperature profiles for the experiments with KCl at 110°C and 120°C, with 24h run and 80 Vol-% H_2O.

5.3 Analysis of electrostatic precipitator ash

The electrostatic precipitator (ESP) ashes that were investigated in this study originate from a pulp mill in Scandinavia. They are named as “PA1” and “PA2” and differentiate from each other by the source of raw material in the pulp digestion. PA1 is based on black liquor from the digestion of hard wood, while PA2 originates from soft wood black liquor.

The ashes were dried in an oven over night at 105°C, after which they were diluted to 5 wt% with ultra-pure ELGA water. The results from the pH measurements are as follows:

- Deposit 1: pH = 11.0
- Deposit 2: pH = 10.2

The difference in pH is due to the difference in the concentration of carbonate in the ash samples.

Three coupons, one from each test runs; Run23, Run24, and Run29 (see table 5.1), were casted in epoxy resin in order to analyze the composition of the corrosion products. However the corrosion was not significant enough to be detected in the SEM. An EDX analysis was although carried out on the ESP ashes used in this study and the results of the elemental composition can be found in table x.

Table 5.3. Elemental composition of ESP ashes from a pulp mill in Scandinavia, where PA1 originates from the pulping of hardwood while PA2 is ESP ash from the combustion of black liquor from softwood pulping

	Na	K	SO4	Cl	CO3 (bal)
PA1	30.3	4.6	58.4	0.9	5.8
PA2	29.8	4.8	61.0	1.0	3.6

6. Results

The experiments give conclusive information about how actual electrostatic precipitator (ESP) ash and different salts, commonly occurring in black liquor recovery boilers, do adsorb moisture at temperatures higher than the pure water vapor dew point and can cause corrosion to carbon steel (ST45) surfaces. All salts tested, except sodium carbonate (Na_2CO_3), do cause corrosion under the right circumstances. In table 6.1 are the lowest temperatures listed, at different water concentrations, when no corrosion was detected.

Table 6.1. The lowest temperatures (°C), at which no corrosion could be detected after a 4h or 24h exposure time at the specific concentration of water vapor

Salt	**H_2O (vol.%)**	**Duration (h)**	**T (°C)**
Na_2SO_4	27	4	90
	60	4	110
$NaHSO_4$	27	4	>90
	60	4	>150
Na_2Co_3	80	24	*
NaCl	80	24	120
KCl	80	24	120
Deposit 1	27	24	**100
	60	4	110
Deposit 2	27	4	110
	60	4	110

*No corrosion detected at any tested temperature and water vapor concentration.

**Disputable if corrosion occurred at 100°C, why 100°C is considered to be a safe temperature if corrosion is to be avoided.

There were two extremes in the experiments, which where sodium bisulfate ($NaHSO_4$) and sodium carbonate (Na_2CO_3). Sodium bisulfate caused corrosion at all temperatures tested (80°C - 150°C) and it is therefore unknown at which temperature it does not cause corrosion. Sodium carbonate on the other hand did not cause corrosion in these

experiments, while it clearly absorbed moisture. It was fully dissolved in absorbed water at 90°C (figure 6.1).

Figure 6.1. Sodium carbonate dissolved in absorbed water on carbon steel coupons after 4h exposure at 90°C with 80 vol% H_2O. No corrosion could be detected.

The most interesting findings are due to the pinpointing of the shifts in corrosive behavior, for a salt, between two experiments with the same water vapor concentration but different temperature. For example sodium chloride (NaCl) showed very evident signs of corrosion at 110°C and none at all at 120°C. In figure 6.2 is a graphical presentation of the highest temperatures, at specific water vapor concentrations, when corrosion did occur.

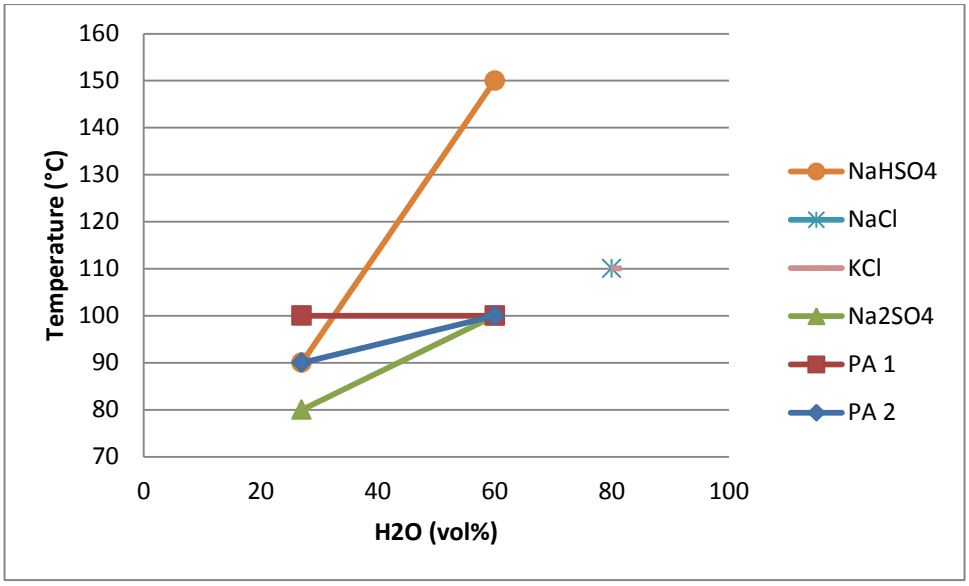

Figure 6.2. The highest temperatures at which different salts caused corrosion at specific water vapor concentration (vol%). The corrosion tendency is not necessarily linear despite that lines are drawn between the points of verified corrosion.

6.1 $NaHSO_4$

Sodium bisulfate ($NaHSO_4$) corroded the carbon steel coupons at all temperatures, where the water vapor concentration in the gas was either 27 vol% or 60 vol%. The only exception, when no corrosion could be verified, was an additional test run that was carried out with 0 vol% H_2O, just to ensure that the equipment worked properly. In table 6.2 are the names of the pictures listed of actual $NaHSO_4$ exposed carbon steel coupons in accordance to the conditions during the experiments.

Table 6.2. Temperature and water concentration (vol%) table for $NaHSO_4$ and the respective figures of the carbon steel coupons

$NaHSO_4$	80°C	90°C	120°C	130°C	140°C	150°C
27 vol%	fig. 6.3	fig. 6.4				
60 vol%			fig. 6.5	fig. 6.6	fig. 6.7	fig. 6.8

In all runs, with a water vapor concentration above O vol%, was $NaHSO_4$ absorbing water from the gas with such intensity that the salts were completely dissolved in a water solution on top of the carbon steel coupons. Salt conditions in table 6.3, are in accordance to water vapor concentration and temperature. This can be seen in the figures 6.2 to 6.7. The corrosion is due to a formation of an acidic solution with water.

Table 6.3. Salt conditions after each experiment with $NaHSO_4$ in accordance to water vapor concentration and temperature

$NaHSO_4$	80°C	90°C	120°C	130°C	140°C	150°C
27 vol%	liquid	liquid				
60 vol%			liquid	liquid	liquid	liquid

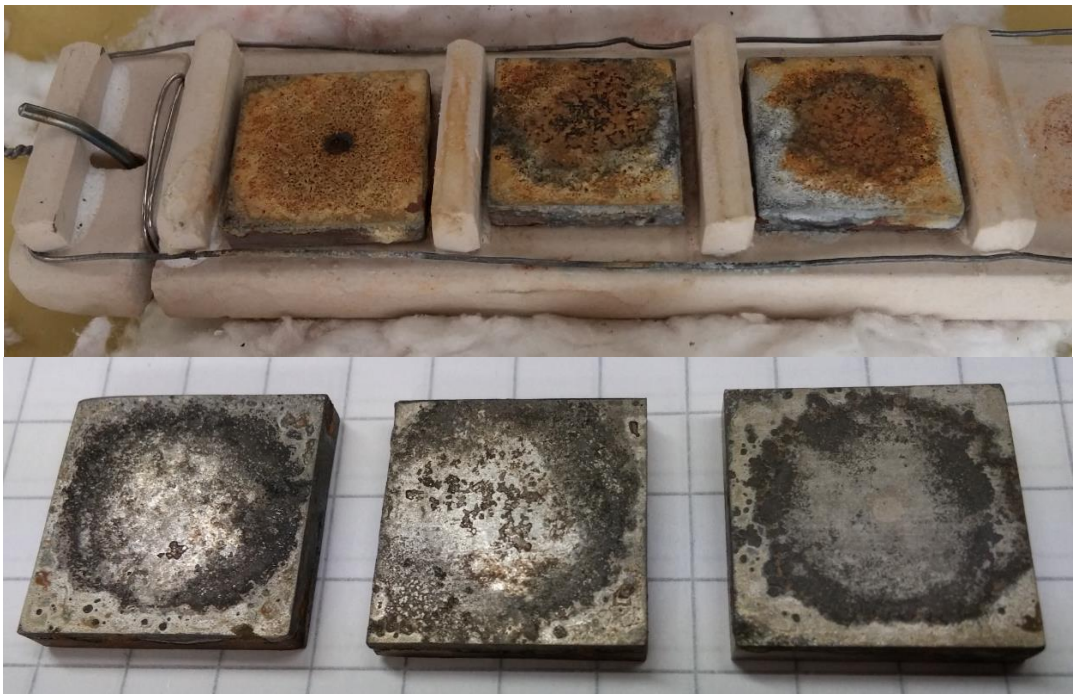

Figure 6.3. Unwashed coupons above and washed coupons below after 4h exposure to $NaHSO_4$ at 80°C and 27 vol% H_2O.

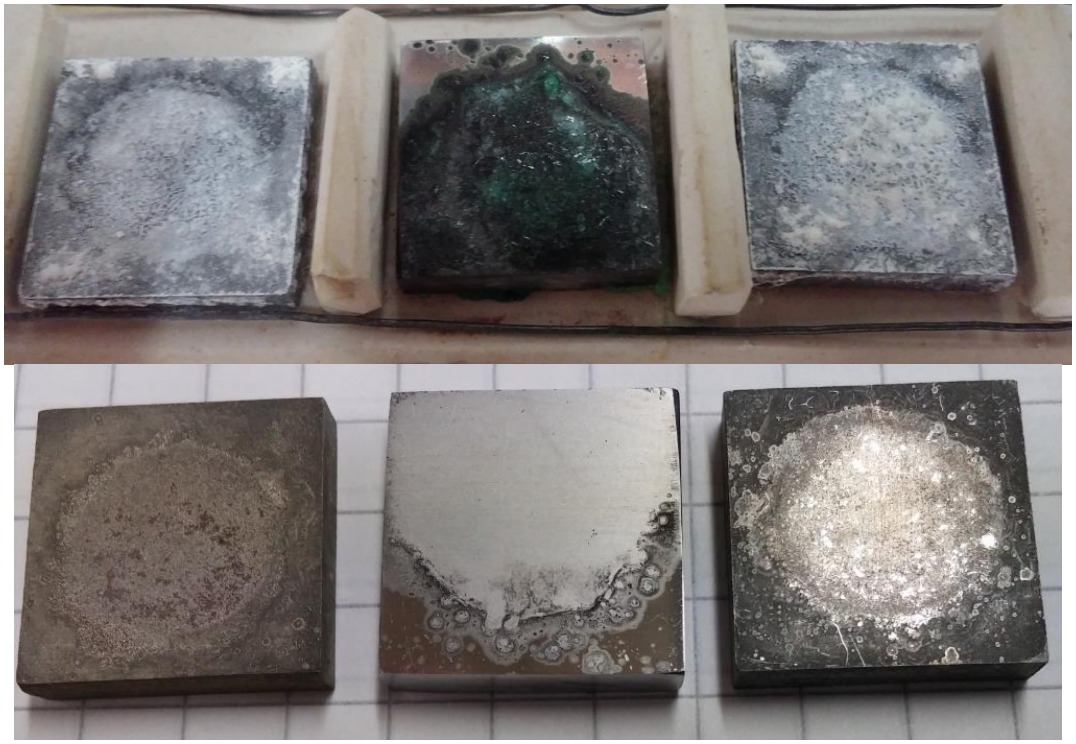

Figure 6.4. Unwashed coupons above and washed coupons below after 4h exposure to $NaHSO_4$ at 90°C and 27 vol% H_2O.

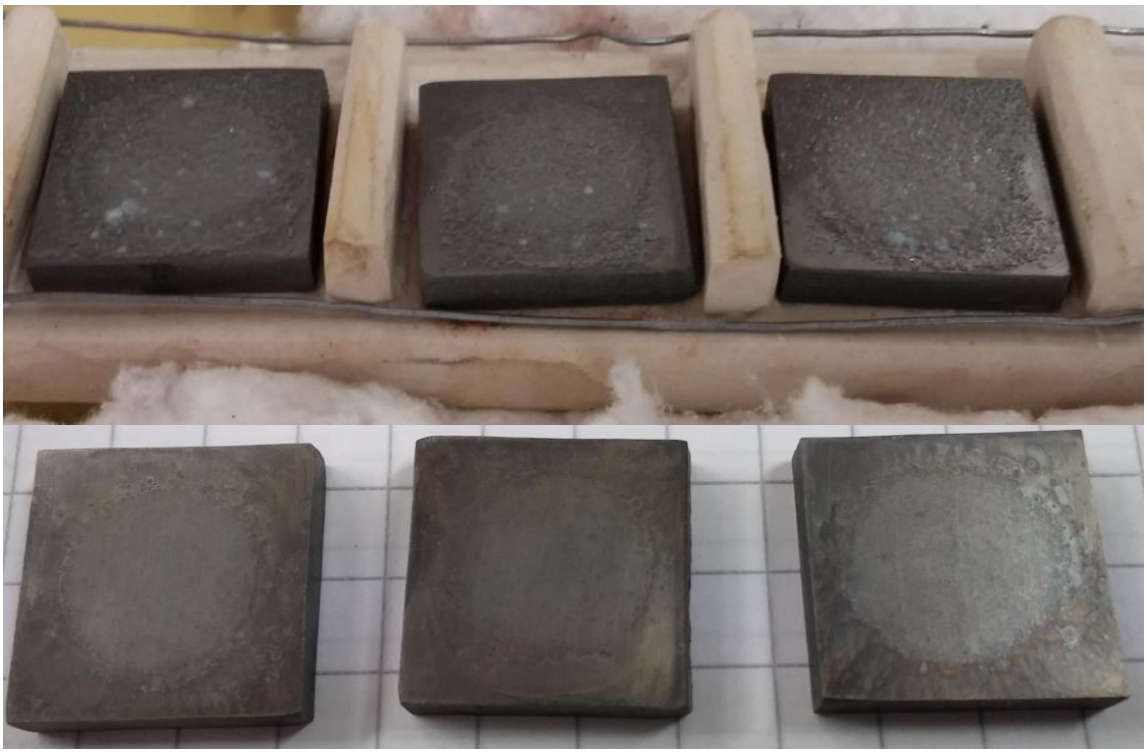

Figure 6.5. Unwashed coupons above and washed coupons below after 4h exposure to $NaHSO_4$ at 120°C and 60 vol% H_2O.

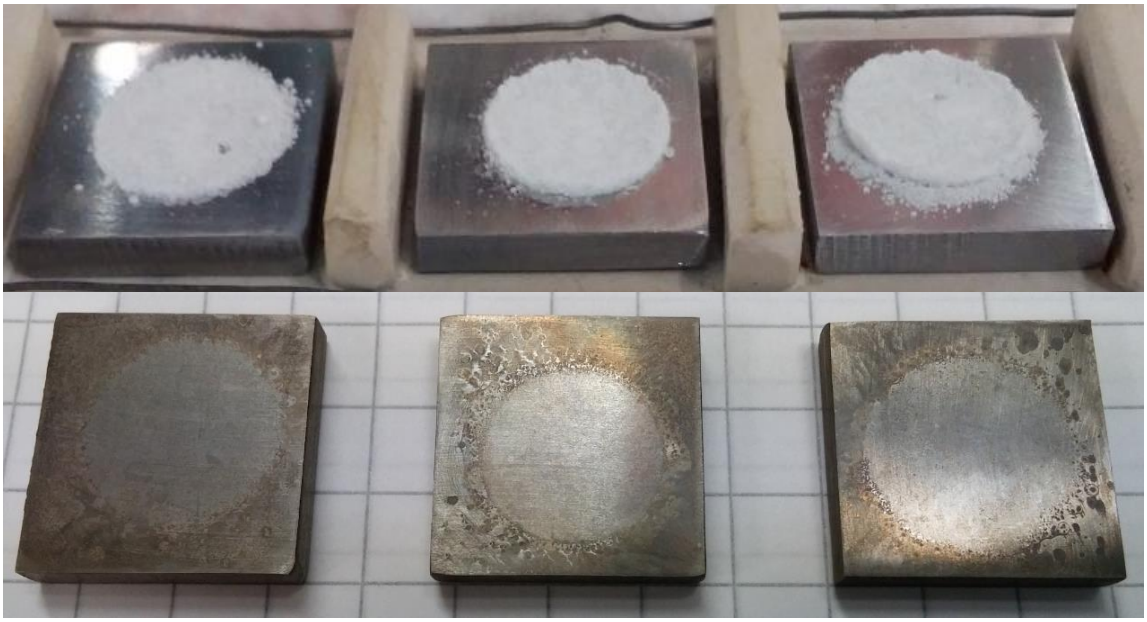

Figure 6.6. Unexposed coupons above and washed coupons below after 4h exposure to $NaHSO_4$ at 130°C and 60 vol% H_2O.

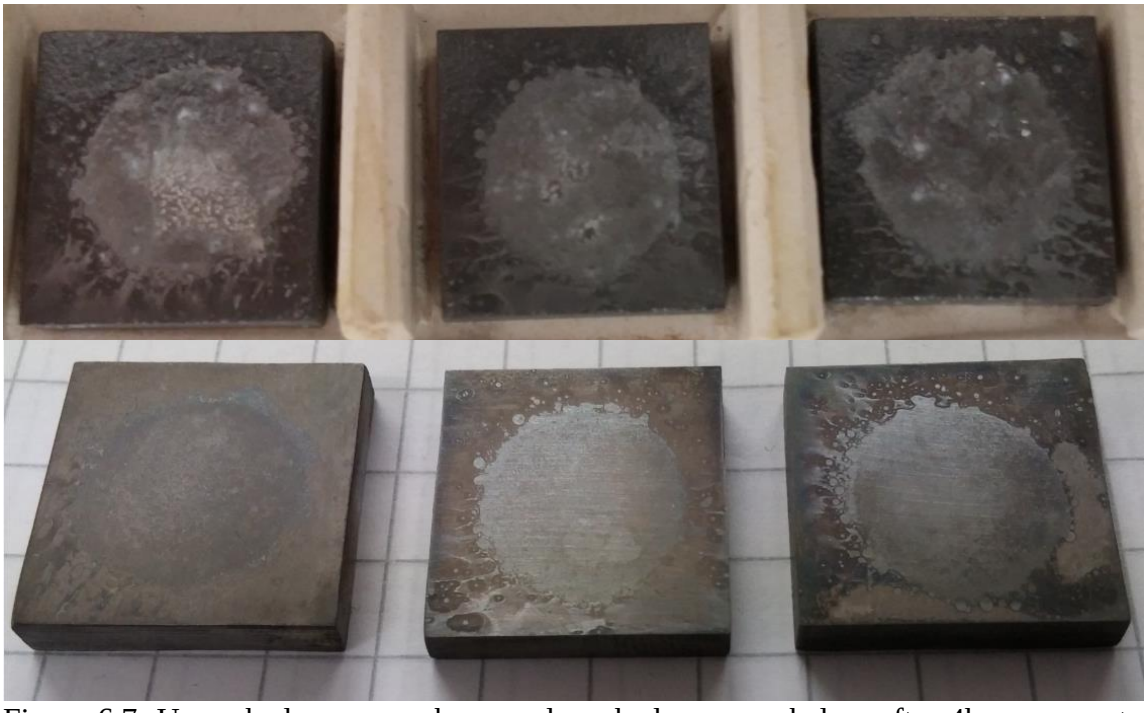

Figure 6.7. Unwashed coupons above and washed coupons below after 4h exposure to $NaHSO_4$ at 140°C and 60 vol% H_2O.

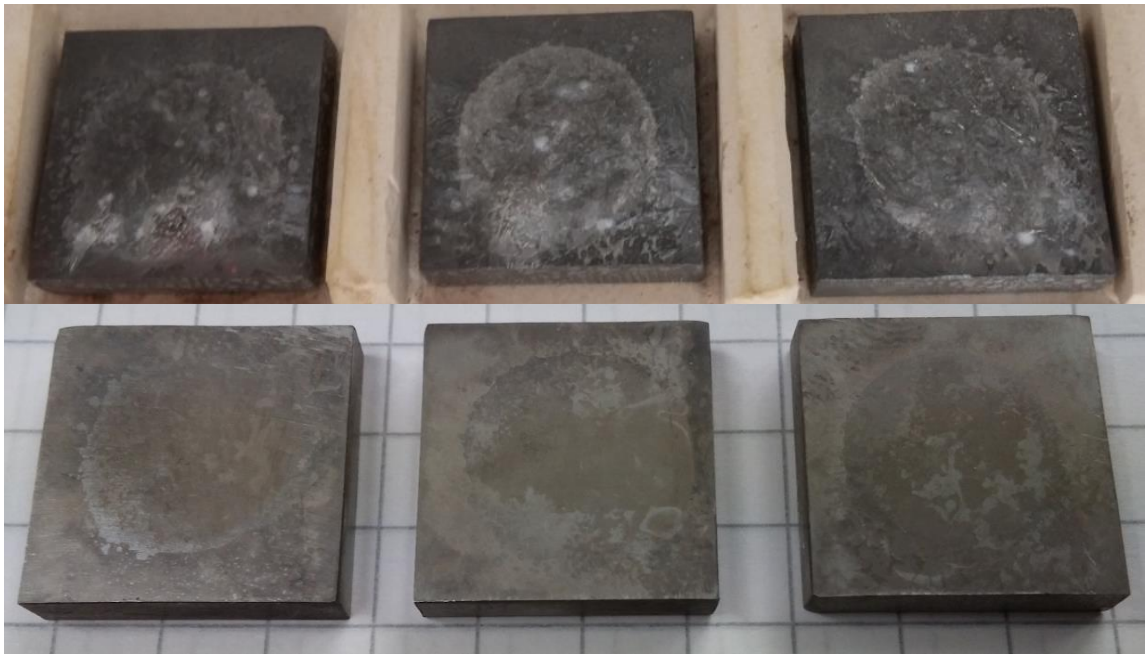

Figure 6.8. Unwashed coupons above and washed coupons below after 4h exposure to $NaHSO_4$ at 150°C and 60 vol% H_2O.

The absorption of water is very aggressive, as could be seen in the figures 6.3 to 6.8. With increasing temperature the severity of material loss seems to decrease, according to figure 6.8, even though a temperature where the corrosion stops was not found in these studies.

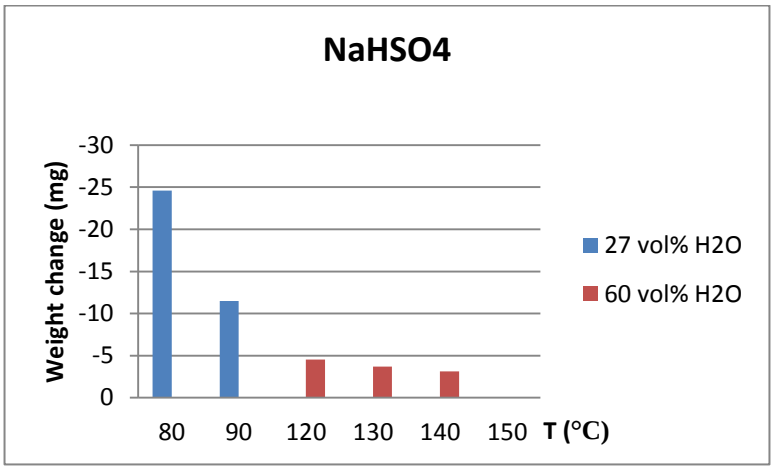

Figure 6.9. The average weight change (mg) of $NaHSO_4$ covered carbon steel coupons after 4h exposure to 27 or 60 vol% H_2O at different temperatures.

6.2 NaCl and KCl

Sodium chloride (NaCl) shows very evident signs of corrosion at 110°C and none at all at 120°C (figure 6.10). The same can be said about KCl (figure 6.12). Here it is quite clear that chlorine, combined with critical amounts of water, has the same type of corrosion mechanism in both cases. Furthermore it is noteworthy how big of a difference there is when the temperature is increased from 110°C to 120°C. This sort of abrupt change from severe corrosion to none at all is quite remarkable. Usually the degree of corrosion tends to decrease for every step, until corrosion can no longer be observed. This is the case with for example precipitator ash 1 (PA1).

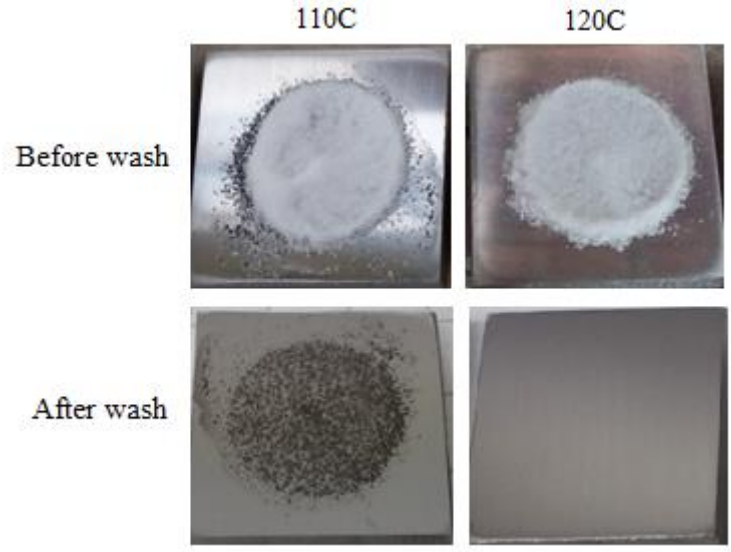

Figure 6.10. NaCl on carbon steel after 24h exposure with 80 vol% H_2O.

The weight measurements of coupons that have been exposed to sodium chloride, does not follow the anticipated logic of a greater change in mass when corrosion has taken place in the steel surface. In figure 6.11, the weight change is far greater after an experiment at 120°C, when no corrosion could be detected, compared to quite intrusive corrosion after equally long exposure time (24h) at 110°C.

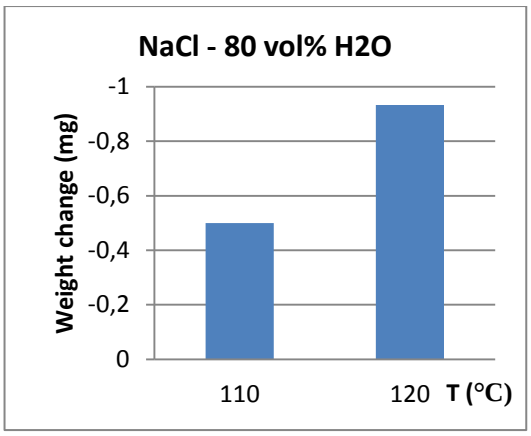

Figure 6.11. The average weight change (mg) of NaCl covered carbon steel coupons after 24h exposure to 80 vol% H_2O at 110°C and 120°C.

Figure 6.12. KCl on carbon steel after 24h exposure with 80 vol% H_2O.

Potassium chloride did perform very much like sodium chloride, with the same type of corrosive pattern with pitting in the steel surface. The temperature, 120°C, when corrosion was not identifiable any more was the same as for sodium chloride during the same humidity of 80 vol%, which gives clear indications of the corrosive properties of chlorides under such conditions. The average weight change in the carbon steel coupons after being exposed to KCl can be seen in figure 6.13.

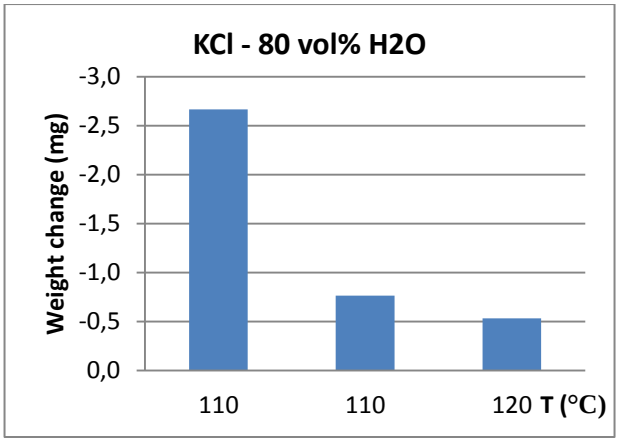

Figure 6.13. The average weight change (mg) of KCl covered carbon steel coupons after 4h (2nd column) and 24h (1st and 3rd columns) exposure to 80 vol% H_2O at different temperatures.

6.3 Na_2SO_4

Sodium sulfate (Na_2SO_4) corroded the carbon steel coupons at 80°C but not at 90°C with 27 vol% H_2O in the gas flow (figure 6.14). With 60 vol% H_2O, the corrosion of the coupon surfaces was inhibited at 110°C (figure 6.15). This indicates that with an increase of the water concentration in the gas flow from 27 vol% to 60 vol%, the non-corrosive temperature increased with 20°C, from 90°C to 110°C. The average weight changes in the carbon steel coupons are presented in figure 6.16.

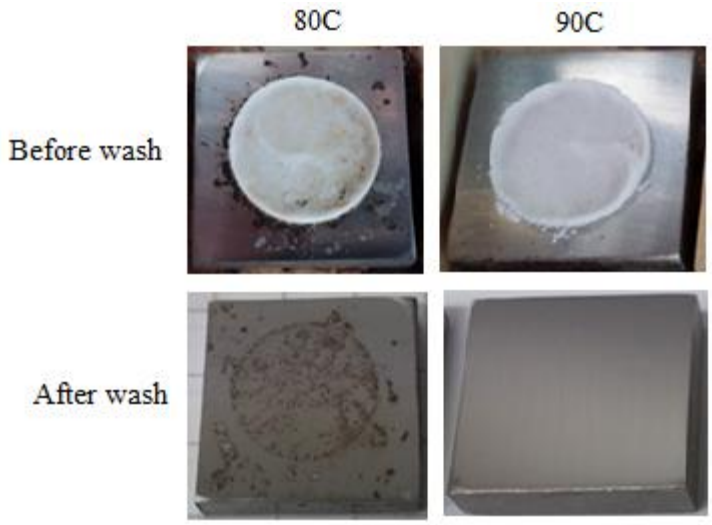

Figure 6.14. Na_2SO_4 on carbon steel after 4h exposure with 27 vol% H_2O.

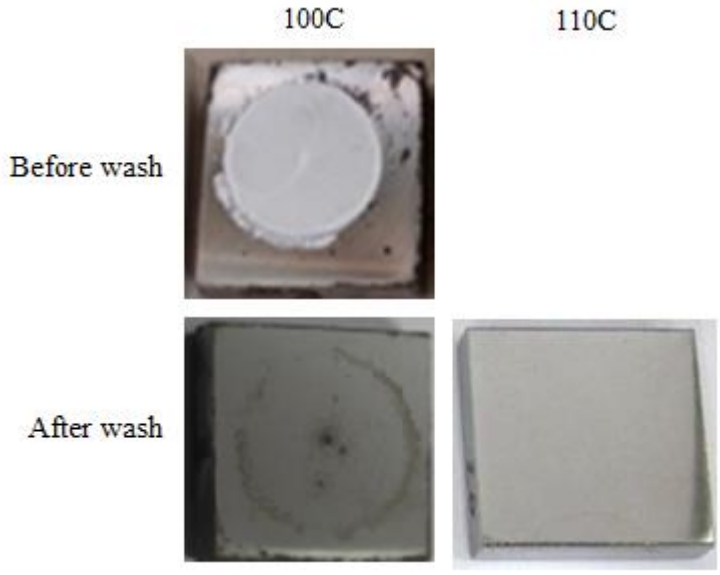

Figure 6.15. Na_2SO_4 on carbon steel after 24h exposure with 60 vol% H_2O.

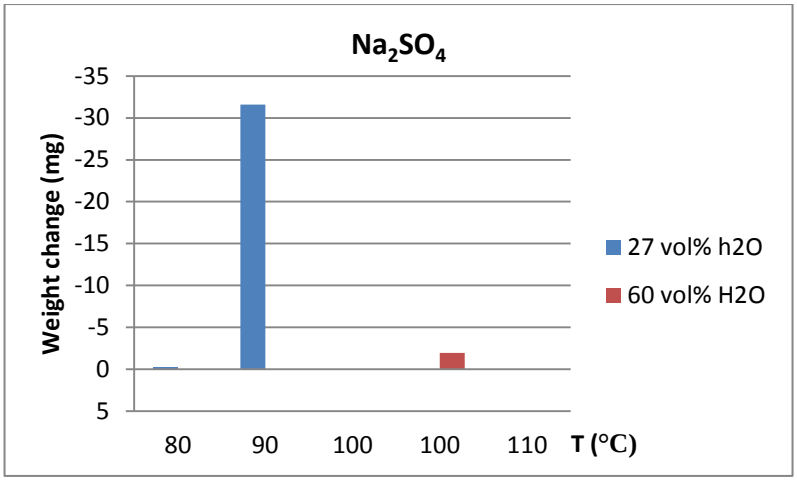

Figure 6.16. The average weight change (mg) of Na_2SO_4 covered carbon steel coupons after 4h and 24h (60 vol% H_2O at 100°C, 4th column) exposure to 27 or 60 vol% H_2O at different temperatures. **[Revise graph]**

6.4 Na_2CO_3

Sodium carbonate did not cause corrosion to the carbon steel coupons (figure 6.17). The weight changes in figure 6.18 tell that some sort of weight change took place after all. This might be due to measurement error. The reason remains as a speculative matter and is discussed further in chapter 7.

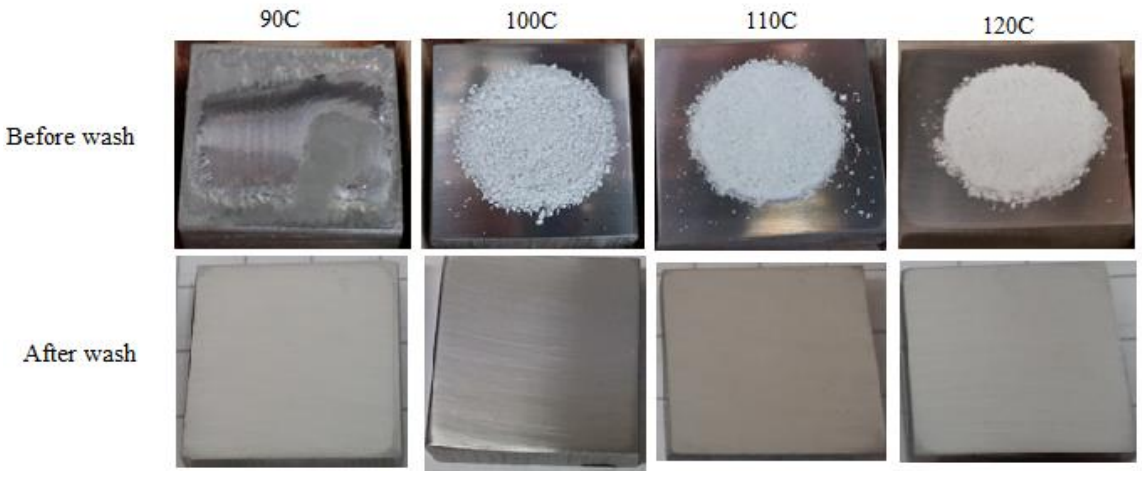

Figure 6.17. Na_2CO_3 on carbon steel coupons after 4h (90°C and 100°C) and 24h (110°C and 120°C) exposure with 80 vol% H_2O. Sodium carbonate dissolved in absorbed water after 4h exposure at 90°C with 80 vol% H_2O. No corrosion.

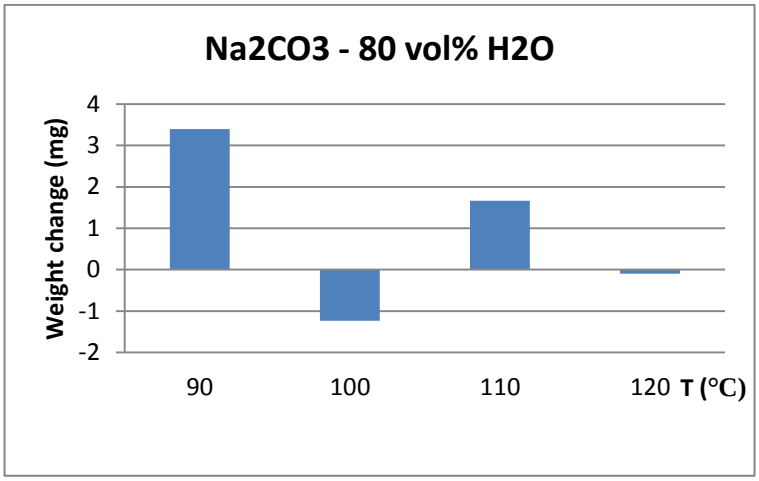

Figure 6.18. The average weight change (mg) of Na_2CO_3 covered carbon steel coupons after 4h (90°C and 100°C) and 24h (110°C and 120°C) exposure to 80 vol% H_2O at different temperatures.

6.5 Precipitator ash

PA1 was ESP ash from the combustion of black liquor originating from hard wood pulp digestion. The maximum temperature at which corrosion could be detected was 100°C in both cases of humidity. Pictures of the coupons after each run, according to temperature and water vapor concentration, are presented in figure 6.19 and 6.20. Average weight changes in the coupons according to temperature and vol% H2O are found in figure 6.21.

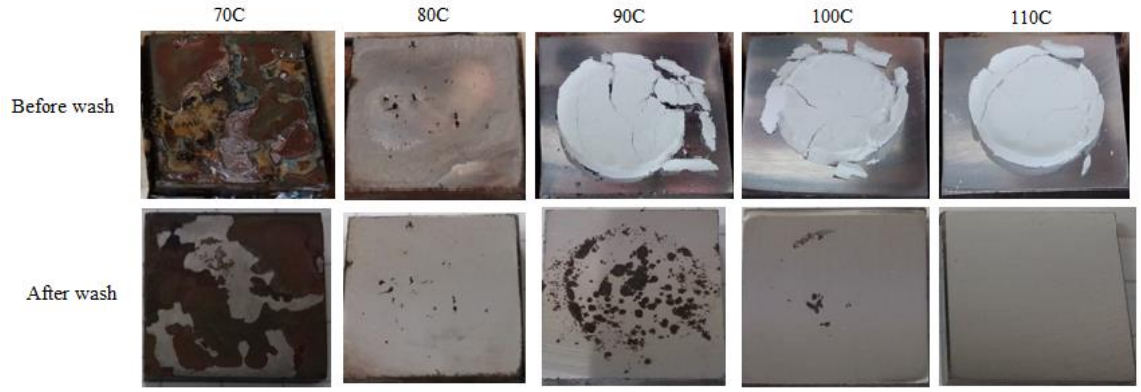

Figure 6.19. Precipitator ash 1 (PA1), on carbon steel coupons after 24h exposure at 70°C to 110°C with 27 vol% H_2O. The ash is dissolved in absorbed water at 70°C and 80°C.

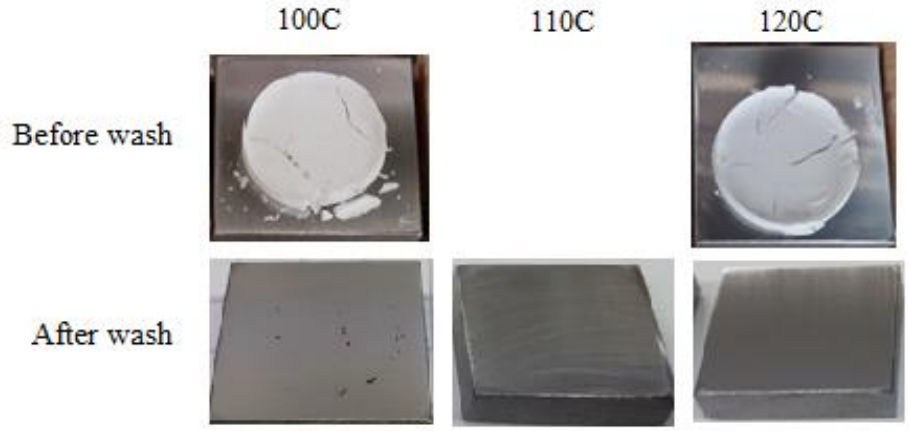

Figure 6.20. Precipitator ash 1 (PA1) on carbon steel coupons after 4h exposure at 100°C to 120°C with 60 vol% H_2O.

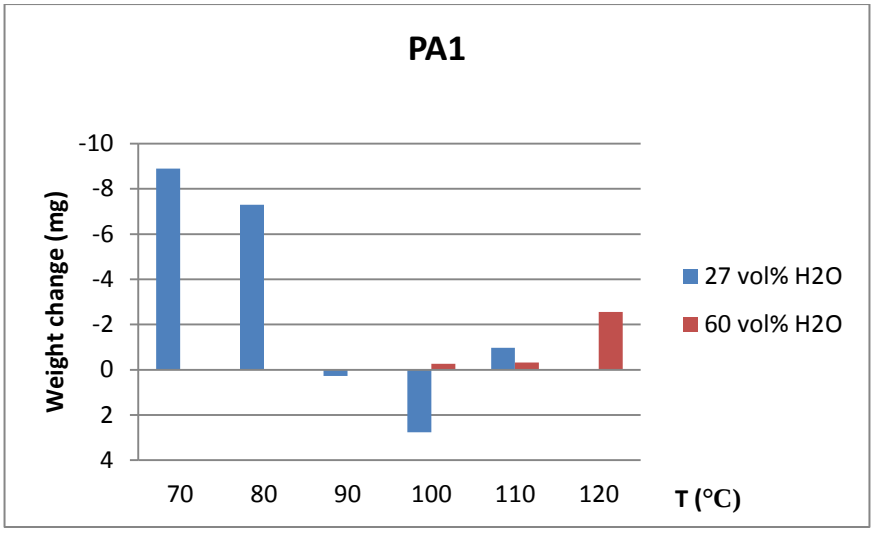

Figure 6.21. The average weight change (mg) of Deposit 1 covered carbon steel coupons after 4h (60 vol% H_2O) and 24h (27 vol% H_2O) exposure at different temperatures.

PA2 was ESP ash from the combustion of black liquor from soft wood pulping. Two runs with 27 vol% H_2O were executed with PA2, at 100°C and 110°C respectively. At 110°C could no corrosion be seen, but at 100°C were some barely visible spots that might be due to corrosion. This is disputable and categorized as "no corrosion" due to it being so insignificant. Coupons are shown in figures 6.22 and 6.23.

Figure 6.22. Precipitator ash 2 (PA2) on carbon steel after 4h exposure at 100°C with 27 vol% H_2O. Possibly extremely weak corrosion categorized as insignificant and thus "no corrosion" at 100°C and 27 vol% H_2O.

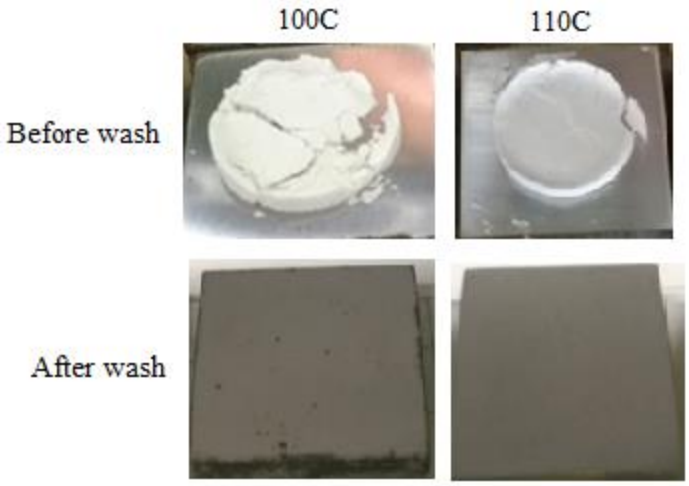

Figure 6.23. Precipitator ash 2 (PA2) on carbon steel coupons after 4h exposure at 100°C and 110°C with 60 vol% H_2O. Corrosion is verified at 100°C and non at 110°C.

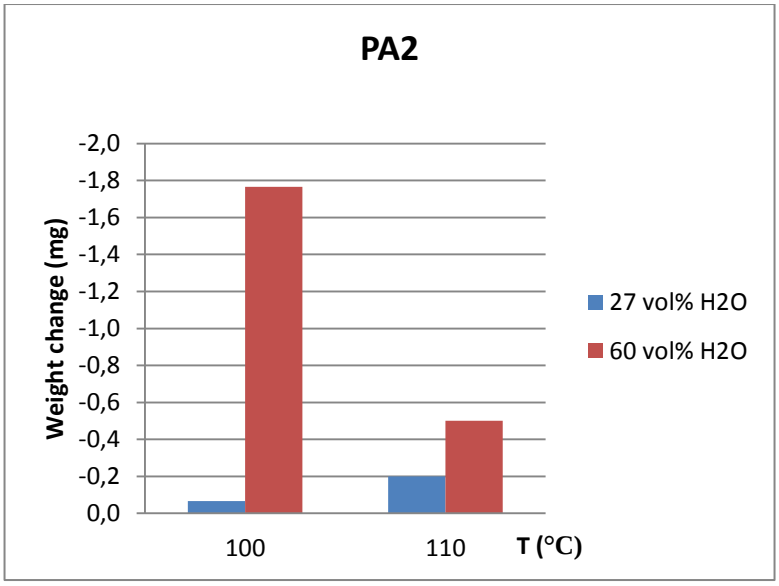

Figure 6.24. The average weight change (mg) of Deposit 2 covered carbon steel coupons after 4h and 24h exposure to 27 or 60 vol% H_2O at different temperatures.

A surface SEM-analysis was carried out on two carbon steel coupons which had been exposed to precipitator ash (PA1) at 70°C (Run 16) and 90°C (Run 18) with 27 vol% water vapor in both occasions. The prevailing hypothesis of the corrosion mechanism with precipitator ash is that mainly chloride ions are responsible for the corrosion in these tests. The pH measurements (section 5.3) of PA1 and PA2 show that both ashes

are highly alkaline at pH 11.0 and pH 10.2 respectively. Acidic bisulfates are not the cause of corrosion due to the high pH values. According to a SEM analysis of a washed coupon from Run 18 (table 6.4), exposed to PA1 at 90°C with 27 vol% H_2O, there are some spots with sulfur on the surface of the carbon steel coupon and especially spots that are enriched in chlorine. To some extent are regions with sodium and potassium also present. In measure point 7, in figure 6.25, is the chlorine concentration more than 4 times higher than the concentration of chlorine in PA1 (table 5.3). This indicates that the main reason for corrosion under said conditions (Run 18) with PA1 is due to chlorine, and to some extent sulfur. The significance of sodium and potassium in the actual corrosion mechanism in carbon steel is to be considered as negligible.

At 70°C and 27 vol% H_2O, was the salt so readily dissolved in water that chlorides could probably not interact with the carbon steel to the same extent as when the temperature was 90°C and the salt was kept as a solid. This assumption is to some degree verified by the almost nonexistent presence of chlorine in the surface of the coupon from Run 16, which was analyzed with SEM (figure 6.26 with wt% values of the elemental compositions given in table 6.5). A higher concentration of chlorine can be seen in table 6.4 for Run 18 than the equivalent table 6.5 for Run 16. The PA1 has 0.9 wt% of chlorine; compared to the elemental analysis of the coupon surface (Run 18) where some spots consists of 1 to 4 wt% of chlorine, verifies that some of the corrosion products are enriched in chlorine.

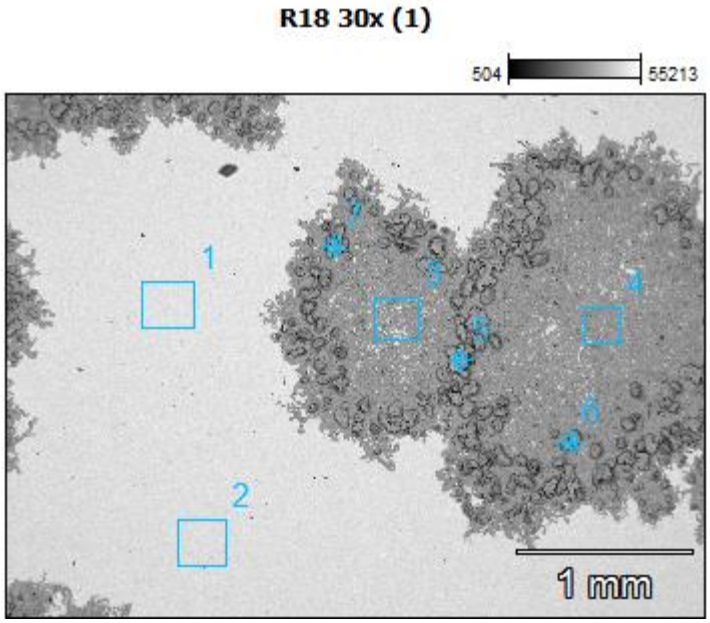

Figure 6.25. SEM image of a carbon steel coupon surface: after 24h exposure to PA1 at 90°C and 27 vol% H_2O. The small spots at the edges of the darker regions are enriched in chlorine. Elemental analysis for the specific measure points in the figure can be found in table 6.4.

Table 6.4. SEM analysis of the elemental composition (wt%) of corroded carbon steel

	O-K	*Na-K*	*Si-K*	*S-K*	*Cl-K*	*K-K*	*Mn-K*	*Fe-K*
R18 30x (1)_pt1			0.27					99.73
R18 30x (1)_pt2			0.30				1.04	98.66
R18 30x (1)_pt3	24.56	1.98	0.21	0.18	0.84	0.55		71.69
R18 30x (1)_pt4	27.57	2.13	0.19		0.79	0.68		68.64
R18 30x (1)_pt5	37.97		0.29	0.43	1.40	0.21	0.81	58.89
R18 30x (1)_pt6	19.17		0.14	0.27	1.27			79.16
R18 30x (1)_pt7	33.75			0.96	4.01			61.28

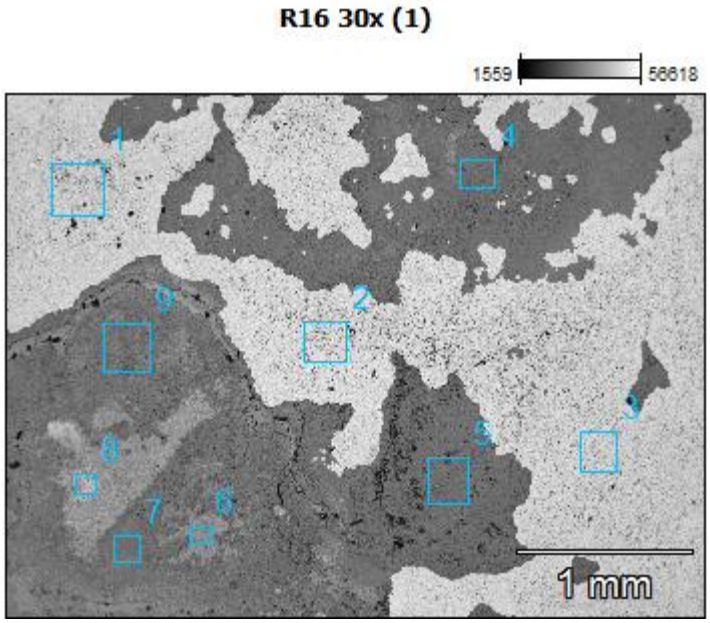

Figure 6.26. SEM image of a carbon steel coupon surface: after 24h exposure to PA1 at 70°C and 27 vol% H_2O. Elemental analysis for the specific measure points in the figure can be found in table 6.5.

Table 6.5. SEM analysis of the elemental composition (wt%) of corroded carbon steel

	O-K	*Na-K*	*Mg-K*	*Si-K*	*S-K*	*Cl-K*	*K-K*	*Ca-K*	*Mn-K*	*Fe-K*
R16 30x (1)_pt1	3.10					0.15			1.36	95.39
R16 30x (1)_pt2	2.83	0.32							1.23	95.62
R16 30x (1)_pt3	3.60			0.19					1.39	94.83
R16 30x (1)_pt4	39.90	2.03							1.08	56.99
R16 30x (1)_pt5	43.18			0.29	0.32			0.47	1.12	54.62
R16 30x (1)_pt6	30.63			0.25			0.17		1.19	67.76
R16 30x (1)_pt7	39.79	1.65	0.43					0.61	1.35	56.17
R16 30x (1)_pt8	16.88							0.22	1.36	81.53
R16 30x (1)_pt9	36.21	1.61							1.87	60.31

7. Discussion

The reason to examine the hygroscopic and corrosion promoting behavior of different salts and actual ash at low temperature becomes quite apparent, when new studies imply that the old hypothesis of acid dew point is not an issue in modern black liquor recovery boilers. This investigation of low temperature corrosion suggest there is no need for an acid dew point for corrosion to take place, under such circumstances where both temperature and water concentrations are at sufficient levels for salts to absorb enough water to cause corrosion on carbon steel.

The set-up that was built, tested and used throughout this set of experiments turned out to work as anticipated and gave interesting results and great reasons for further investigations. The only questionable part of this investigation is due to the seemingly irregular weight changes in the steel coupons that where measured. In some cases coupons that showed no signs of corrosion, had a greater average weight difference compared to coupons with severe corrosion. This was something unexpected and gives reasons to question the weight measuring procedure. The answer to the question is most certainly due to the washing procedure after exposure time. The coupons were probably not washed carefully enough. The general procedure was to wash with water and ethanol and dry them with a paper towel. This way of unstandardized washing of the steel coupons may give room for weight measuring error, if not careful enough, due to a possibly varying amount of corrosion products being removed. The accuracy of the scale (±0.1 mg) is also something to consider when the measured difference can be less than 1 mg. In future work, a standardized washing procedure could be beneficial to develop, so that corrosion can be more precisely quantified by removing the corrosion products from the steel coupons.

In spite of assumed inaccurate weight difference measurements, the study itself is of no less value due to the fact that in first hand, the target was set to investigate hygroscopic properties and to map at which temperatures and water vapor concentration there is

corrosion. The visual inspections give sufficient evidence of whether there is corrosion or not. In other cases, for example with sodium carbonate ($NaCO_3$), the visual inspections shows no signs of corrosion, but instead shows clearly how hygroscopic a salt sodium carbonate is when all of the samples, at 90°C, 27 vol. % water vapor and 24 h exposure time, have absorbed so much water that they are fully soaked and liquefied on top of the steel coupons, yet there are no signs of corrosion. In future work it would be of great interest to investigate the CRH of different salts and ashes by measuring the electric currents in metals, imposed by the corrosion mechanism**.** Then the adsorption and initiated corrosion at different temperatures and water vapor concentrations could be better understood.

The duration of the experiments could be something to reconsider in future work, because experiments with 4 or even 24 hour exposure time might not be long enough in all occasions. In experiments with for example sodium sulfate (Na_2SO) at 100°C and 60 vol% H_2O, there was a significant difference between 4h and 24h test runs, which could be an indication of that there might have been occasions when corrosion could possibly have been detected with a longer exposure time.

8. Summary and conclusions

The results gathered from the experiments, which were carried out in this study, gives insightful information about under which conditions that different salts and precipitator ashes do cause corrosion to carbon steel in a simulated synthetic flue gas. Temperatures ranged from 70°C to 150°C, with water vapor concentrations in the gas flow of N_2, CO_2, and O_2, equaling to 27, 60, and 80 vol% H_2O.

The corrosion mechanism at low temperatures is dependent of the presence of water in the gas phase. Due to the lowering of partial pressure and the activity of water, by salts with hygroscopic properties, water can condense in higher concentrations in the salt than the concentration of the water vapor in the gas at a given temperature. Adsorbed water that condenses to the metal surface enables an ion, and/or electron exchange between the salt particles and the carbon steel. Alkali sulfates, bisulfates and chlorides are heavily promoting corrosion under the right conditions. Sodium carbonate does not cause corrosion to carbon steel, and can at sufficient concentrations inhibit the corrosive properties of acidic sulfates. This passivation of carbon steel can however be disrupted by chlorides, which is the main hypothesis to why the studied precipitator ashes do cause corrosion to carbon steel, while the measured pH of 10 – 11 in the precipitator ashes are due to relatively high concentrations of carbonates.

9. References

[1] Vainio E., Fleig D., Brink A., Andersson K., Johnsson F., Hupa M.: *Experimental Evaluation and Field Application of a Salt Method for SO_3 Measurements in Flue Gases*, Energy & Fuels 2013, 27, pp 2767-2775.

[2] Perrish D.: *Black Liquor Recovery Boilers – An introduction* (1998), The National Board of Boiler and Pressure Vessel Inspectors, 1998. Retrieved from: http://www.nationalboard.org/index.aspx?pageID=164&ID=231 [Accessed: 27 September 2015]

[3] Salmenoja K.: *Field and Laboratory Studies on Chlorine-induced Superheater Corrosion in Boilers Fired with Biofuels*, Academic Dissertation. Report 00-1. Åbo Akademi University, Faculty of Chemical Engineering.

[4] Tran H., Vaikkalainen E.K.: *The Kraft Chemical Recovery Process*, 2008. Retrieved from: http://www.tappi.org/content/events/08kros/manuscripts/1-1.pdf [Accessed: 27 September 2015]

[5] Andritz: *ANDRITZ to supply the world's largest High Energy Recovery Boiler to OKI Pulp & Paper Mills, Indonesia*, 2014, Retrieved from: http://www.andritz.com/group/gr-news/gr-news-detail.htm?id=27097 [Accessed: 27 September 2015]

[6] Li, J., van Heiningen, A. R. P.: *Kinetic Study of Carbonate Reduction with Black Liquor Char*, Tappi Journal, 1990, 73, p 213.

[7] Silva W. L., Ribeiro, J.C.T., da Costa E.F., da Costa A.O.S.: *Reduction Efficiency Prediction of Cenibra´s Recovery Boiler by Direct Minimization of Gibbs Free Energy*, Brazilian Journal of Chemical Engineering 2008, 25(03), pp 603-611.

[8] Hupa M.: *Recovery Boiler Chemistry,* Chapter 2 in Kraft Recovery Boilers, 1997, TAPPI Press, Atlanta, ISBN 0-9625985-9-3.

[9] Parker K. R., Porle K.: *Dry type precipitator applications,* chapter 12 in Applied Electrostatic Precipitation, 1997, Chapman & Hall, London, ISBN 0-7514-0266-4

[10] Hupa M.: *Recovery boiler chemistry – the picture becomes sharper,* Paperi ja Puu – Paper and timber, 1993, 75(5), pp 310-219.

[11] Marklund M.: *Black Liquor Recovery: How does it work?,* 2001, Retrieved from: http://etcpitea.se/blg/document/PBLG_or_RB.pdf [Accessed: 5 April 2015]

[12] Raiko R., Kurki-Suonio I., Saastamoinen J., Hupa M.: *Poltto ja palaminen,* International Flame Research Foundation (IFRF), 1995, Suomen Kansallinen osasto.

[13] Adams T. N.: *General Characteristics of Kraft Black liquor Recovery Boilers,* chapter 1 in Kraft Recovery Boilers, 1997, TAPPI Press, Atlanta, ISBN 0-9625985-9-3.

[14] Pöyry, J.: *Reduction of Atmospheric Emissions from Pulp Industry, on behalf of Swedish EPA*, 1992, SEPA report 4008.

[15] Björklund H., Warnqvist B., Pettersoson B.: *Inside a Kraft Recovery Boiler: Combustion of high sulphidity black liquor at high dry solids,* 1991, Pulp & Paper Canada, 92(8), pp 206-208.

[16] Vakkilainen E. K.: *Kraft recovery boilers – Principles and practice,* 2005, Finnish Recovery Boiler Committee.

[17] Jokiniemi J. K., Pyykkönen J., Mikkanen P., Kauppinen E. I.: *Modeling fume formation and deposition in Kraft recovery boilers*, Tappi Journal, 1996, 79(7).

[18] McKeough P. J., Kurkela M., Arpiainen V., Mikkanen P., Kauppinen E., Jokiniemi J.: *The release of Carbon, Sodium and Sulphur During Rapid Pyrolysis of Black liquor,* TAPPI International Chemical Recovery Conf., 1995, Toronto, Canada, pp A217-A226.

[19] Feuerstein D. L., Thomas J. F., Brink D. L.: *Malodorous Products from the Combustion of Kraft Black Liquor.* I. *Pyrolysis and Combustion Aspects,* Tappi J., 1967, 50(6), pp 258-262.

[20] McKeough P. J., Vakkilainen E. K.: *Effects of black composition and furnace conditions on recovery boiler fume chemistry,* International Chemical Recovery Conference, 1998, pp 487-594.

[21] Vainio E.: *Fate of Fuel-Bound Nitrogen and Sulfur in Biomass-Fired Industrial Boilers,* Doctoral Thesis, Åbo Akademi University, Department of Chemical Engineering, 2014, Report 14-01, ISBN 978-952-12-3010-3

[22] Tran H.: *Recovery boiler fireside deposits and plugging prevention,* University of Toronto, Tappi Kraft Recovery Course, 2007.

[23] Mikkanen P.: *Fly ash particle formation in kraft recovery boilers,* Technical Research Centre of Finland (VTT), 2000, Otamedia Oy, Espoo, Finland, ISBN 951-38-5584-8.

[24] Tran H.: *Recovery Boiler Corrosion,* chapter 10 in Kraft Recovery Boilers, 1997, TAPPI Press, Atlanta, ISBN 0-9625985-9-3.

[27] Mobin M., Malik A. U., Al-Hajri M.: *Investigations on the Failure of Economizer Tubes in a High-Pressure Boiler,* J Fail. Anal. And Preven., 2008, 8(1), pp 69-74.

[26] Crowe D. C.: *Corrosion of Electrostatic Precipitators,* 1987, IPC Technical paper series, number 212.

[27] Sharp W. B. A.: *Corrosion and Cracking in Recovery Boilers,* 2008, SharpConsultant, Columbia, Maryland, USA. Retrieved from: http://www.tappi.org/content/events/08kros/manuscripts/5-4.pdf [Accessed: 27 September 2015].

[28] Speller F. N., Texter C. R.: *Effect of Alkaline Solutions on the Corrosion of Steel Immersed in Water,* National Tube Company and Mellon Institute of Industrial Research, Industrial and Engineering Chemistry, April 1924, p 393.

[29] Charng T., Lansing F.: *Review of Corrosion Causes and Corrosion Control In a Technical Facility*, National Aeronautics and Space Administration (NASA), 1982, TDA Progress Report 42-69.

[30] U.S. Department of Energy: *DOE Fundamentals Handbook Chemistry*, 1993, Vol. 1 of 2, DOE-HDBK-1015/1-93. Washington D.C.

[31] Ameer M. A., Fekry A. M., Ghoneim A. A.: *Electrochemical Corrosion Inhibition of Steel in Alkaline Chloride Solution*, 2010, Int. J. Electrochem. Sci., 5, 1847-1861.

[32] Herzog T., Müller W., Spiegel W., Brell J., Molitor D., Schneider D.: *Corrosion Caused by Dew Point and Deliquescent Salts in the Boiler and Flue Gas Cleaning*, Waste Management, vol. 3, Recycling and Recovery, Neuroppin: TK Verlag, 2012, pp 343-358.

[33] Lindau L., Goldschmidt B.: *Low temperature corrosion in bark fueled, small boilers,* Värmeforsk Service AB: Stockholm, Sweden, 2002, ISSN 0282-3772.

[34] Jacobs M., Z.: *Fundamentals of Atmospheric Modeling 2nd Edition,* chapter 17, part 2, Stanford University, Stanford, 2005.

[35] Retschitzegger S., Brunner T., Obernberger I.: *Low-Temperature Cossorion in Biomass Boilers Fired with Chemically Untreated Wood Chips and Bark*, Energy & Fuels, 2015.

[36] Bechtel SAIC Company, LLC: *Enivornment on the Surfaces of the Drip Shield and Waste Package Outer Barrier,* 2004, prepared for U.S. Department of Energy: Las Vegas, Nevada, USA.

[37] Lide D. R. *CRC Handbook of Chemistry and Physics*, 84th Edition, 2003, CRC Press: Boca Raton, Florida, USA, ISBN 9780849304842 - CAT# 484

[38] Tang I. N., Munkelwitz H. R.: *Composition and temperature dependence of the deliquescence properties of hygroscopic aerosols*, Atmospheric Environment, 1993, 27A (4), pp 467-473.

[39] Yang L., Pabalan R. T., Browning L., Dunn D. S.: *Corrosion behavior of Carbon Steel and Stainless Steel Materials under Salt Deposits in Simulated Dry Repository Environments*, 2003, Mat. Res. Soc. Symp. Vol. 757.

[40] Yang L. Pabalan R. T., Juckett M. R.: *Deliquescence Relative Humidity Measurements Using an Electrical Conductivity Method,* Journal of Solution Chemistry, 2006, 35(4).

Appendix A

Na_2SO_4 on carbon steel (ST45) - 27 vol. % H_2O

Unwashed coupons after 4h run at 80°C and 27 vol. % H_2O.

Washed coupons after 4h run at 80°C and 27 vol. % H_2O.

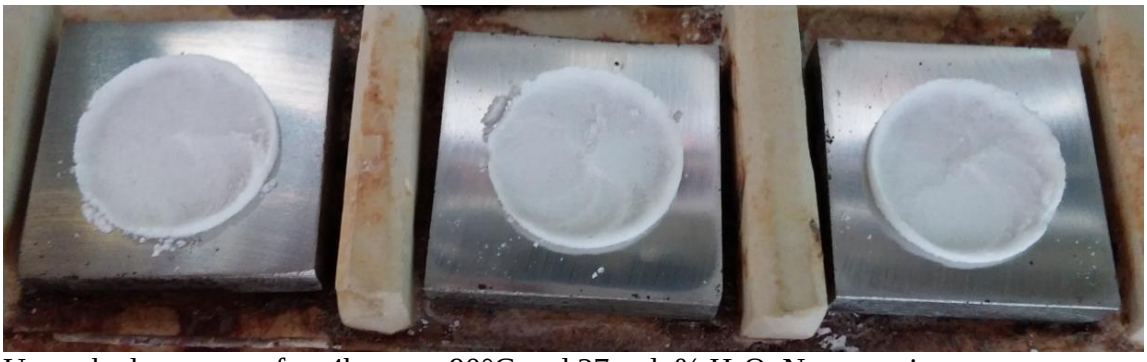

Unwashed coupons after 4h run at 90°C and 27 vol. % H_2O. No corrosion.

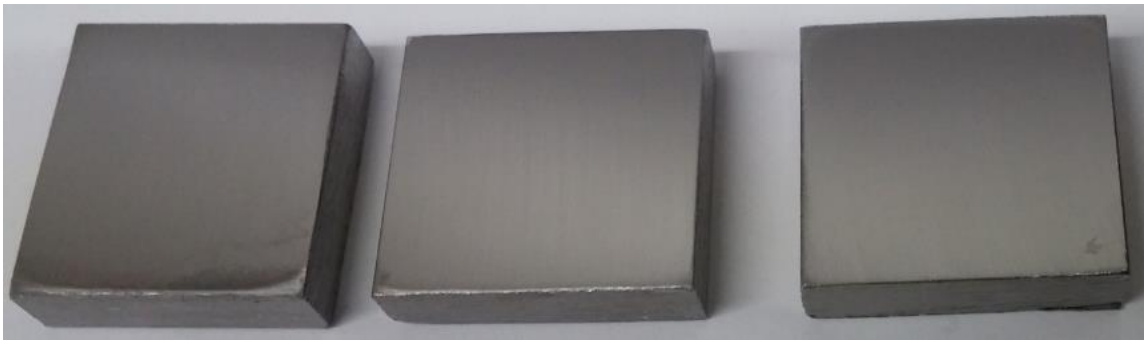

Washed coupons after 4h run at 90°C and 27 vol. % H_2O. No corrosion.

Na_2SO_4 on carbon steel (ST45) - 60 vol. % H_2O

Unwashed coupons after 4h run at 100°C.

Washed coupons after 4h run at 100°C.

Unwashed coupons after 24h run at 100°C.

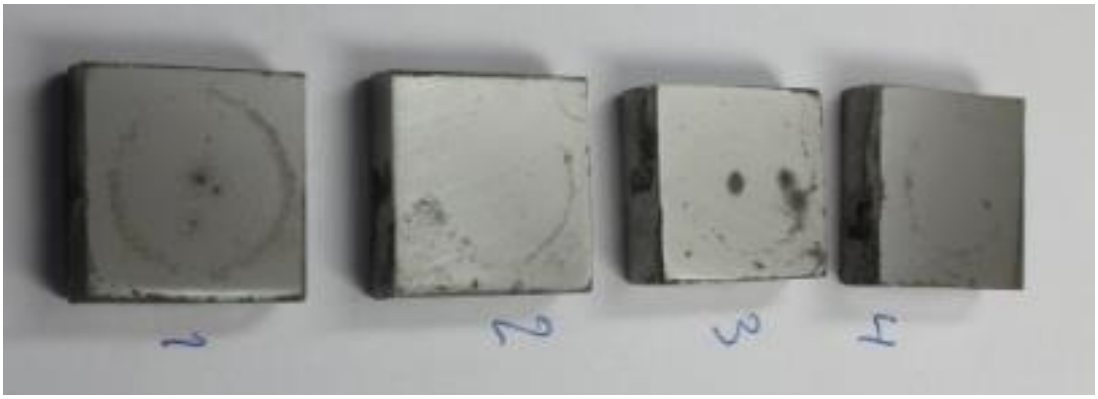

Washed coupons after 24h run at 100°C.

Washed coupon after 24h run 110°C. No corrosion.

$NaHSO_4$ on carbon steel (ST45) - 27 vol. % H_2O

Unwashed coupons after 4h run at 80°C.

Washed coupons after 4h run at 80°C.

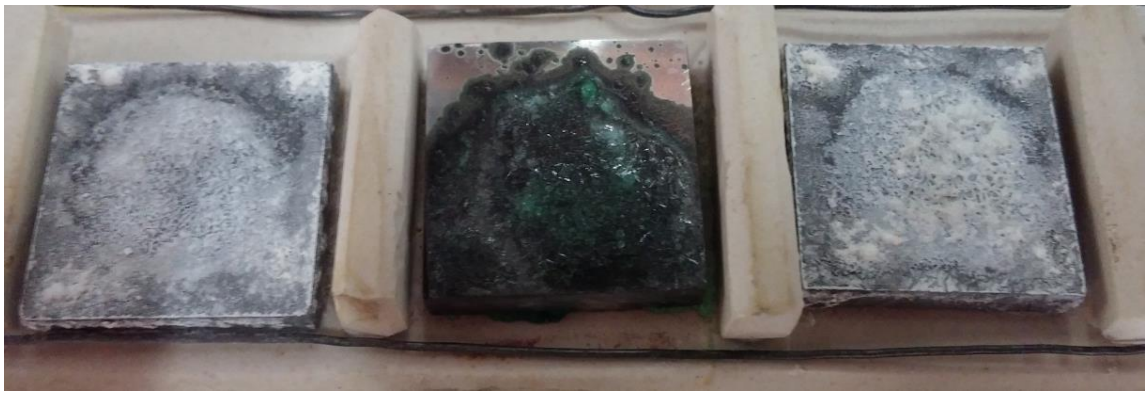

Unwashed coupons after 4h run at 90°C.

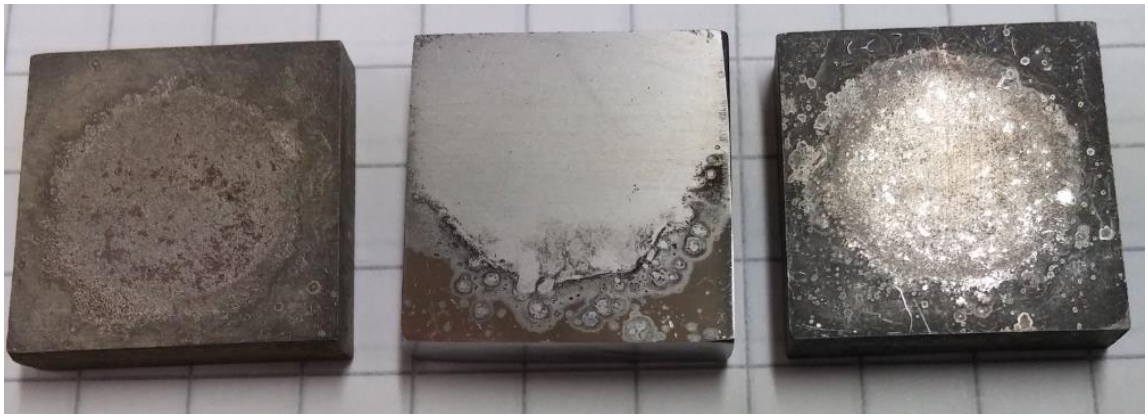

Washed coupons after 4h run at 90°C.

$NaHSO_4$ on carbon steel (ST45) - 60 vol. % H_2O

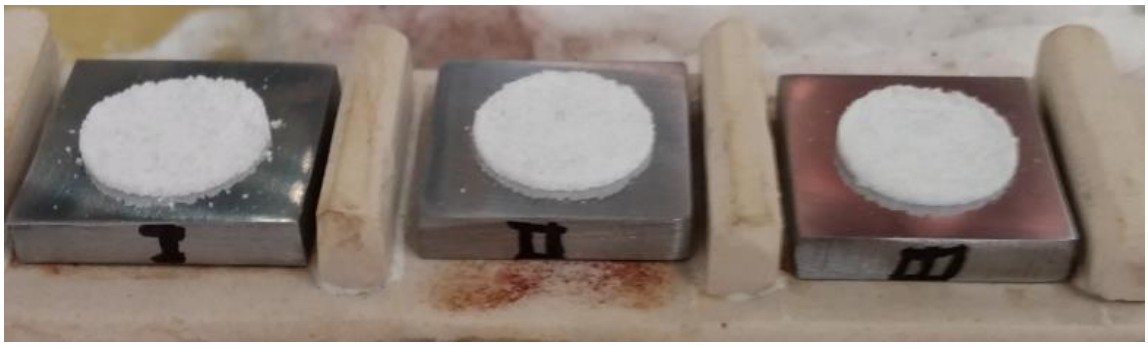

Unexposed coupons before 4h run at 120°C.

Unwashed coupons after 4h run at 120°C.

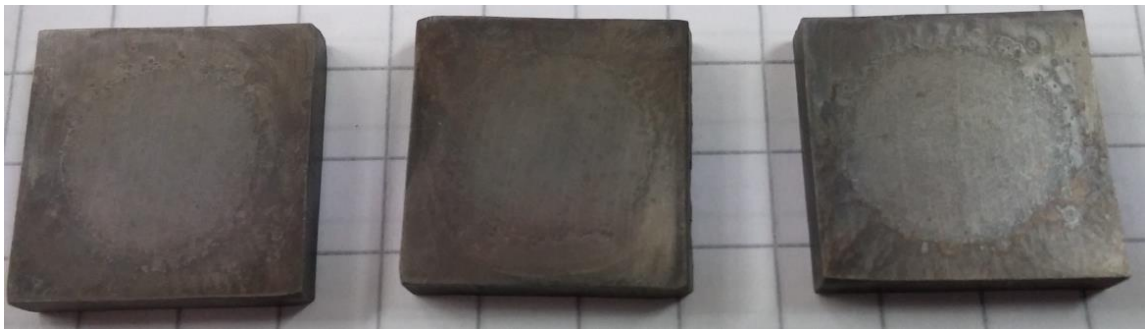

Washed coupons after 4h run at 120°C.

Unexposed coupons before 4h run at 130°C.

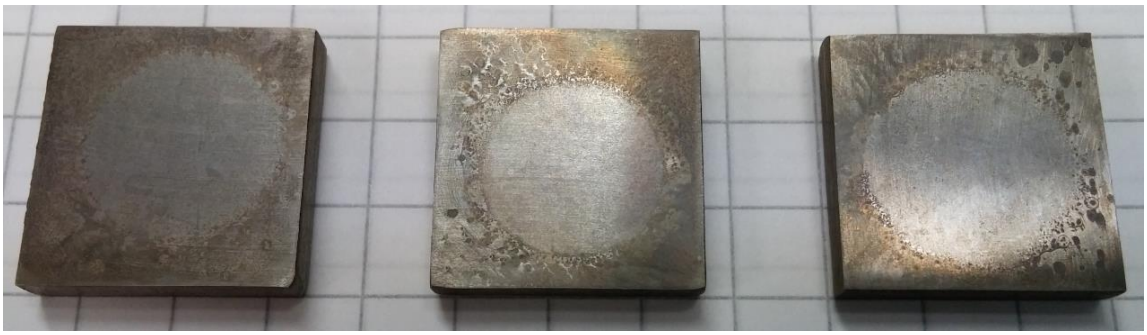

Washed coupons after 4h run at 130°C.

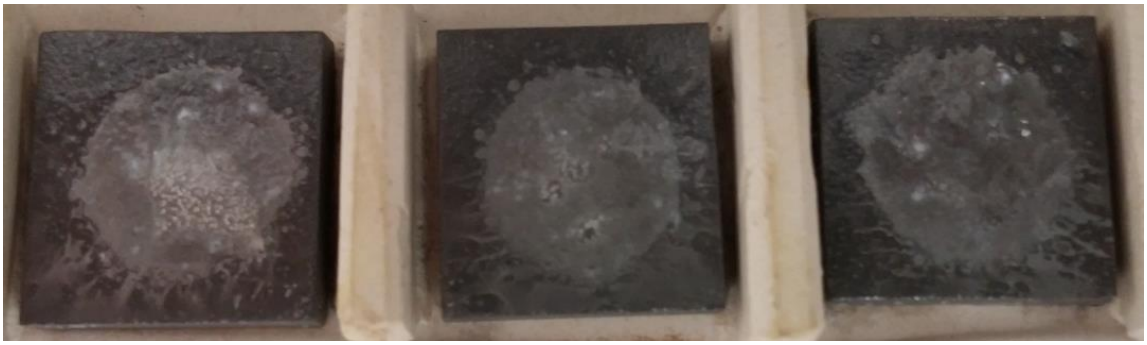

Unwashed coupons after 4h run at 140°C.

Washed coupons after 4h run at 140°C.

Unexposed coupons before 4h run at 150°C.

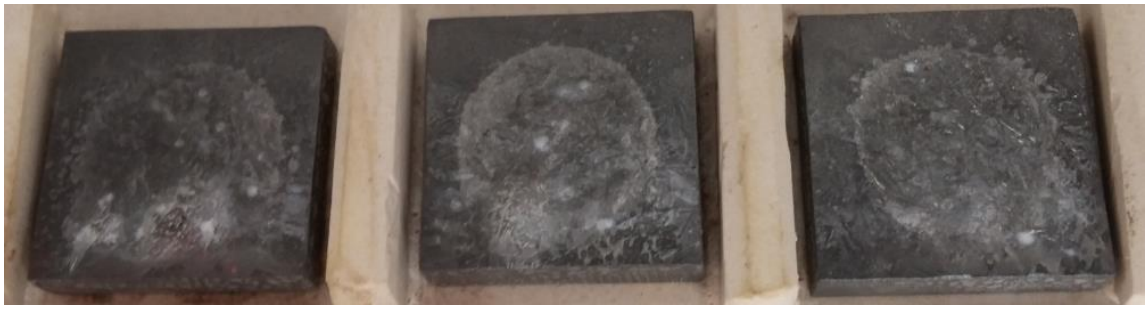

Unwashed coupons after 4h run at 150°C.

Washed coupons after 4h run at 150°C.

$NaHSO_4$ on carbon steel (ST45) - 0 vol. % H_2O

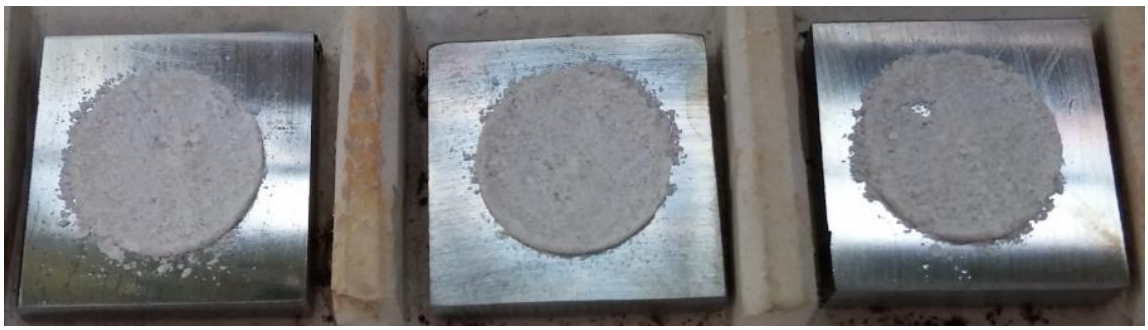

Unwashed coupons after 4h run at 150°C.

Washed coupons after 4h run at 150°C.

Na_2CO_3 on carbon steel (ST45) - 80 vol. % H_2O

Unwashed coupons after 4h run at 90°C.

Washed coupons after 4h run at 90°C. No corrosion.

Unwashed coupons after 4h run at 100°C.

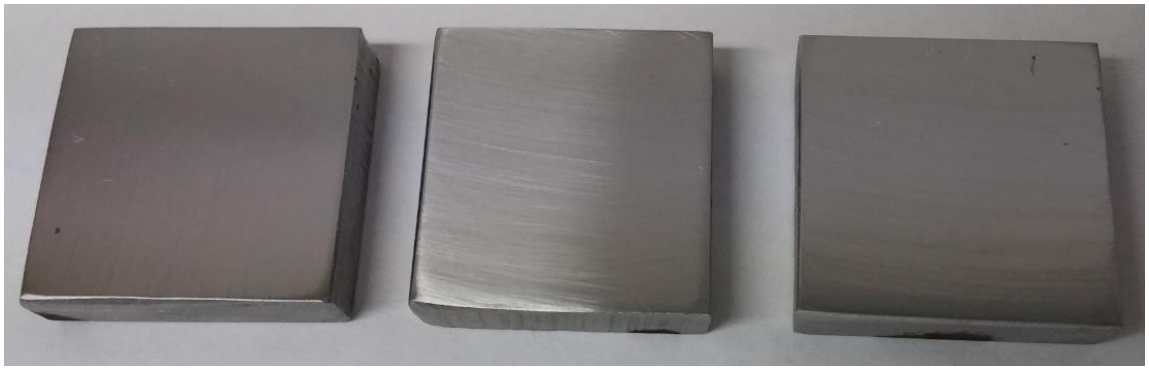

Washed coupons after 4h run at 100°C. No corrosion

Unwashed coupons after 4h run at 110°C.

Washed coupons after 4h run at 110°C. No corrosion.

Unwashed coupons after 4h run at 120°C.

Washed coupons after 4h run at 120°C. No corrosion.

NaCl on carbon steel (ST45) - 80 vol. % H_2O

Unwashed coupons after 4h run at 110°C.

Washed coupons after 4h run at 110°C.

Unwashed coupons after 4h run at 120°C.

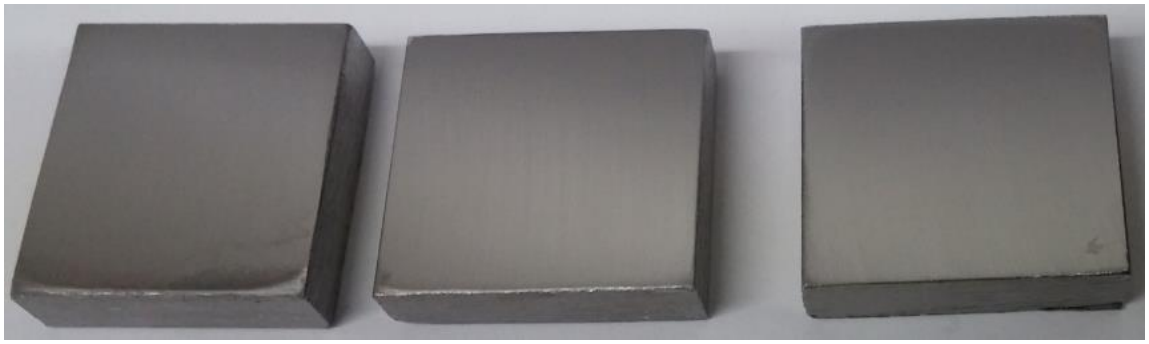

Washed coupons after 4h run at 120°C.

KCl on carbon steel (ST45) - 80 vol. % H_2O

Unwashed coupons after 24h run at 110°C.

Washed coupons after 24h run at 110°C.

Unwashed coupons after 4h run at 110°C.

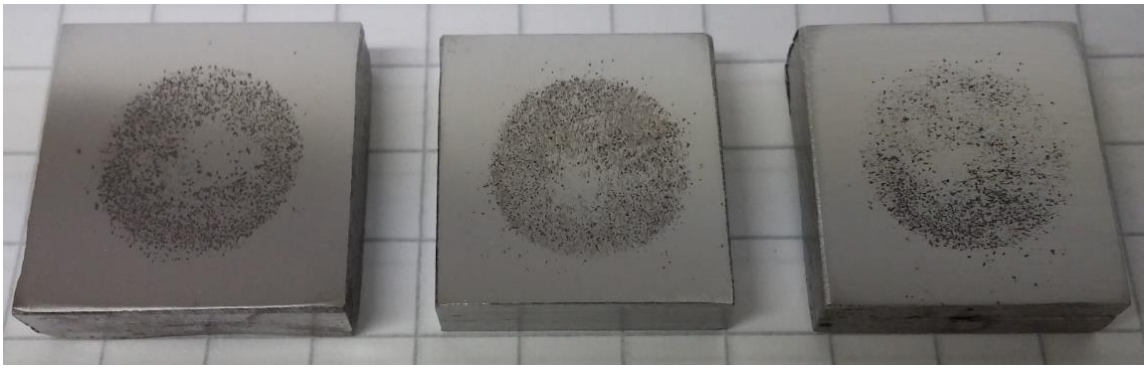

Washed coupons after 4h run at 110°C. One coupon taken to SEM/EDX analysis.

Unwashed coupons after 24h run at 120°C.

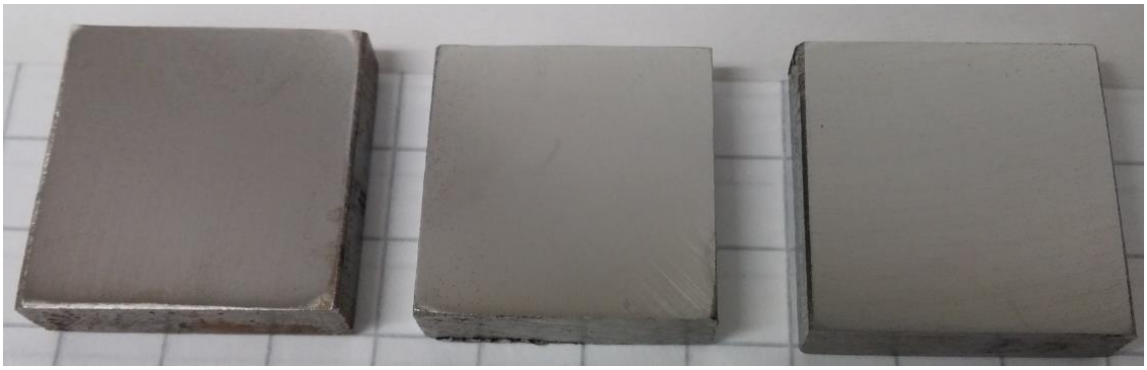

Washed coupons after 24h run at 120°C.

Deposit 1 (modern ESP ash) on carbon steel (ST45) - 27 vol. % H_2O

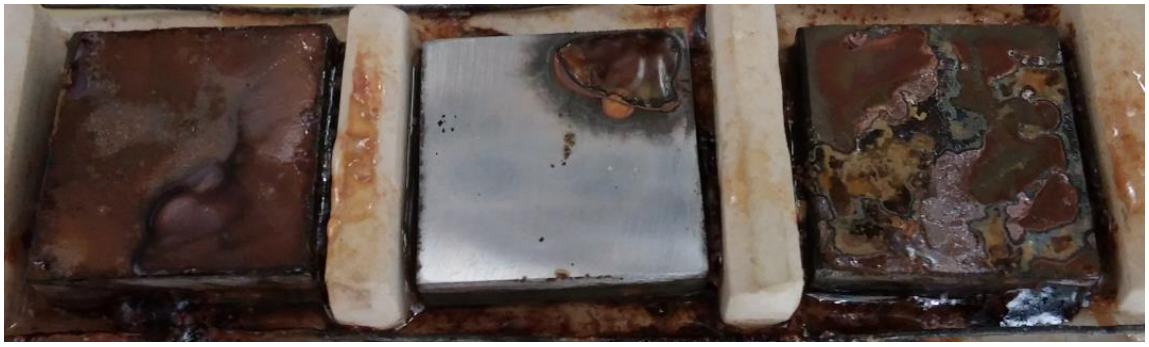

Unwashed coupons after 24h run at 70°C.

Washed coupons after 24h run at 70°C.

Unwashed coupons after 24h run at 80°C.

Washed coupons after 24h run at 80°C.

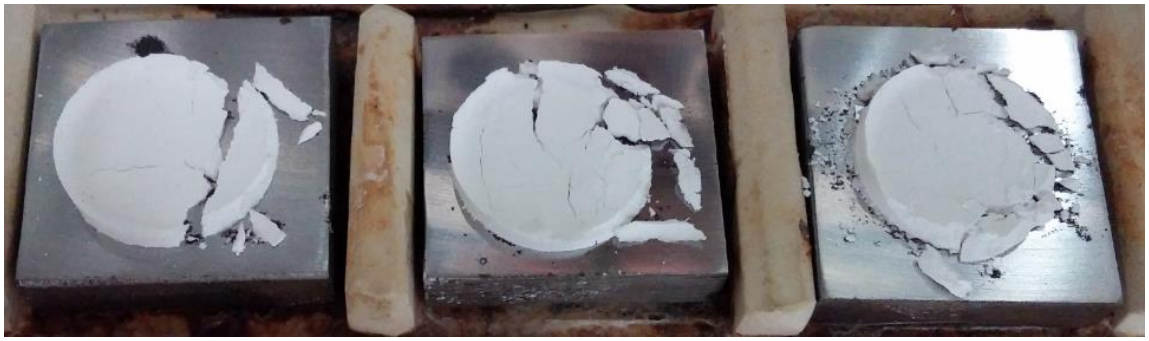

Unwashed coupons after 24h run at 90°C.

Washed coupons after 24h run at 90°C.

Unwashed coupons after 24h run at 100°C.

Washed coupons after 24h run at 100°C.

Unwashed coupons after 24h run at 110°C.

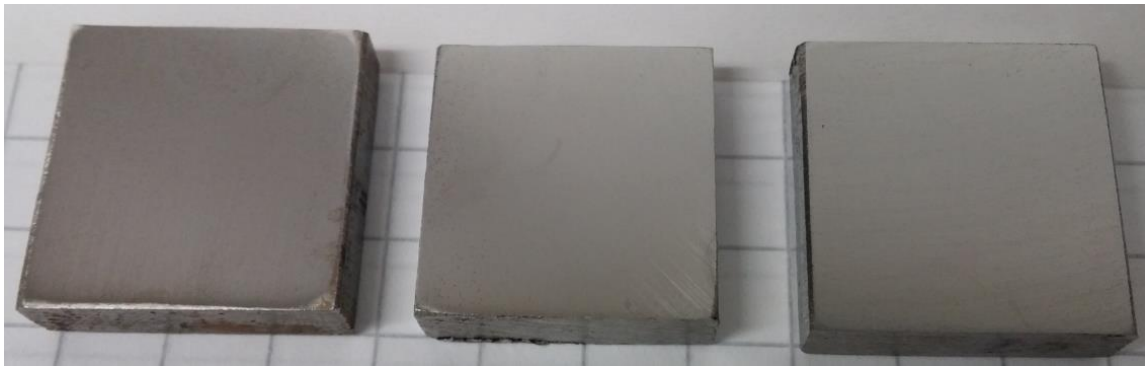

Washed coupons after 24h run at 110°C.

Deposit 1 (modern ESP ash) on carbon steel (ST45) - 60 vol. % H_2O

Unwashed coupons after 4h run at 100°C.

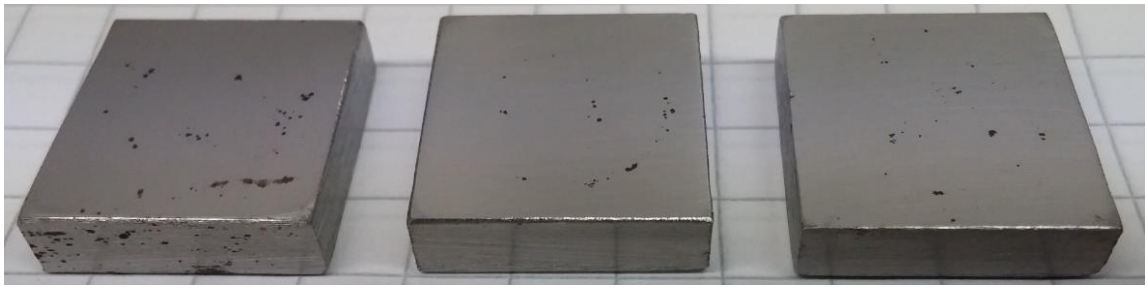

Washed coupons after 4h run at 100°C.

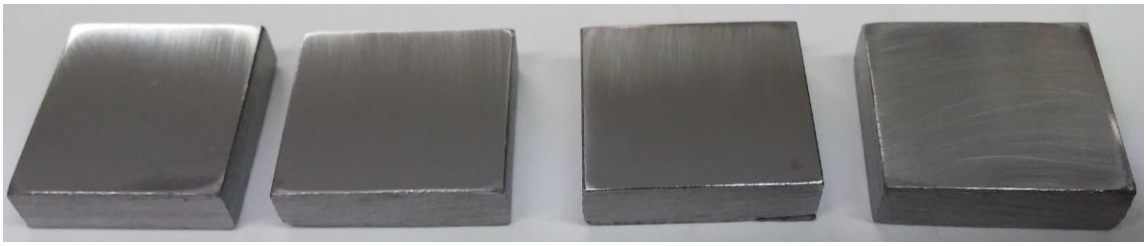

Washed coupons after 4h run at 110°C.

Unwashed coupons after 4h run at 120°C. Salt cakes broke to pieces when samples were taken out from the oven.

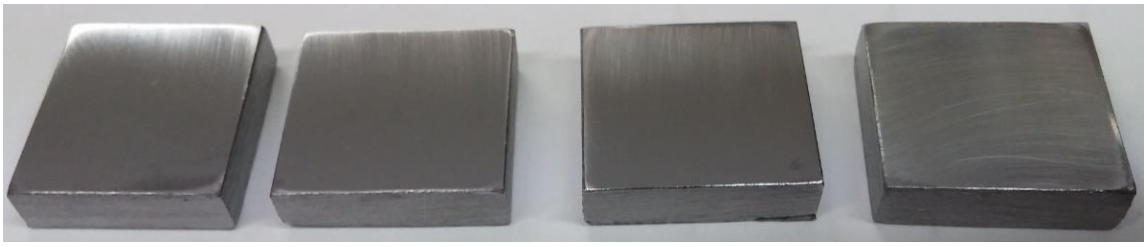

Washed coupons after 4h run at 120°C.

Deposit 2 (modern ESP ash) on carbon steel (ST45) - 27 vol. % H_2O

Unwashed coupons after 4h run at 100°C.

Washed coupons after 4h run at 100°C. Extremely weak corrosion in just a few sporadic spots. One coupon was taken to SEM/EDX analysis.

Unwashed coupons after 4h run at 110°C.

Washed coupons after 4h run at 110°C.

Deposit 2 (modern ESP ash) on carbon steel (ST45) - 60 vol. % H_2O

Unwashed coupons after 4h run at 100°C.

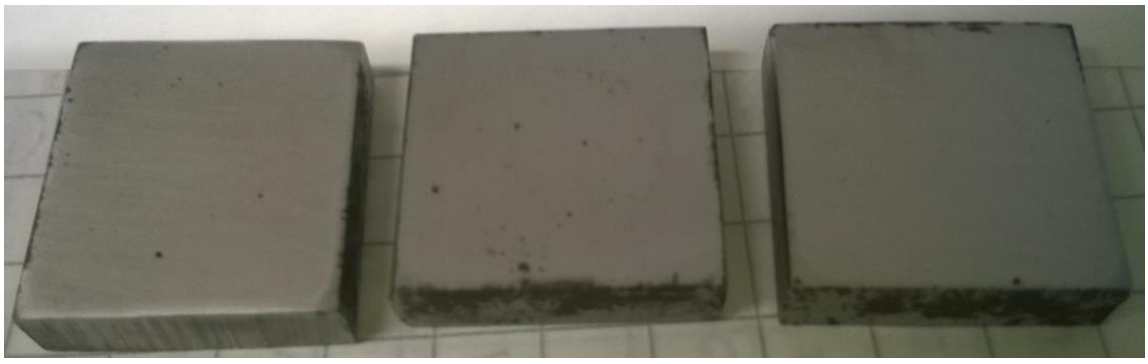

Washed coupons after 4h run at 100°C.

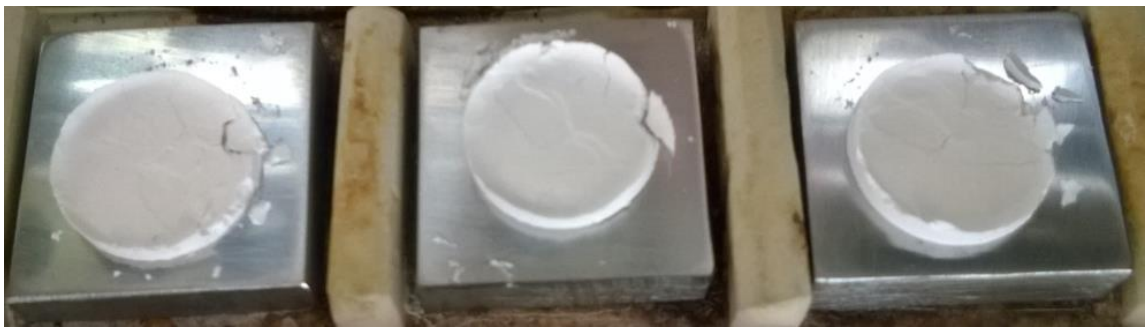

Unwashed coupons after 4h run at 110°C.

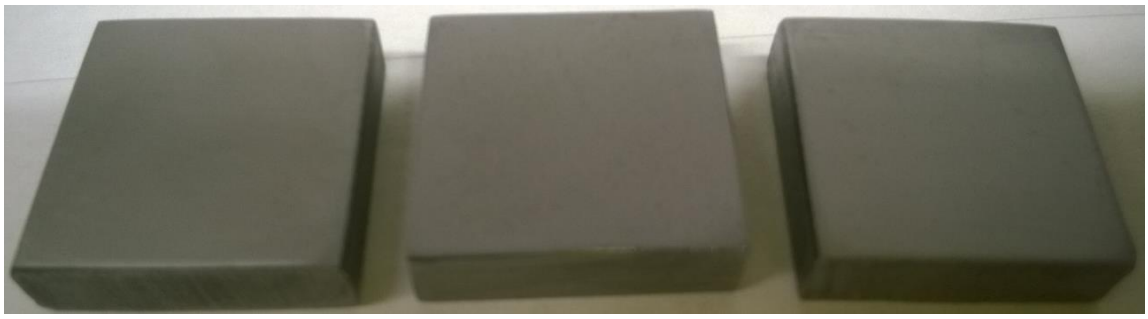

Washed coupons after 4h run at 110°C.

Appendix B

Na_2SO_4

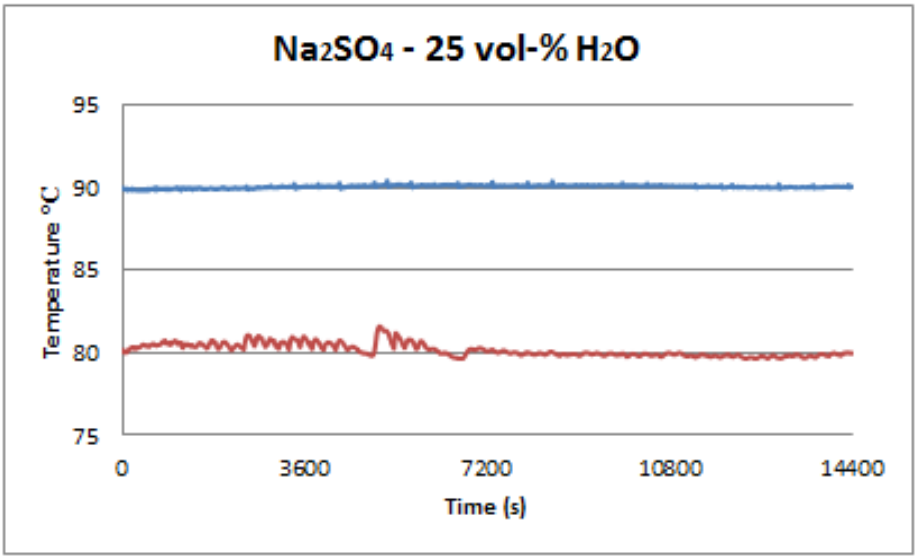

$NaHSO_4$

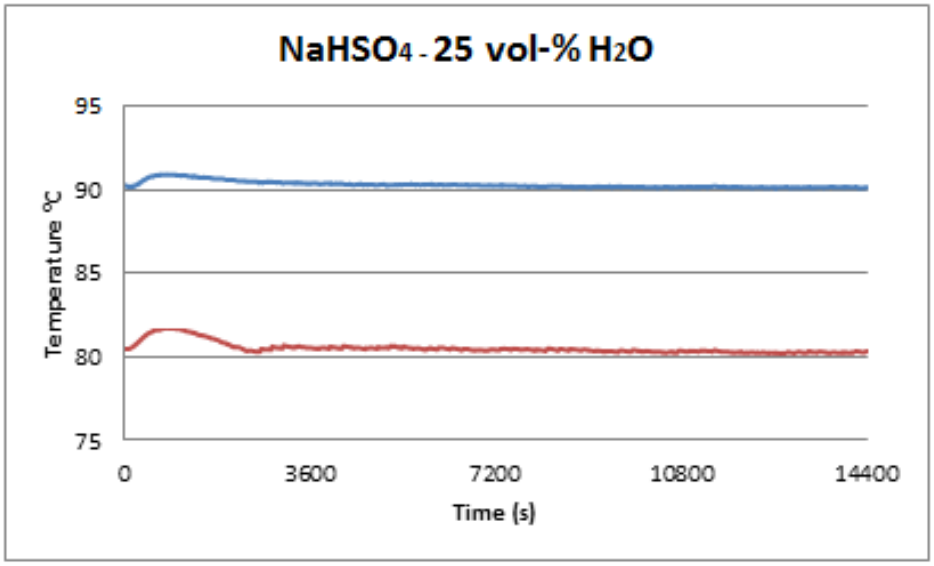
NaHSO4 - 25 vol-% H2O
95
90
85
80
75
Temperature °C
0
3600
7200
10800
14400
Time (s)

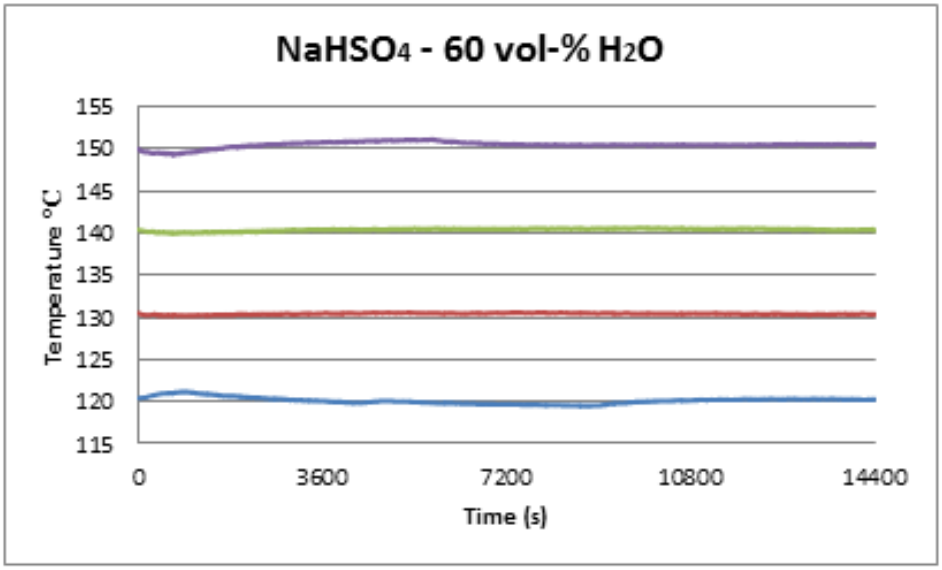
NaHSO4 - 60 vol-% H2O
155
150
145
140
135
130
125
120
115
Temperature °C
0
3600
7200
10800
14400
Time (s)

Na_2CO_3

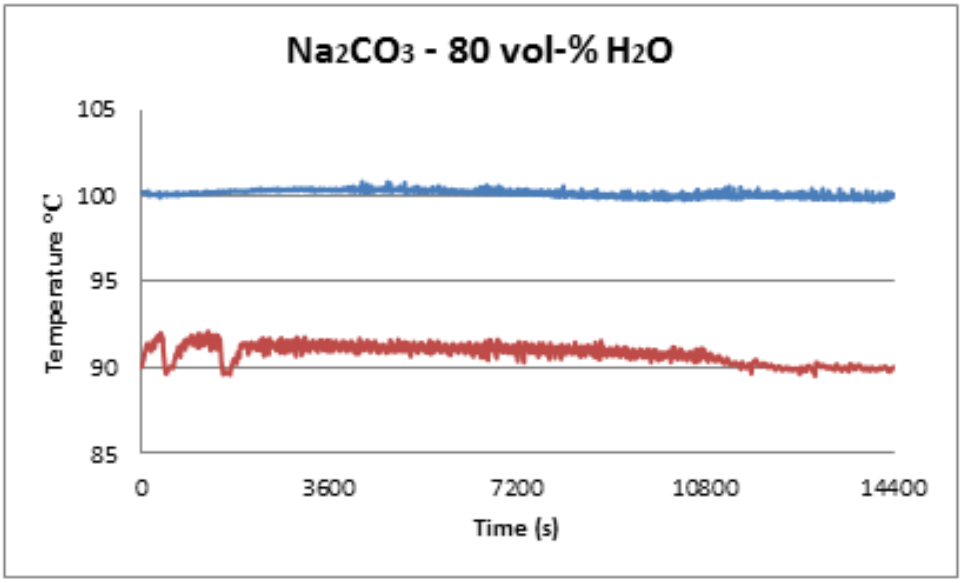
Na2CO3 - 80 vol-% H2O
105
100
95
90
85
Temperature °C
0
3600
7200
10800
14400
Time (s)

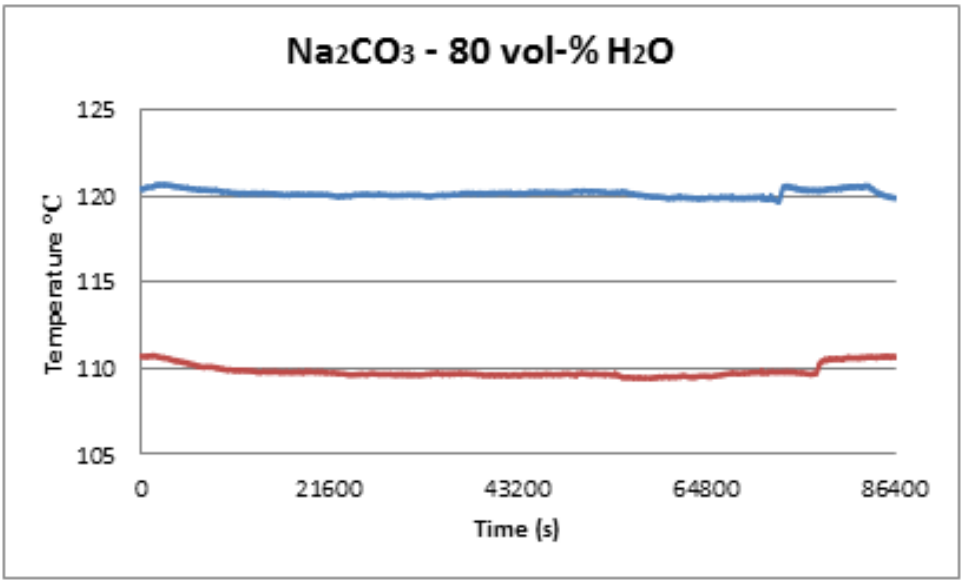
Na2CO3 - 80 vol-% H2O
125
120
115
110
105
Temperature °C
0
21600
43200
64800
86400
Time (s)

NaCl

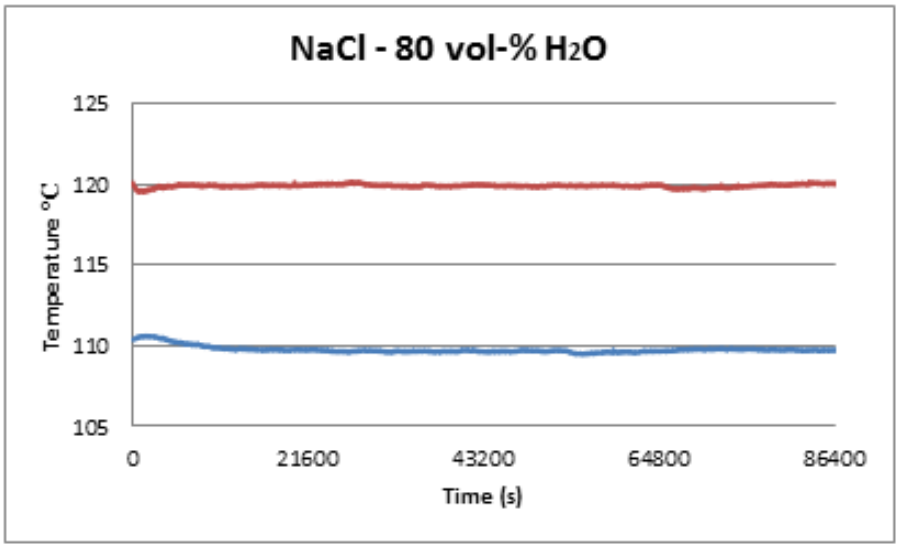
NaCl - 80 vol-% H2O
125
120
115
110
105
Temperature °C
0
21600
43200
64800
86400
Time (s)

KCl

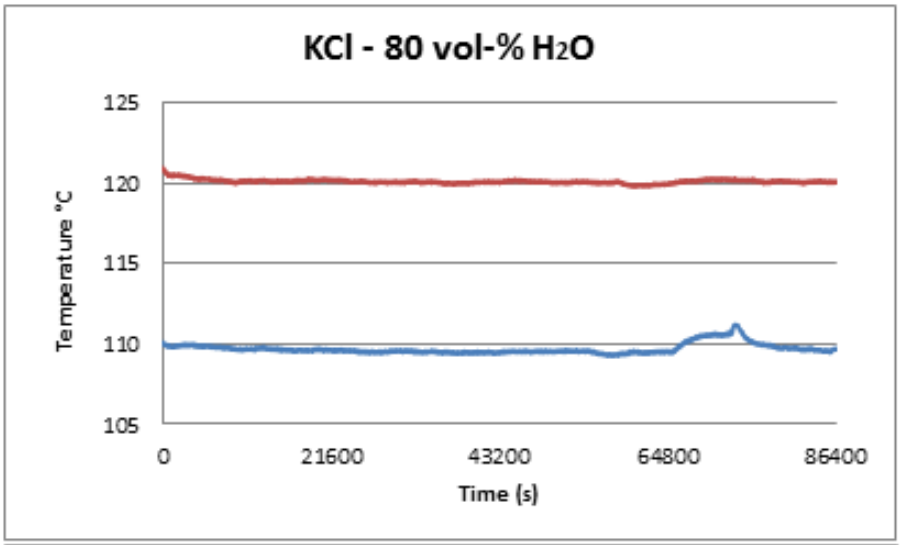
KCl - 80 vol-% H2O
125
120
115
110
105
Temperature °C
0
21600
43200
64800
86400
Time (s)

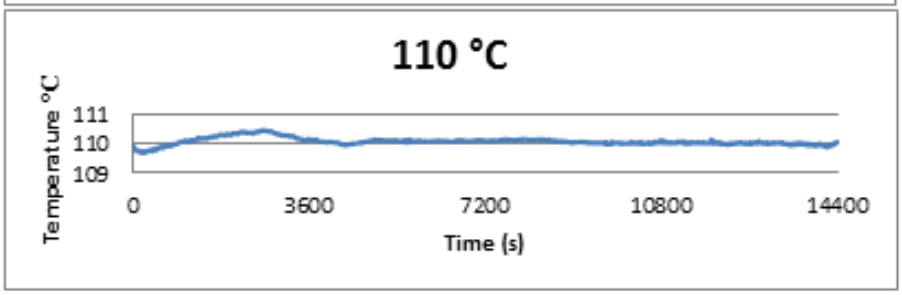
110 °C
111
110
109
Temperature °C
0
3600
7200
10800
14400
Time (s)

Electrostatic precipitator ash 1 (AP1)

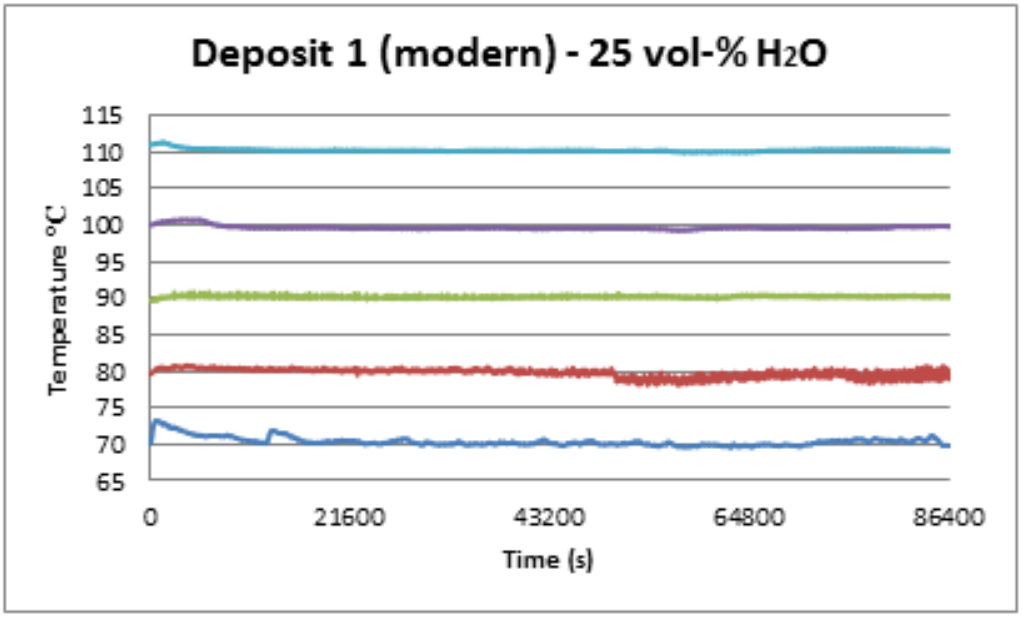

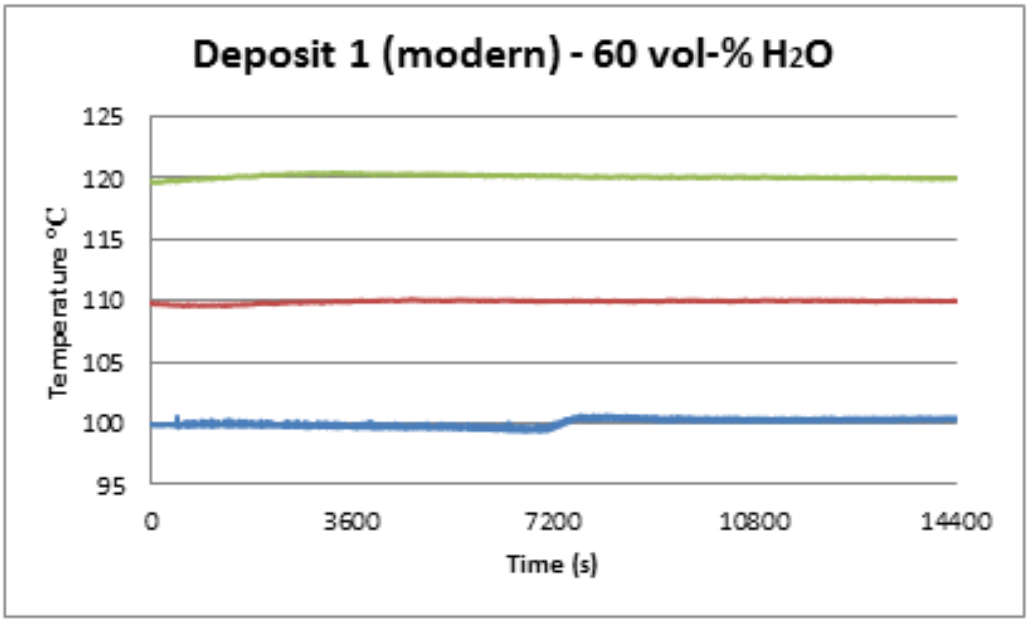

Electrostatic precipitator ash 2 (AP2)

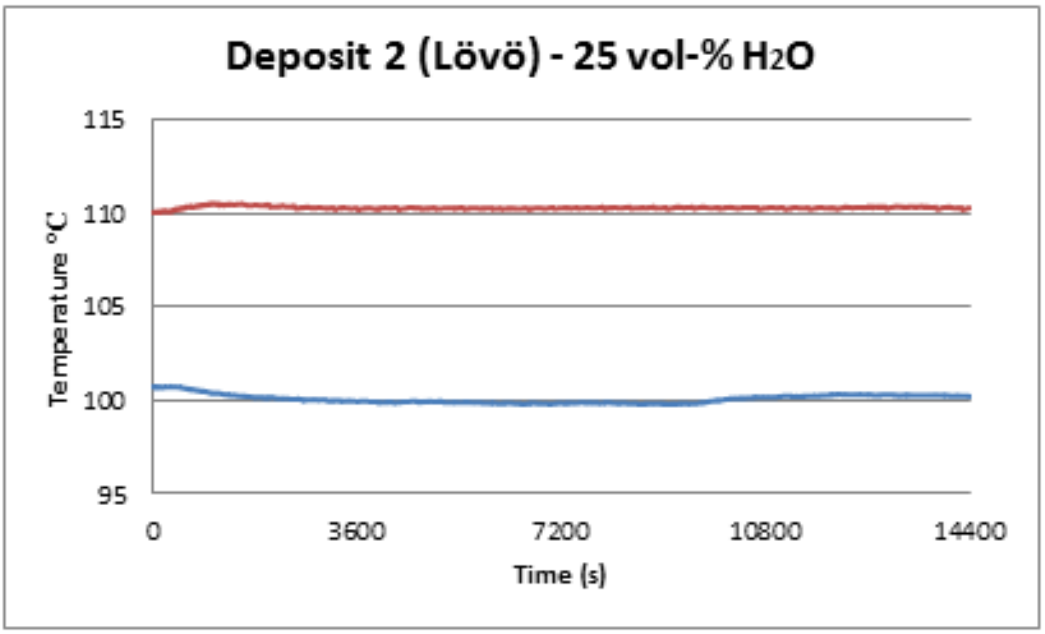

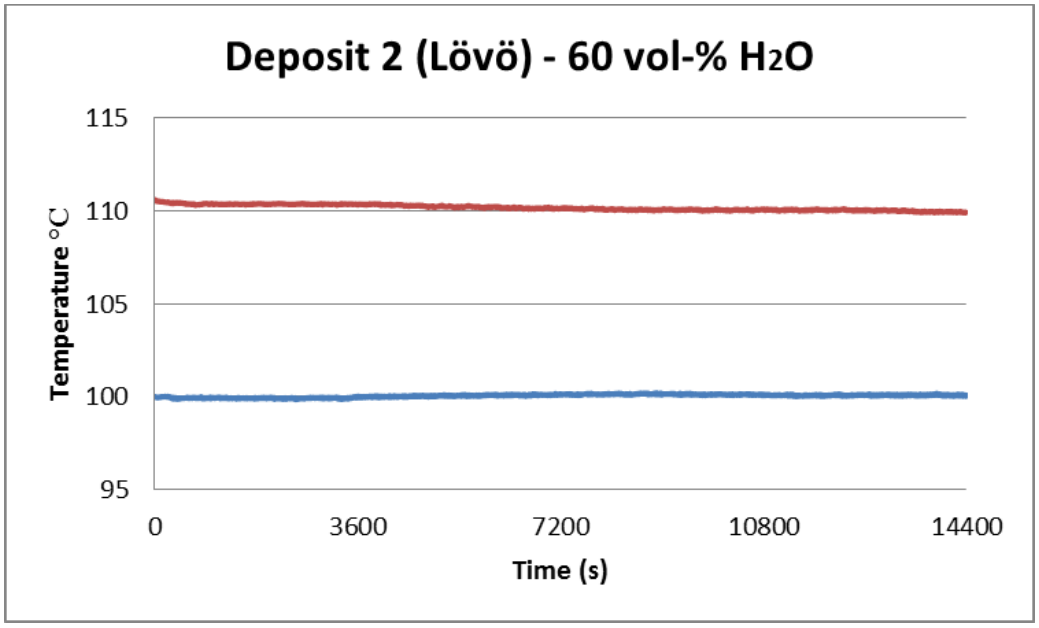

Appendix C

Table x. The total average change of mass, in coupons, before and after exposure

Na2SO4	**25 vol. %**	*Δm (mg)*	*T (°C)*	*Time (h)*	*Corrosion:*
Run26		-0,3	80	4	Yes
Run25		-31,6	90	4	No
Na2SO4	**60 vol. %**	*Δm (mg)*	*T (°C)*	*Time (h)*	
Run1		0,1	100	4	Yes
Run2		-1,95	100	24	Yes
RunX		0	110	24	No
NaHSO4	**25 vol. %**	*Δm (mg)*	*T (°C)*	*Time (h)*	*Corrosion:*
Run8		-24,6	80	4	Yes
Run7		-11,5	90	4	Yes
NaHSO4	**60 vol. %**	*Δm (mg)*	*T (°C)*	*Time (h)*	*Corrosion:*
Run3		-4,5	120	4	Yes
Run4		-3,7	130	4	Yes
Run5		-3,1	140	4	Yes
Run6		0	150	4	Yes
NaHSO4	**0 vol. %**	*Δm (mg)*	*T (°C)*	*Time (h)*	*Corrosion:*
Run9		0,3	150	4	No
Na2CO3	**80 vol. %**	*Δm (mg)*	*T (°C)*	*Time (h)*	*Corrosion:*
Run28		3,4	90	4	No
Run27		-1,2	100	4	No
Run11		1,7	110	24	No
Run10		-0,1	120	24	No
NaCl	**80 vol. %**	*Δm (mg)*	*T (°C)*	*Time (h)*	*Corrosion:*
Run12		-0,5	110	24	Yes
Run13		-0,9	120	24	No
KCl	**80 vol. %**	*Δm (mg)*	*T (°C)*	*Time (h)*	*Corrosion:*
Run14		-2,7	110	24	Yes
Run24		-0,8	110	4	Yes
Run15		-0,5	120	24	No

Deposit 1	**25 vol. %**	*Δm (mg)*	*T (°C)*	*Time (h)*	*Corrosion:*
Run16		-8,9	70	24	Yes
Run17		-7,3	80	24	Yes
Run18		0,3	90	24	Yes
Run19		2,8	100	24	Yes
Run20		-1,0	110	24	No
Deposit 1	**60 vol. %**	*Δm (mg)*	*T (°C)*	*Time (h)*	*Corrosion:*
Run23		-0,3	100	4	Yes
Run22		-0,3	110	4	No
Run21		-2,5	120	4	No
Deposit 2	**25 vol. %**	*Δm (mg)*	*T (°C)*	*Time (h)*	*Corrosion:*
Run29		-0,1	100	4	Yes
Run30		-0,2	110	4	No
Deposit 2	**60 vol. %**	*Δm (mg)*	*T (°C)*	*Time (h)*	*Corrosion:*
Run32		-1,8	100	4	Yes
Run31		-0,5	110	4	No

Table x. Weight measurements for all coupons and their average change in mass

Weight:	before (g)	after (g)	Diff (g)	Avg. Diff. (mg)
Run1	18,4962	18,4963	1E-04	
	20,1905	20,1905	0	
	16,9758	16,9758	0	
	18,6909	18,6910	1E-04	
	17,4550	17,4551	0,0001	
			6E-05	0,06
Run2	17,0948	17,0940	-0,0008	
	17,5544	17,5515	-0,0029	
	17,0585	17,0587	0,0002	
	19,7954	19,7911	-0,0043	
			-0,0019	-1,95
Run3	12,3388	12,3351	-0,0037	
	12,0347	12,0303	-0,0044	
	12,3297	12,3242	-0,0055	
			-0,00453	-4,53333

Run4	12,6376	12,6354	-0,0022	
	12,5522	12,5538	0,0016	
	12,4694	12,4663	-0,0031	
			-0,0037	-3,7
Run5	12,5658	12,5633	-0,0025	
	12,2200	12,2204	0,0004	
	12,4886	12,4813	-0,0073	
			-0,00313	-3,13333
Run6	12,1326	12,1321	-0,0005	
	12,3032	12,3039	0,0007	
	12,3757	12,3755	-0,0002	
			0	0
Run7	12,6561	12,6385	-0,0176	
	12,4409	12,4268	-0,0141	
	11,3221	11,3193	-0,0028	
			-0,0115	-11,5
Run8	12,3699	12,3468	-0,0231	
	11,9351	11,9089	-0,0262	
	12,6089	12,5844	-0,0245	
			-0,0246	-24,6
Run9	12,2927	12,2936	0,0009	
	12,2375	12,2370	-0,0005	
	12,2503	12,2508	0,0005	
			0,0003	0,3
Run10	12,6477	12,6484	0,0007	
	12,5329	12,5321	-0,0008	
	12,5161	12,5159	-0,0002	
			-1E-04	-0,1
Run11	12,2005	12,2005	0	
	12,0175	12,0218	0,0043	
	12,5611	12,5618	0,0007	
			0,001667	1,666667

Run12	12,4695	12,4696	1E-04	
	12,1601	12,1599	-0,0002	
	12,2572	12,2559	-0,0013	
			-0,00047	-0,46667
Run13	12,2598	12,2597	-1E-04	
	12,4910	12,4892	-0,0018	
	12,1406	12,1397	-0,0009	
			-0,00093	-0,93333
Run14	12,2987	12,2942	-0,0045	
	12,3730	12,3696	-0,0034	
	12,5377	12,5376	-1E-04	
			-0,00267	-2,66667
Run15	12,4777	12,4760	-0,0017	
	12,6215	12,6209	-0,0006	
	12,4654	12,4661	0,0007	
			-0,0005	-0,53333
Run16	17,4154	17,4036	-0,0118	
	11,7629	11,7578	-0,0051	
	12,5824	12,5726	-0,0098	
			-0,0089	-8,9
Run17	19,2657	19,2545	-0,0112	
	16,9154	16,9113	-0,0041	
	19,5825	19,5759	-0,0066	
			-0,0073	-7,3
Run18	19,5426	19,5447	0,0021	
	17,9734	17,9724	-0,001	
	20,0157	20,0154	-0,0003	
			0,000267	0,266667
Run19	19,6718	19,6780	0,0062	
	19,0006	19,0027	0,0021	
	17,8558	17,8558	0	
			0,002767	2,766667
Run20	16,9486	16,9468	-0,0018	

	18,4485	18,4476	-0,0009	
	18,6513	18,6511	-0,0002	
			-0,00097	-0,96667
Run21	16,7751	16,7737	-0,0014	
	16,3998	16,3962	-0,0036	
	16,3405	16,3391	-0,0014	
	16,7918	16,7880	-0,0038	
			-0,00255	-2,55
Run22	16,6816	16,6829	0,0013	
	16,3809	16,3786	-0,0023	
	16,5620	16,5615	-0,0005	
	16,7552	16,7554	0,0002	
			-0,00033	-0,325
Run23	16,6829	16,6804	-0,0025	
	16,3786	16,3802	0,0016	
	16,5615	16,5616	1E-04	
	xxx	sem/edx		
			-0,00027	-0,26667
Run24	20,1511	20,1528	0,0017	
	17,4205	17,4188	-0,0017	
	16,6602	16,6579	-0,0023	
	xxx	sem/edx		
			-0,00077	-0,76667
Run25	12,0340	12,0282	-0,0058	
	12,5474	12,5367	-0,0107	
	12,2167	12,2016	-0,0151	
			-0,0316	-31,6
Run26	12,2016	12,2010	-0,0006	
	12,0282	12,0280	-0,0002	
	12,5367	12,5366	0	
			-0,0003	-0,26667
Run27	18,1248	18,1260	0,0012	
	17,9854	17,9818	-0,0036	
	17,6399	17,6386	-0,0013	

			-0,0012	-1,23333
Run28	17,6171	17,6183	0,0012	
	18,1045	18,1045	0	
	17,9603	17,9625	0,0022	
			0,0034	3,4
Run29	18,0511	18,0511	0	
	xxx	sem/edx		
	18,1071	18,107	-1E-04	
	17,9774	17,9773	-1E-04	
			-6,7E-05	-0,06667
Run30	18,2081	18,2081	0	
	17,3137	17,3135	-0,0002	
	17,9665	17,9661	-0,0004	
			-0,0002	-0,2
Run31	17,9415	17,9435	0,002	
	18,1849	18,1848	-1E-04	
	17,2921	17,2887	-0,0034	
			-0,0005	-0,5
Run32	17,9433	17,9423	-0,001	
	18,1864	18,1846	-0,0018	
	17,2922	17,2897	-0,0025	
			-0,00177	-1,76667

LIITE 4

ÅA, Understanding Low Temperature Corrosion in BL Combustion
Phase 2 – esitys 29.10.2015

Johan Gadolin
PROCESS CHEMISTRY CENTRE

Åbo Akademi University

Understanding Low Temperature Corrosion in BL Combustion

Nikolai DeMartini, Henri Holmblad, Emil Vainio

Background

- This SKY project has funded the DI work of Henri Holmblad at ÅAU

Background

- Industrial interest in extracting more energy from flue gases
- Some historical industrial observation of low temperature corrosion – not well documented
- H_2SO_4 acid dewpoint previously thought to exist in recovery boilers

Background - dew point at Rauma

● = measured dew point

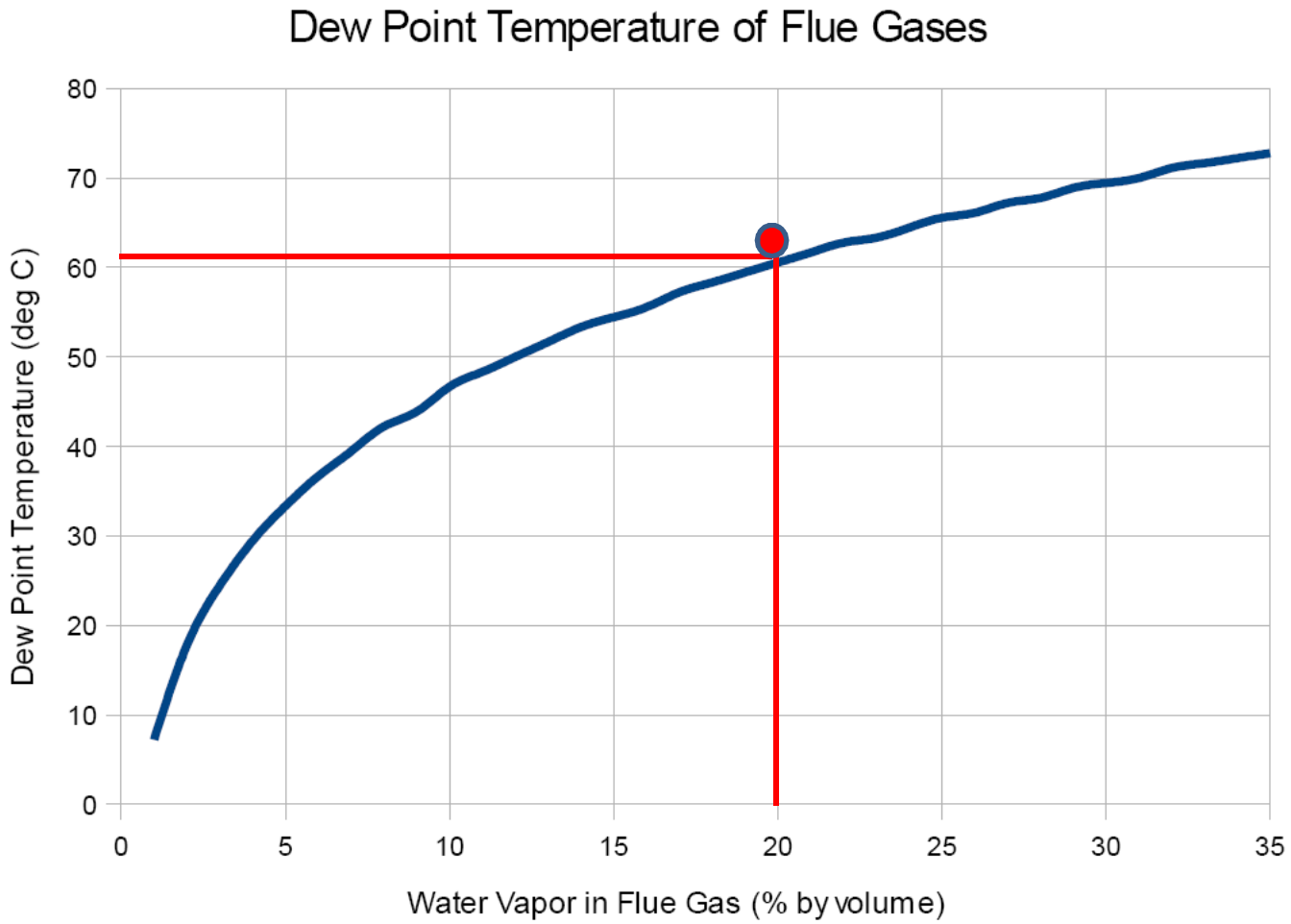

Background - corrosion probe results at Rauma

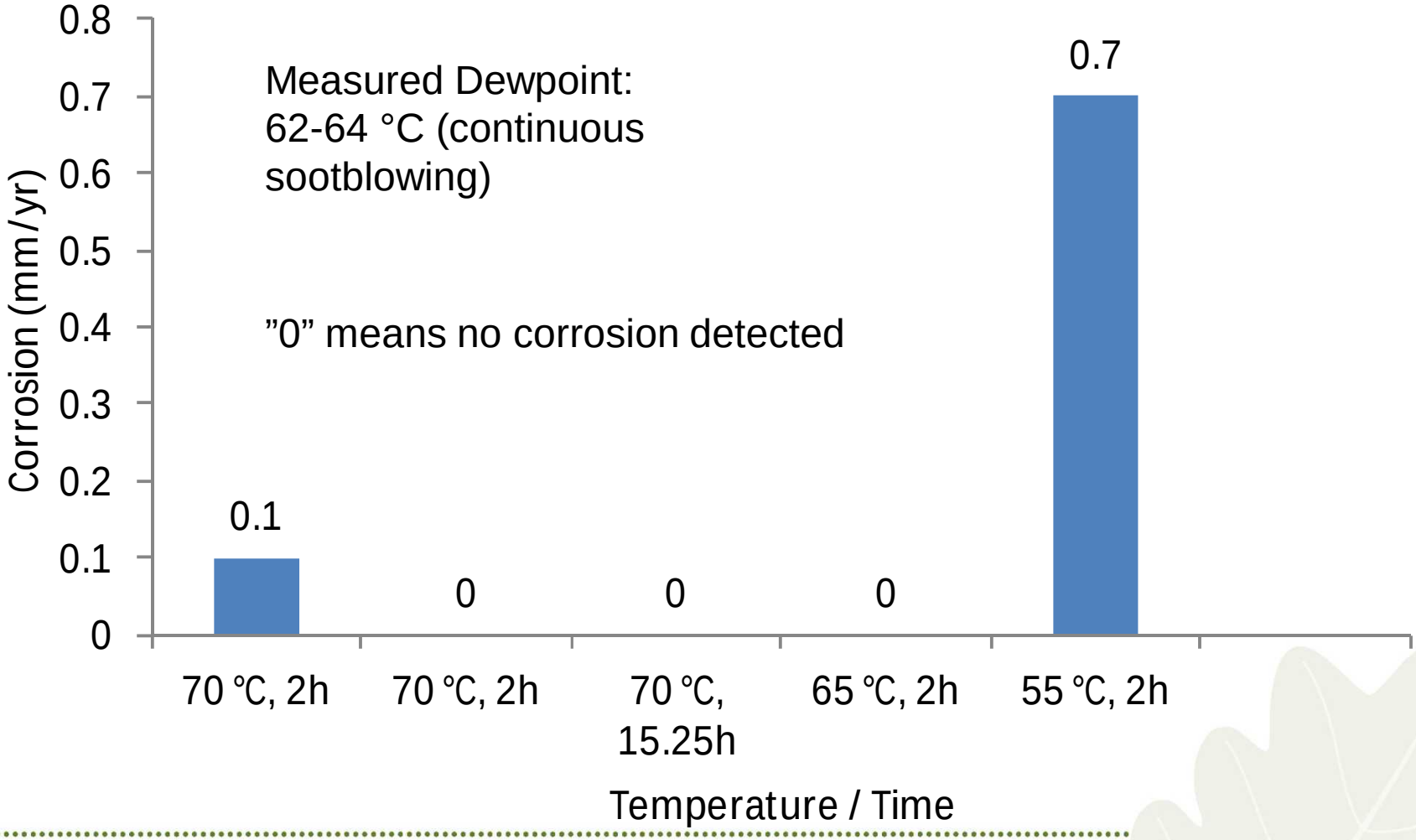

Background - dew point at Heinola

= measured dew point

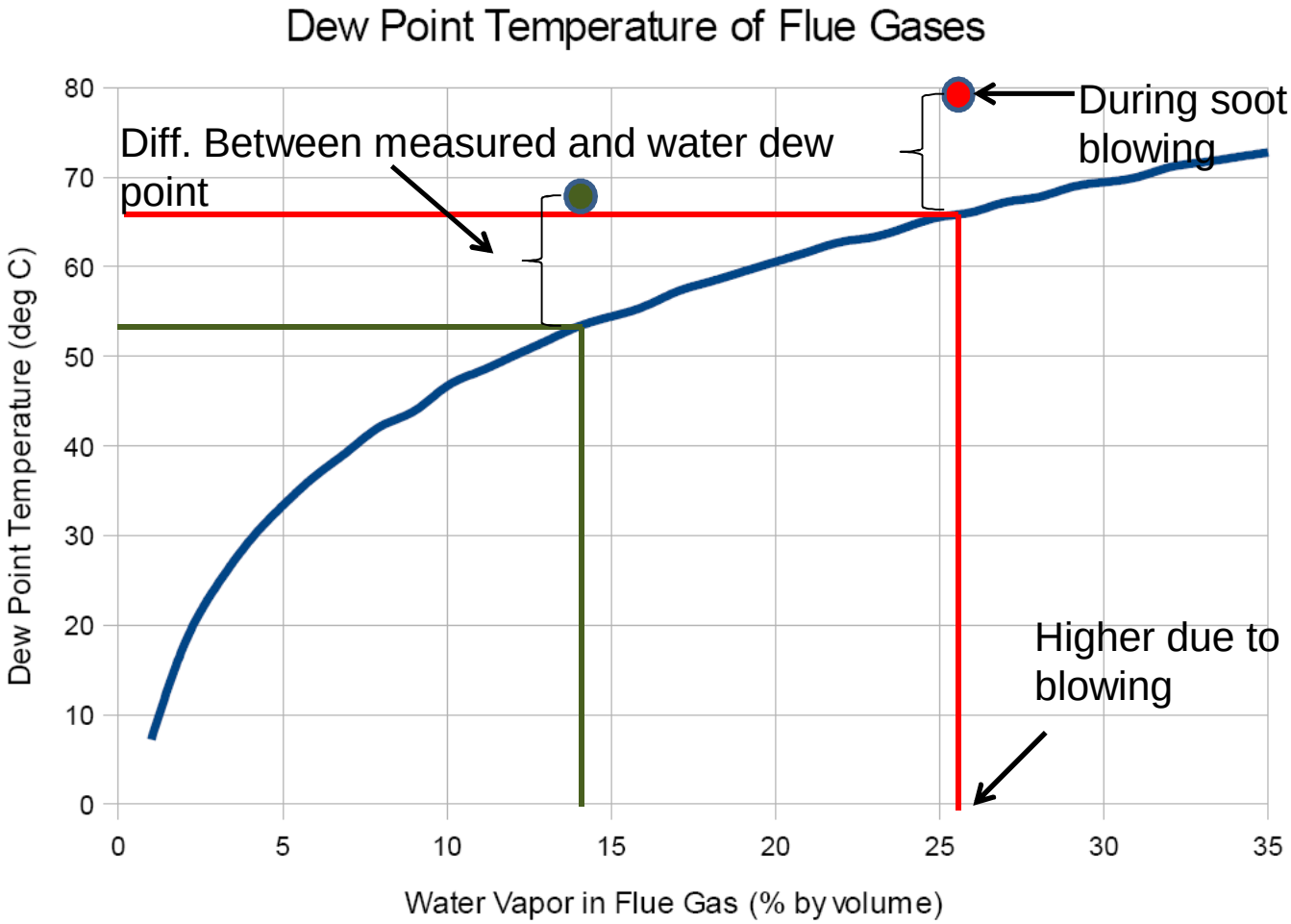

Background - corrosion probe results at Heinola

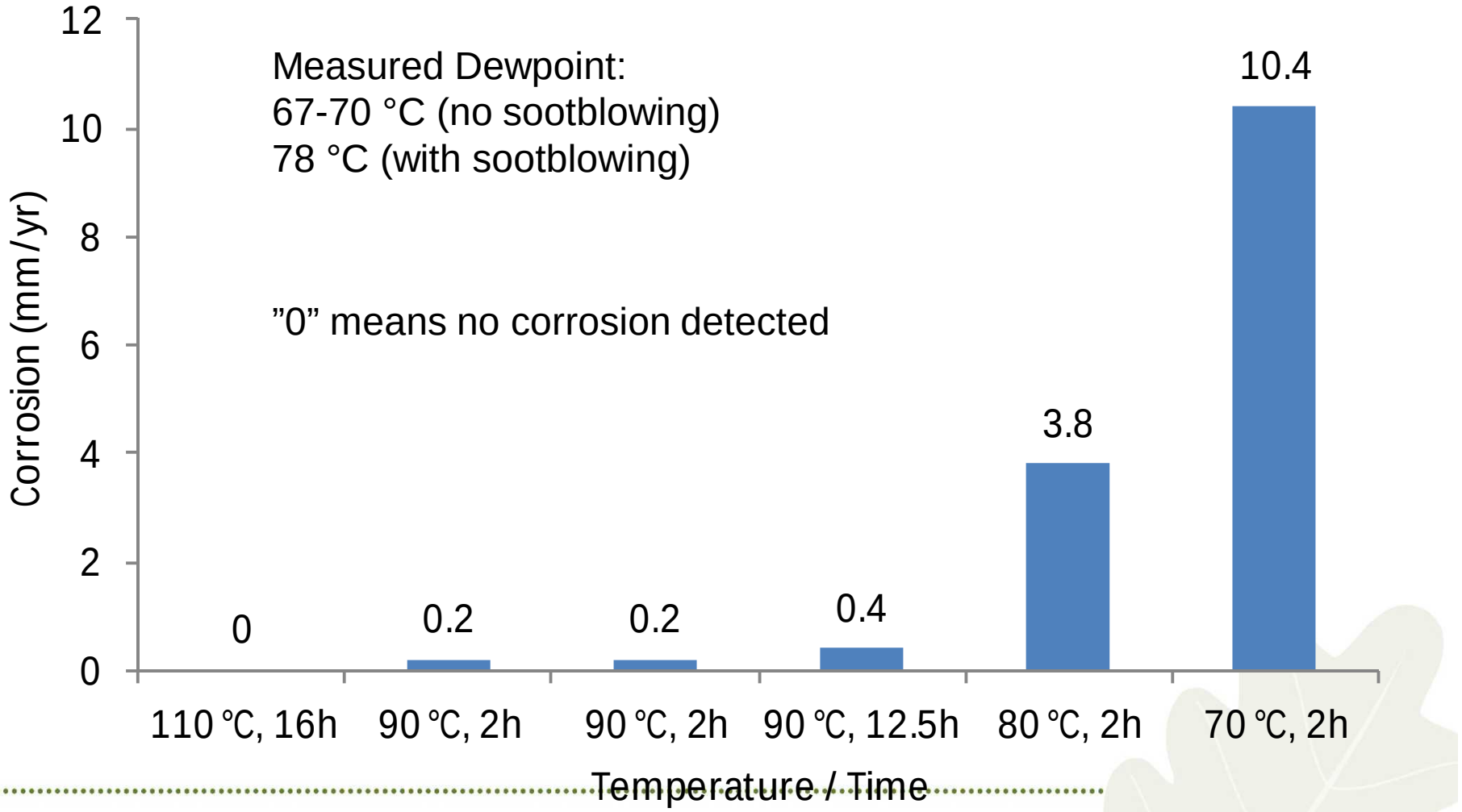

Objectives

- Hypothesis: hygroscopic salts absorb water, resulting in dew point corrosion
- Hygroscopic nature of salts in recovery boilers not yet understood
- This study – Start to map out at what temperatures/vol-% H_2O carbon steel corrodes

Experimental setup

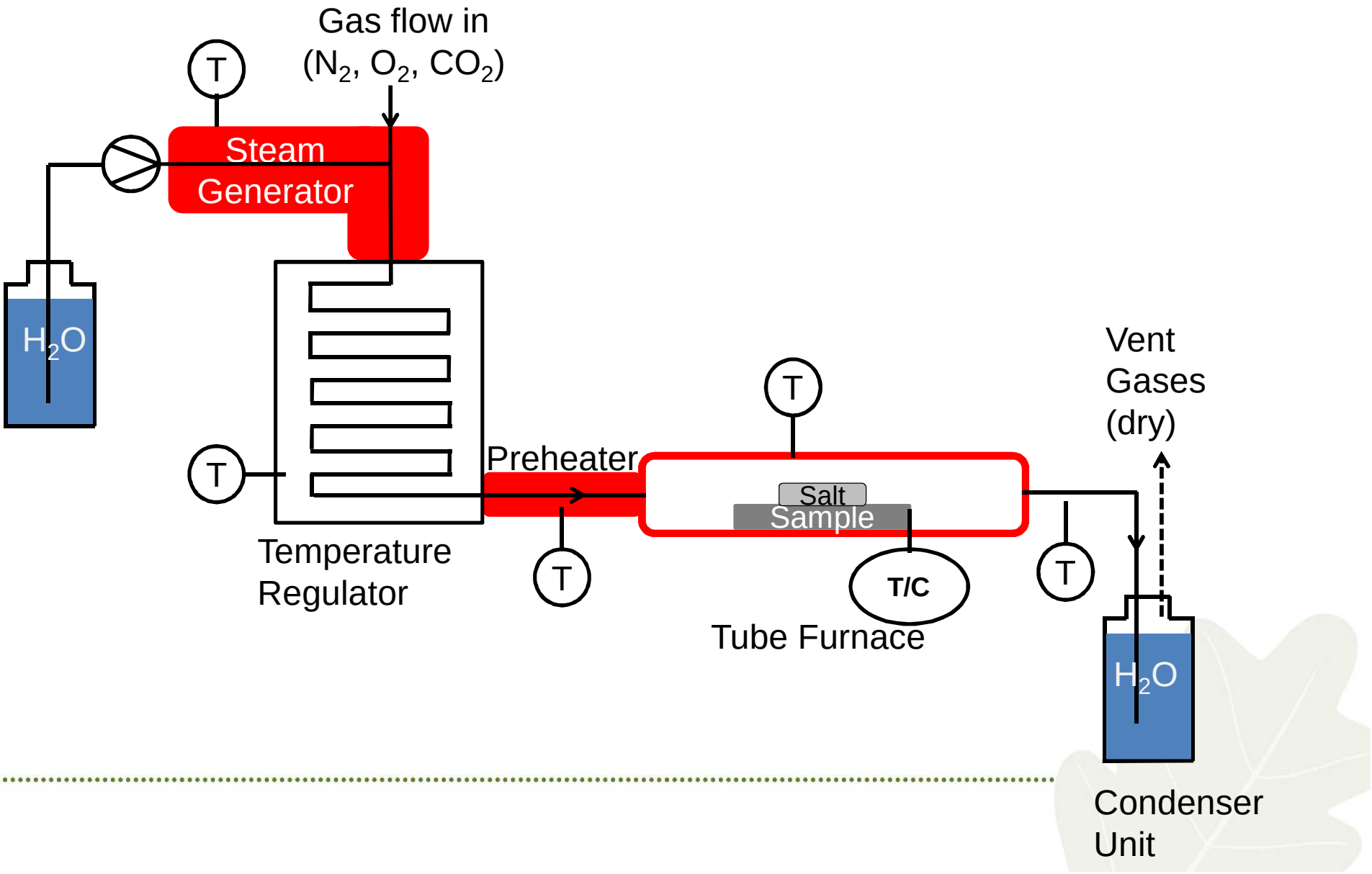

Experimental setup

Gases in

Steam Generator

Gas temperature regulator

Water in

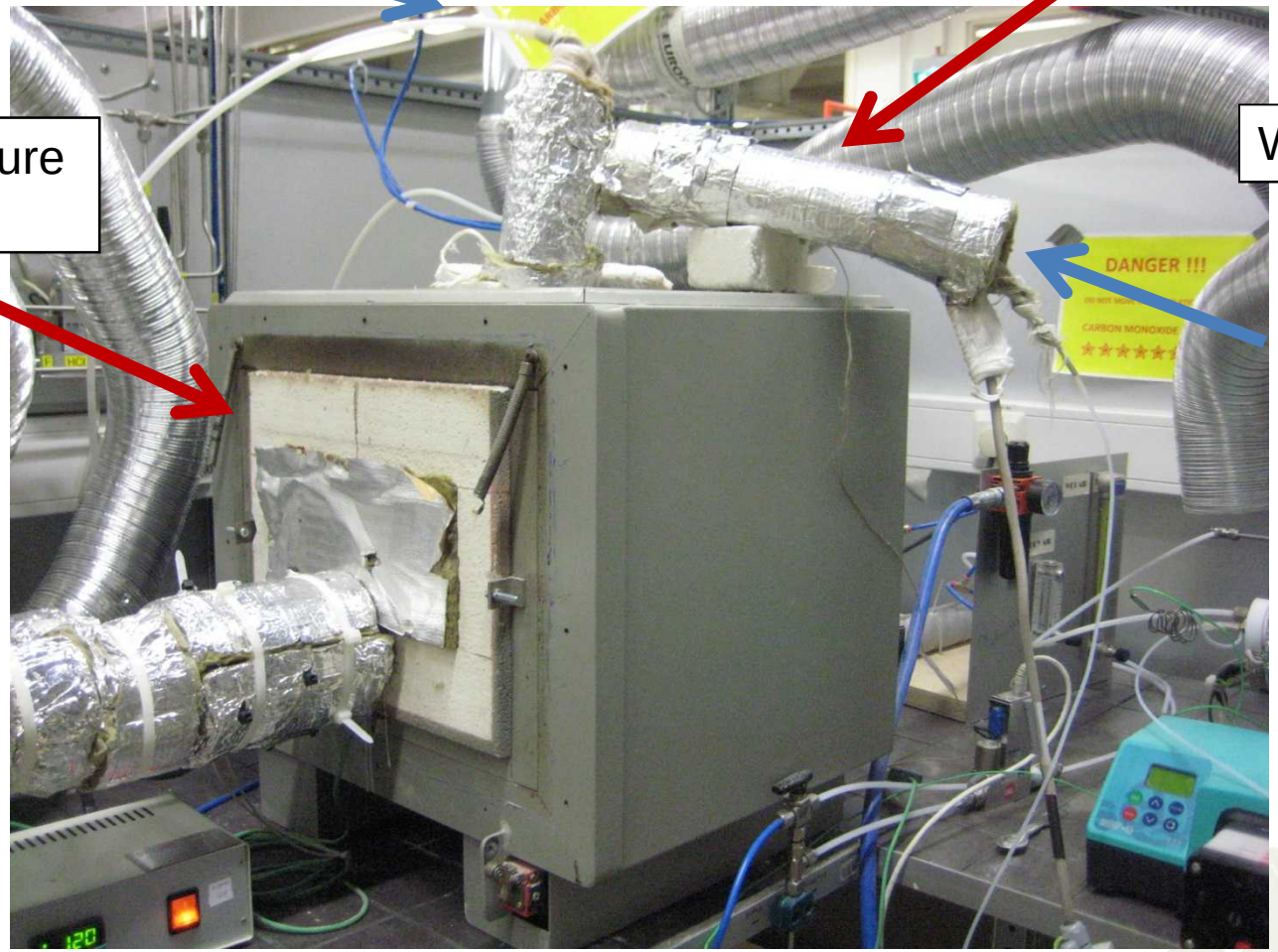

Experimental setup

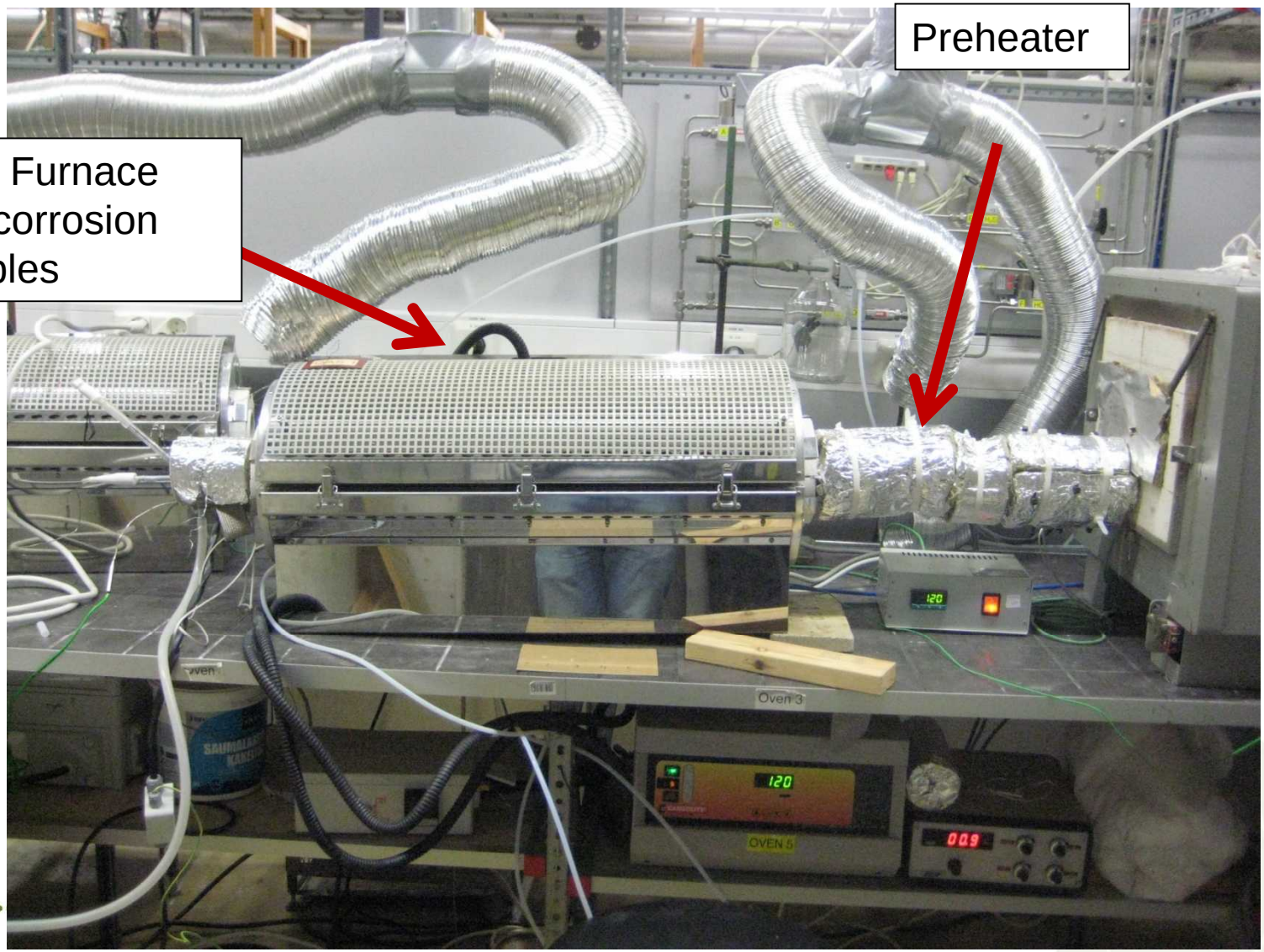

Experimental work

- corrosion sample:
  - 2x2 cm carbon steel coupon
  - 3-4 coupons per experiment
- ~0.1 g of salt on the coupon
- Ratio of dry gases during experimental runs: 15.5:3.5:1 N_2:CO_2:O_2
  - (31% N_2, 7% CO_2 & 2% O_2 at 60% H_2O)
- Corrosion determined by:
  - Visual inspection
  - (Weight loss)
  - (SEM analysis)

Experimental setup

Temparature

Na_2SO_4 4 h experiments

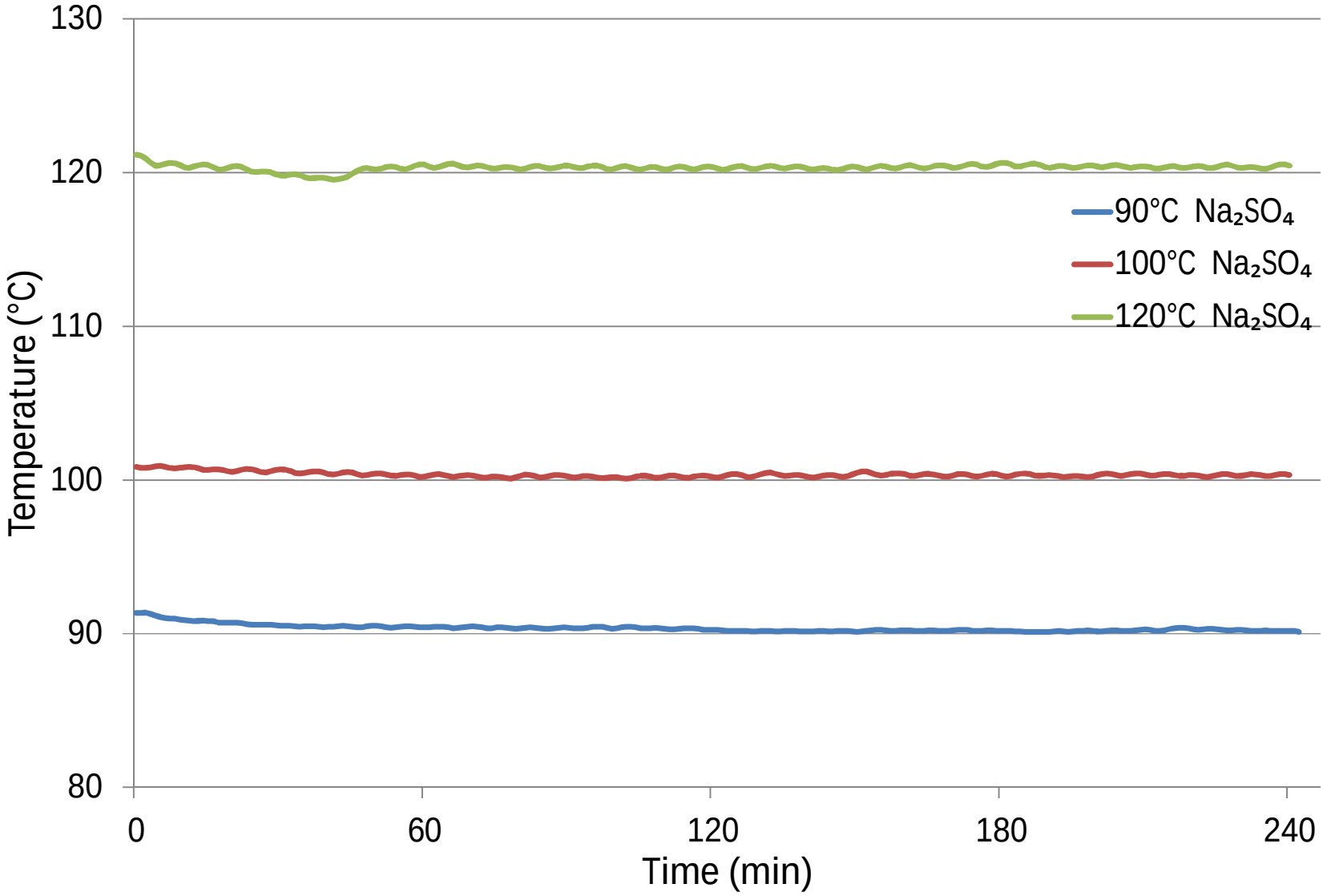

Experimental Plan 1

Salt	Temperature (°C)	H_2O (vol-%)	Time (h)
$NaHSO_4$	90	60	4
	100		
	110		
	120		
Na_2SO_4	90	60	4
	90		24
	100		4
	100		24
	110		24
	120		4

Salt Tests – Phase 2

Salt	H_2O (vol%)	Temp (°C)	Time (h)
Na_2SO_4	27	80	4
		90	4
	60	100	4
		100	24
		110	24
Na_2CO_3	80	90	4
		100	4
		110	24
		120	24
Na_2SO_4-Na_2CO_3 (90:10)	27	80	24
NaCl	80	110	24
		120	24
KCl	80	110	24
		110	4
		120	24

Precipitator Ash Tests – Phase 2

Salt	H_2O (vol%)	Temp (°C)	Time (h)
PA1	27	70	24
		80	24
		90	24
		100	24
		110	24
	60	100	4
		110	4
		120	4
	80	110	24
PA2	27	100	4
		110	4
	60	100	4
		110	4

$NaHSO_4$ tests – Phase 2

Salt	H_2O (vol%)	Temp (°C)	Time (h)
$NaHSO_4$	0	150	4
	27	80	4
		90	4
	60	120	4
		130	4
		140	4
		150	4

Precipitator Ash Composition

	Na (wt-%)	K (wt-%)	SO_4 (wt-%)	Cl (wt-%)	CO_3 (bal) (wt-%)
PA1	30.3	4.6	58.4	0.9	5.8
PA2	29.8	4.8	61.0	1.0	3.6

Results

Na_2SO_4

Salt: Na_2SO_4
Temperature: 90°C
H_2O: 60 vol-%
Exposure: 4h

Salt: Na_2SO_4
Temperature: 90°C
H_2O: 60 vol-%
Exposure: **24h**

Salt: Na_2SO_4
Temperature: 90°C
H_2O: 60 vol-%
Exposure: 4h

Top view

	WT%			
	Fe	S	Na	O
1	64.0	1.1	1.4	31.7
2	40.7	5.7	16.6	35.1
3	62.9	3.9	20.9	11.7

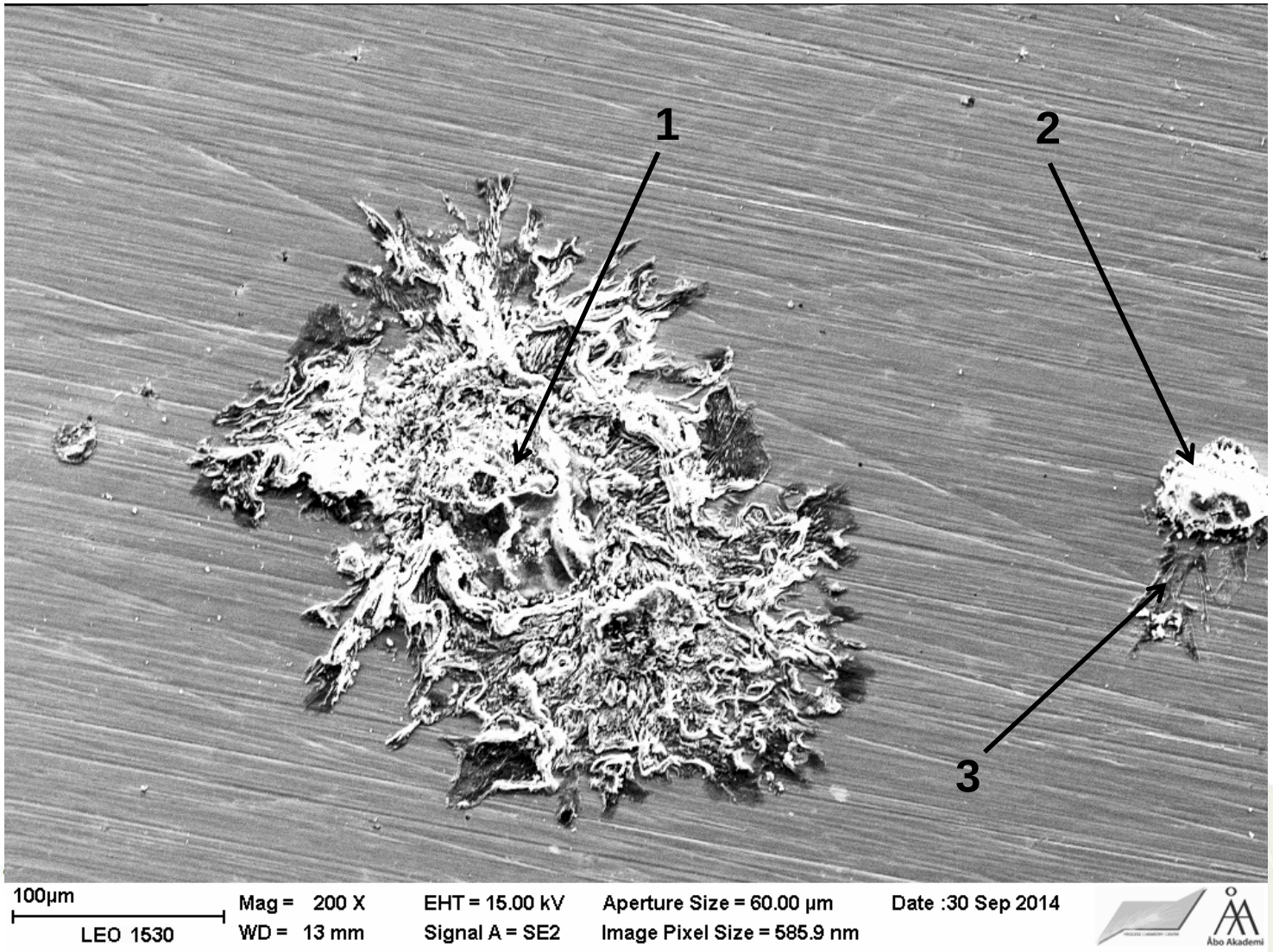

$NaHSO_4$ – Na_2SO_4 Comparison
(60 vol-% H_2O)

Na_2SO_4 – comparison of 27vol-% and 60 vol-% H_2O

Na_2SO_4, 27 vol-% H_2O

Na_2SO_4, 60 vol-% H_2O

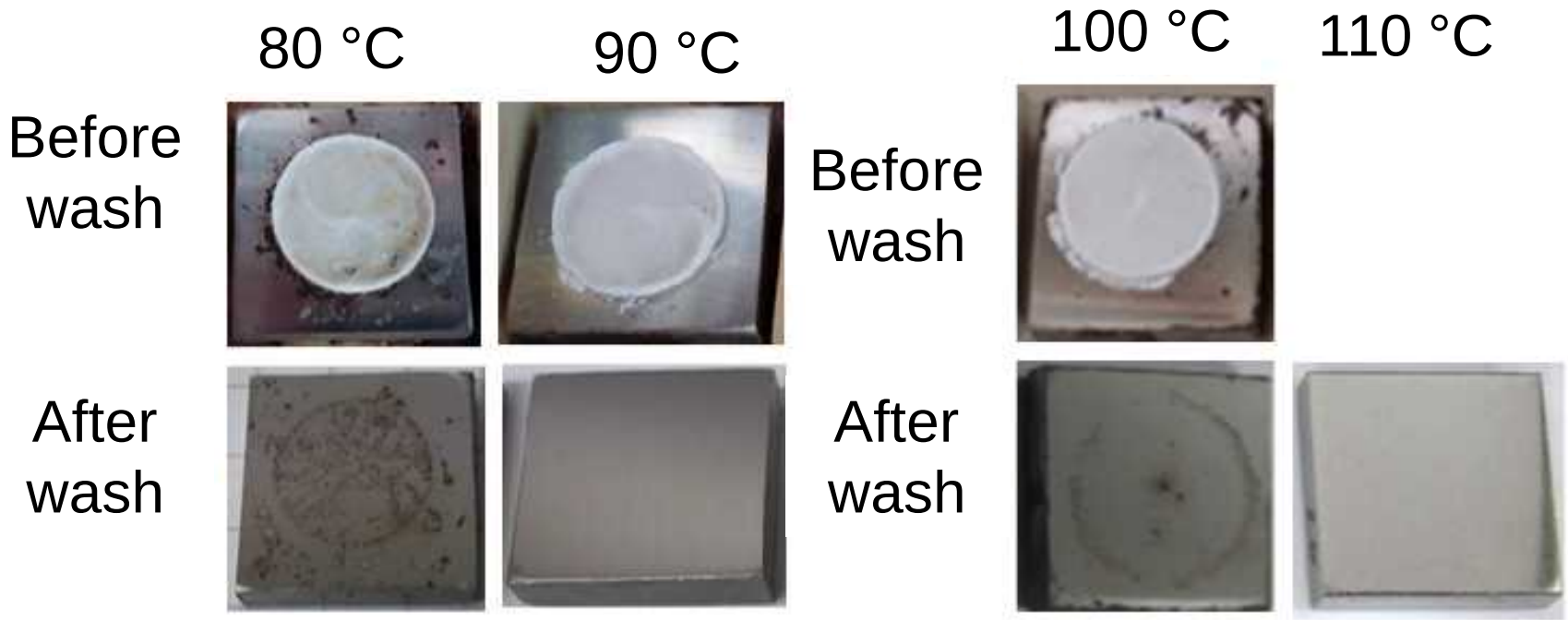

Na_2CO_3

Salt: Na_2CO_3
H_2O: 80 vol-%
Exposure: 4h (90 & 100 °C),
24h (110 & 120 °C)

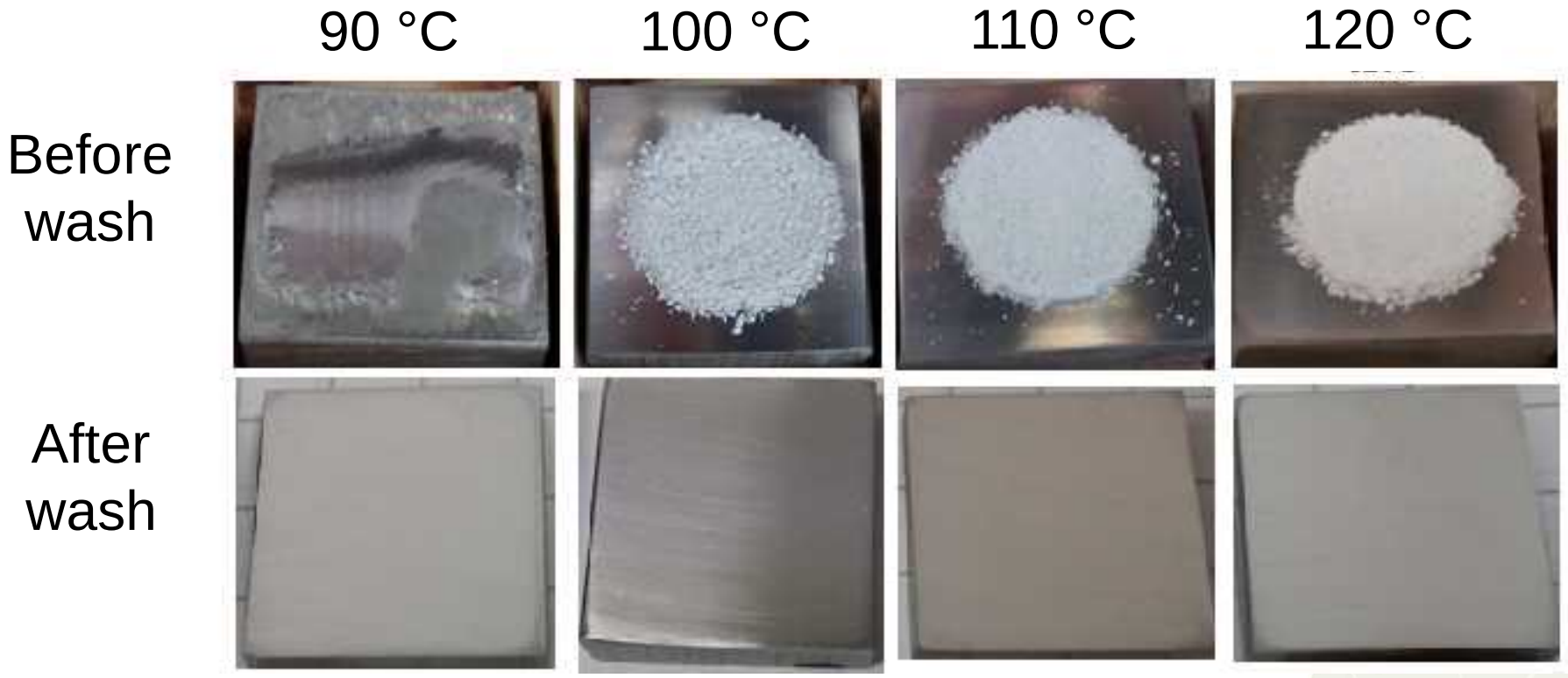

Salt mixture

90% Na_2SO_4 – 10%Na_2CO_3

Salt: 90% Na_2SO_4 & 10% Na_2CO_3
Temperature: 80 °C
H_2O: 27 vol-%
Exposure: 24h

Precipitator Ash 1

Salt: Precipitator Ash 1

H_2O: 27 vol-%

Exposure: 24h

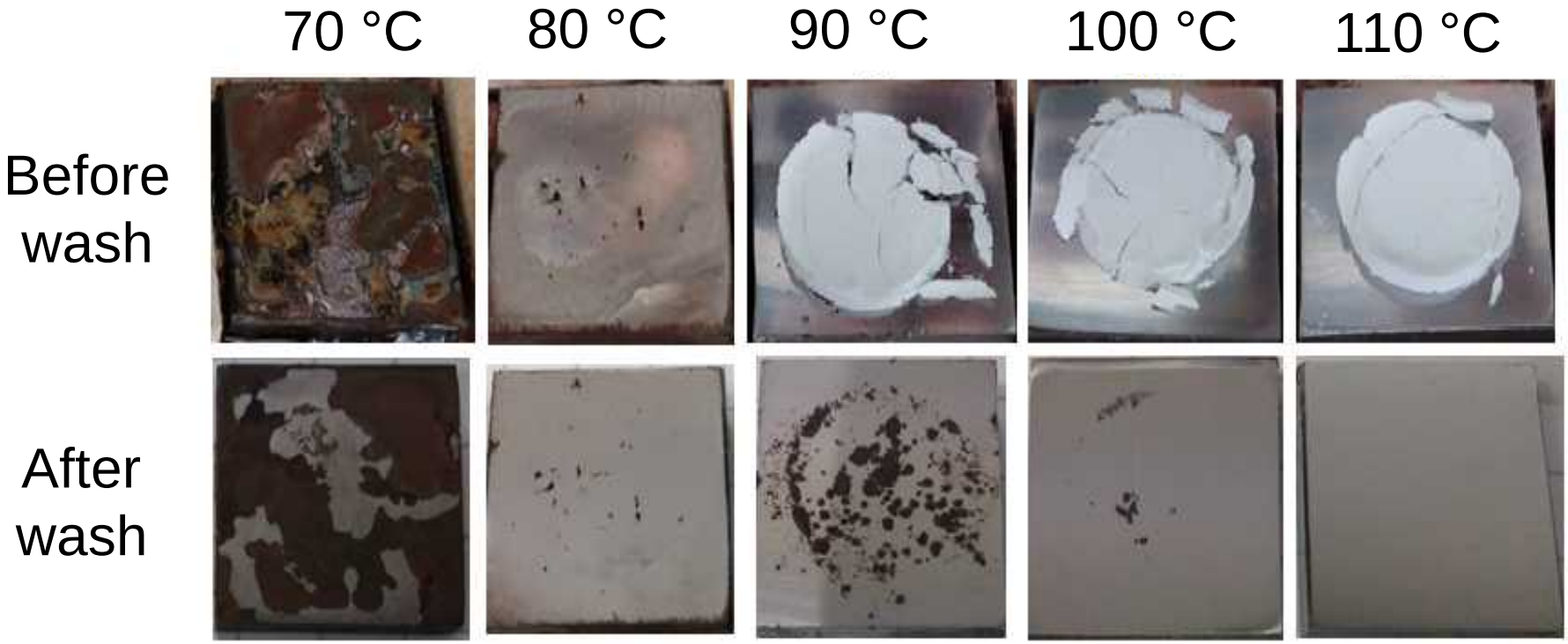

Salt: Precipitator Ash 1

H_2O: 60 vol-%

Exposure: 4h

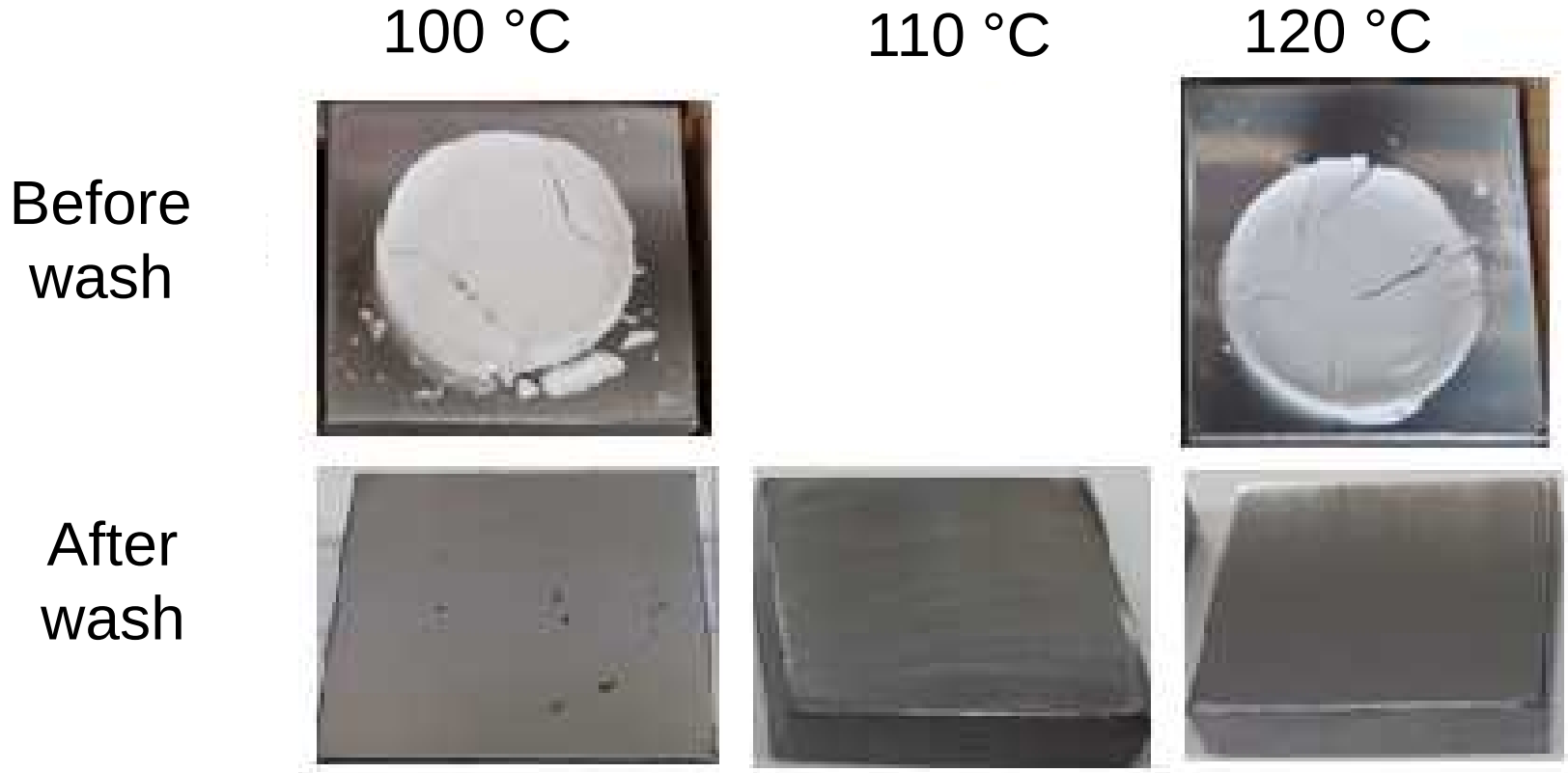

Salt: Precipitator Ash 1
Temperature: 110 °C
H_2O: 80 vol-%
Exposure: 24h

Precipitator Ash 2

Salt: Precipitator Ash 2
Temperature: 100 °C
H_2O: 27 vol-%
Exposure: 4h

Before wash

After wash

Salt: Precipitator Ash 2

H_2O: 60 vol-%

Exposure: 4h

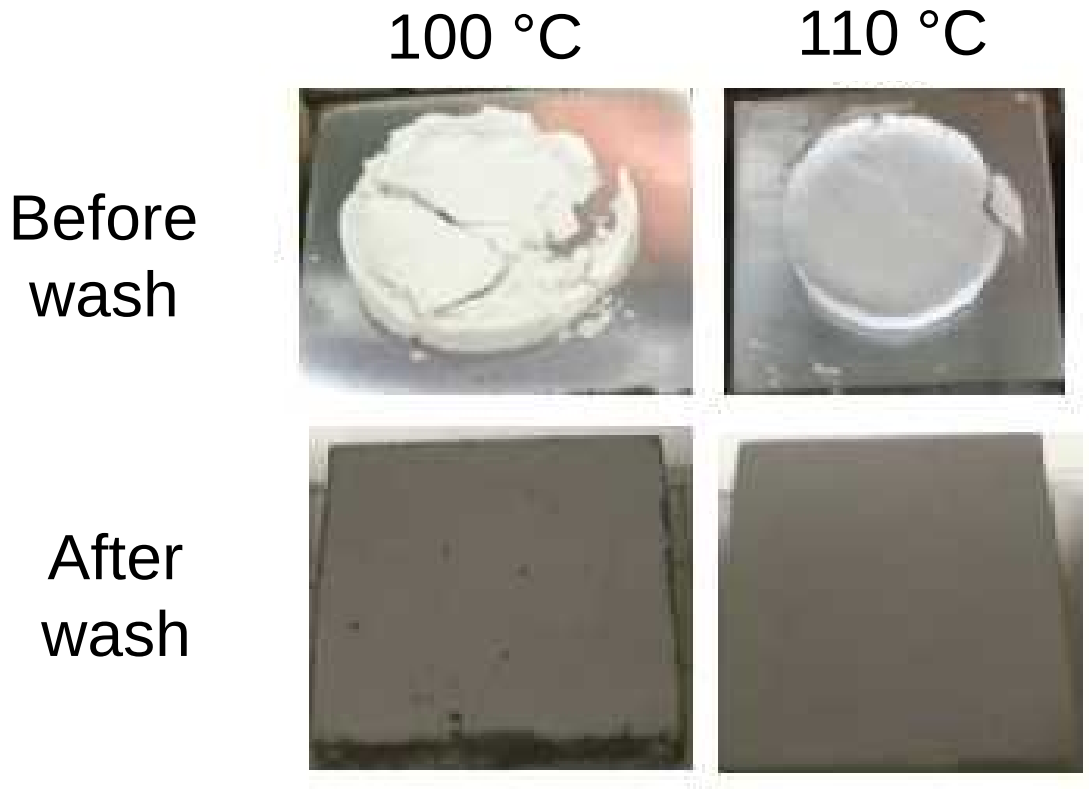

Conclusions

	27% H_2O	60% H_2O	80% H_2O
Na_2SO_4	90 °C	110 °C	
Na_2CO_3			-[a]
PA1	110 °C	110 °C	120 °C[b] (?)
PA2	100 °C	110 °C	

[a]No corrosion seen even though salt absorbed enough water to be totally dissolved

[b]Very light corrosion seen at 110 °C, so expect no corrosion at 120 °C

Conclusions

- Absorbtion of H_2O by hygroscopic salts appears to be the mechanism for low temperature corrosion

- Academy of Finland support for Emil Vainio to understand this phenomena of water adsorption by salts in biomass fueled boilers

Conclusions

- **These results indicated 110 °C (both gas and steel) is a safe temperature from a corrosion perspective**
- More deposits should be tested
- Some corrosion studies in a gradient needed
- Tests with moments of higher H_2O to similuate local fluctuations seen with sootblowing

Acknowledgements

- Our thanks to SKY and member companies for continued support of projects at ÅAU

- We’d like to acknowledge Niklas Vähä-Savo now with Vapo Oy for his work in phase 1

LIITE 5

ÅA, CFD Modeling of Reduced Lignin Black Liquor Combustion
Phase 2 – esitys 23.10.2015

PROCESS CHEMISTRY CENTRE

ÅBO AKADEMI UNIVERSITY

CFD Modeling of Reduced Lignin Black Liquor Combustion – Phase 2

Markus Engblom, Niko DeMartini
Åbo Akademi

SKY meeting 11.11.2015

Background and objective

- CFD modeling for studying what operational changes may be needed when firing reduced lignin black liquor
- Phase 1 conclusion: vol-C / char-C split an important model parameter
  - Phase 1 assumption

Modeled Black Liquors (3/3)

	Original Black Liquor	10% lower lignin	20% lower lignin
Liquor d.s. (wt-%)	81.3	81.3	81.3
Volatiles (kg/kg d.s.)	0.337	0.337	0.337
Char-C (kg/kg d.s.)	0.143	0.103	0.074
Inorganics (kg/kg d.s.)	0.516	0.555	0.585
Na_2S (kg/kg d.s.)	0.115	0.120	0.121
Na_2SO_4 (kg/kg d.s.)	0.080	0.101	0.118
Na_2CO_3 (kg/kg d.s.)	0.320	0.335	0.345
HHV (MJ/kg d.s.)	13.2	12.4	11.6
LHV (MJ/kg liquor)	8.4	7.8	7.2

  - Phase 2 objective
    - Determine vol-C / char-C experimentally
    - CFD runs 8-15
      - Including simultaneous change in air and spraying

CFD runs 8-15

- **Run 1:** Wisa Base Case, 100% MCR, flue gas O_2 3% (wet)
- **Runs 8-15:** using vol-C / char-C based on experimental data
  - **Runs 8 and 9:** 10% (97% MCR) and 20% (94% MCR) lignin removed, total air adjusted for flue gas O_2 3% (wet), other variables unchanged (similar to Phase 1 runs 2&3) (results in carbon balance ≠ 0)
  - **Runs 10 and 11:** 10% (97% MCR) & 20% (94% MCR) lignin removed, modifications to air distribution **and** liquor spraying for carbon balance = 0
  - **Runs 12 and 13:** same as runs 10&11 but with 100% MCR
  - **Runs 14 and 15:** 10% (97% MCR) & 20% (94% MCR) lignin removed, modifications to liquor spraying for carbon balance = 0 (similar to Phase 1 runs 6&7)

Experimental results

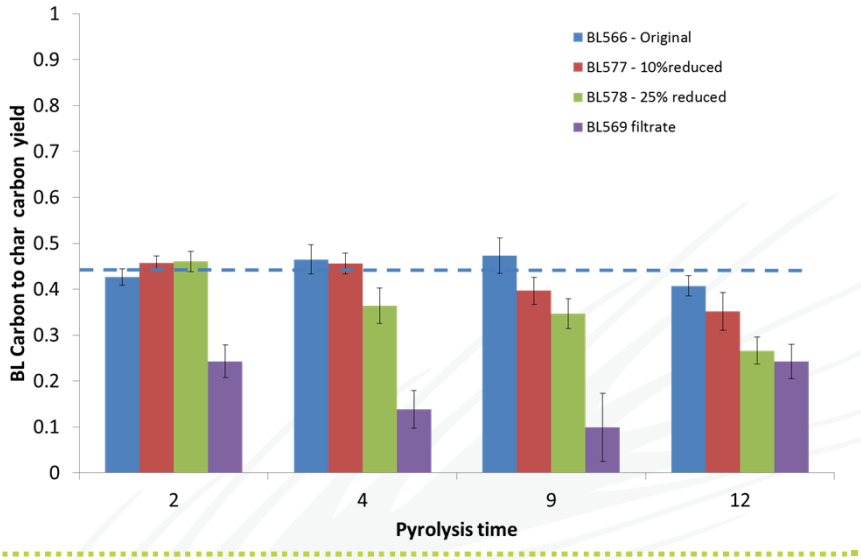

Modeled Black Liquors (1/3)

	Original Black Liquor (wt% d.s.)	Lignin [1] (wt% d.s.)
C	32.2	64.5
H	3.3	6
N	0.09	0.1
Na	21.4	0.3
K	2.4	0.05
Cl	0.3	0
Tot. S	6.4	2.5
SO4	5.4	0
OH	1.74	0
HHV (MJ/kg d.s.)	13.2	26.5

Composition of reduced lignin BL based:

- Lignin content of BL: 36 wt-%
- 175 kg H_2SO_4/ton lignin precipitated [1]

1 Tomani, P. The lignoboost process. In Proceedings to The 2nd Nordic Wood Biorefinery Conf., 2-4 Sept. 2009, Helsinki, Finland, pp. 181-188.

Modeled Black Liquors (2/3)

	Original Black Liquor (wt% d.s.)	10% lower lignin (wt% d.s.)	20% lower ligning (wt% d.s.)
C	32.2	30.9	28.9
H	3.3	3.2	3.03
N	0.09	0.09	0.09
Na	21.4	22.8	23.9
K	2.4	2.6	2.7
Cl	0.3	0.32	0.34
Tot. S	6.4	7.0	7.5
SO_4	5.4	6.7	7.87
OH	1.74	1.4	1.1
HHV (MJ/kg d.s.)	13.2	12.4	11.6

Modeled Black Liquors (3/3)

Phase2: Vol-C/char-C 50/50 split based on laboratory data, This split is the same as used for the original liquor

	Original Black Liquor	10% lower lignin	20% lower ligning
Liquor d.s. (wt-%)	81.3	81.3	81.3
Volatiles (kg/kg d.s.)	0.337	0.337 / 0.305	0.337 / 0.286
Char-C (kg/kg d.s.)	0.143	0.103 / 0.136	0.074 / 0.125
Inorganics (kg/kg d.s.)	0.516	0.555	0.585
Na_2S (kg/kg d.s.)	0.115	0.120	0.121
Na_2SO_4 (kg/kg d.s.)	0.080	0.101	0.118
Na_2CO_3 (kg/kg d.s.)	0.320	0.335	0.345
HHV (MJ/kg d.s.)	13.2	12.4	11.6
LHV (MJ/kg liquor)	8.4	7.8	7.2

Liquor feed and combustion air (Runs 1 and 8&9)

	Original Black Liquor	10% lower lignin	20% lower ligning
Liquor feed (tds/d)	5320	5160	5000
Of MCR (%)	100	97	94
Air (kg/s)	272	256	232
Air (Nm3/s)	211	199	180
Primary	22%	22%	22%
Secondary	43%	43%	43%
Tertiary	35%	35%	35%
Target flue gas O_2 (% wet)	3.0	3.0	3.0
HHRR (MW/m^2) based on (HHV / LHV)	3.6 / 2.9	3.3 / 2.6	3.0 / 2.3
$T_{adiabatic}$	1580 °C	1490 °C	1450 °C

Guidelines for changes to combustion air

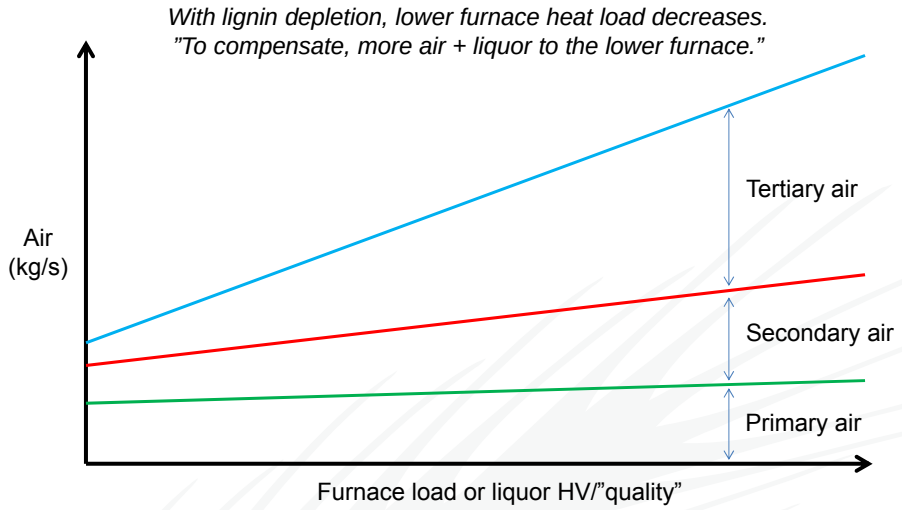

Schematic illustration of combustion air delivery strategy as function of furnace load or liquor HV/"quality"

Conclusions

- Less char-C with lignin removal
  - Less C to the lower furnace with lignin removal if drop size stays the same
  - Changes to operation needed to compensate
- For up to 20% lignin removal
  - With air distribution unchanged (p22%/s43%/t35%) decrease in liquor temperature by approximately 1 °C
  - Combined change in air+spray (p28%/s40%/t32%) decrease in liquor temperature by approximately 3.6 °C

CFD results

- **Run 1:** Wisa Base Case, 100% MCR, flue gas O_2 3% (wet)
- **Runs 8-15:** using vol-C / char-C based on experimental data
  - **Runs 8 and 9:** 10% (97% MCR) and 20% (94% MCR) lignin removed, total air adjusted for flue gas O_2 3% (wet), other variables unchanged (similar to Phase 1 runs 2&3) (results in carbon balance ≠ 0)
  - **Runs 10 and 11:** 10% (97% MCR) & 20% (94% MCR) lignin removed, modifications to air distribution **and** liquor spraying for carbon balance = 0
  - **Runs 12 and 13:** same as runs 10&11 but with 100% MCR
  - **Runs 14 and 15:** 10% (97% MCR) & 20% (94% MCR) lignin removed, modifications to liquor spraying for carbon balance = 0 (similar to Phase 1 runs 6&7)

Temperature

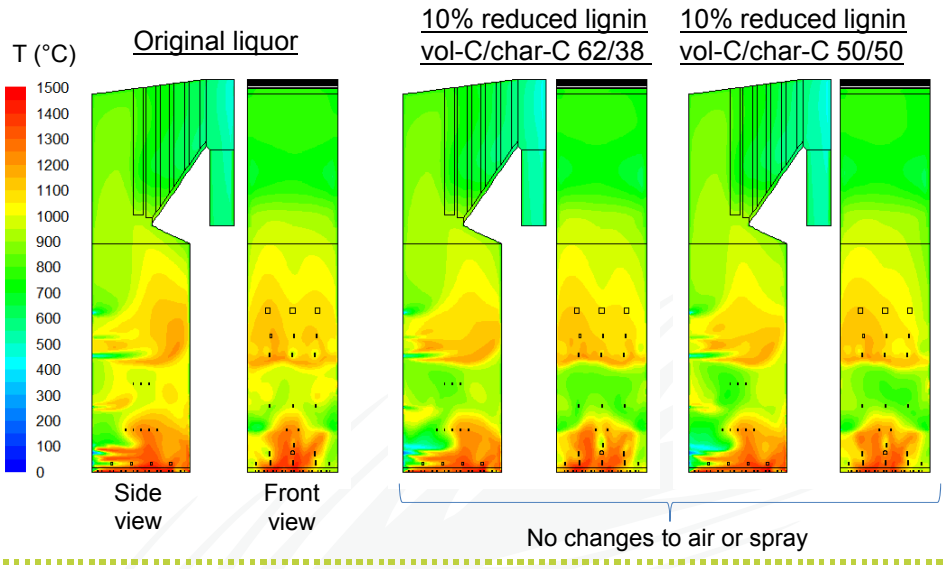

O_2 concentration

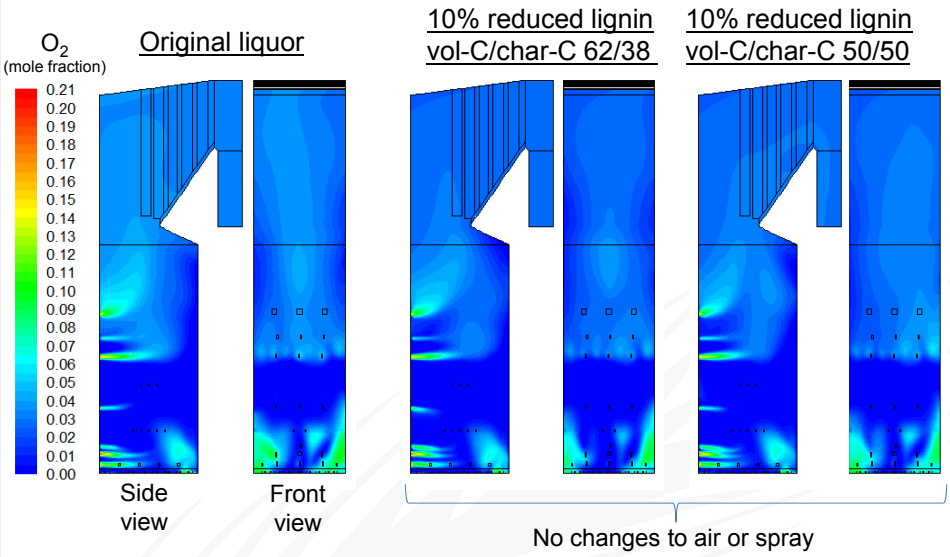

Carbon to walls/bed

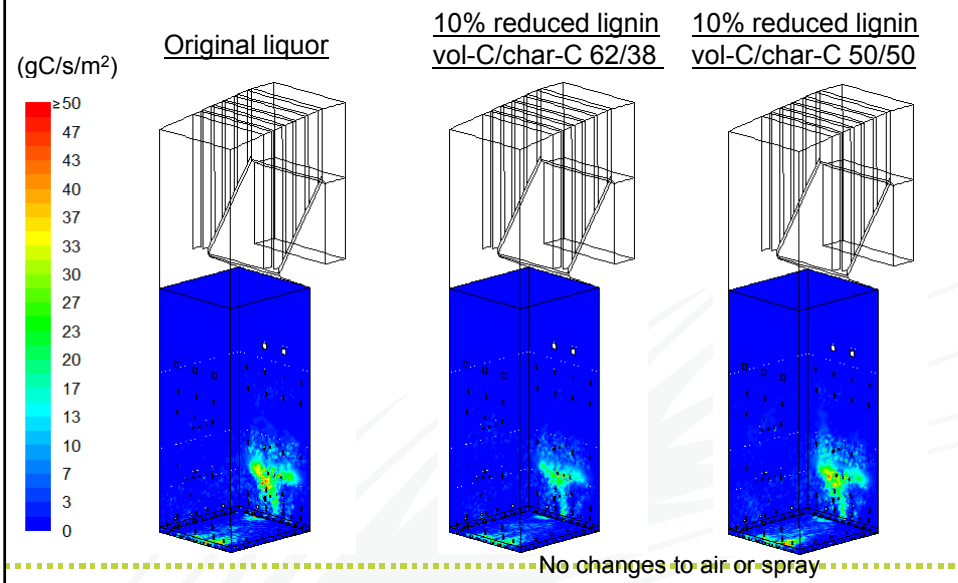

Carbon to walls/bed

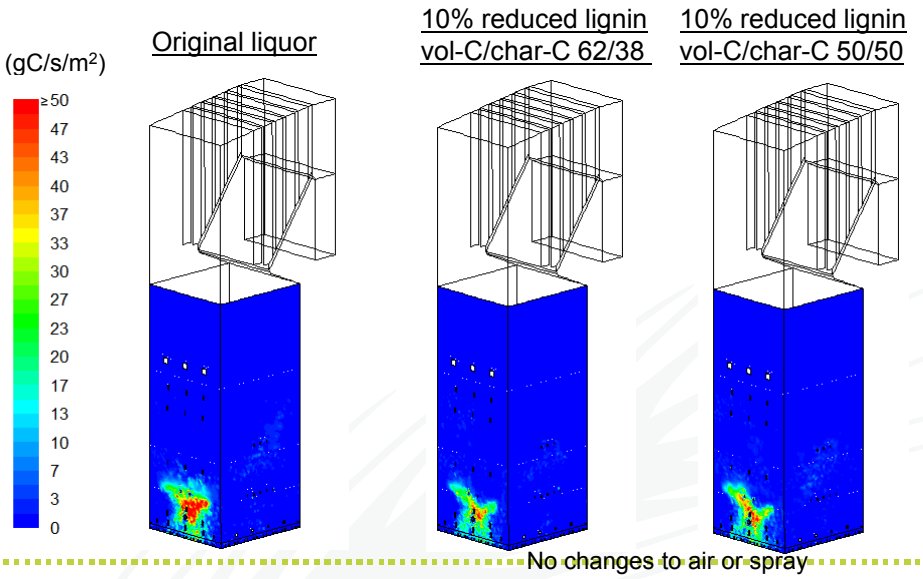

No changes to air or spray

Right wall and front wall

Furnace carbon loading

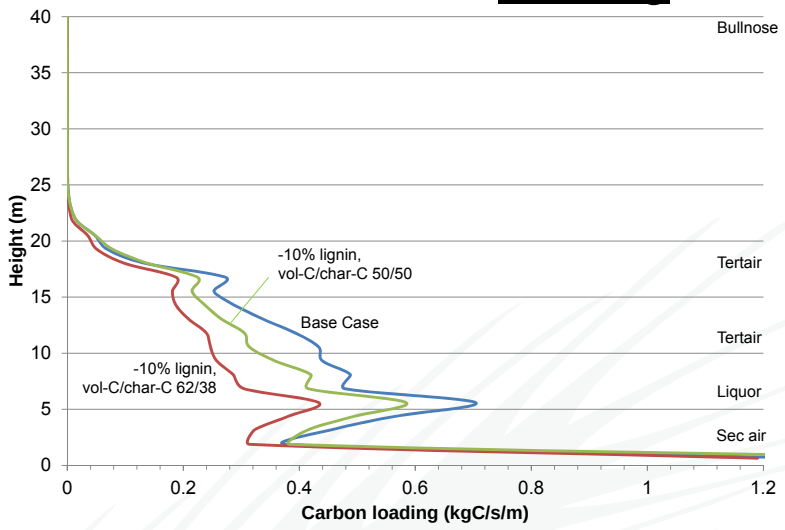

Furnace carbon conversion

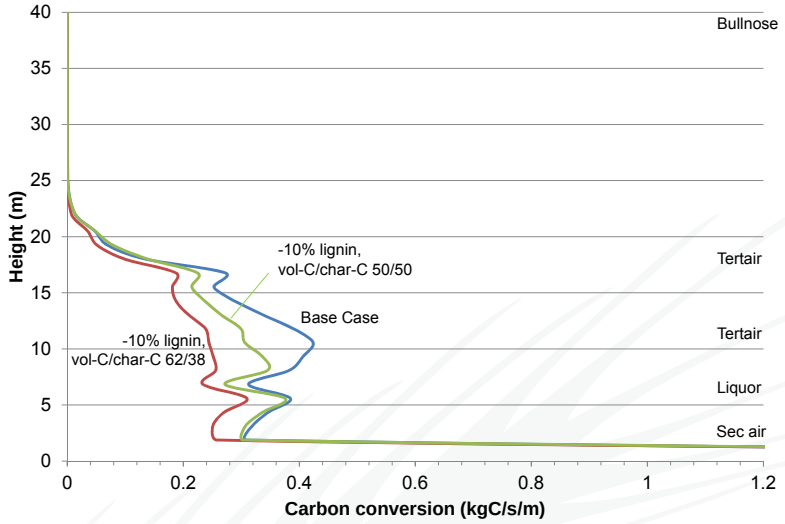

Fate of char carbon

(kg/s)	Base Case	10% reduced lignin, vol-C/char-C 62/38	10% reduced lignin, vol-C/char-C 50/50
In liquor feed	8.81	6.19	8.12
in-flight conversion	3.90	2.60	3.39
to bed/walls	4.91	3.59	4.74
conversion on bed/walls	4.70	4.37	4.95
carbon accumulation	0.21	-0.78	-0.21

Fate of char carbon

(%)	Base Case	10% reduced lignin, vol-C/char-C 62/38	10% reduced lignin, vol-C/char-C 50/50
In liquor feed	100.0	100.0	100.0
in-flight conversion	44.3	42.0	41.7
to bed/walls	55.7	58.0	58.3
conversion on bed/walls	53.4	70.5	61.0
carbon accumulation	2.3	-12.5	-2.6

Temperature

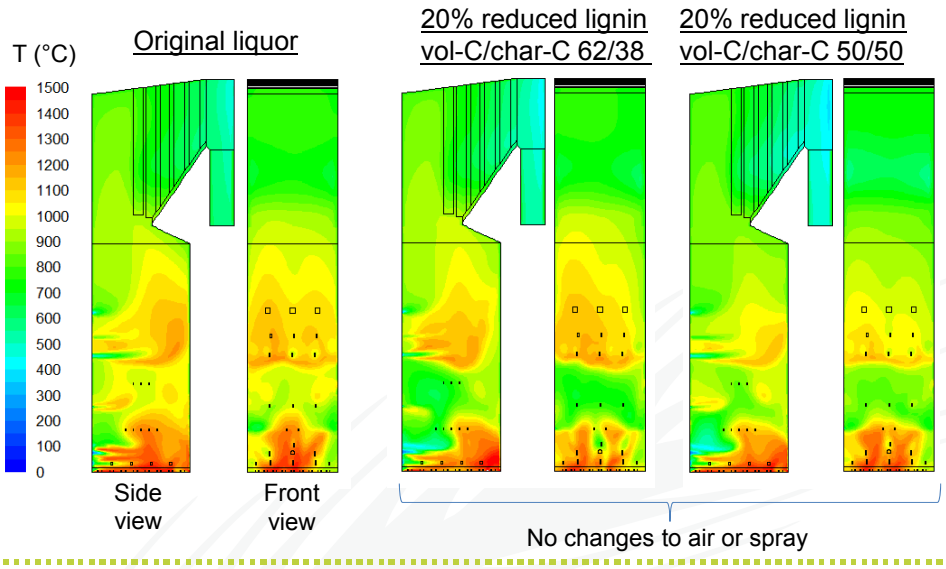

O_2 concentration

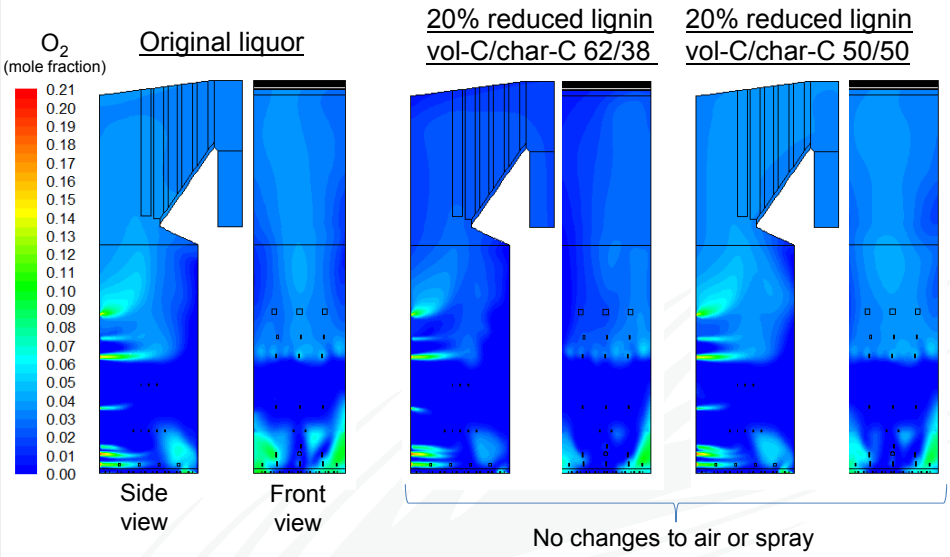

Carbon to walls/bed

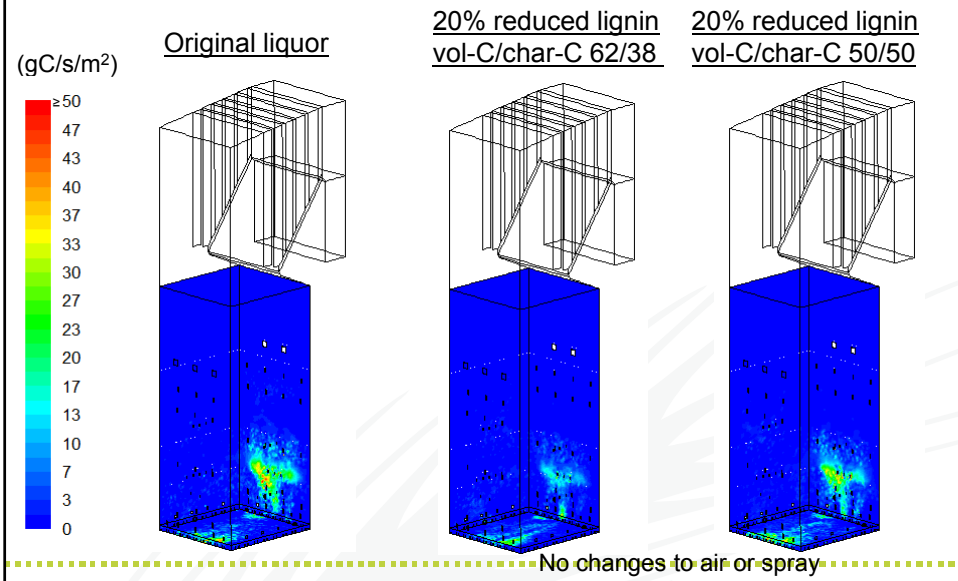

Carbon to walls/bed

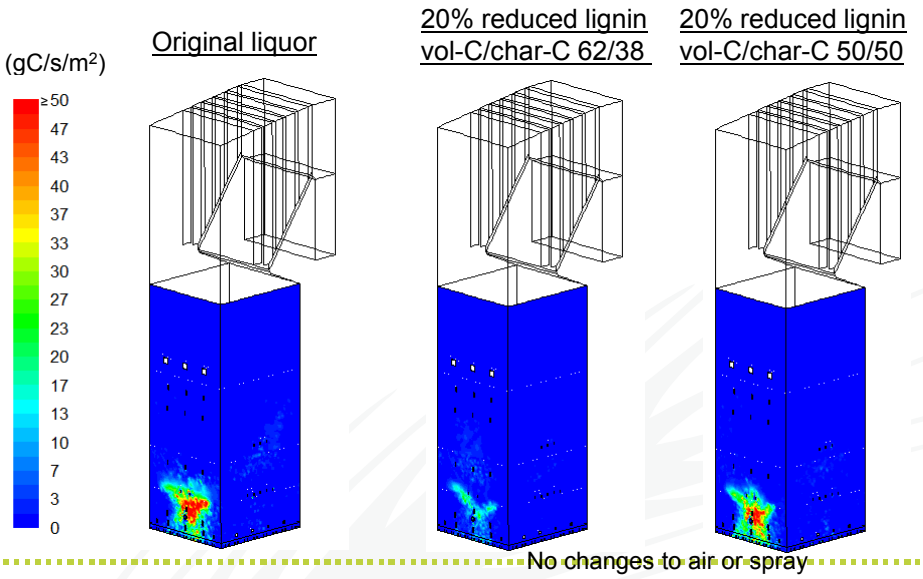

No changes to air or spray

Right wall and front wall

Furnace carbon loading

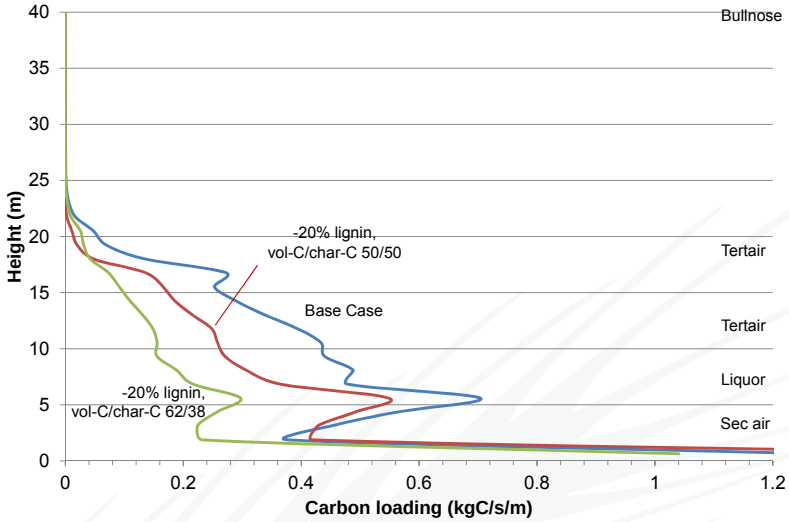

Furnace carbon conversion

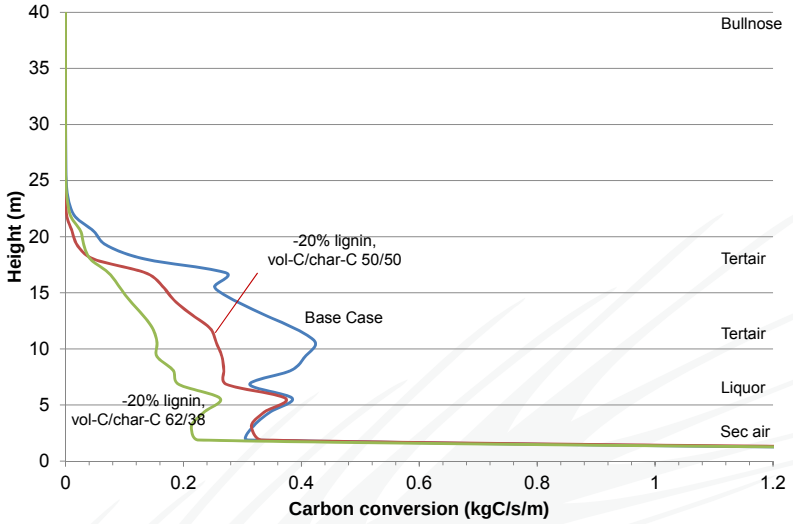

Fate of char carbon

(kg/s)	Base Case	20% reduced lignin, vol-C/char-C 62/38	20% reduced lignin, vol-C/char-C 50/50
In liquor feed	8.81	4.30	7.25
in-flight conversion	3.90	1.79	2.80
to bed/walls	4.91	2.51	4.45
conversion on bed/walls	4.70	4.10	4.84
carbon accumulation	0.21	-1.59	-0.39

Fate of char carbon

(%)	Base Case	20% reduced lignin, vol-C/char-C 62/38	20% reduced lignin, vol-C/char-C 50/50
In liquor feed	100.0	100.0	100.0
in-flight conversion	44.3	41.6	38.6
to bed/walls	55.7	58.4	61.4
conversion on bed/walls	53.4	95.5	66.8
carbon accumulation	2.3	-37.1	-5.4

CFD results

- **Run 1:** Wisa Base Case, 100% MCR, flue gas O_2 3% (wet)
- **Runs 8-15:** using vol-C / char-C based on experimental data
  - **Runs 8 and 9:** 10% (97% MCR) and 20% (94% MCR) lignin removed, total air adjusted for flue gas O_2 3% (wet), other variables unchanged (similar to Phase 1 runs 2&3) (results in carbon balance ≠ 0)
  - **Runs 10 and 11:** 10% (97% MCR) & 20% (94% MCR) lignin removed, modifications to air distribution **and** liquor spraying for carbon balance = 0
  - **Runs 12 and 13:** same as runs 10&11 but with 100% MCR
  - **Runs 14 and 15:** 10% (97% MCR) & 20% (94% MCR) lignin removed, modifications to liquor spraying for carbon balance = 0 (similar to Phase 1 runs 6&7)

Liquor feed and combustion air (Runs 1 and 10 & 11)

	Original Black Liquor	10% lower lignin Run 10	20% lower ligning Run 11
Liquor feed (tds/d)	5320	5160	5000
Of MCR (%)	100	97	94
Air (kg/s)	272	256	232
Air (Nm3/s)	211	199	180
Primary	22%	25% *	28% *
Secondary	43%	40%	40%
Tertiary	35%	35%	32%
Target flue gas O_2 (% wet)	3.0	3.0	3.0
Dp average (mm)	5.7	6.5	11
ΔT spray (°C)	0	-0.6	-3.6

Air distribution changed after which average droplet size "optimized" for carbon balanced situation.
Air change based on discussion with industry: "with a lower HV/quality liquor, more of the combustion (air+liquor) to lower furnace".
*) these percentages give ~same mass flow (kg/s) primary

Temperature

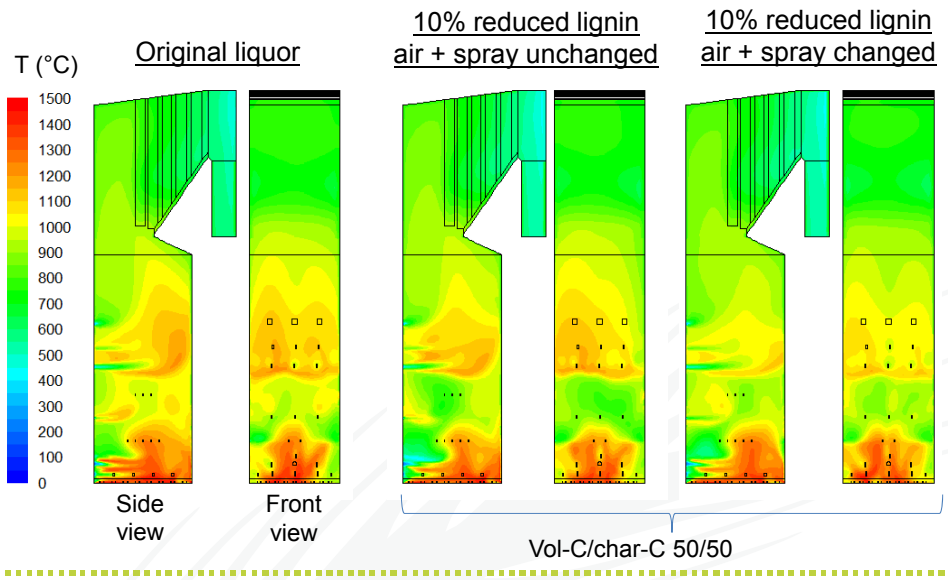

O_2 concentration

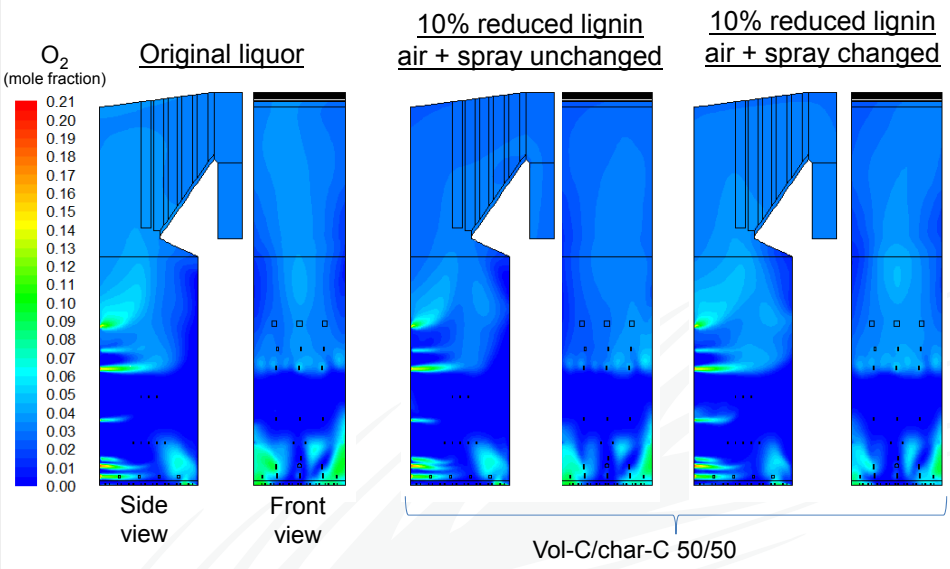

Carbon to walls/bed

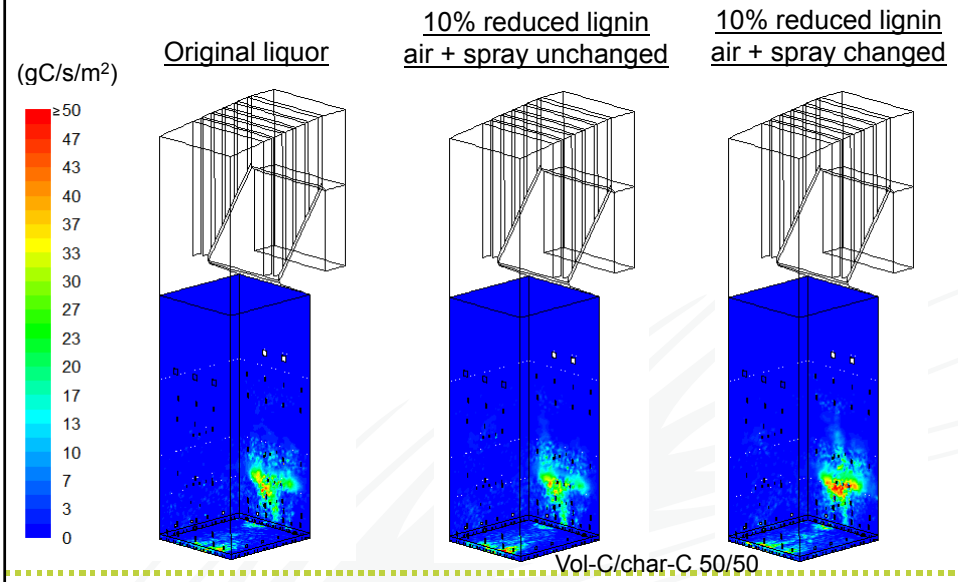

Left wall, back wall, and char bed

Carbon to walls/bed

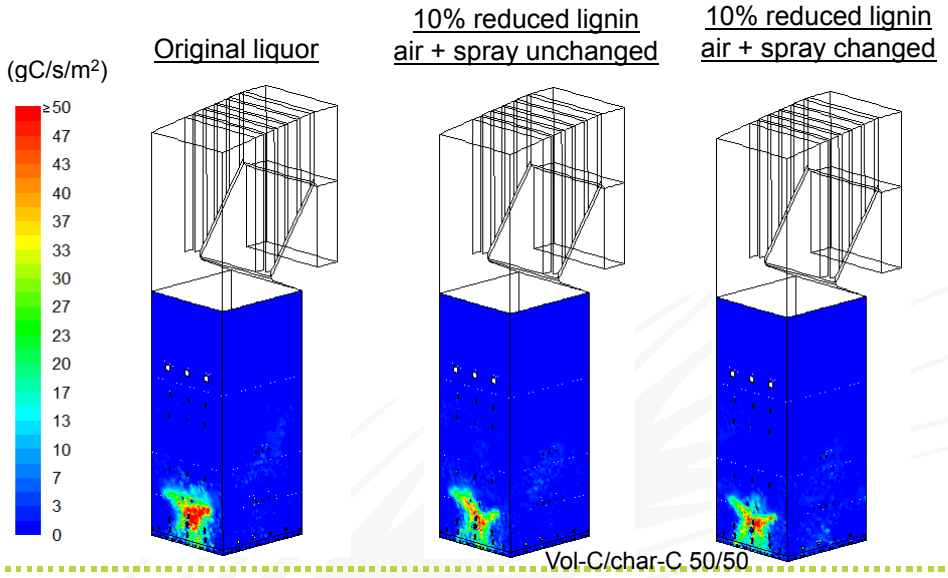

Right wall and front wall

Furnace carbon loading

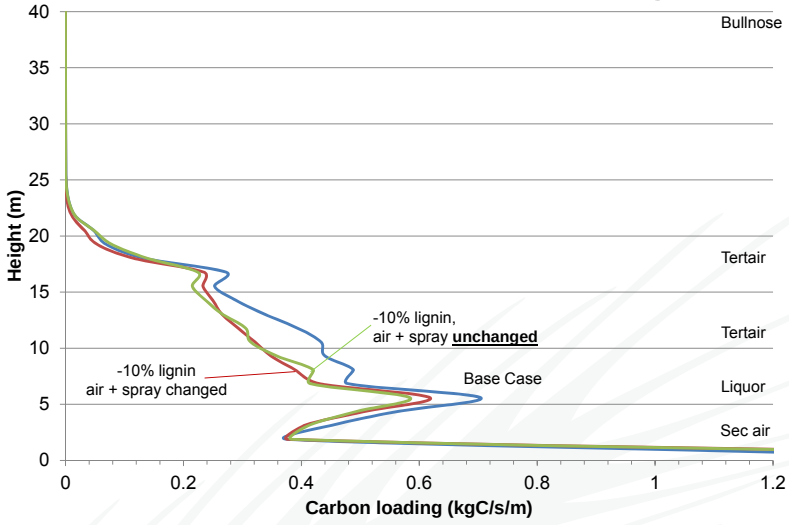

Furnace carbon conversion

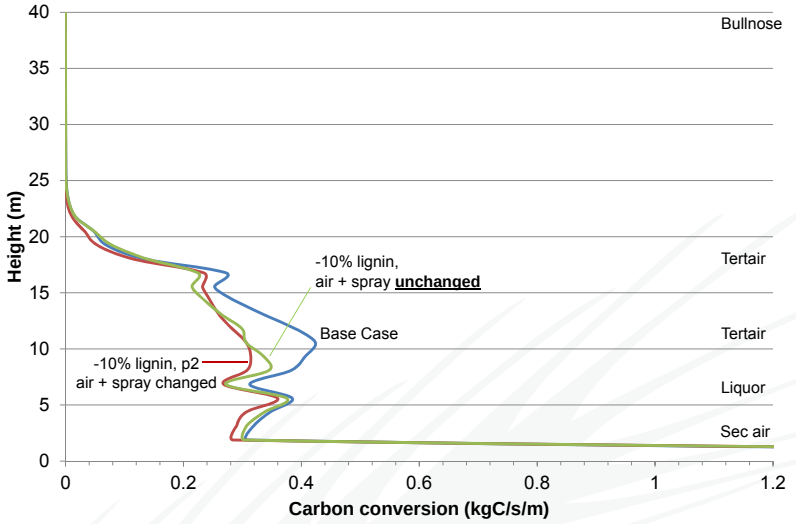

Fate of char carbon

(kg/s)	Base Case	10% reduced lignin, air + spray unchanged	10% reduced lignin, air + spray changed
In liquor feed	8.81	8.12	8.12
in-flight conversion	3.90	3.39	2.94
to bed/walls	4.91	4.74	5.19
conversion on bed/walls	4.70	4.95	5.20
carbon accumulation	0.21	-0.21	-0.01

Fate of char carbon

(%)	Base Case	10% reduced lignin, air + spray unchanged	10% reduced lignin, air + spray changed
In liquor feed	100.0	100.0	100.0
in-flight conversion	44.3	41.7	36.2
to bed/walls	55.7	58.3	63.8
conversion on bed/walls	53.4	61.0	64.0
carbon accumulation	2.3	-2.6	-0.2

Temperature

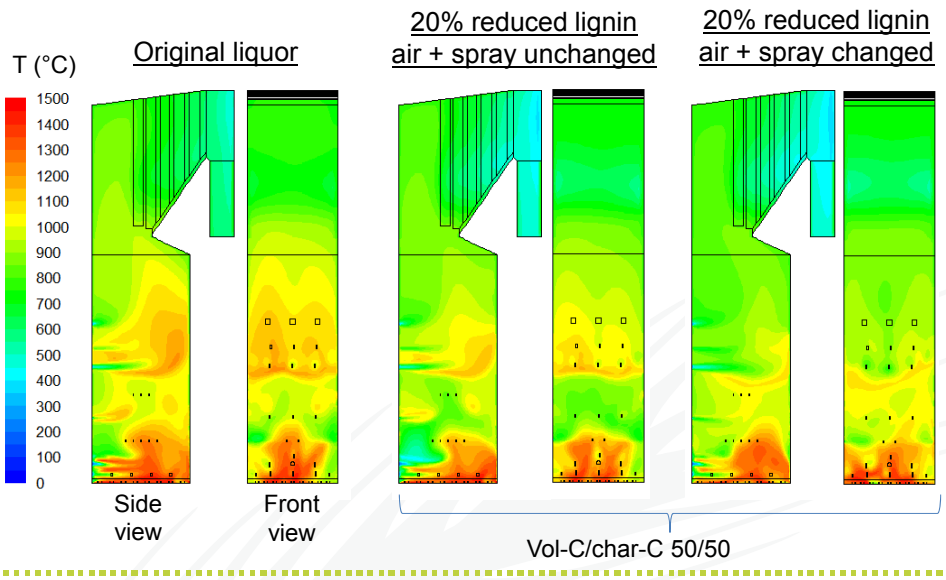

O_2 concentration

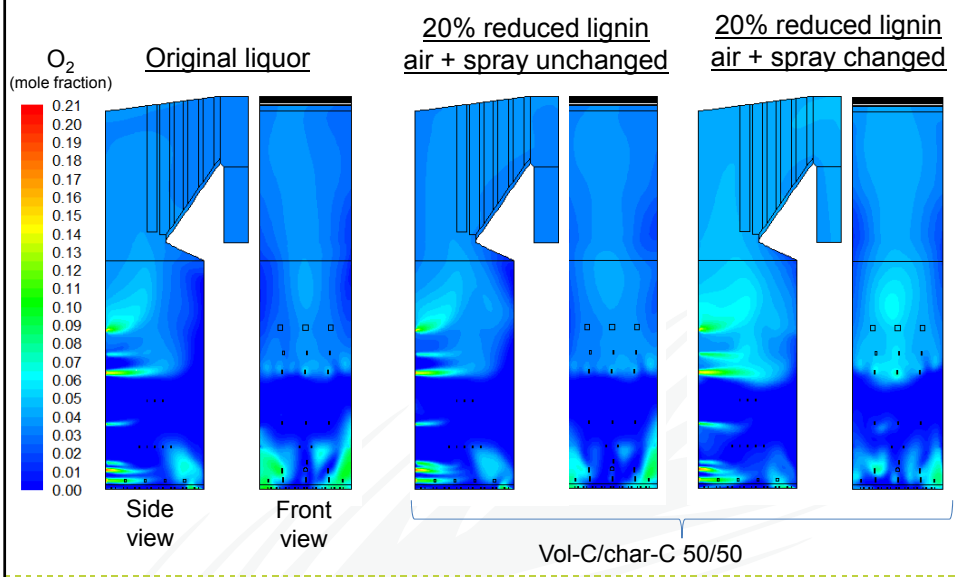

Carbon to walls/bed

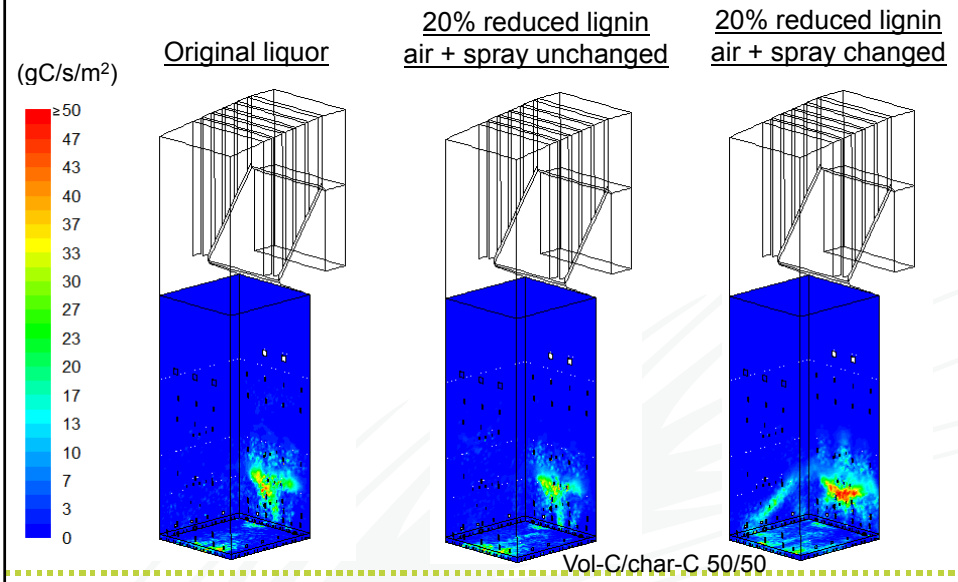

Left wall, back wall, and char bed

Carbon to walls/bed

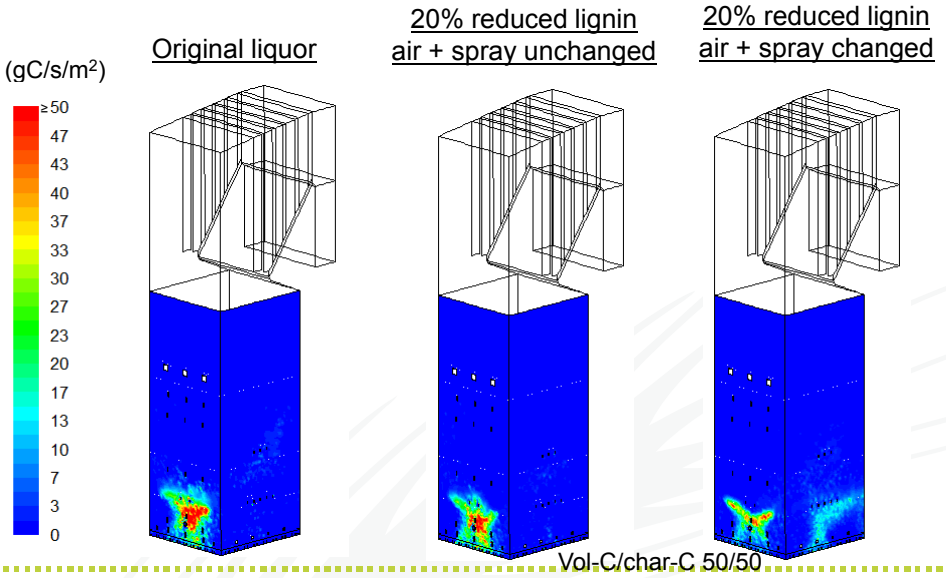

Right wall and front wall

Furnace carbon loading

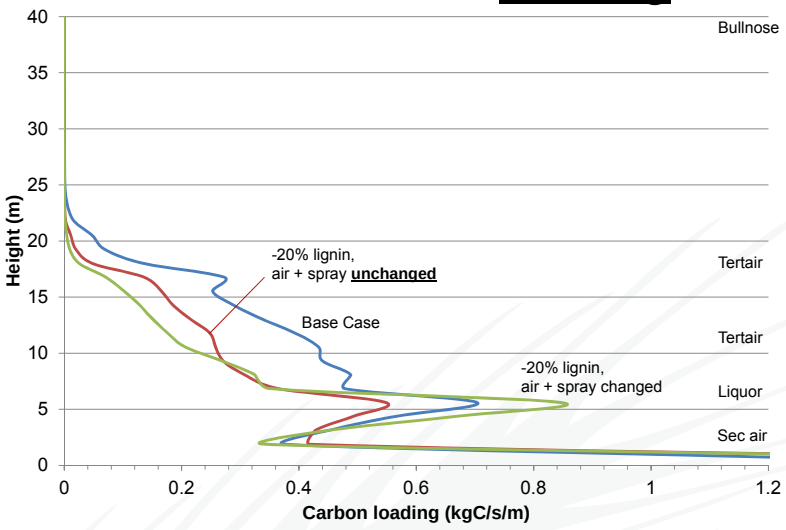

Furnace carbon conversion

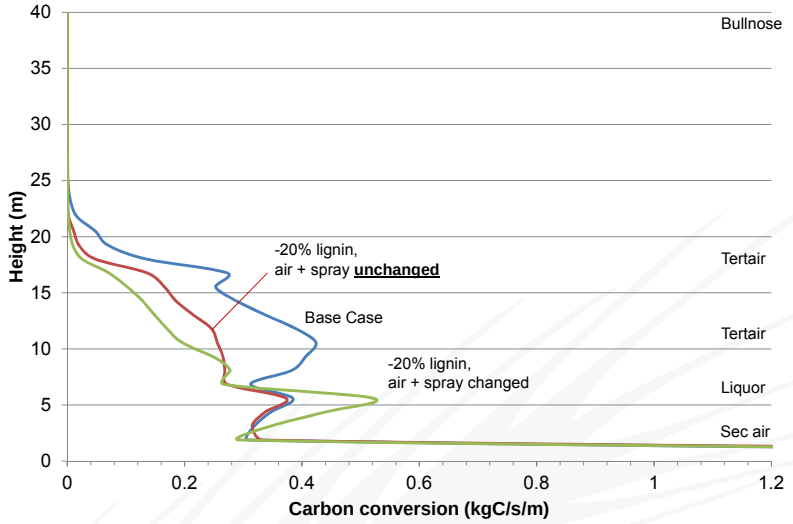

Fate of char carbon

(kg/s)	Base Case	20% reduced lignin, air + spray unchanged	20% reduced lignin, air + spray changed
In liquor feed	8.81	7.25	7.25
in-flight conversion	3.90	2.80	1.42
to bed/walls	4.91	4.45	5.83
conversion on bed/walls	4.70	4.84	5.74
carbon accumulation	0.21	-0.39	0.09

Fate of char carbon

(%)	Base Case	20% reduced lignin, air + spray unchanged	20% reduced lignin, air + spray changed
In liquor feed	100.0	100.0	100.0
in-flight conversion	44.3	38.6	19.6
to bed/walls	55.7	61.4	80.4
conversion on bed/walls	53.4	66.8	79.2
carbon accumulation	2.3	-5.4	1.2

CFD results

- **Run 1:** Wisa Base Case, 100% MCR, flue gas O_2 3% (wet)
- **Runs 8-15:** using vol-C / char-C based on experimental data
  - **Runs 8 and 9:** 10% (97% MCR) and 20% (94% MCR) lignin removed, total air adjusted for flue gas O_2 3% (wet), other variables unchanged (similar to Phase 1 runs 2&3) (results in carbon balance ≠ 0)
  - **Runs 10 and 11:** 10% (97% MCR) & 20% (94% MCR) lignin removed, modifications to air distribution **and** liquor spraying for carbon balance = 0
  - **Runs 12 and 13:** same as runs 10&11 but with 100% MCR
  - **Runs 14 and 15:** 10% (97% MCR) & 20% (94% MCR) lignin removed, modifications to liquor spraying for carbon balance = 0 (similar to Phase 1 runs 6&7)

Liquor feed and combustion air (Runs 1 and 10-13)

	Original Black Liquor	10% lower lignin Run 10	20% lower ligning Run 11	10% lower lignin Run 12	20% lower ligning Run 13
Liquor feed (tds/d)	5320	5160	5000	5320	5320
Of MCR (%)	100	97	94	100	100
Air (kg/s)	272	256	232	264	247
Air (Nm3/s)	211	199	180	205	191
Primary	22%	25% *	28% *	24% *	26% *
Secondary	43%	40%	40%	40%	40%
Tertiary	35%	35%	32%	36%	34%
Target flue gas O_2 (% wet)	3.0	3.0	3.0	3.0	3.0
Dp average (mm)	5.7	6.5	11	6.0	9.3
ΔT spray (°C)	0	-0.6	-3.6	-0.2	-2.5

Air distribution changed after which average droplet size "optimized" for carbon balanced situation.
Air change based on discussion with industry: "with a lower HV/quality liquor, more of the combustion (air+liquor) to lower furnace".
*) these percentages give ~same mass flow (kg/s) primary

Temperature

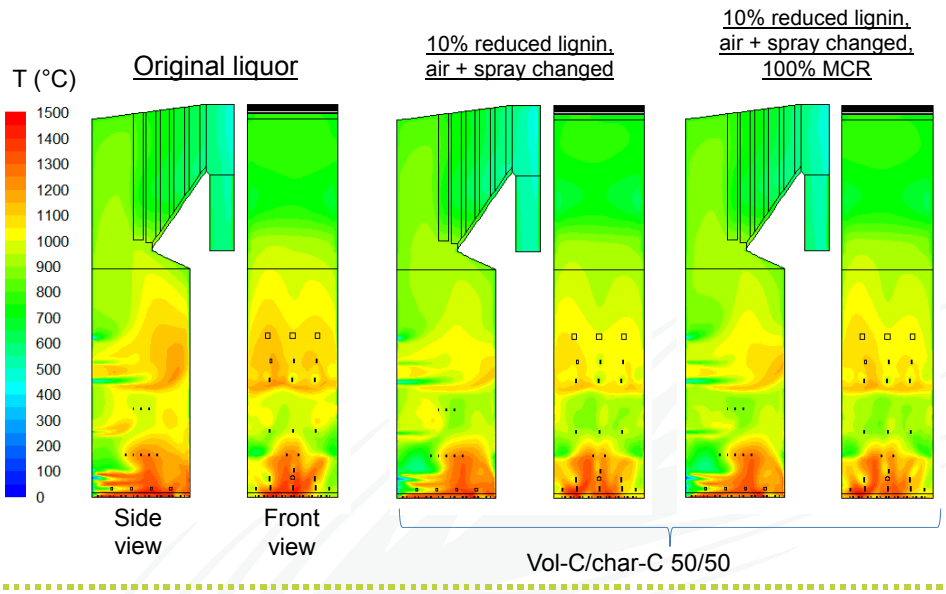

O_2 concentration

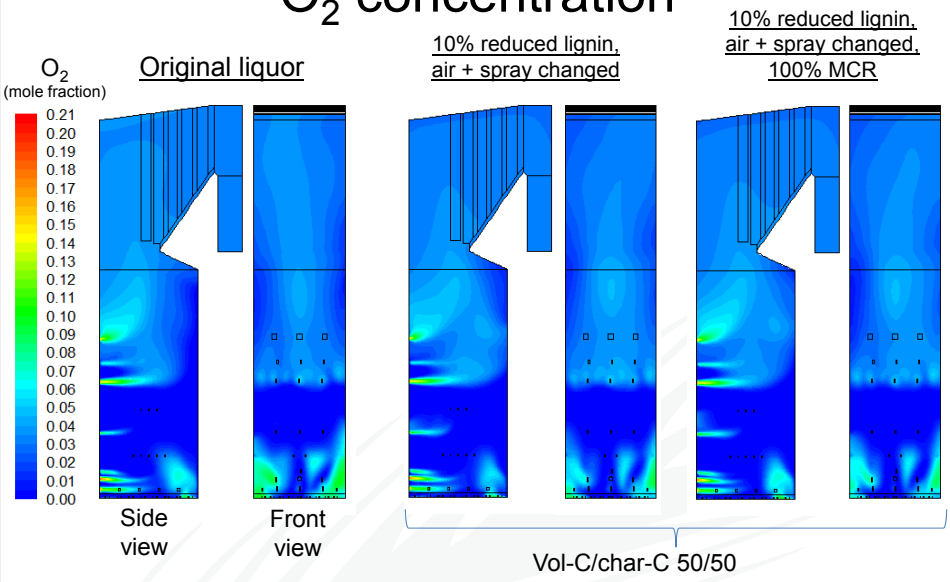

Carbon to walls/bed

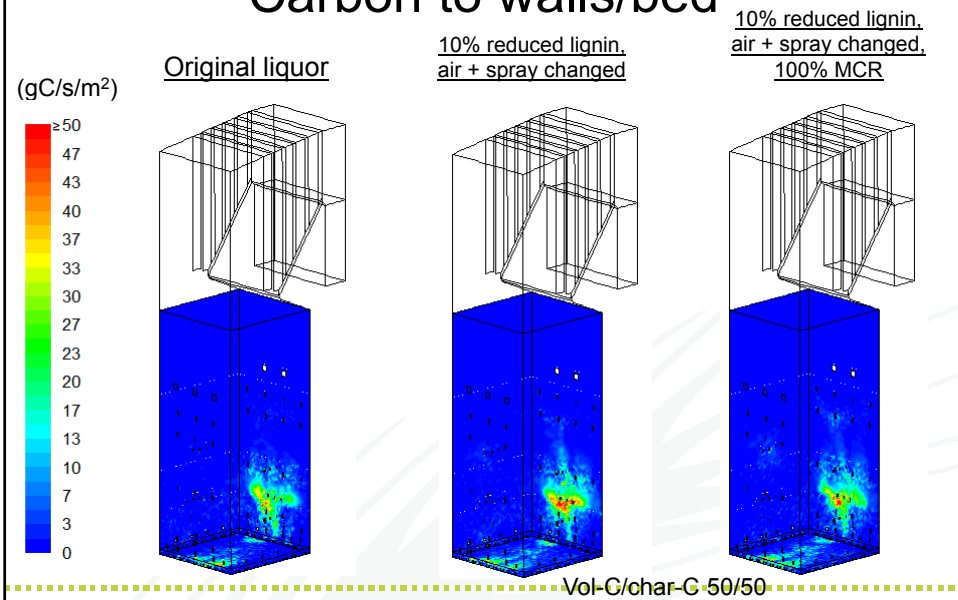

Left wall, back wall, and char bed

Carbon to walls/bed

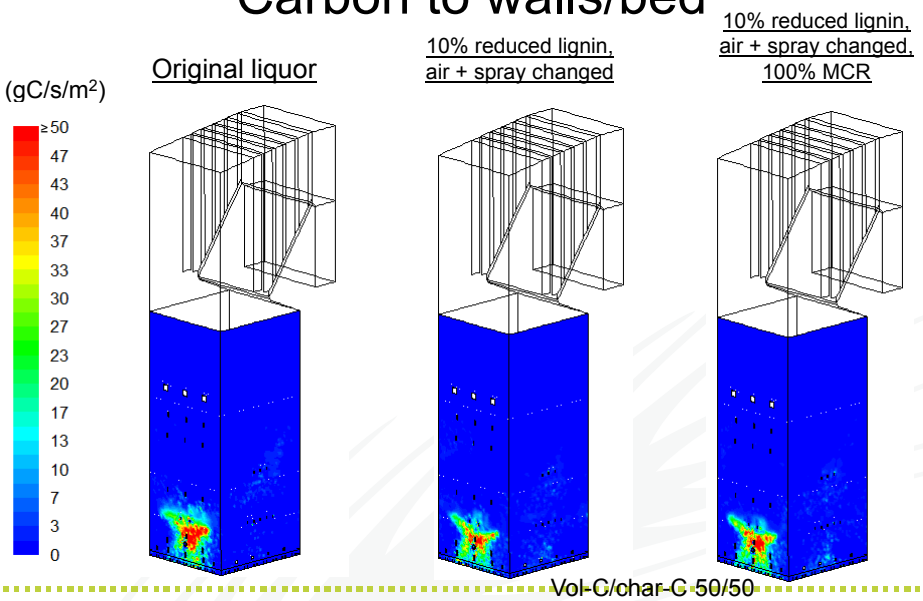

Vol-C/char-C 50/50

Right wall and front wall

Furnace carbon loading

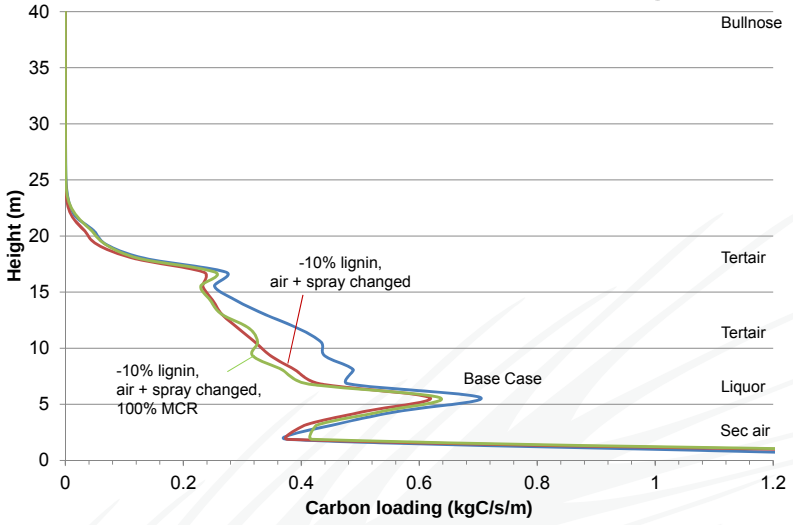

Furnace carbon conversion

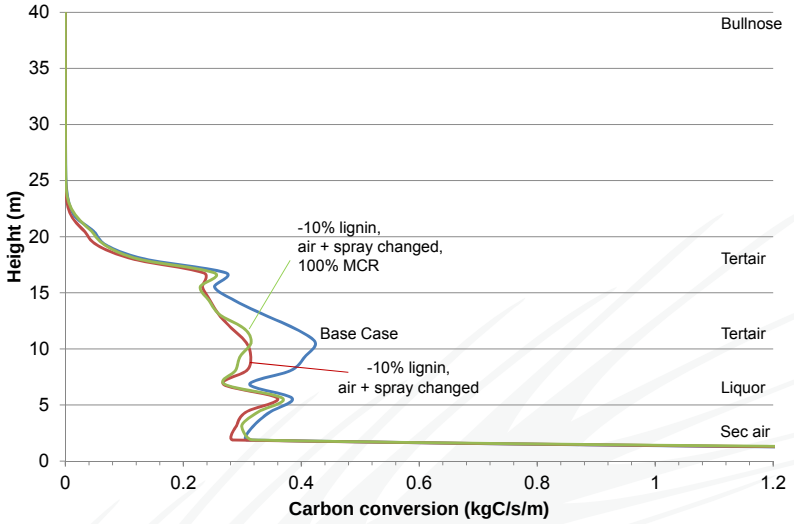

Fate of char carbon

(kg/s)	Base Case	10% reduced lignin, air + spray changed	10% reduced lignin, p2, air + spray changed 100% MCR
In liquor feed	8.81	8.12	8.37
in-flight conversion	3.90	2.94	3.18
to bed/walls	4.91	5.19	5.20
conversion on bed/walls	4.70	5.20	5.13
carbon accumulation	0.21	-0.01	0.06

Fate of char carbon

(%)	Base Case	10% reduced lignin, air + spray changed	10% reduced lignin, p2, air + spray changed 100% MCR
In liquor feed	100.0	100.0	100.0
in-flight conversion	44.3	36.2	37.9
to bed/walls	55.7	63.8	62.1
conversion on bed/walls	53.4	64.0	61.3
carbon accumulation	2.3	-0.2	0.7

Temperature

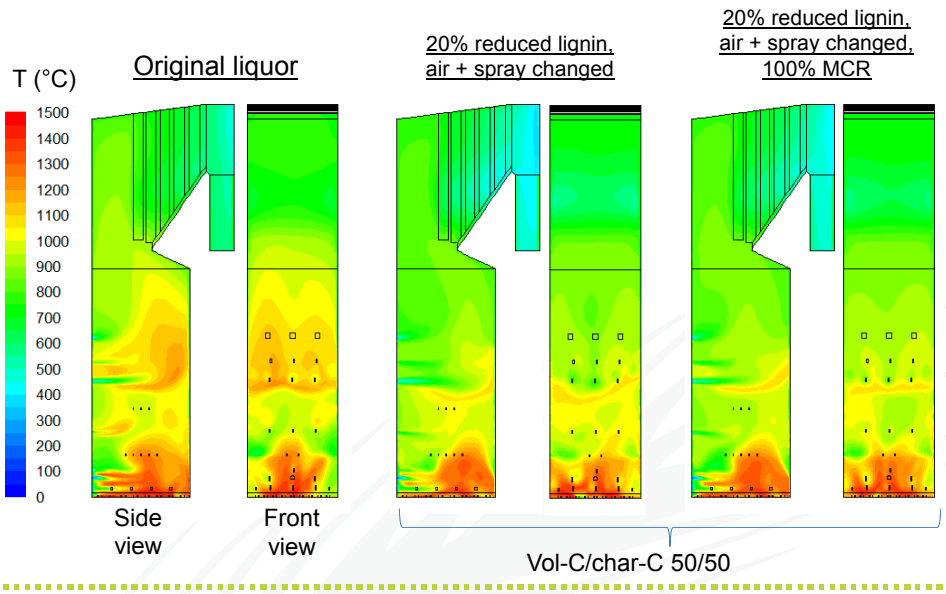

O_2 concentration

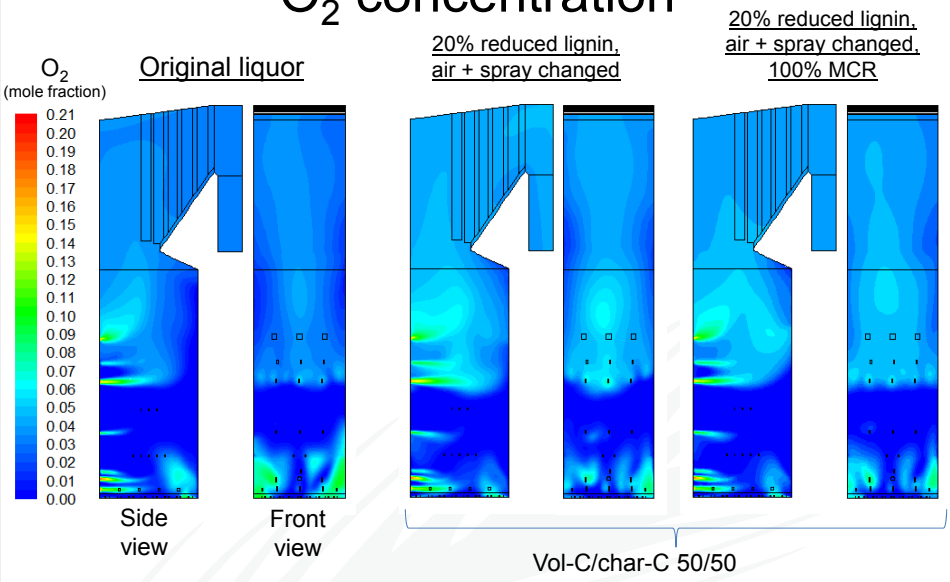

Carbon to walls/bed

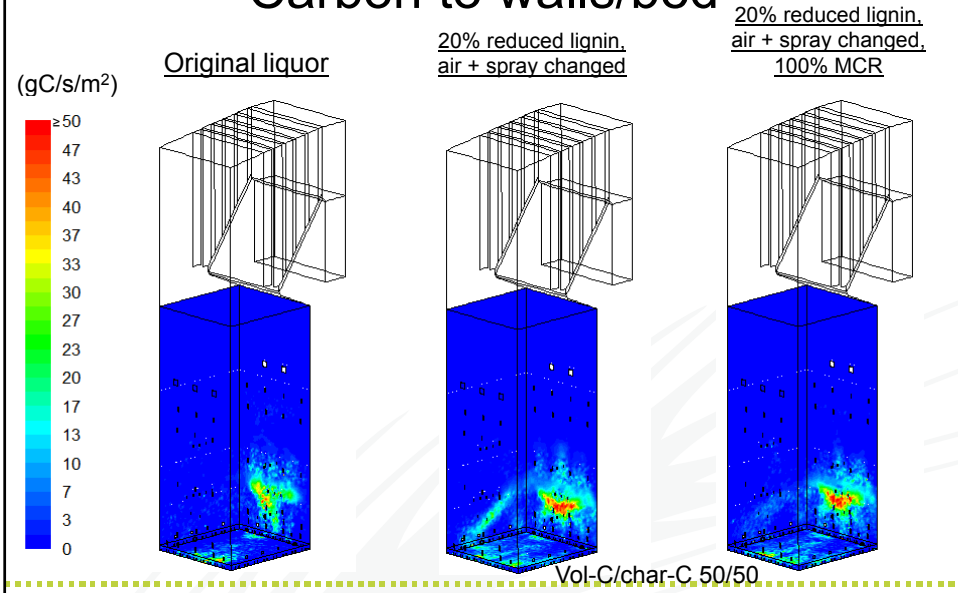

Left wall, back wall, and char bed

Carbon to walls/bed

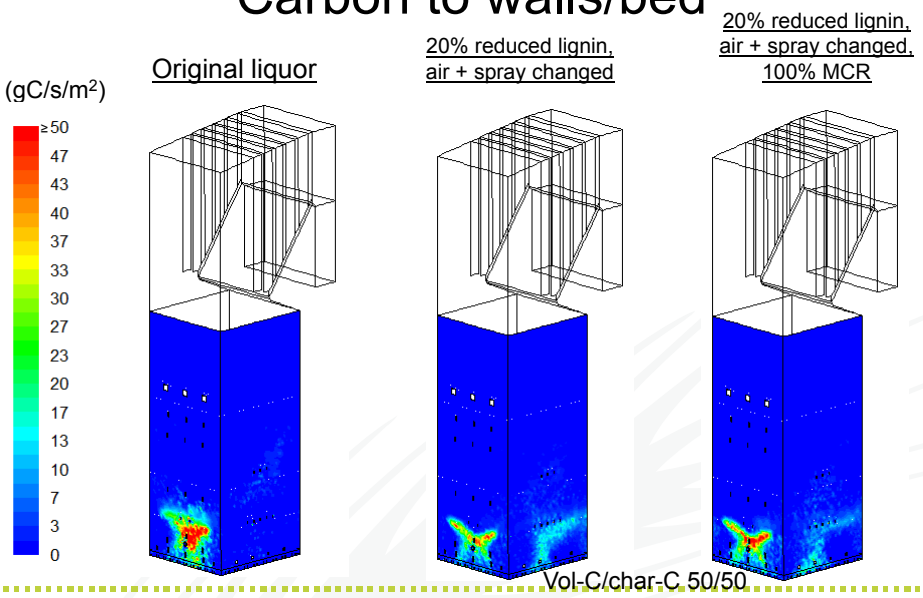

Right wall and front wall

Furnace carbon loading

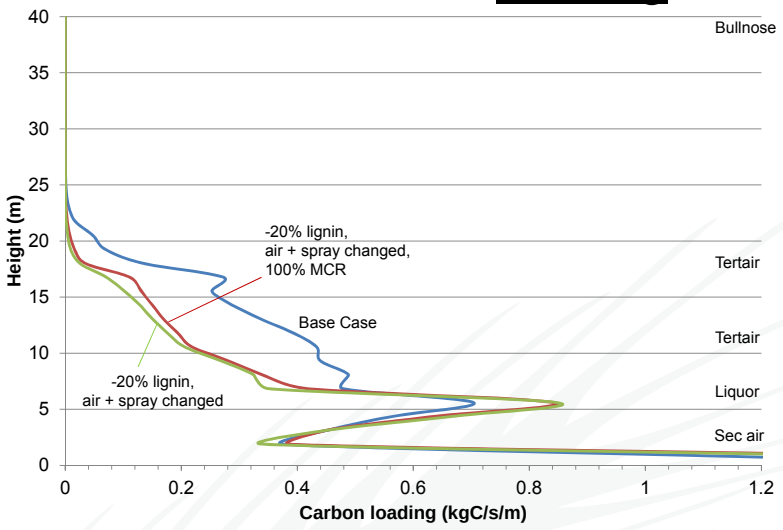

Furnace carbon conversion

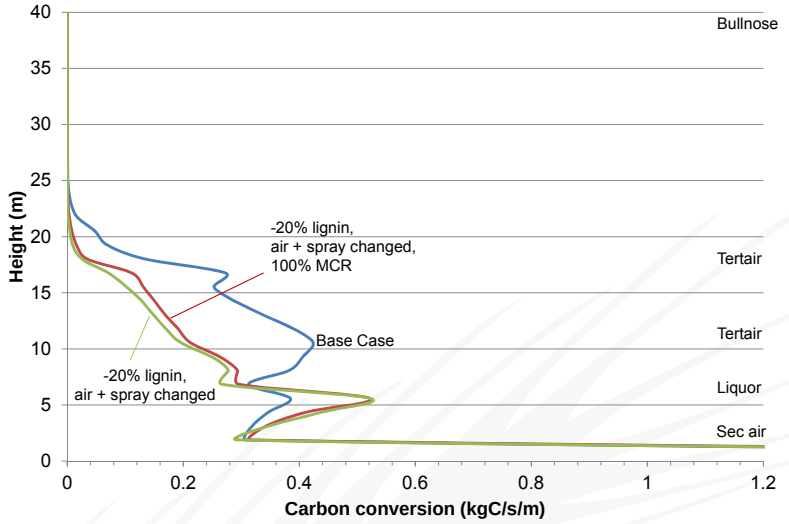

Fate of char carbon

(kg/s)	Base Case	20% reduced lignin, air + spray changed	20% reduced lignin, p2, air + spray changed 100% MCR
In liquor feed	8.81	7.25	7.71
in-flight conversion	3.90	1.42	1.84
to bed/walls	4.91	5.83	5.86
conversion on bed/walls	4.70	5.74	5.82
carbon accumulation	0.21	0.09	0.04

Fate of char carbon

(%)	Base Case	20% reduced lignin, air + spray changed	20% reduced lignin, p2, air + spray changed 100% MCR
In liquor feed	100.0	100.0	100.0
in-flight conversion	44.3	19.6	23.9
to bed/walls	55.7	80.4	76.1
conversion on bed/walls	53.4	79.2	75.6
carbon accumulation	2.3	1.2	0.5

CFD results

- **Run 1:** Wisa Base Case, 100% MCR, flue gas O_2 3% (wet)
- **Runs 8-15:** using vol-C / char-C based on experimental data
  - **Runs 8 and 9:** 10% (97% MCR) and 20% (94% MCR) lignin removed, total air adjusted for flue gas O_2 3% (wet), other variables unchanged (similar to Phase 1 runs 2&3) (results in carbon balance ≠ 0)
  - **Runs 10 and 11:** 10% (97% MCR) & 20% (94% MCR) lignin removed, modifications to air distribution **and** liquor spraying for carbon balance = 0
  - **Runs 12 and 13:** same as runs 10&11 but with 100% MCR
  - **Runs 14 and 15:** 10% (97% MCR) & 20% (94% MCR) lignin removed, modifications to liquor spraying for carbon balance = 0 (similar to Phase 1 runs 6&7)

Liquor feed and combustion air (Runs 1, 6&7, 10&11, 14&15)

	Original Black Liquor	10% lower lignin Run 6	20% lower ligning Run 7	10% lower lignin Run 10	20% lower ligning Run 11	10% lower lignin Run 14	20% lower ligning Run 15
Liquor feed (tds/d)	5320	5160	5000	5160	5000	5160	5000
Of MCR (%)	100	97	94	97	94	97	94
Air (kg/s)	272	256	232	256	232	256	232
Air (Nm3/s)	211	199	180	199	180	199	180
Primary	22%	22%	22%	25% *	28% *	22%	22%
Secondary	43%	43%	43%	40%	40%	43%	43%
Tertiary	35%	35%	35%	35%	32%	35%	35%
Target flue gas O_2 (% wet)	3.0	3.0	3.0	3.0	3.0	3.0	3.0
	Phase 1	Phase 1	Phase 1	Phase 2	Phase 2	Phase 2	Phase 2
Vol-C/char-C	**50/50**	**62/38**	**70/30**	**50/50**	**50/50**	**50/50**	**50/50**
Dp average (mm)	**5.7**	**12.5**	**23.0**	**6.5**	**11**	**6.3**	**7.2**
ΔT spray (°C)	**0**	**-4.7**	**-11.9**	**-0.6**	**-3.6**	**-0.4**	**-1.0**

Air distribution changed after which average droplet size "optimized" for carbon balanced situation.
Air change based on discussion with industry: "with a lower HV/quality liquor, more of the combustion (air+liquor) to lower furnace".
*) these percentages give ~same mass flow (kg/s) primary

Liquor feed and combustion air (Runs 1, 6&7, 10&11, 14&15)

	Original Black Liquor	10% lower lignin Run 6	20% lower ligning Run 7	10% lower lignin Run 10	20% lower ligning Run 11	10% lower lignin Run 14	20% lower ligning Run 15
Liquor feed (tds/d)	5320	5160	5000	5160	5000	5160	5000
Of MCR (%)	100	97	94	97	94	97	94
Air (kg/s)	272	256	232	256	232	256	232
Air (Nm3/s)	211	199	180	199	180	199	180
Primary	22%	22%	22%	25% *	28% *	22%	22%
Secondary	43%	43%	43%	40%	40%	43%	43%
Tertiary	35%	35%	35%	35%	32%	35%	35%
Target flue gas O_2 (% wet)	3.0	3.0	3.0	3.0	3.0	3.0	3.0
	Phase 1	Phase 1	Phase 1	Phase 2	Phase 2	Phase 2	Phase 2
Vol-C/char-C	**50/50**	**62/38**	**70/30**	**50/50**	**50/50**	**50/50**	**50/50**
Dp average (mm)	**5.7**	**12.5**	**23.0**	**6.5**	**11**	**6.3**	**7.2**
ΔT spray (°C)	**0**	**-4.7**	**-11.9**	**-0.6**	**-3.6**	**-0.4**	**-1.0**

Air distribution changed after which average droplet size "optimized" for carbon balanced situation.
Air change based on discussion with industry: "with a lower HV/quality liquor, more of the combustion (air+liquor) to lower furnace".
*) these percentages give ~same mass flow (kg/s) primary

Temperature

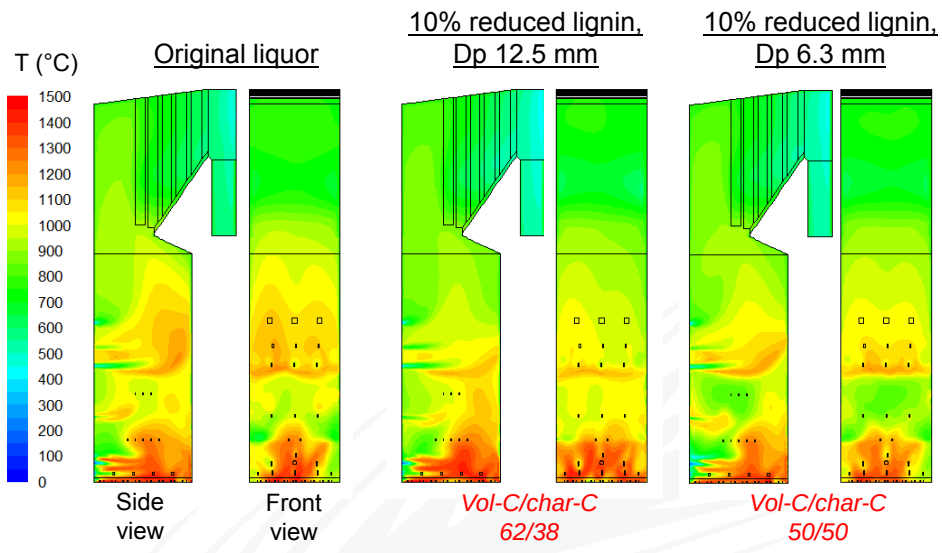

O_2 concentration

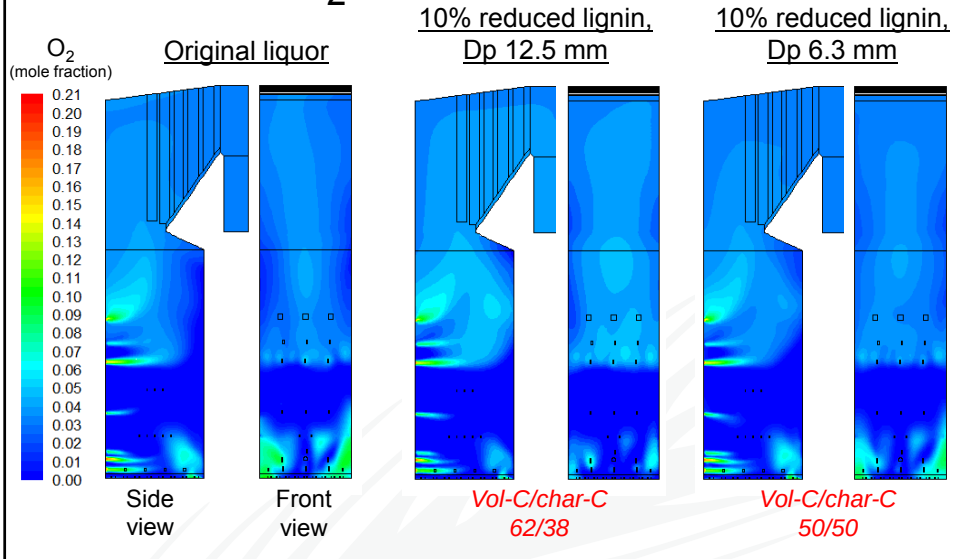

Carbon to walls/bed

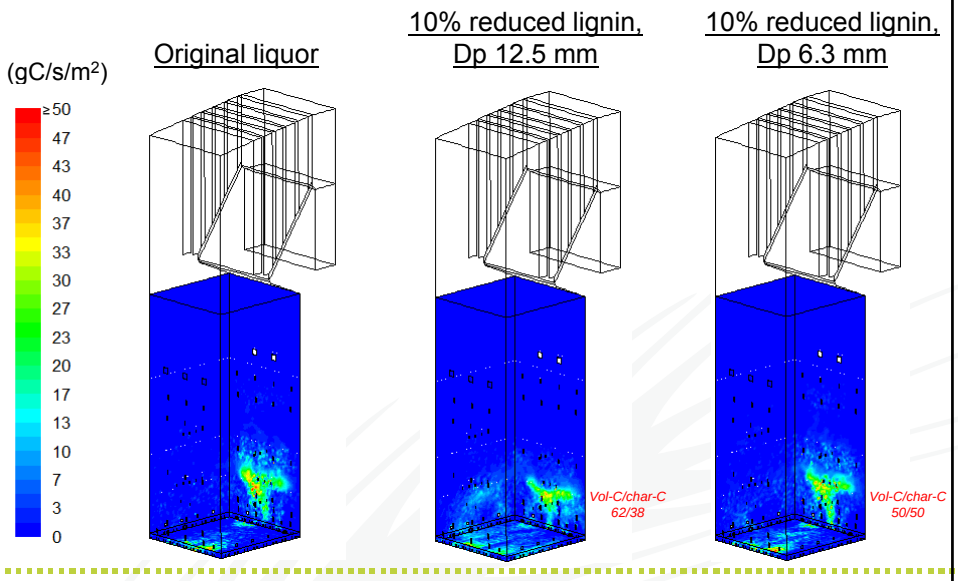

Left wall, back wall, and char bed

Carbon to walls/bed

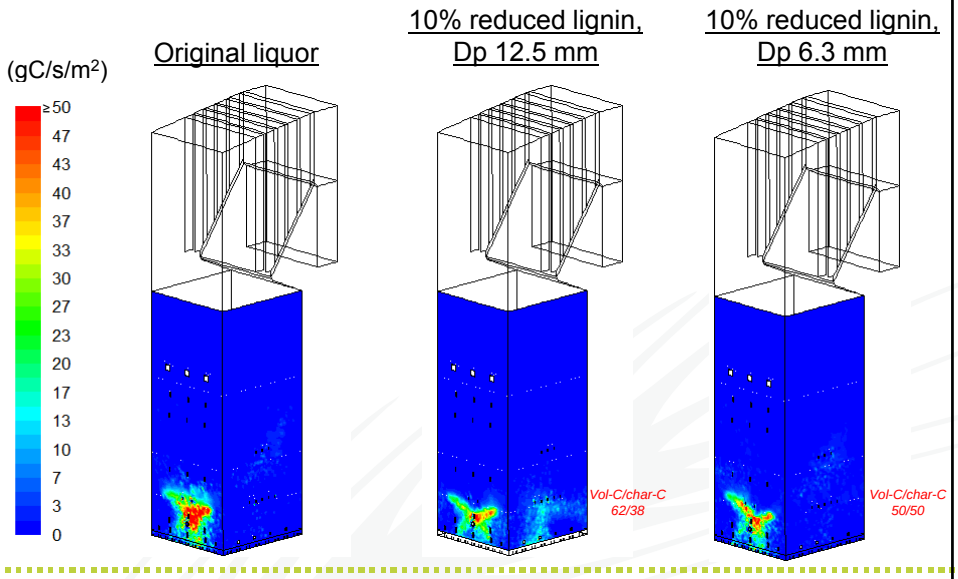

Right wall and front wall

Furnace carbon loading

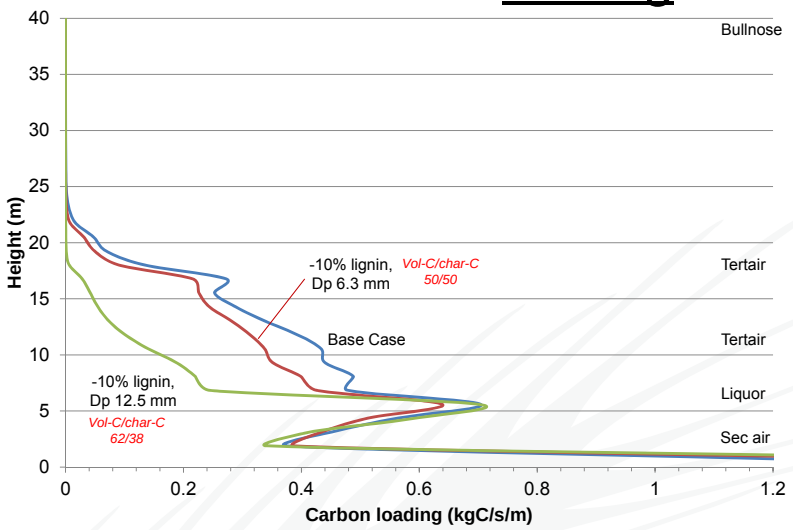

Furnace carbon conversion

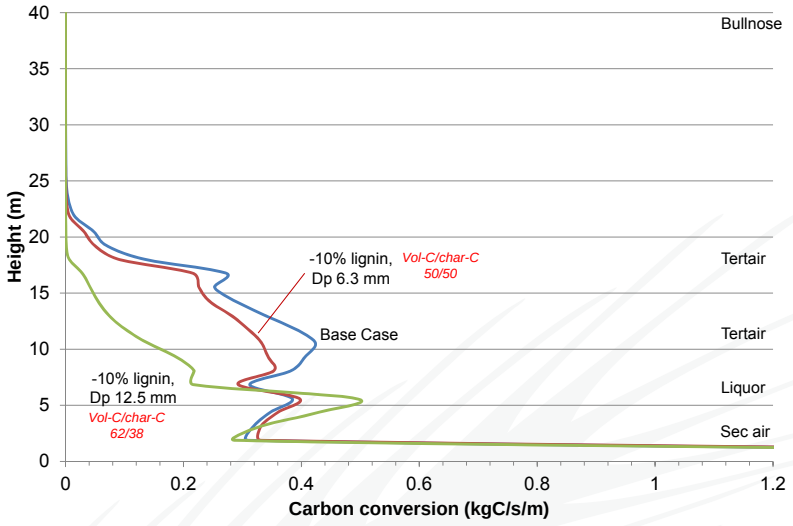

Fate of char carbon

(kg/s)	Base Case	10% reduced lignin, Dp 12.5 mm	10% reduced lignin, Dp 6.3 mm
In liquor feed	8.81	6.19	8.12
in-flight conversion	3.90	1.01	3.08
to bed/walls	4.91	5.18	5.04
conversion on bed/walls	4.70	5.16	5.01
carbon accumulation	0.21	0.02	0.03
		Vol-C/char-C 62/38	*Vol-C/char-C 50/50*

Fate of char carbon

(%)	Base Case	10% reduced lignin, Dp 12.5 mm	10% reduced lignin, Dp 6.3 mm
In liquor feed	100.0	100.0	100.0
in-flight conversion	44.3	16.3	38.0
to bed/walls	55.7	83.7	62.0
conversion on bed/walls	53.4	83.4	61.7
carbon accumulation	2.3	0.3	0.3
		Vol-C/char-C 62/38	*Vol-C/char-C 50/50*

Temperature

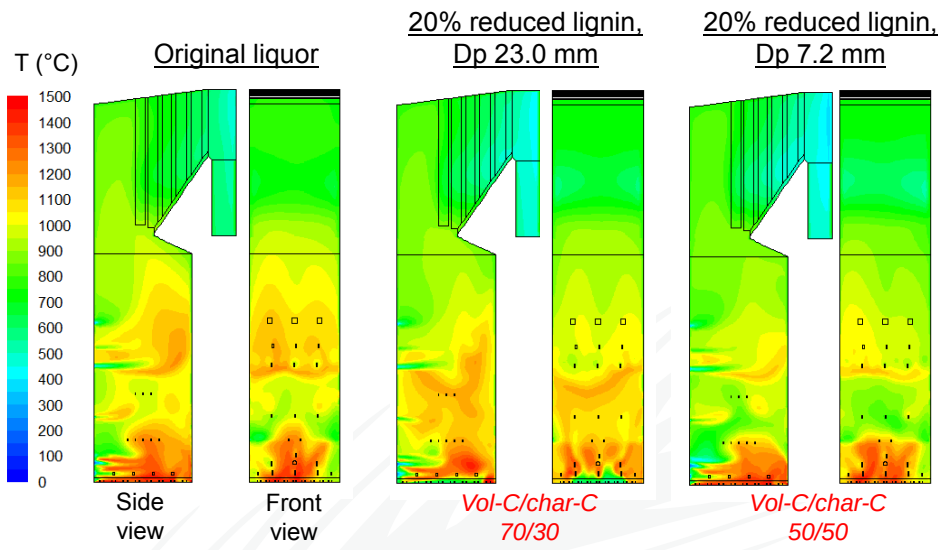

O_2 concentration

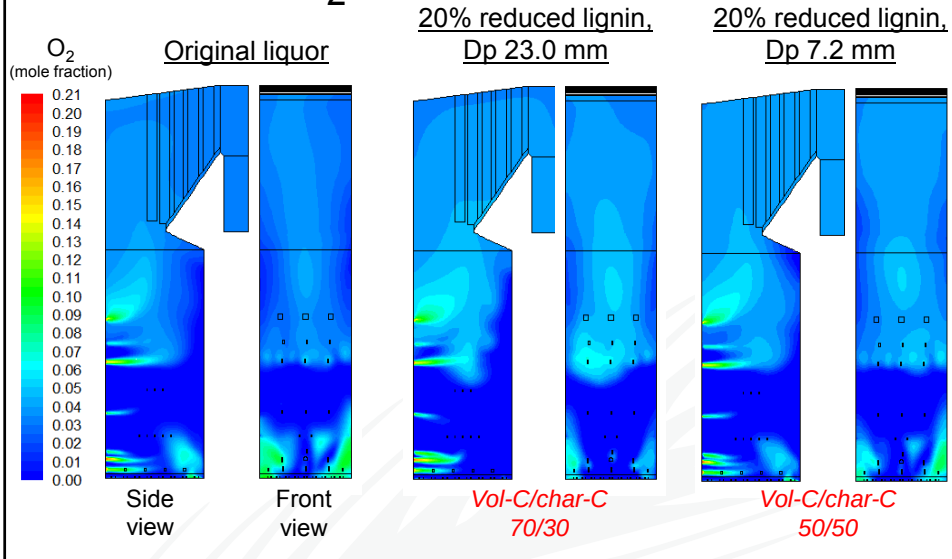

Carbon to walls/bed

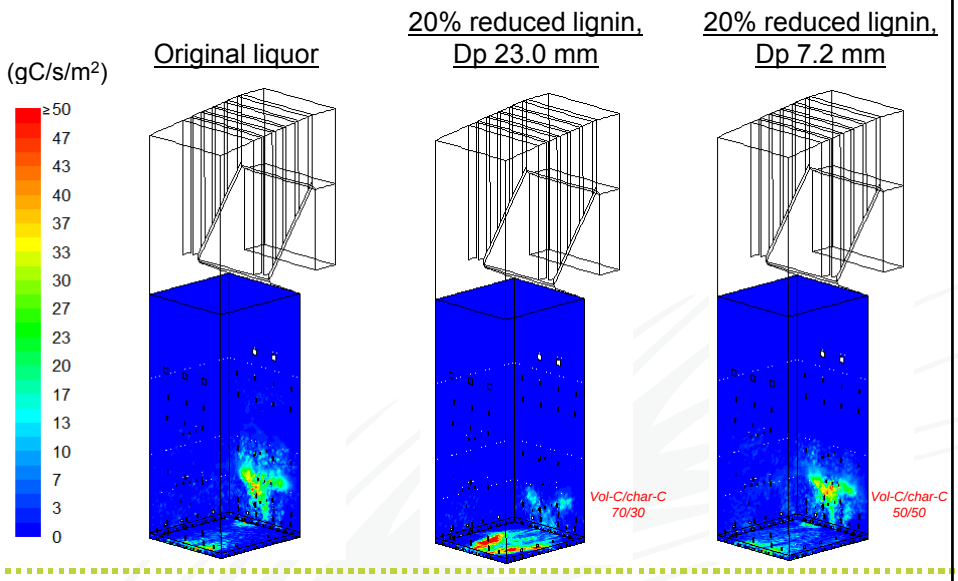

Left wall, back wall, and char bed

Carbon to walls/bed

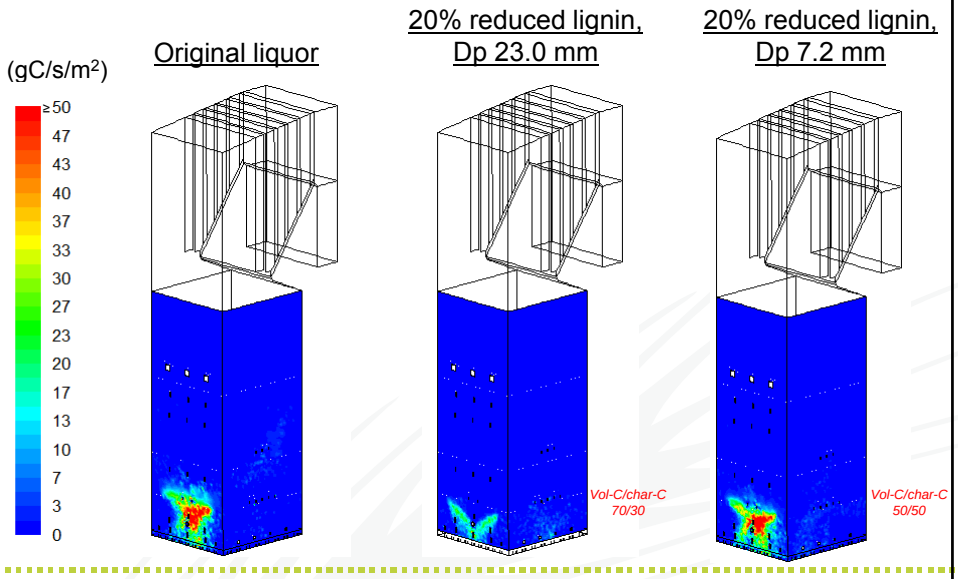

Right wall and front wall

Furnace carbon loading

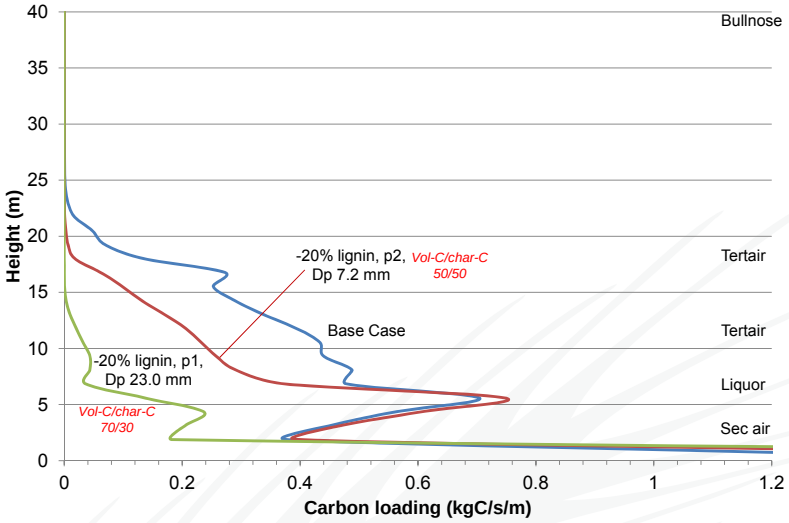

Furnace carbon conversion

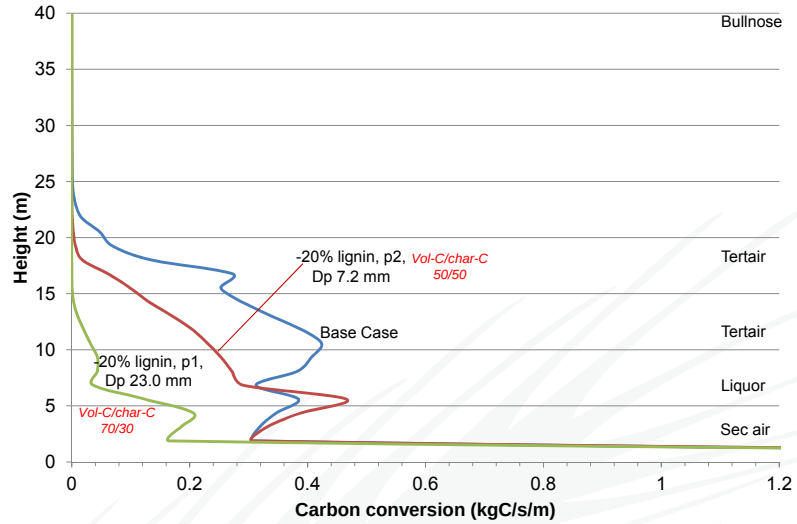

Fate of char carbon

(kg/s)	Base Case	20% reduced lignin, Dp 23.0 mm	20% reduced lignin, Dp 7.2 mm
In liquor feed	8.81	4.30	7.25
in-flight conversion	3.90	0.24	2.07
to bed/walls	4.91	4.05	5.18
conversion on bed/walls	4.70	4.02	5.15
carbon accumulation	0.21	0.03	0.03
		Vol-C/char-C 70/30	*Vol-C/char-C 50/50*

Fate of char carbon

(%)	Base Case	20% reduced lignin, Dp 23.0 mm	20% reduced lignin, Dp 7.2 mm
In liquor feed	100.0	100.0	100.0
in-flight conversion	44.3	5.7	28.5
to bed/walls	55.7	94.3	71.5
conversion on bed/walls	53.4	93.6	71.0
carbon accumulation	2.3	0.7	0.4
		Vol-C/char-C 70/30	*Vol-C/char-C 50/50*

Conclusions

- Less char-C with lignin removal
  - Less C to the lower furnace with lignin removal if drop size stays the same
  - Changes to operation needed to compensate
- For up to 20% lignin removal
  - With air distribution unchanged (p22%/s43%/t35%) decrease in liquor temperature by approximately 1 °C
  - Combined change in air+spray (p28%/s40%/t32%) decrease in liquor temperature by approximately 3.6 °C